

CRANIOFACIAL MORPHOLOGY OF *SIMOSUCHUS CLARKI* (CROCODYLIFORMES: NOTOSUCHIA) FROM THE LATE CRETACEOUS OF MADAGASCAR

NATHAN J. KLEY,^{*,1} JOSEPH J. W. SERTICH,¹ ALAN H. TURNER,¹ DAVID W. KRAUSE,¹ PATRICK M. O'CONNOR,² and JUSTIN A. GEORGI³

¹Department of Anatomical Sciences, Stony Brook University, Stony Brook, New York, 11794-8081, U.S.A.,
Nathan.Kley@stonybrook.edu; jsertich@ic.sunysb.edu; Alan.Turner@stonybrook.edu; David.Krause@stonybrook.edu;

²Department of Biomedical Sciences, Ohio University College of Osteopathic Medicine, Athens, Ohio 45701, U.S.A.,
oconnorp@oucom.ohiou.edu;

³Department of Anatomy, Arizona College of Osteopathic Medicine, Midwestern University, Glendale, Arizona 85308, U.S.A.,
jgeorgi@midwestern.edu

ABSTRACT—*Simosuchus clarki* is a small, pug-nosed notosuchian crocodyliform from the Late Cretaceous of Madagascar. Originally described on the basis of a single specimen including a remarkably complete and well-preserved skull and lower jaw, *S. clarki* is now known from five additional specimens that preserve portions of the craniofacial skeleton. Collectively, these six specimens represent all elements of the head skeleton except the stapedes, thus making the craniofacial skeleton of *S. clarki* one of the best and most completely preserved among all known basal mesoeucrocodylians. In this report, we provide a detailed description of the entire head skeleton of *S. clarki*, including a portion of the hyobranchial apparatus. The two most complete and well-preserved specimens differ substantially in several size and shape variables (e.g., projections, angulations, and areas of ornamentation), suggestive of sexual dimorphism. Assessment of both external and internal morphological features indicates a habitual head posture in which the preorbital portion of the dermal skull roof was tilted downward at an angle of ~45°. Functional and comparative assessment of the feeding apparatus strongly indicates a predominantly if not exclusively herbivorous diet. Other features of the craniofacial skeleton of *S. clarki* are consistent with the interpretation developed from analysis of the postcranial skeleton of a terrestrial habitus, but the current working hypothesis of a burrowing lifestyle is not supported. The atypical appearance of the skull and lower jaw of *S. clarki* is underscored by the identification of at least 45 autapomorphic features, many of them related to the greatly foreshortened snout.

INTRODUCTION

The Upper Cretaceous (Maastrichtian) Maevarano Formation in the Mahajanga Basin of northwestern Madagascar has yielded the articulated or associated cranial remains of several vertebrate taxa, including the frog *Beelzebufo ampinga* Evans, Jones, and Krause, 2008; the turtle *Kinkonychelys rogersi* Gaffney, Krause, and Zalmout, 2009; the lizard *Konkasaurus mahalana* Krause, Evans, and Gao, 2003; the snake *Menarana nosymena* LaDuke, Krause, Scanlon, and Kley, 2010; the crocodyliforms *Araripesuchus tsangatsangana* Turner, 2006, *Mahajangasuchus insignis* Buckley and Brochu, 1999 (see also Turner and Buckley, 2008), and *Miadanasuchus oblita* (Buffetaut and Taquet, 1979) Simons and Buckley, 2009; the abelisauroid theropods *Majungasaurus crenatissimus* (Depéret, 1896) Lavocat, 1955 (see also Sampson et al., 1998; Sampson and Witmer, 2007), and *Masiakasaurus knopfleri* Sampson, Carrano, and Forster, 2001 (see also Carrano et al., 2002, in press); and the titanosaurian sauropod *Rapetosaurus krausei* Curry Rogers and Forster, 2001 (see also Curry Rogers and Forster, 2004). None, however, are as complete and undistorted, or preserve surface detail as well, as the head skeleton in the holotype (Université d'Antananarivo [UA] specimen number 8679) of the blunt-snouted basal mesoeucrocodylian *Simosuchus clarki*. This specimen, which also includes a large portion of the postcranial skeleton, was rapidly buried in a debris flow over 65.5 million years ago (Rogers 2005; Krause et al., this volume), discovered and collected by a field crew of the joint Stony Brook University/Université d'Antananarivo Mahajanga Basin Project in 1998, and described in a preliminary report by Buckley et al. in 2000.

The discovery of *Simosuchus clarki* and description of many other notosuchian taxa with unusual cranial architecture (e.g.,

Chimaerasuchus paradoxus Wu, Sues, and Sun, 1995, see also Wu and Sues, 1996; *Malawisuchus mwakasyungutiensis* Gomani, 1997; *Mariliasuchus amarali* Carvalho and Bertini, 1999, see also Zaher et al., 2006; *Baurusuchus salgadoensis* Carvalho, Campos, and Nobre, 2005; *Adamantinasuchus navae* Nobre and Carvalho, 2006; *Sphagesaurus montealtensis* Andrade and Bertini, 2008; *Notosuchus terrestris*, see Fiorelli and Calvo, 2008; *Armadillosuchus arrudai* Marinho and Carvalho, 2009; *Yacarerani boliviensis* Novas, Pais, Pol, Carvalho, Scanferla, Mones, and Riglos, 2009; *Pakasuchus kapilimai* O'Connor, Sertich, Stevens, Roberts, Gottfried, Hieronymus, Jinnah, Ridgely, Ngasala, and Temba, 2010) over the last 10–15 years have effectively dismantled the concept that crocodyliforms varied little in cranial morphology during their evolutionary history (Langston, 1973). Buckley et al. (2000) described the skull of *Simosuchus clarki* as being dorsoventrally vaulted with a very abbreviated, squared snout, foliform, multi-cusped teeth, and an anteriorly shifted jaw joint, and therefore deviating significantly from the 'typical' crocodyliform Bauplan of a dorsoventrally flattened skull with an elongate snout, recurved, conical teeth, and posteriorly positioned jaw articulation. The morphology and placement of the jaw articulation and the shape of the teeth of *Simosuchus* were interpreted by Buckley et al. (2000) as reflective of an herbivorous diet. The lateral position of the orbits and the anterior position of the external nares indicated to the authors a terrestrial habit. The deep cranium, short, shovel-like snout, posteroventrally positioned occipital condyle, and underslung lower jaw were interpreted as evidence that *Simosuchus* may have been a burrower. Finally, the presence of two unambiguous synapomorphies—"internal nares divided by a septum and strongly spatulate posterior teeth" (Buckley et al., 2000:943)—linked *Simosuchus* with the Late Cretaceous (Cenomanian) South American form *Uruguaysuchus* as sister taxa.

Since the collection and description of the holotype specimen of *Simosuchus clarki*, several additional cranial specimens of this species have been recovered that add relatively little in terms

*Corresponding author.

of anatomical detail but do permit a preliminary assessment of intraspecific variability. The discovery of these additional specimens, further preparation of the holotype skull, the ability to discern anatomical structure in greater detail (e.g., positions of sutures, pathways of neurovascular canals) through the use of computed tomography (CT) scanning and image-processing software, and the recent discovery, description, and analysis of numerous other notosuchian taxa from elsewhere allow a more detailed, comparative, and comprehensive assessment of the anatomy, life habits, and phylogenetic position of *Simosuchus* than was possible a decade ago when the holotype was first described.

This report is focused exclusively on the head skeleton, including the dentition, of *Simosuchus clarki*. Its objectives are to (1) provide a detailed description of the skull, lower jaw, and dentition in a comparative context; (2) evaluate aspects of intraspecific variability in cranial size, shape, relative proportions, and ontogenetic maturity, and to determine the likelihood of sexual dimorphism; (3) assess attributes of the head skeleton that might provide insight into life habits, particularly feeding and locomotion; and (4) discuss the implications of craniofacial morphology for phylogeny reconstruction.

Institutional Abbreviations—**AMNH**, American Museum of Natural History, New York, U.S.A.; **BMNH**, British Museum of Natural History, London, U.K.; **BP**, Bernard Price Institute for Palaeontological Research, University of the Witwatersrand, Johannesburg, South Africa; **BSP**, Bayerische Staatssammlung für Paläontologie und Geologie, München, Germany; **CNRST-SUNY**, Centre National de la Recherche Scientifique et Technologique de Mali, Bamako, Mali—Stony Brook University, Stony Brook, U.S.A.; **CPPLIP**, Centro de Pesquisas Paleontológicas Llewellyn Ivor Price, Peirópolis, Brazil; **DGM**, Departamento de Produção Mineral, Rio de Janeiro, Brazil; **FMNH**, The Field Museum, Chicago, U.S.A.; **GMPKU-P**, School of Earth and Space Sciences, Peking University, Beijing, People's Republic of China; **IGM**, Mongolian Institute of Geology, Ulaan Baatar, Mongolia; **IVPP**, Institute of Vertebrate Paleontology and Paleoanthropology, Beijing, People's Republic of China; **LACM**, Los Angeles County Museum, Los Angeles, U.S.A.; **MACN-PV**, Museo Argentino de Ciencias Naturales, Buenos Aires, Argentina; **MAL**, Malawi Department of Antiquities, Lilongwe, Malawi; **MCZ**, Museum of Comparative Zoology, Cambridge, U.S.A.; **MLP**, Museo de La Plata, La Plata, Argentina; **MN**, Museu Nacional, Universidade Federal do Rio de Janeiro, Rio de Janeiro, Brazil; **MNHN**, Muséum National d'Histoire Naturelle, Paris, France; **MNK**, Museo de Historia Natural Noel Kempff Mercado, Universidad Autónoma Gabriel René Moreno, Santa Cruz de la Sierra, Bolivia; **MNN**, Musée National du Niger, Niamey, Republic of Niger; **MOZ**, Museo Prof. Dr. Juan A. Olsacher, Zapala, Argentina; **MPCA-PV**, Museo Provincial Carlos Ameghino, Cipoletti, Argentina; **MPMA**, Museu de Paleontologia de Monte Alto, Monte Alto, Brazil; **MTM**, Magyar Természettudományi Múzeum, Budapest, Hungary; **MUCPv**, Museo de Geología y Paleontología, Universidad Nacional del Comahue, Neuquén, Argentina; **MZSP-PV**, Museu de Zoologia, Universidade de São Paulo, São Paulo, Brazil; **NMC**, Canadian Museum of Nature, Ottawa, Canada; **PVL**, Instituto Miguel Lillo, Tucumán, Argentina; **QM**, Queensland Museum, Brisbane, Australia; **RCL**, Museo de Ciencias Naturales, Pontificia Universidade Católica de Minas Gerais, Belo Horizonte, Brazil; **ROM**, Royal Ontario Museum, Toronto, Canada; **RRBP**, Rukwa Rift Basin Project, Tanzanian Antiquities Unit, Dar es Salaam, Tanzania; **SAM**, South African Museum, Cape Town, South Africa; **TMM**, Texas Memorial Museum, Austin, U.S.A.; **TMP**, Royal Tyrrell Museum of Palaeontology, Drumheller, Canada; **UA**, Université d'Antananarivo, Antananarivo, Madagascar; **UCMP**, University of California Museum of Paleontology, Berkeley, U.S.A.; **UFRJ**, Universidade Federal do Rio de Janeiro, Rio de Janeiro, Brazil; **UNC**, University of North Carolina Department of Geological

Sciences, Chapel Hill, U.S.A.; **URC**, Museu de Paleontologia e Estratigrafia Prof. Dr. Paulo Milton Barbosa Landim, Universidade Estadual Paulista, Rio Claro, Brazil.

Anatomical Abbreviations—See Appendix 1.

MATERIALS AND METHODS

Specimens of *Simosuchus clarki*

Three specimens of *Simosuchus clarki* are now known in which the skull and lower jaw are preserved nearly completely: UA 8679, FMNH PR 2596, and FMNH PR 2597. (See Krause et al. [this volume] for provenance information and an accounting of the postcranial elements associated with each of these specimens.)

UA 8679—This specimen, which serves as the holotype for *Simosuchus clarki*, includes a fully articulated head skeleton (although its anterior and posterior palpebrals were removed from both sides of the skull during preparation). This specimen includes nearly all elements of the skull (only the stapedes and epipterygoids are missing), all elements of the lower jaw, and a single fragmentary piece of the hyobranchial apparatus. In general, the entire head skeleton is preserved extraordinarily well; distortion is minimal, and externally visible breakage is limited primarily to one region of the left quadrate within the adductor chamber and to a few small, isolated areas along the very thinnest portions of the pterygoid and palatine bones where they surround the internal nares. Internally, the anteroventral-most portion of the cranial cavity is incompletely preserved and both left and right tympanic bullae are partially damaged.

FMNH PR 2596—This specimen includes a nearly complete head skeleton that remains at least partially articulated. However, both the skull and lower jaw of this specimen have been fragmented extensively through severe crushing, and the skull in particular exhibits additional significant distortion. Most notably, the snout has broken away from the remainder of the skull near the level of the preorbital crest, and this entire segment of the facial skeleton has been forced ventrally far beyond its already strongly ventroflexed natural position. Despite such extensive damage, however, certain elements of the skull and lower jaw (e.g., articulars, premaxillary teeth) remain remarkably well preserved.

FMNH PR 2597—This specimen includes a head skeleton that remains nearly fully articulated and largely complete. The only elements missing entirely are the stapedes and the right articular and splenial, as well as the (extracranial) anterior and posterior supratemporal ossifications and the right posterior palpebral. However, both the skull and lower jaw of this specimen exhibit significant distortion and isolated areas of breakage, with most of the latter appearing to have been caused primarily, if not exclusively, by the former. The comparatively poor preservation of this specimen (and that of FMNH PR 2596, described above) relative to that of the holotype specimen (UA 8679) may relate to the fact that both FMNH PR 2596 and FMNH PR 2597 were preserved in the Masorobe Member of the Maevarano Formation, whereas UA 8679 was collected from facies 2 of the Anembalemba Member, the latter being well known for its exquisite preservation of fossil vertebrate specimens (Rogers et al., 2000, 2007; Rogers, 2005).

The most significant distortion evident in the head skeleton of FMNH PR 2597 is a sagittal shearing that resulted in the right side of the skull and lower jaw being forced anteriorly relative to the left side. Specifically, the right squamosal has been forced strongly anteroventrally. The anterior component of this movement was transmitted to the right postorbital, and thus to the right jugal, consequently resulting in breakage of several bones near the anteroventral margin of the right orbital fenestra (i.e., anterior process of the jugal, descending process of the lacrimal,

and posterior-most portion of the alveolar process of the maxilla), as well as deformation of the right antorbital fenestra (due to an anterior displacement of the descending process of the lacrimal and ascending process of the maxilla) (see Krause et al., this volume:fig. 4). Ultimately, anterior displacement of the entire right half of the snout resulted in significant crushing of the anterior surfaces of both the right premaxilla and maxilla.

Simultaneously, the ventral component of the anteroventral displacement of the right squamosal was transmitted to the right quadrate, and ultimately to both the pterygoid and the right mandibular ramus. In the case of the former, anterodorsal rotation of the pterygoid process of the quadrate was transmitted to the quadrate process of the pterygoid, forcing the more anterior portions of the pterygoid to rotate ventrally (likely the cause of breakage to both the anterior process and right transverse process of the pterygoid, and to the palatines as well). In the case of the latter, anteroventral rotation of the distal portion of the body of the right quadrate (and thus the quadratic hemicondyles) not only forced the entire right half of the lower jaw anteriorly relative to the left half, but also apparently caused significant damage in the region of the right craniomandibular joint; the body of the right quadrate is badly broken and no portion of the right articular was preserved. Despite this extensive distortion and breakage, however, FMNH PR 2597 preserves the majority of the head skeleton more or less articulated and intact, thus making possible at least some additional, though limited, observations concerning intraspecific variability in the morphology of the skull and lower jaw of *Simosuchus clarki*. Perhaps even more significantly, it is the only specimen of *Simosuchus* currently known to preserve the epipterygoids.

Other Specimens—In addition to the three articulated specimens listed above, three other specimens include isolated elements, or fragments of elements, of the head skeleton of *Simosuchus clarki*: UA 9754 includes a nearly complete right ectopterygoid (missing only the posterior process); UA 9762 includes a partial frontal (right posterolateral portion); and FMNH PR 2598 includes fragments of the right quadratojugal (ventral three-quarters of the central plate, together with the tubercle and proximal-most portion of the anterior process), surangular (anterior half of ramus), and angular (three separate fragments collectively comprising nearly the entire ventrolateral flange).

Due to the near completeness and generally exquisite preservation of UA 8679, together with the exceptional quality of the high-resolution X-ray computed tomographic (HRXCT) scans taken of its skull and lower jaw, our description of the head skeleton of *S. clarki* is based predominantly on this specimen. Moreover, due to the extensive crushing and distortion of FMNH PR 2596, and the significant (albeit far less severe) distortion of FMNH PR 2597, all measurements given in the text refer specifically to UA 8679, unless otherwise indicated (but see Tables 1 and 2 for morphometric comparisons of the two most complete articulated specimens, UA 8679 and FMNH PR 2597). Nevertheless, despite the distortion and breakage evident in both FMNH PR 2596 and FMNH PR 2597, these specimens provide useful comparative data that serve to further corroborate our anatomical interpretations of the holotype and provide information on intraspecific variability in this taxon.

Comparative Material

In addition to the specimens of *Simosuchus clarki* referenced above, the following specimens representing other crocodyliform taxa, both extinct and extant, were examined to facilitate the comparisons made in this paper. Where published illustrations and descriptions were used to supplement information obtained through direct observation of specimens, appropriate references follow specimen numbers. Where only published illustrations and

descriptions of individual specimens were available, the appropriate references are enclosed in brackets.

Adamantinasuchus navae (UFRJ-DG 107-R [Nobre and Carvalho, 2006]); *Alligator mississippiensis* (FMNH 8201; Iordansky, 1973; Brochu, 1999); *Anatosuchus minor* (MNN nos. GAD17, GAD603; Sereno et al., 2003; Sereno and Larsson, 2009); *Araripesuchus buitreaensis* (MPCA-PV nos. 235, 236; Pol and Apesteguía, 2005); *Araripesuchus gomesii* (AMNH FR 24450; DGM-DNPM 432-R [Price, 1959]); *Araripesuchus patagonicus* (MUCPv nos. 267, 269, 270, 283; Ortega et al., 2000); *Araripesuchus tsangatsangana* (FMNH nos. PR 2297–PR 2299, UA 8720; Turner, 2006); *Araripesuchus wegneri* (MNHN-GDF 700, MNN GAD19; Buffetaut and Taquet, 1979; Sereno and Larsson, 2009); *Armadillosuchus arrudai* (UFRJ-DG 303-R, MPMA-64-0001-04 [Marinho and Carvalho, 2009]); *Baurusuchus pachecoi* (DGM 299-R [Price, 1945, Carvalho et al., 2005]); *Baurusuchus salgadoensis* (MPMA 62-0001-02 [Carvalho et al., 2005; Vasconcelos and Carvalho, 2007]); *Bretesuchus bonapartei* (PVL 4735; Gasparini et al., 1993); *Caiman crocodilus* (AMNH R 43291; Brochu, 1999); *Caiman latirostris* (AMNH nos. R 62555, R 143183; Brochu, 1999); *Caiman yacare* (AMNH nos. R 97295, R 97296, R 97309; Brochu, 1999); *Calsosayusuchus valliceptus* (TMM 43631-1; Tykoski et al., 2002); *Candidodon itapecuriense* (MN-4355-V [Carvalho, 1994]; UFRJ-DG 114-R [Nobre and Carvalho, 2002]); *Chimaerasuchus paradoxus* (IVPP V8274 [Wu and Sues, 1996]); *Comahuesuchus brachybuccalis* (MUCPv 202, MACN-PV nos. N 30, N 31 [Bonaparte, 1991]; MOZ P 6131 [Martinelli, 2003]); *Crocodylus acutus* (AMNH R 66635; Iordansky, 1973); *Crocodylus niloticus* (FMNH nos. 17157, 217153); *Dibothrosuchus elaphros* (IVPP V 7907; Wu and Chatterjee, 1993); *Dromicosuchus grallator* (UNC 15574 [Sues et al., 2003]); *Edentosuchus tienshanensis* (IVPP V 3236; GMPKU-P 200101 [Pol et al., 2004]); Fruita Form (LACM 120455a [Clark, 1985]); *Gavialis gangeticus* (FMNH nos. 82681, 98864; Iordansky, 1973); *Goniopholis simus* (BMNH 41098; Salisbury et al., 1999); *Goniopholis stovalli* (AMNH FR 5782; Mook, 1964); *Hamadasuchus rebouli* (ROM 52620; Larsson and Sues, 2007); *Hesperosuchus agilis* (AMNH FR 6758 [Clark et al., 2000]); *Hylaeochampsia vectiana* (BMNH R177; Clark and Norell, 1992); *Iharkutosuchus makadii* (MTM 2006.52.1 [Ösi et al., 2007; Ösi, 2008]); *Isisfordia duncani* (QM nos. F36211, F44320 [Salisbury et al., 2006]); *Junggarsuchus sloani* (IVPP V 14010 [Clark et al., 2004]); *Kaprosuchus saharicus* (MNN IGU12; Sereno and Larsson, 2009); *Laganosuchus thaumastos* (MNN IGU13; Sereno and Larsson, 2009); *Leidyosuchus canadensis* (AMNH FR 5352; NMC 2279; ROM 1903; TMP 74.10.8; Wu et al., 2001); *Libycosuchus brevirostris* (BSP 1912.VIII.574; Stromer, 1914); *Litargosuchus leptorhynchus* (BP/1/5273 [Clark and Sues, 2002]); *Lomasuchus palpebrosus* (MOZ 4084 PV; Gasparini et al., 1991); *Mahajangasuchus insignis* (FMNH nos. PR 2389, PR 2448–PR 2450; UA nos. 8654, 9046, 9047, 9737; Turner and Buckley, 2008); *Malawisuchus mwakasyungutiensis* (MAL nos. 46, 48, 49; Gomani, 1997); *Mariliasuchus amarali* (MZSP-PV nos. 50, 51 [Zaher et al., 2006]; UFRJ-DG 106-R [Nobre et al., 2008]; URC R-68 [Andrade and Bertini, 2008b]); *Melanosuchus niger* (AMNH nos. R 58135, R 110179; Brochu, 1999); *Montealtosuchus arrudacamposi* (MPMA-16-0007-04 [Carvalho et al., 2007]); *Notosuchus terrestris* (MACN-PV nos. N 20, N 22, N 24, N 43, RN 1037–RN 1044, RN 1046, RN 1048, RN 1118, RN 1119; MLP nos. 64-IV-16-1, 64-IV-16-5, 64-IV-16-6, 64-IV-16-10–64-IV-16-13, 64-IV-16-23; MPCA-PV nos. 249, 250; MUCPv nos. 35, 147, 287; Fiorelli and Calvo, 2008); *Pakasuchus kapilimai* (RRBP nos. 05103, 08631; O'Connor et al., 2010); *Paleosuchus palpebrosus* (AMNH nos. R 97326, R 97328; Brochu, 1999); *Paleosuchus trigonatus* (AMNH nos. R 137174, R 137175; Brochu, 1999); *Peirosaurus torminni* (MOZ 1750 PV; Gasparini et al., 1991; DGM-433-R [Price, 1955]); *Pristichampsus vorax* (FMNH nos. PR 74, PR 399, PR 479; UCMP 154329; Troxell, 1925); *Protosuchus richardsoni*

(AMNH FR 3024; MCZ 6727; UCMP nos. 130860, 131827; Colbert and Mook, 1951); *Rhabdognathus aslerensis* (CNRST-SUNY 190; Brochu et al., 2002); *Sarcosuchus imperator* (MNH GDF 662; MNN 603, 604; Broin and Taquet, 1966; Sereno et al., 2001); *Shamosuchus djadochtaensis* (AMNH FR 6412, IGM 100/1195; Pol et al., 2009); *Sphagesaurus huenei* (RCL 100 [Pol, 2003]); *Sphagesaurus montealtensis* (MPMA 15–001/90 [Andrade and Bertini, 2008a]); *Sphenosuchus acutus* (SAM 3124 [Walker, 1990]); *Stolokrosuchus lapparenti* (MNH GDF600, Larsson and Gado, 2000); *Stomatosuchus inermis* (see Stromer, 1925); *Terminonaris robusta* (AMNH nos. FR 5849, FR 5850; Wu et al., 2001); *Theriosuchus pusillus* (BMNH nos. R 48216, R 48218, R 48227, R 48328, R 48330; Clark, 1986); *Tomistoma schlegelii* (AMNH R 15177, MCZ 12459 [Mook, 1921b; Iordansky, 1973]); *Uberabasuchus terrificus* (CPPLIP 630 [Carvalho et al., 2004]); *Uruguaysuchus aznarezi* (see Rusconi, 1933); *Yacarerani bolivienensis* (MNK-PAL5063 [Novas et al., 2009]); *Zaraasuchus shepardii* (IGM 100/1321; Pol and Norell, 2004b); *Zosuchus davidsoni* (IGM nos. 100/1304–100/1308; Pol and Norell, 2004a).

Comparisons made to ‘mesoeucrocodylians’ refer to all taxa contained within the clade Mesoeucrocodylia as defined by Whetstone and Whybrow (1983), whereas comparisons made to ‘basal mesoeucrocodylians’ refer only to members of Mesoeucrocodylia basal to Neosuchia. Comparisons made to ‘crocodylians’ refer to all members of the clade Crocodylia as defined by Brochu (2003) (i.e., the most recent common ancestor of *Gavialis gangeticus*, *Alligator mississippiensis*, and *Crocodylus niloticus*, and all of its descendants).

Computed Tomography

The skull and lower jaw of the holotype (UA 8679) of *Simosuchus clarki* were μ CT-scanned at the High-Resolution X-ray Computed Tomography (HRXCT) Facility of The University of Texas at Austin. The specimen was scanned in the transverse plane (field of reconstruction = 121 mm), resulting in a total of 999 slices, each 0.131 mm thick, with an interslice spacing of 0.131 mm, and a pixel resolution of 1024 \times 1024. The original transverse slices were then resliced in both the frontal and sagittal planes, with reslicing done on every pixel, resulting in interslice spacings of 0.118 mm in these reslicings.

HRXCT images of UA 8679 were examined directly using OsiriX software (available at <http://www.osirix-viewer.com/>). In addition, these images were further processed (by M. Colbert and J. Maisano of The University of Texas at Austin) using VGStudioMAX software (Volume Graphics, Heidelberg, Germany) to create three-dimensional (3-D) animations of the head skeleton of this specimen. Specifically, four sets of QuickTime animations were created: (1) 3-D rotations around the three principal orthogonal axes; (2) 3-D rotations around the three principal orthogonal axes, with the remaining matrix digitally removed; (3) 3-D dynamic cutaways along the three principal orthogonal axes, with the remaining matrix digitally removed; and (4) slice-by-slice animations along the three principal orthogonal axes. An interactive version of the HRXCT data set, including animations of 3-D reconstructions, as well as additional technical information concerning the scans and image processing, can be viewed at http://www.digimorph.org/specimens/Simosuchus_clarki. The original full-resolution HRXCT data are available from the corresponding author upon request.

The head skeletons of FMNH PR 2596 and FMNH PR 2597 were CT-scanned on a GE Lightspeed VCT scanner at the Stony Brook University Medical Center. FMNH PR 2596 was scanned in the transverse plane (field of reconstruction = 124 mm), resulting in a total of 501 slices, each 0.625 mm thick, with an interslice spacing of 0.200 mm, and a pixel resolution of 512 \times 512. FMNH PR 2597 was also scanned in the transverse plane (field of reconstruction = 96 mm), resulting in a total of 410

slices, each 0.625 mm thick, with an interslice spacing of 0.310 mm, and a pixel resolution of 512 \times 512. These transverse slices were examined directly (and resliced in both the frontal and sagittal planes) using both OsiriX and ImageJ software (available at <http://rsb.info.nih.gov/ij/>; developed by W. Rasband, National Institutes of Health, Bethesda, U.S.A.). In addition, 3-D QuickTime animations of the head skeletons of these referred specimens (i.e., rotations around the three principal orthogonal axes) were created using OsiriX software.

Measurements

All external linear measurements of the skull and lower jaw of *Simosuchus clarki* were taken using a hand-held Mitutoyo CD-8”C digital caliper, with the specimens held under either a Zeiss SteREO Discovery.V12 stereomicroscope or a Ledu 120 mm magnifying lamp. Each reported measurement represents the mean of 10 individual measurements, rounded to the nearest 0.1 mm. Comparative measurements taken on the head skeletons of UA 8679 and FMNH PR 2597 are described and reported in Tables 1 and 2.

Whereas external anatomical structures were generally measured by hand with a caliper, internal structures within the head skeleton of UA 8679 were measured digitally from HRXCT scans using OsiriX and Image J software. In addition, a small number of non-linear measurements were made digitally from photographs using Image J software.

Conventions Adopted Regarding Directional Anatomical Nomenclature

The potential advantages and disadvantages of adopting a standardized system of anatomical nomenclature for all non-human tetrapods continue to be debated in the literature (see Harris, 2004, and Wilson, 2006, for recent reviews). Nevertheless, at present, no standardized ‘Nomina Anatomica Tetrapodum’ exists. Although some vertebrate morphologists have adopted the standardized terminologies formalized in Nomina Anatomica Veterinaria (ICVGAN, 2005) (developed for domesticated mammals) or Nomina Anatomica Avium (Baumel et al., 1993) (developed for birds), and have applied them to other distantly related tetrapod taxa, others continue to use the well-entrenched, traditional anatomical terminology that arose historically in parallel with the early development and subsequent growth of comparative vertebrate anatomy as a formal discipline. In our description of the skull and lower jaw of *Simosuchus clarki*, we follow the latter approach by using the anatomical nomenclature traditionally applied to reptiles, initially developed principally by Owen (1854, 1866), and subsequently elaborated by Williston (1925) and, most significantly, Romer (1956). Most notably, we use the traditional directional terms ‘anterior’ and ‘posterior’ rather than their veterinary equivalents, ‘rostral’ and ‘caudal.’ However, given the extreme angulation of both the upper and lower dental arcades in *Simosuchus*, we use standard terms from dental anatomy (i.e., ‘mesial,’ ‘distal,’ ‘labial,’ and ‘lingual’) (e.g., Peyer, 1968) to describe the orientations of teeth and certain portions of the three paired bones that possess them in *Simosuchus* (i.e., premaxillae, maxillae, and dentaries).

One additional, taxon-specific consideration regarding our usage of directional anatomical nomenclature relates to the strongly angulated skull of *Simosuchus*. If, for example, the posterior portion of the cranial table is oriented horizontally, then the preorbital portion of the skull must be considered to be directed not anteriorly, but rather anteroventrally (i.e., pitched downward at an angle of 45°). Although this is indeed precisely the orientation that we infer to be the habitual head posture for *S. clarki* (see ‘Habitual Head Posture’ [below]), our anatomical description is written—largely for pragmatic reasons—as

if the natural orientation of the head skeleton was essentially 'neutral' (i.e., with both the snout and posterior cranial table pitched downward by $\sim 22.5^\circ$); not coincidentally, this is the orientation of the skull when it is positioned in articulation with the lower jaw, with the latter resting on a horizontal surface (i.e., supported on each side between the retroarticular process and the posterior portion of the ventral lamina of the splenial).

SYSTEMATIC PALEONTOLOGY

ARCHOSAURIA Cope, 1869

CROCODYLOMORPHA Walker, 1970

CROCODYLIFORMES Hay, 1930 (sensu Clark, in Benton and Clark, 1988)

MESOEUCROCODYLIA Whetstone and Whybrow, 1983

NOTOSUCHIA Gasparini, 1971

SIMOSUCHUS CLARKI Buckley, Brochu, Krause, and Pol, 2000

Type Specimen—UA 8679, complete skull and lower jaw and anterior portion of postcranial skeleton.

Age and Distribution—Late Cretaceous (Maastrichtian), Madagascar.

Referred Specimens—See complete listing in Krause et al. (this volume).

Diagnosis—See Turner and Sertich (this volume).

DESCRIPTION AND COMPARISONS

General Description of the Skull and Lower Jaw

The skull of *Simosuchus clarki*, if preserved in its entirety, would have been comprised of 41 individual elements, 17 of them paired (unfused, left and right, for a total of 34—premaxillae, maxillae, nasals, lacrimals, prefrontals, squamosals, postorbitals, quadratojugals, jugals, ectopterygoids, palatines, vomers, laterosphenoids, prootics, epipterygoids, stapedes, and quadrates) and seven unpaired (fused at midline—frontal, parietal, pterygoid, parabasisphenoid, basioccipital, otoccipital, and supraoccipital) (Fig. 1A–E). Of these elements, the only ones not preserved in the known specimens of *S. clarki* are the stapedes. The lower jaw, which we believe to be preserved in its entirety, is comprised of five paired elements (unfused, left and right, for a total of 10—articulars, surangulars, angulars, splenials, and dentaries) (Fig. 1A, C–E). The boundaries of each of the preserved skull and lower jaw elements, including the sutures separating contiguous elements, were delineated primarily by gross and light microscopic observation of external surfaces, but also by tracing their subsurface projections internally using high-resolution X-ray computed tomographic (HRXCT) scans. The prootics, having no external exposure, were visualized exclusively through HRXCT scans. Significantly, because of its rare preservation in fossil crocodylomorphs, a nearly complete element of the hyobranchial apparatus, the right first ceratobranchial, is preserved in the holotype specimen (UA 8679) of *S. clarki*.

In addition to these primary elements of the dermatocranium, chondrocranium, and splanchnocranium, there are four dermal ossifications associated with each side of the skull (preserved in their entirety only in the holotype specimen [UA 8679]). These consist of two palpebrals (one large anterior element and a much smaller posterior one; Fig. 1A, B, D), which, in life, would have been embedded in the fixed upper eyelids, and two small supratemporal ossifications (a small anterior element and a slightly smaller posterior one; Fig. 1A), which, in life, would have been embedded in the skin overlying each supratemporal fenestra.

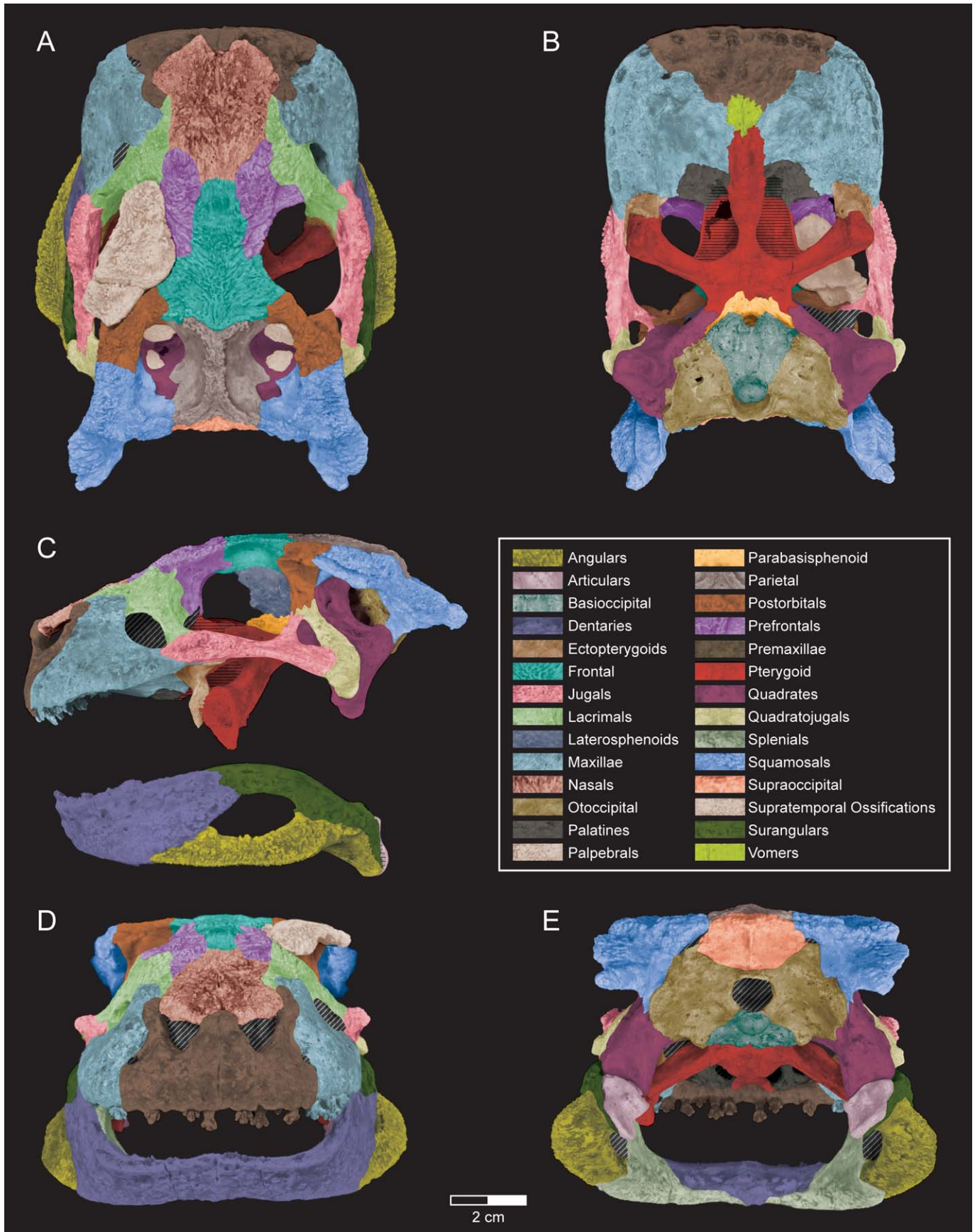
Dorsal View—In dorsal view (Fig. 2), the most notable feature of the skull of *Simosuchus clarki* is its remarkable brevity, a result of its greatly foreshortened snout. Indeed, the anteroposterior length of the rostrum is only slightly more than half its transverse

width, proportions that are unique among adult basal mesoeucrocodylians (though approached by *Comahuesuchus brachybucalis*). The rostrum is also considerably shorter than the remainder of the skull that follows posteriorly. In this view, it is subrectangular with an anterior margin that is essentially flat, parallel lateral margins, and rounded anterolateral corners. The length of the head skeleton along the dorsal midline is only slightly greater than its maximum width, in part a result of the bowed jugals, but especially because of the lateral flaring of the ventral margins of the angulars of the lower jaw. The external nares face anterolaterally and the very large orbits face dorsolaterally. However, each orbit is roofed dorsally by two substantial, articulating palpebrals—the anterior one being approximately four times larger than the posterior one—which effectively alter the orientation of the orbits such that they face almost directly laterally. Between the nares and orbits are relatively small, lenticular (in this view) antorbital fenestrae that face anterolaterally. The salient features of the posterior region of the skull as seen in dorsal view are the supratemporal fossae, each of which preserves two small supratemporal ossifications that, in life, helped to cover the subtrapezoidal supratemporal fenestrae, and the prominent posterior processes of the squamosals, which extend relatively far posterolaterally from the occipital surface of the skull.

With the exception of the lateral surface of the anterior process of the jugal, the external surfaces of the skull bones are much more heavily sculptured on the dorsal aspect of the skull than those that are visible anteriorly and laterally. Prominent sculpturing is also evident on the ventrolateral flanges of the angulars, which can be seen in this view because they extend further laterally than does the skull itself.

Ventral View—The ventral view of the skull (Fig. 3) reveals that the palatal processes of the maxillae are separated from one another along the midline by the anterior process of the pterygoid (posteriorly) and by the palatal processes of the vomers (anteriorly). Similarly, the internal narial fenestrae (choanae) are divided completely in the midline by the anterior process of the pterygoid. The palate is remarkably short and broad, with the premaxillae and maxillae forming the margins of the snout and bearing teeth that are foliform, multicusped, and arranged in anterior transverse and posterior longitudinal series. More posteriorly, the ventral surface of the skull is dominated by robust, anteroventrolaterally projecting transverse processes of the pterygoid that articulate anteriorly with the descending processes of the ectopterygoids. The midline of the posterior portion of the skull features a large median Eustachian foramen as well as a foramen magnum and occipital condyle that face posterovertrally. The anteroventrally sloping occipital region is bordered laterally on each side by the articular condyle of the quadrate and the tubercle of the quadratojugal and posterolaterally by the prominent posterior process of the squamosal.

Lateral View—The combination of brevity and height of the skull and lower jaw of *Simosuchus clarki* is best visualized in lateral view (Fig. 4). The snout, in addition to being anteroposteriorly short and dorsoventrally tall, is strongly downturned, a result of prominent ventroflexion about a transverse axis passing through the orbits. The antorbital fenestra is amygdaloid in shape and relatively small, much smaller than the external mandibular fenestra and especially the orbital fenestra; it is roughly comparable in size to the external narial fenestra. The orbits are essentially round, directed dorsolaterally (but almost directly laterally with the palpebrals in place), and very large, occupying more than one-quarter the total length of the skull (i.e., including the posterior processes of the squamosals), and nearly meeting in the midline (where they were likely largely or completely separated from one another by a cartilaginous interorbital septum). The transverse process of the pterygoid, coupled with the descending process of the ectopterygoid, extend ventrally to a level well below a line connecting the ventral margins of the premaxilla and



maxilla anteriorly and the ventral margins of the hemicondyles of the quadrate posteriorly. The craniomandibular joint is located well forward of the posterior end of the skull, lying anteroventral to the otic aperture and immediately ventral to the central plate of the quadratojugal. The posterior margin of the skull, in lateral view and with the head in what we refer to as a ‘neutral position’ (i.e., as if placed in articulation with the lower jaw on a horizontal surface), is oriented obliquely, bounded by the posterior descending process of the squamosal posterodorsally and the body of the quadrate anteroventrally. As a result of the oblique orientation of the posterior part of the skull, the occipital condyle and foramen magnum are directed posteroventrally rather than directly posteriorly. However, if the skull is oriented into the position that we infer to represent the habitual head posture of *S. clarki* (i.e., with the snout pitched downward at an angle of $\sim 45^\circ$; see ‘Habitual Head Posture’ [below]), the posterior margin of the skull, formed largely by the body of the quadrate, would be oriented more nearly vertically, the occipital condyle would be directed more posteriorly than ventrally, and the foramen magnum would face directly posteriorly.

The lower jaw is deepest in the region of the external mandibular fenestra, tapering anteroventrally along the alveolar process of the dentary and posteroventrally toward a robust, yet relatively short, retroarticular process formed by the articular, angular, and surangular. The dentary, like the premaxilla and maxilla, supports foliform, multicusped teeth. The large external mandibular fenestra is bordered anterodorsally by the dentary, dorsally and posterodorsally by the surangular, and ventrally and posteroventrally by the angular. The angular, which flares strongly laterally, is prominently sculptured along its external surface.

Anterior View—The anterior view of the skull (Fig. 5) is dominated by tall, dentigerous premaxillae that meet in the midline to form a dorsally peaked internarial bar, anterolaterally facing external nares, rounded lateral margins of the maxillae, laterally flaring jugals, and nearly flat, highly sculptured dorsal surfaces of the bones of the anterior portion of the dermal skull roof. The overall shape of the skull in this view is subrectangular except for the large orbits that scallop the lateral margins.

The ventrolateral flaring of the angulars is most obvious in this view; they render the lower jaw considerably wider than the skull itself. The dentaries each send a dorsoventrally shallow ramus medially from the anterolateral corners of the lower jaw to meet at the midline at the fused (but still very visible) mandibular symphysis.

Posterior View—The posterior region of the skull deviates less in relative size and shape from the typical crocodyliform pattern than does the anterior portion. The posterior view (Fig. 6) exhibits a nearly flat dorsal margin, laterally projecting posterior processes of the squamosals at the dorsolateral corners, and nearly vertically oriented quadrates laterally that articulate ventrally with the lower jaw. At the posterior midline is a prominent nuchal crest, a nearly circular foramen magnum (directed posteroventrally, but inferred to have been most typically held in a posteriorly facing orientation in life; see ‘Habitual Head Posture’ [below]), and a short, posteroventrally directed occipital condyle.

In posterior view, the lower jaw exhibits a prominent tubercle extending ventrally from the fused mandibular symphysis, rami that deepen slightly as they extend laterally, prominent flanges of the angular that extend ventrolaterally, and prominent ventromedial processes of the angular, surangular, and articular that join to form a retroarticular process lying ventral to the jaw joint.

Major Cranial Fenestrae, Foramina, and Fossae

External Narial Fenestrae—The external narial fenestrae (Figs. 2, 4, 5) are oriented anterolaterally, as in many basal mesoeucrocodylians, and are subtriangular in shape, their anteroventral corners being somewhat rounded. Each is bounded anteromedially by the dorsolateral margin of the dorsomedial process of the premaxilla, posterolaterally by a prominent anterodorsally facing crest on the dorsolateral process of the premaxilla, and dorsally by the anterolateral edge of the nasal. They measure ~ 17 mm in maximum width and ~ 8.7 mm in maximum height. In the floor of each external narial fenestra, where the dorsomedial and dorsolateral processes of the premaxilla converge toward one another, there is a shallow groove extending anterolaterally for a short distance onto the anterior lamina of the alveolar process of the premaxilla. The external narial fenestrae are well separated from one another by the broad, triangular internarial bar (‘septum’) formed by the dorsomedial processes of the premaxillae; as noted originally by Buckley et al. (2000), this condition is unique to *Simosuchus clarki* among crocodyliforms.

Perinarial Fossae—The perinarial fossae (Figs. 2, 4, 5) are approximately ovoid in shape and are positioned immediately lateral to the external narial fenestrae. Each is oriented such that its floor faces predominantly anteriorly, but also slightly dorsally and laterally as well. The medial half of each fossa is formed by a concavity along the anterolateral surface of the dorsolateral process of the premaxilla. The lateral half is formed by the anteromedially concave anterior margin of the ascending process of the maxilla. Extending along the long axes of these fossae are the dorsal portions of the premaxillomaxillary sutures. Straddling each of these sutures, just dorsal to the ventral margin of each fossa, is a prominent perinarial foramen, which lies directly dorsal to the ipsilateral anterior palatal foramen. The perinarial fossae are quite prominent, with each reaching a depth of several millimeters and measuring ~ 17 mm along its major axis and ~ 12 mm along its minor axis.

Although these fossae are almost certainly homologous with the perinarial fossae described previously in various other notosuchian taxa (e.g., *Mariliasuchus amarali* [see Zaher et al., 2006]), they might be more aptly thought of as ‘paranarial fossae’ in *Simosuchus clarki*, as radical structural reorganization—in particular, extreme widening—of the snout has effectively resulted in them being more laterally placed. Thus, the fossae are no longer restricted to the premaxillae, but rather each is formed jointly by the ipsilateral premaxilla and maxilla. This condition represents an autapomorphy of *Simosuchus*.

Internal Narial Fenestrae—The internal narial fenestrae (Fig. 3), or choanae (secondary choanae sensu Witmer, 1995), are relatively large in size, subtriangular in shape (bluntly rounded at their corners), and positioned directly adjacent to the more

← FIGURE 1. Bones of the skull and lower jaw of *Simosuchus clarki*, based on the holotype (UA 8679), in **A**, dorsal; **B**, ventral (lower jaw removed); **C**, reversed right lateral; **D**, anterior; and **E**, posterior views. The anterior and posterior palpebrals are shown in their articulated positions on the left side of the specimen only. See color key inset (right center) for identification of individual elements of the head skeleton and associated dermal ossifications. Foramina, fenestrae, canals, and cavities still filled with matrix, retained to ensure structural integrity, are shown with diagonal hatching. Areas of bones still partially obscured by residual matrix along their surfaces are shown with horizontal hatching. Note: neither the epipterygoids nor the stapedes are preserved in this specimen (nor would they have been visible in these views), and the prootics, although well preserved, are almost exclusively internal structures and therefore not visible in these external views.



FIGURE 2. Skull and lower jaw of the holotype (UA 8679) of *Simosuchus clarki* in dorsal view. **A**, photograph; **B**, interpretive drawing. The anterior and posterior palpebrals are shown in their articulated positions on the left side of the specimen only. See Appendix 1 for anatomical abbreviations.

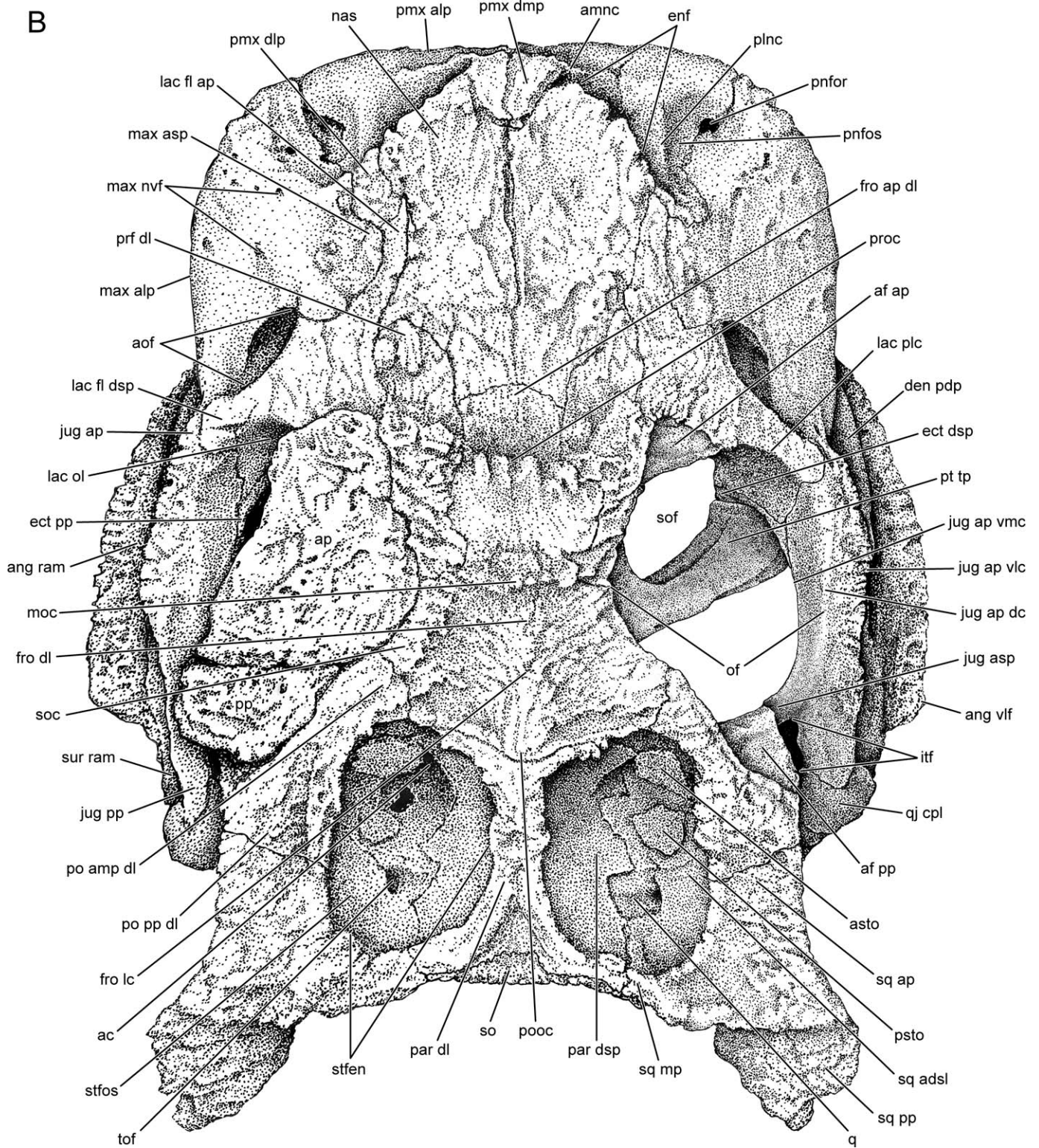


FIGURE 2. Continued.

laterally placed suborbital fenestrae, as is typical of nearly all crocodyliforms except derived neosuchians. They measure ~21 mm in maximum length (an estimate because portions of both palatines are broken away in UA 8679) and ~12 mm in

maximum width. The anterior, medial, and posterior borders of each fenestra are approximately coplanar, being formed by the posteromedial edge of the palatal process of the palatine, the lateral edge of the ventral lamina of the anterior process of the



FIGURE 3. Skull of the holotype (UA 8679) of *Simosuchus clarki* in ventral (palatal) view. **A**, photograph; **B**, interpretive drawing. The anterior and posterior palpebrals are shown in their articulated positions on both sides of the specimen. See Appendix 1 for anatomical abbreviations.

B

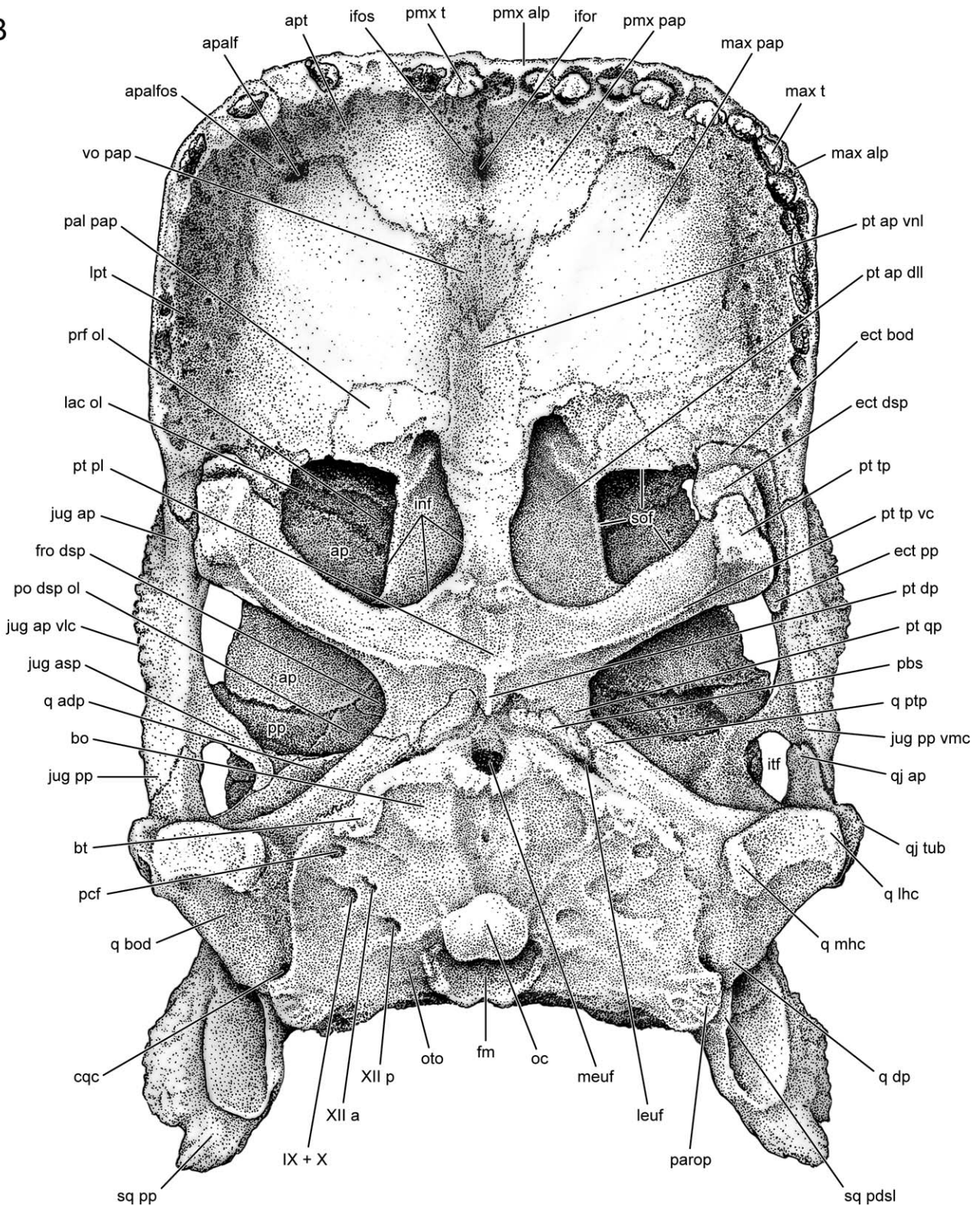


FIGURE 3. Continued.

pterygoid, and the anterior edge of the transverse process of the pterygoid, respectively. The lateral borders of the internal nares fenestrae are situated somewhat more dorsally, being formed by the ventrolateral edges of the dorsolateral laminae of the an-

terior process of the pterygoid, similar to the condition exhibited by *Uruguaysuchus aznarezi*. The internal nares are divided completely by a septum formed by the ventral and vertical laminae of the anterior process of the pterygoid. Similar internarial

A



FIGURE 4. Skull and lower jaw of the holotype (UA 8679) of *Simosuchus clarki* in reversed right lateral view. **A**, photograph; **B**, interpretive drawing. The skull and lower jaw are separated so that the latter does not obstruct ventrally projecting portions of the former. The anterior and posterior palpebrals are not shown. See Appendix 1 for anatomical abbreviations.

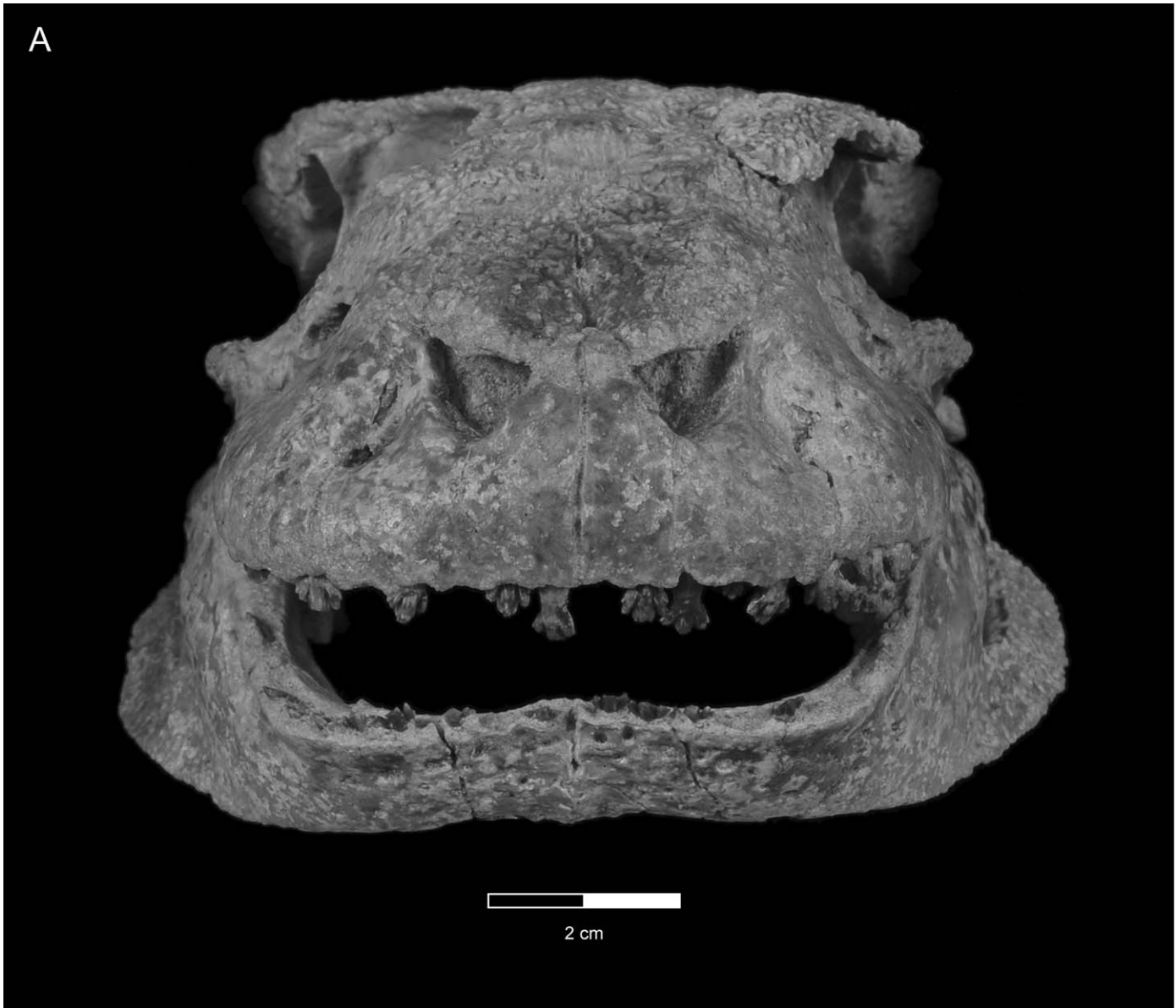


FIGURE 5. Skull and lower jaw of the holotype (UA 8679) of *Simosuchus clarki* in anterior view. **A**, photograph; **B**, interpretive drawing. The lower jaw is shown in a partially depressed position and the anterior and posterior palpebrals are shown in their articulated positions on the left side of the specimen only. See Appendix 1 for anatomical abbreviations.

(choanal) septa are present in *Araripesuchus*, *Uruguaysuchus*, peirosaurids, and various neosuchian taxa.

Incisive Fossa—The incisive fossa (Fig. 3) is a dome-shaped recess that projects dorsally from the center of the palatal portion of the interpremaxillary suture. It is relatively deep, extending more than 5 mm above the already-vaulted roof of the anterior-most portion of the bony palate (i.e., anterior palatal trough), and it is pierced at its dorsal apex by a prominent incisive foramen. The incisive fossa is formed entirely by the premaxillae; on each side, it is bounded anteriorly by the medial-most portion of the posterior lamina of the alveolar process, and laterally and posteriorly by the ventral lamina of the palatal process.

Antorbital Fenestrae—The antorbital fenestrae (Figs. 2, 4, 5) are moderate in size and approximately amygdaloid in shape,

their major axes slanting (from anterodorsal to posteroventral) at an angle of $\sim 60^\circ$ relative to the flat (antero)dorsal surface of the snout. Each lies directly anterior to the ventral half of the ipsilateral orbit and is bounded predominantly by the posterior margin of the ascending process of the maxilla anteroventrally and by the ventral margin of the facial lamina of the lacrimal posterodorsally. However, the anterior-most tip of the anterior process of the jugal also contributes slightly to the margin of the fenestra at its posteroventral corner. The left lacrimal of UA 8679 is partially broken, thereby slightly distorting the morphology of the left antorbital fenestra. However, the right antorbital fenestra in this specimen is undistorted and measures 17.3 mm along its major axis (i.e., about one-half the diameter of the orbital fenestra) and 8.7 mm across its minor axis (i.e., about one-quarter

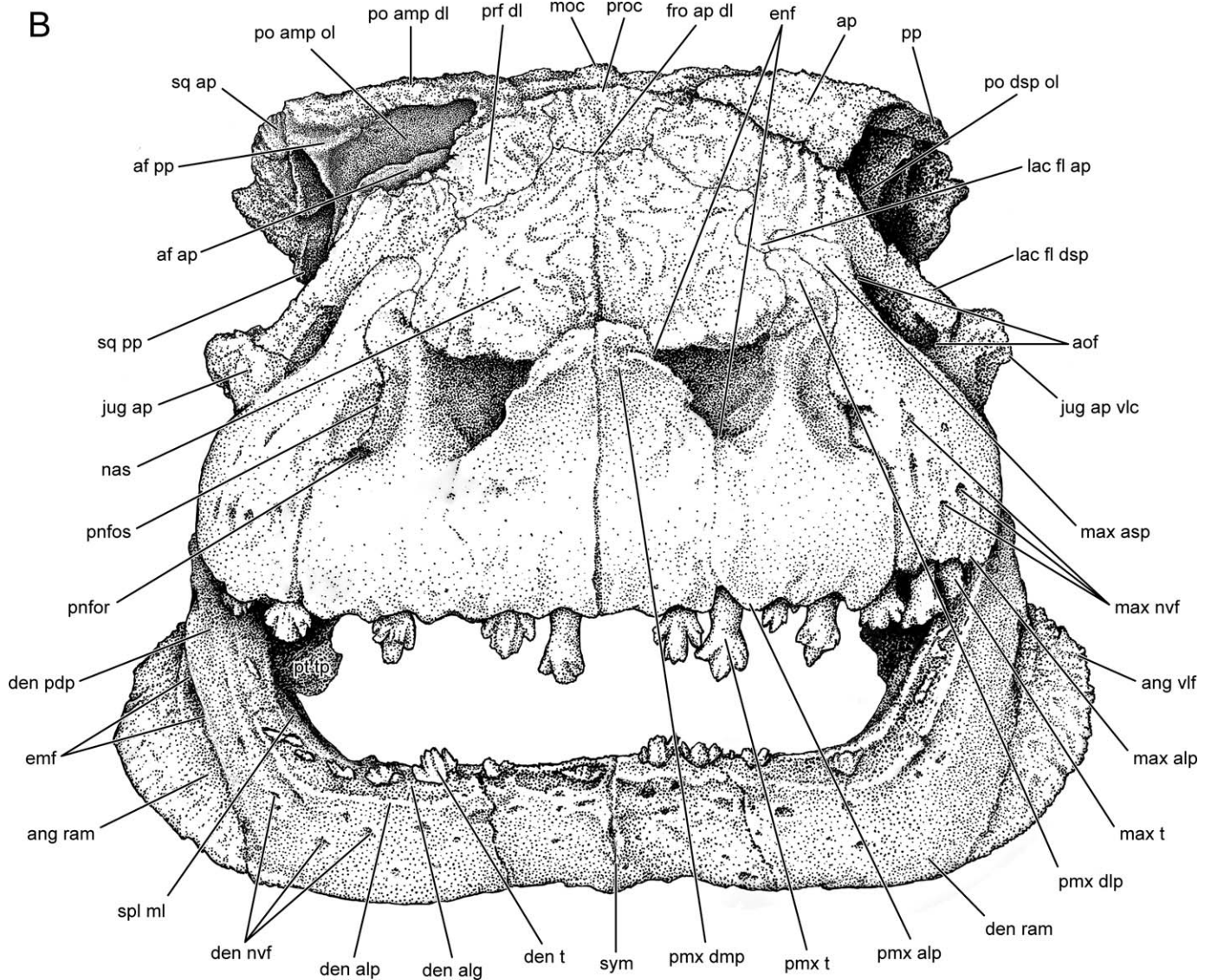


FIGURE 5. Continued.

the diameter of the orbital fenestra). The antorbital fenestrae are directed primarily laterally, although they do face very slightly dorsally and anteriorly as well.

The distinct amygdaloid shape of the antorbital fenestrae of *Simosuchus clarki*, with their acutely angled anterodorsal and posteroventral vertices, is unique among crocodyliforms. In addition, the anterodorsal-to-posteroventral orientation of the long axes of these fenestrae is unusual, having been described previously in relatively few other basal mesoeucrocodylians (e.g., *Montealtosuchus arrudacamposi* [see Carvalho et al., 2007]; *Sphagesaurus montealtensis* [see Andrade and Bertini, 2008a]).

Orbital Fenestrae—As in many basal mesoeucrocodylians, the orbital fenestrae (Figs. 2, 4) are oriented primarily laterally, but somewhat dorsally as well. They are nearly circular in shape and are by far the largest of the cranial openings in *Simosuchus*, having maximum diameters of ~35 mm. However, with the dorsally positioned anterior and posterior palpebrals in place, the effective orientation of the orbits is nearly entirely lateral, and their effective height is reduced by approximately one-third. Each or-

bitral fenestra is bordered dorsally by the lateral margin of the dorsal lamina of the frontal, posterodorsally by the anterolateral margin of the anteromedial process of the postorbital, posteriorly by the anterolateral margin of the descending process of the postorbital, posteroventrally by the anterior margin of the ascending process of the jugal, ventrally by the dorsal crest of the anterior process of the jugal, anteroventrally by the posterior margin of the descending process of the facial lamina of the lacrimal, and anterodorsally by the posterior margin of the dorsal lamina of the prefrontal.

Suborbital Fenestrae—The suborbital fenestrae (Fig. 3) (palatal fenestrae sensu Iordansky, 1973) lie immediately lateral to the internal narial fenestrae and directly ventral to the anterior halves of the orbits. They are roughly kite-shaped in palatal view, with their major axes oriented at an angle of ~25° relative to the longitudinal axis of the skull. They measure ~17 mm along their major axes and ~14 mm across their minor axes. Each suborbital fenestra is bounded anteromedially by the posterior edge of the palatal process of the palatine, medially by the ventrolateral edge of the dorsolateral lamina of the anterior process of

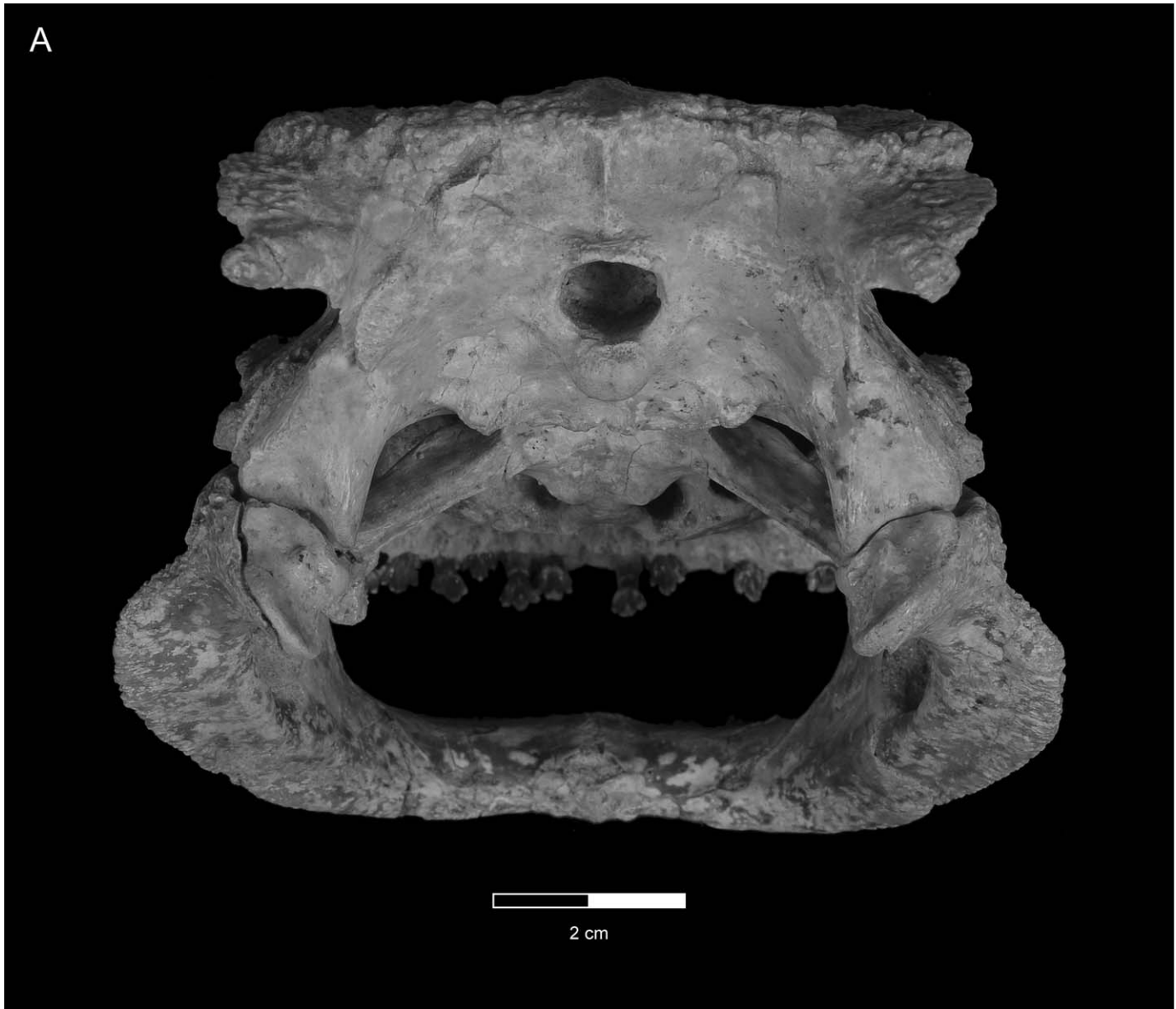


FIGURE 6. Skull and lower jaw of the holotype (UA 8679) of *Simosuchus clarki* in posterior view. **A**, photograph; **B**, interpretive drawing. The lower jaw is shown in a partially depressed position. See Appendix 1 for anatomical abbreviations.

the pterygoid, posterolaterally by the anteromedial edge of the transverse process of the pterygoid, laterally by the medial edge of the descending process of the ectopterygoid, and anterolaterally by the central portion of the posterior edge of the palatal process of the maxilla.

Otic Apertures—The otic apertures (Fig. 4) are subelliptical in shape, measuring ~14 mm along their long axes in UA 8679. Each aperture is formed in large part by the semilunar otic incisure of the quadrate; this forms the anterodorsal, anterior, anteroventral, ventral, and posteroventral margins of the aperture. The remainder of the aperture is formed by the anteroventrally concave anterior margin of the posterior descending lamina of the squamosal.

Supratemporal Fenestrae—The supratemporal fenestrae (Fig. 2) are relatively large, measuring ~28 mm in maximum length and ~20 mm in maximum width. They are subtrapezoidal in shape (their corners slightly rounded), with both their lateral

and medial margins oriented approximately parallel to the longitudinal axis of the skull. The longer lateral margin of each fenestra, which is formed anteriorly by the dorsomedial edge of the posterior process of the postorbital and posteriorly by the dorsomedial edge of the anterior process of the squamosal, lies slightly ventral to the shorter medial margin, which is formed entirely by the central portion of the lateral edge of the dorsal lamina of the parietal. Thus, the anterior margin of each supratemporal fenestra angles not only anterolaterally, but also slightly ventrally. Similarly, the posterior margin angles not only posterolaterally, but slightly ventrally as well. The anterior margin of each fenestra is formed medially by the anterior-most part of the dorsolateral edge of the parietal, centrally by the lateral portion of the posterior edge of the dorsal lamina of the frontal, and laterally by the posterodorsal edge of the anteromedial process of the postorbital. The posterior margin is formed medially by the posterior portion of the dorsolateral edge of the

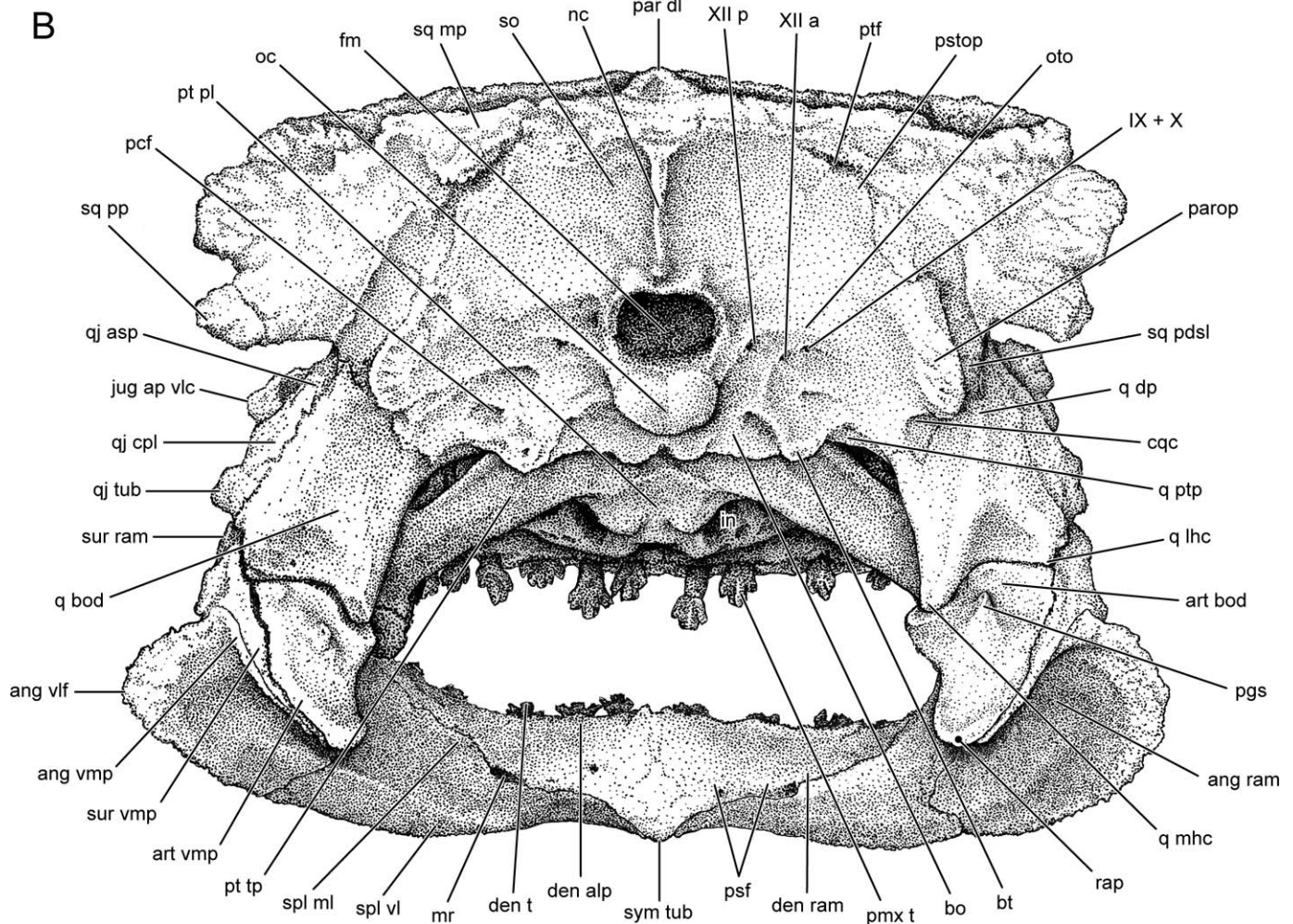


FIGURE 6. Continued.

parietal and laterally by the anterodorsal edge of the medial process of the squamosal.

Supratemporal Fossae—The supratemporal fossae (Fig. 2) extend ventrally from the margins of the supratemporal fenestrae. The medial wall of each fossa is formed entirely by the parietal, dorsally by the lateral surface of its dorsal lamina, and ventrally by the lateral surface of the ipsilateral descending process. The anterior wall is formed medially by the dorsolateral surface of the anterior portion of the descending process of the parietal and laterally by the posteromedial surface of the anteromedial process of the postorbital. Immediately dorsomedial to the postorbitoparietal suture, the posterior surface of the dorsal lamina of the frontal also contributes slightly to the anterior wall of the fossa. The lateral wall of each fossa is formed anteriorly by the medial surface of the posterior process of the postorbital and posteriorly by the medial surface of the anterior process of the squamosal. Finally, the posterior wall is formed laterally by the anterodorsal surface of the medial process of the squamosal and medially by the dorsolateral surface of the posterior portion of the descending process of the parietal. In the lower portion of this posterior part of the supratemporal fossa, immediately ventral to the parietosquamosal suture, there is a prominent diamond-shaped gap, formed anteromedially by a triangular emargination along the posterolateral margin of the descending process of the

parietal, and posterolaterally by the nearly right-angled intersection between the medial and anterior processes of the squamosal. Projecting into the medial three-quarters of this gap is the dorso-medial tip of the quadrate. Immediately lateral to this is a prominent temporo-orbital foramen.

Positioned within each supratemporal fossa are two supratemporal ossifications, one anterior and one posterior. The morphology of these ossifications, which are interpreted as osteoderms that were positioned horizontally directly above the supratemporal fossae in life, is described below.

Infratemporal Fenestrae—The infratemporal fenestrae (Figs. 2–4) are subtriangular in shape in lateral view, their three corners being somewhat rounded. Each is bounded predominantly by the posterior margin of the ascending process of the jugal anteriorly, the anteroventral margin of the ascending process of the quadratojugal posterodorsally, and the dorsal margin of the posterior process of the jugal ventrally. However, the dorsal edge of the proximal part of the anterior process of the quadratojugal contributes slightly to the posterior-most part of the ventral margin of the fenestra. In contrast to the condition exhibited by most mesoeucrocodylians, the postorbital does not contribute to the margins of the infratemporal fenestra in *Simosuchus clarki*. The infratemporal fenestrae are very small in size, measuring ~7 mm in width across their bases, and are oriented

such that they face primarily laterally, but somewhat dorsally as well.

The extraordinarily small relative size of the infratemporal fenestra in *S. clarki*—approximately one-fifth the diameter of the orbital fenestra—is unique among basal mesoecrocodylians. Within Notosuchia, this condition is most closely approximated by *Anatosuchus minor*; however, even in this taxon, the antero-posterior length of the infratemporal fenestra is more than one-third the diameter of the orbital fenestra (Sereno and Larsson, 2009:table 3).

Posttemporal Fenestrae—The posttemporal fenestrae (Fig. 6) exist as narrow, slit-like grooves between the temporal and occipital portions of the skull. Specifically, each is centered where the supraoccipital-otoccipital suture intersects with the posterior surface of the medial process of the squamosal. The posttemporal fenestrae are angled strongly from dorsomedial to ventrolateral and measure ~8.5 mm along their long axes, but only 1–2 mm across their minor axes.

Foramen Magnum—The foramen magnum (Figs. 3, 6) is oriented posteroventrally (but see ‘Conventions Adopted Regarding Directional Anatomical Nomenclature’ [above] and ‘Habitual Head Posture’ [below]) and is nearly circular in shape, having a maximum width of 10.8 mm and a maximum height of 9.3 mm. It is bordered ventrally by the posterodorsal margin of the basioccipital, whereas the remainder of its circumference is formed entirely by the central margins of the otoccipital; as in other mesoecrocodylians, the supraoccipital is excluded from the foramen magnum by a narrow bridge of bone connecting the left and right halves of the otoccipital. From this narrow portion of the otoccipital, a well-developed crest projects posteroventrally to overhang the dorsal margin of the foramen magnum.

External Mandibular Fenestrae—The external mandibular fenestrae (Figs. 4, 5) are relatively large and roughly amygdaloid in shape. They are bordered ventrally by the dorsolateral margin of the angular, anterodorsally by the posteroventral margin of the posterodorsal process of the dentary, and posterodorsally by the ventrolateral margin of the surangular ramus. Each is angled slightly (from anteroventral to posterodorsal) such that its long axis is tilted ~10° relative to the horizontally oriented ventral margin of the angular. The external mandibular fenestrae measure ~23 mm along their major axes and ~11 mm across their minor axes.

Mandibular Adductor Fossae—The mandibular adductor fossae are relatively large, having accommodated a considerable volumetric proportion of the M. adductor mandibulae complex. Each is bounded dorsally by the dorsomedial margin of the surangular ramus, anteriorly by the posterior margin of the medial lamina of the splenial, and ventrally by the elevated dorsomedial margin of the angular ramus. The posterior boundary of the fossa is less well defined, but corresponds approximately to a transverse plane passing vertically through the posterior apex of the external mandibular fenestra and the anterior terminus of the anterior process of the articular. From the slightly curved surface described by these boundaries, the fossa extends laterally to a similarly curved surface described by the boundaries of the external mandibular fenestra.

Bones of the Dermatocranium

Premaxillae—The paired premaxillae (Figs. 1A–E, 2–5) are extraordinarily well preserved and complete in the holotype (UA 8679) of *Simosuchus clarki*, but badly damaged in both FMNH PR 2596 and FMNH PR 2597. They are very broad and form nearly the entire anterior surface of the snout, as well as the anterior-most part of the central portion of the bony palate. They also form the anteromedial, anteroventral, and posterolateral margins of the anterolaterally directed external narial fenestrae. Each premaxilla bears four distinct processes: an alveolar

process, a palatal process, a dorsomedial process, and a dorsolateral process.

Uniquely among crocodylomorphs, the ventrally directed alveolar process of the premaxilla is oriented transversely and restricted entirely to the anterior surface of the rostrum in *Simosuchus clarki*. It consists of two nearly parallel laminae of bone, one anterior (labial) and one posterior (lingual) (Fig. 7A–E). Positioned between these two laminae are five alveoli to accommodate the premaxillary teeth (Fig. 8E, F). These alveoli are complete only dorsally, however; ventrally, the mesial (medial) and distal (lateral) walls of the alveoli are lost, and thus the lower portions of the roots of the premaxillary teeth are contained within a common alveolar groove, which is only partially subdivided by moderately developed interdental ridges that project into the groove from both the posterior surface of the anterior lamina and the anterior surface of the posterior lamina. This arrangement is unique to *Simosuchus* among crocodylomorphs. Due to the great height of the roots of the premaxillary teeth, the alveolar process is extraordinarily tall, extending dorsally to a level approaching that of the ventral margin of the external narial fenestra (Fig. 7C); this prodigious dorsoventral expansion of the alveolar process of the premaxilla represents an autapomorphy of *Simosuchus clarki*.

The external surface of the anterior lamina of the alveolar process consists entirely of smooth, unsculptured bone. It is anteriorly convex in both lateral and dorsal views, but only very slightly so; thus, these subtle convexities do not contribute significantly to the overall shape of the snout, which appears subrectangular (with slightly rounded corners) in dorsal and ventral views and essentially flat in lateral view (Figs. 2–4). In anterior view, the ventral margin of the anterior lamina of the alveolar process is heavily scalloped, with a prominent semilunar emargination associated with each individual tooth (Fig. 5). The ventral margin of the posterior lamina of the alveolar process is also scalloped in appearance, but in a rather different way. No prominent, dorsally directed emarginations are seen in posterior view as they are in anterior view, but heavy, anteriorly directed scalloping is clearly evident in ventral view (Fig. 3). This is due to the fact that, in contrast to the condition seen along the anterior lamina, where the bone adjacent to each interdental ridge is thickened, the opposite occurs along the posterior lamina, with the bone adjacent to each interdental ridge becoming thinner than the bone directly posterior to the teeth themselves. Thus, the posterior lamina of the alveolar process more closely follows the tubular shapes of the roots of the premaxillary teeth than does the anterior lamina. The distinct scalloping present along the free margins of both the anterior and posterior laminae of the alveolar process of the premaxilla is unique to *Simosuchus* among basal mesoecrocodylians.

The alveolar process extends the entire width of the premaxilla (Figs. 3, 5). At the anterior midline, the medial edge of the alveolar process contacts that of the contralateral premaxilla in a relatively straight and vertically oriented interpremaxillary suture. At its lateral end, the alveolar process of the premaxilla meets the anteromedial edge of the alveolar process of the maxilla in a similarly straight and nearly vertical premaxillomaxillary suture.

Extending posteriorly from the alveolar process is the palatal process of the premaxilla (Fig. 3). It consists of distinct dorsal and ventral laminae, with the latter being significantly thicker than the former. Intervening between these two laminae is a pneumatized space containing numerous bony trabeculae (Figs. 7B, C, 8F, 9A). The palatal process is relatively small in size, forming well less than one-quarter of the total area of the ipsilateral half of the bony palate, but is somewhat complex in its overall shape (Fig. 3). Its medial edge is relatively straight, contacting that of its contralateral partner at the palatal midline, thereby forming the ventral-most portion of the interpremaxillary suture. However, its lateral edge is angled from anterolateral to posteromedial.

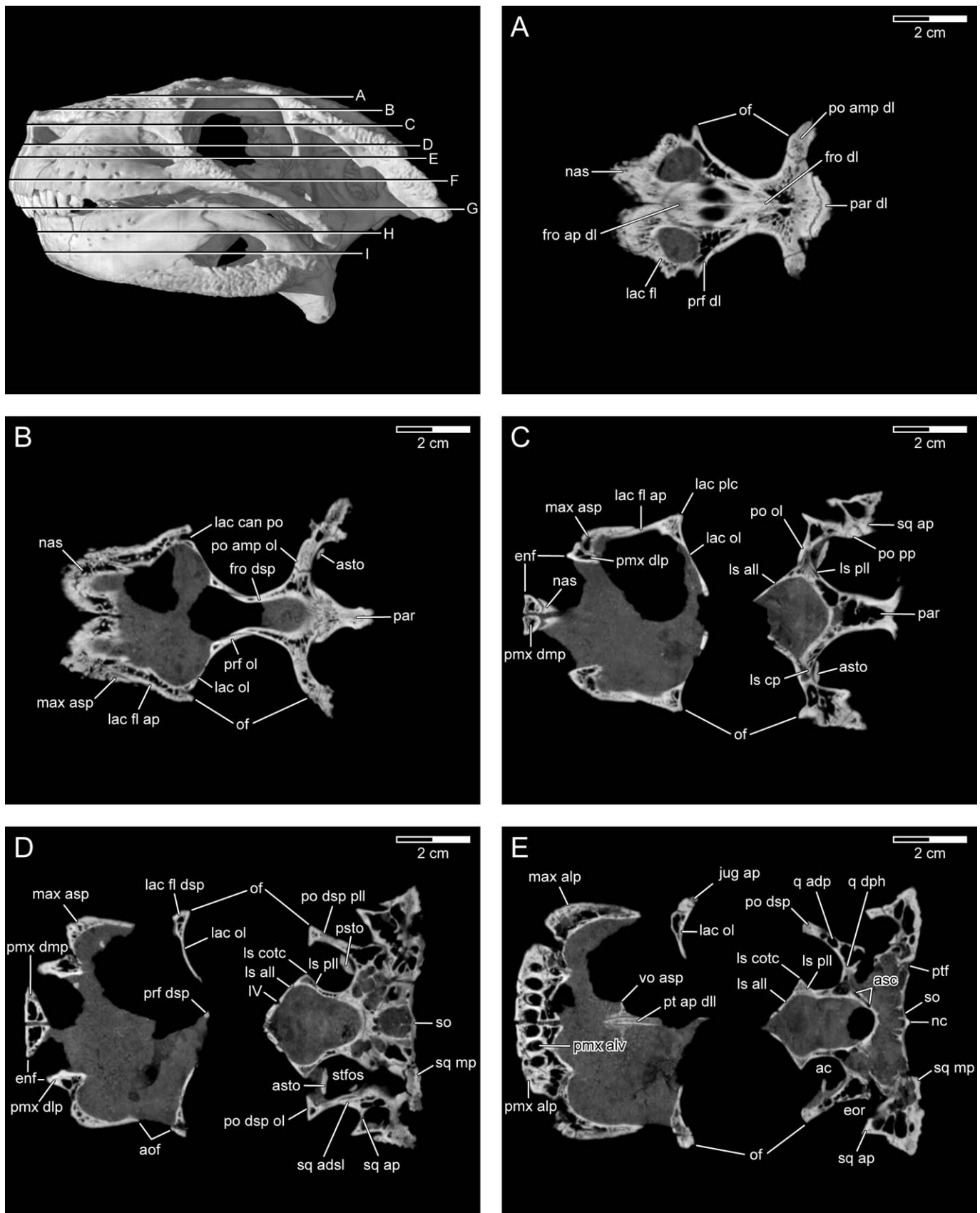


FIGURE 8. Serial frontal (horizontal) slices through the skull and lower jaw of the holotype (UA 8679) of *Simosuchus clarki* obtained via HRXCT scanning. The position of each frontal slice (A–I) along the vertical axis of the skull is indicated on the three-dimensional HRXCT reconstruction in the upper left panel. **A**, Fro 56; **B**, Fro 85; **C**, Fro 125; **D**, Fro 170; **E**, Fro 200; **F**, Fro 252; **G**, Fro 330; **H**, Fro 389; **I**, Fro 444. (Individual slices numbered according to their respective positions along a dorsoventral axis passing through the horizontally resliced HRXCT data set, which consisted of 623 total slices.) See Appendix 1 for anatomical abbreviations.

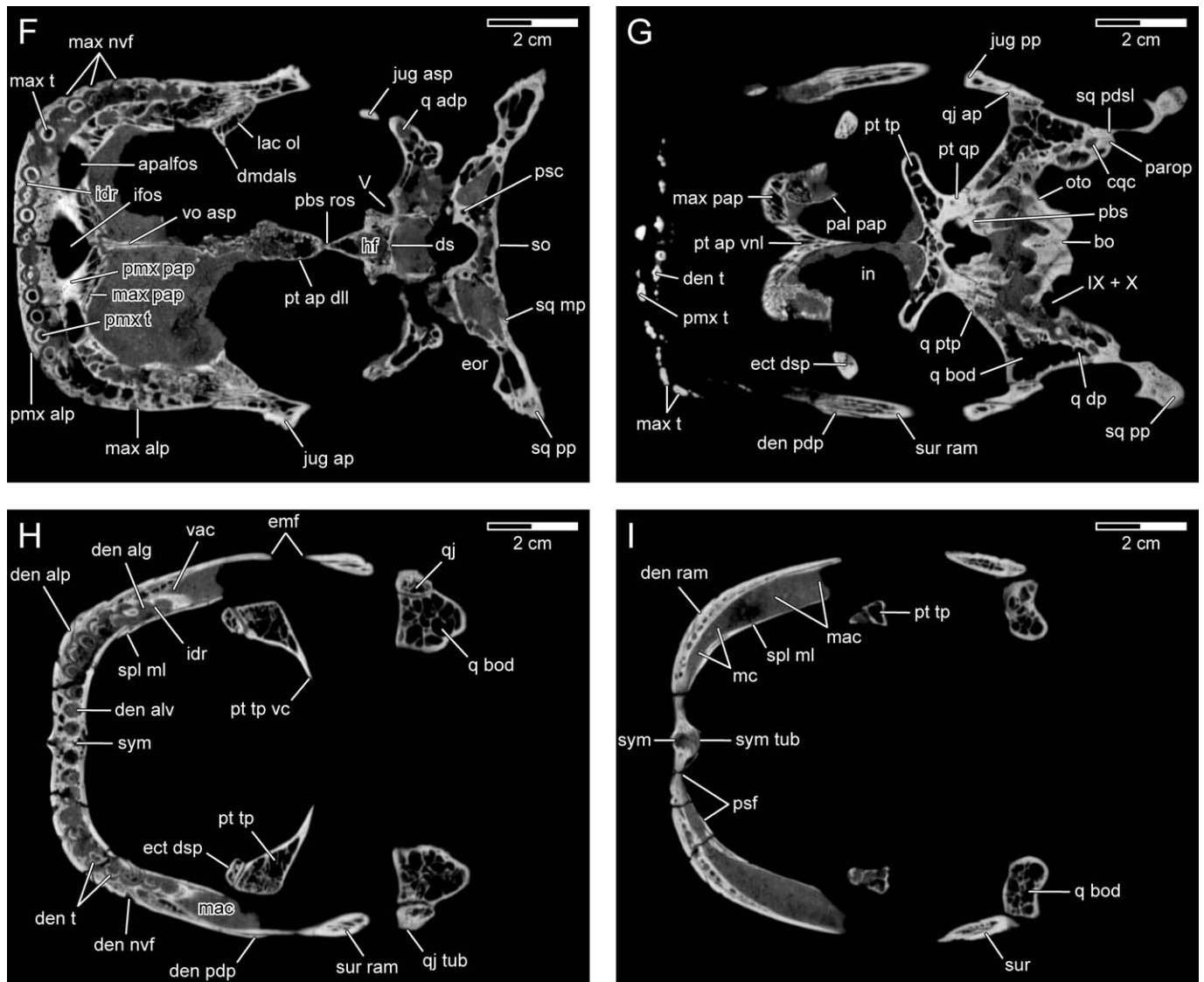


FIGURE 8. Continued.

addition, in the center of the roof of this trough is an even deeper fossa straddling the interpremaxillary suture; this is the incisive fossa, which contains at its apex a prominent incisive foramen (Figs. 3, 7A, 8F). The well-developed anterior palatal trough of *Simosuchus clarki* represents an autapomorphy of this taxon. In contrast, however, the position of the incisive foramen—directly abutting the alveolar process of the premaxilla—resembles that seen in numerous other notosuchians (e.g., *Marilia-suchus*, *Chimaerasuchus*, *Sphagesaurus huenei*, *Hamadasuchus*, *Montealtosuchus*).

The dorsomedial process (internarial process sensu Iordansky, 1973; ascending process sensu Buckley et al., 2000) of the premaxilla consists of distinct anterior, posterolateral, and medial laminae (Figs. 7B, 8C, D). The anterior lamina of the dorsomedial process essentially represents a continuation of that of the alveolar process, extending dorsally and slightly anteriorly from the medial half of the latter. It tapers gradually toward the midline as it extends dorsally, thus giving it the approximate shape

of a right triangle in anterior view, with the hypotenuse of the triangle forming the anteromedial margin of the external narial fenestra (Fig. 5). However, the dorsal angle of this triangle is squared off slightly because the dorsomedial process terminates rather abruptly once it rises slightly above the dorsal surface of the posterolaterally adjacent nasal. The posterolateral lamina of the dorsomedial process represents a continuation of the anterior portion of the dorsal lamina of the palatal process. It curves anteriorly and dorsally to meet the anterior lamina of the dorsomedial process. Where the two laminae intersect laterally, they form a sharp crest along the anteromedial margin of the external narial fenestra (Figs. 2, 4). Finally, the medial lamina of the dorsomedial process runs between the medial ends of the anterior and posterolateral laminae, thereby connecting the two. It is vertically oriented and perfectly flat. The medial laminae of the left and right premaxillae directly abut one another at the midline. Intervening between the anterior, posterolateral, and medial laminae is a pneumatized space containing numerous bony

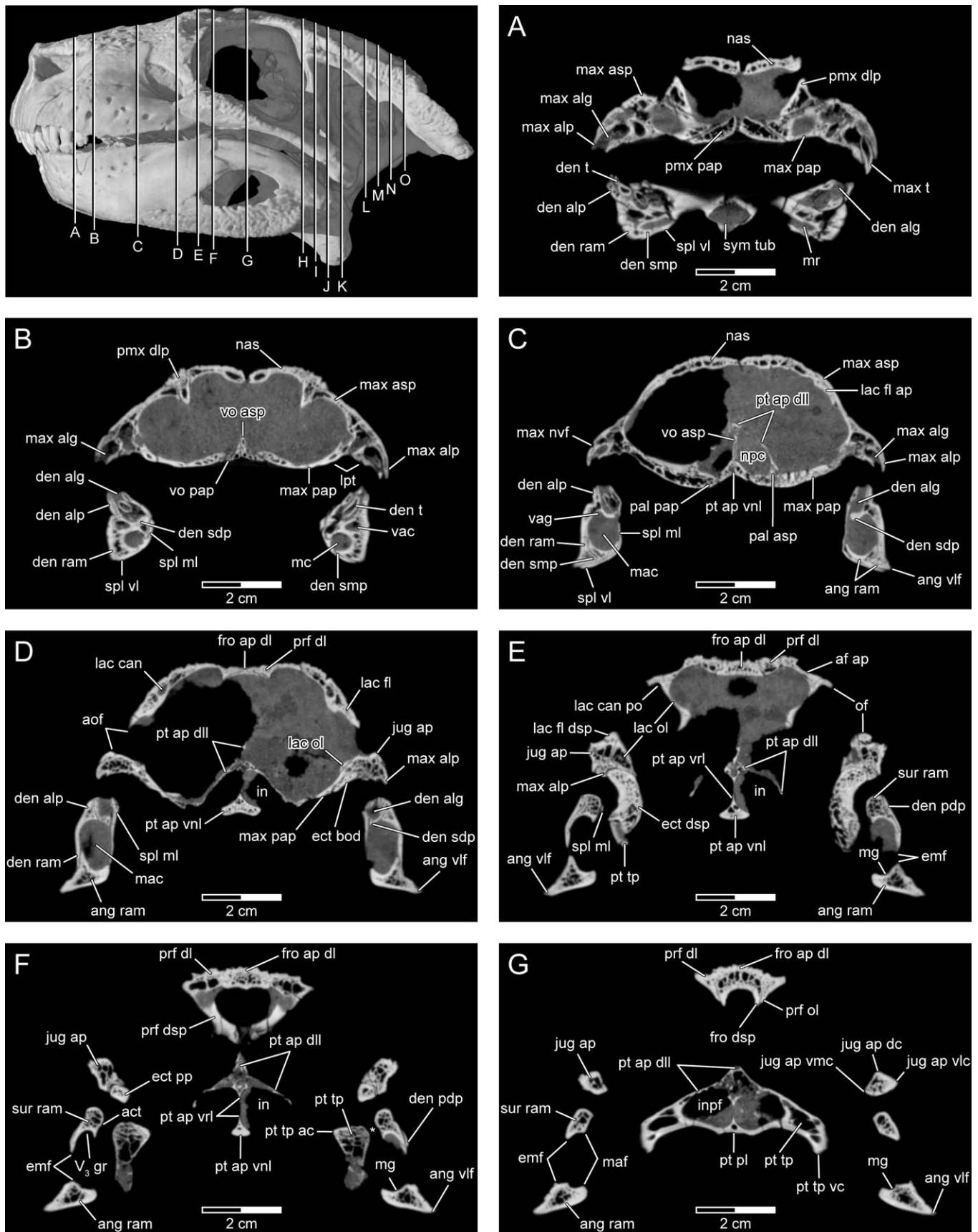


FIGURE 9. Serial transverse slices through the skull and lower jaw of the holotype (UA 8679) of *Simosuchus clarki* obtained via HRXCT scanning. The position of each transverse slice (A–O) along the longitudinal axis of the skull is indicated on the three-dimensional HRXCT reconstruction in the upper left panel. **A**, Tra 137; **B**, Tra 177; **C**, Tra 268; **D**, Tra 352; **E**, Tra 396; **F**, Tra 428; **G**, Tra 499; **H**, Tra 616; **I**, Tra 643; **J**, Tra 669; **K**, Tra 698; **L**, Tra 748; **M**, Tra 774; **N**, Tra 800; **O**, Tra 830. (Individual slices numbered according to their respective positions along an anteroposterior axis passing through the original transversely sliced HRXCT data set, which consisted of 999 total slices.) The asterisk in **F** represents the inferred position of the cartilage transiliens. See Appendix 1 for anatomical abbreviations.

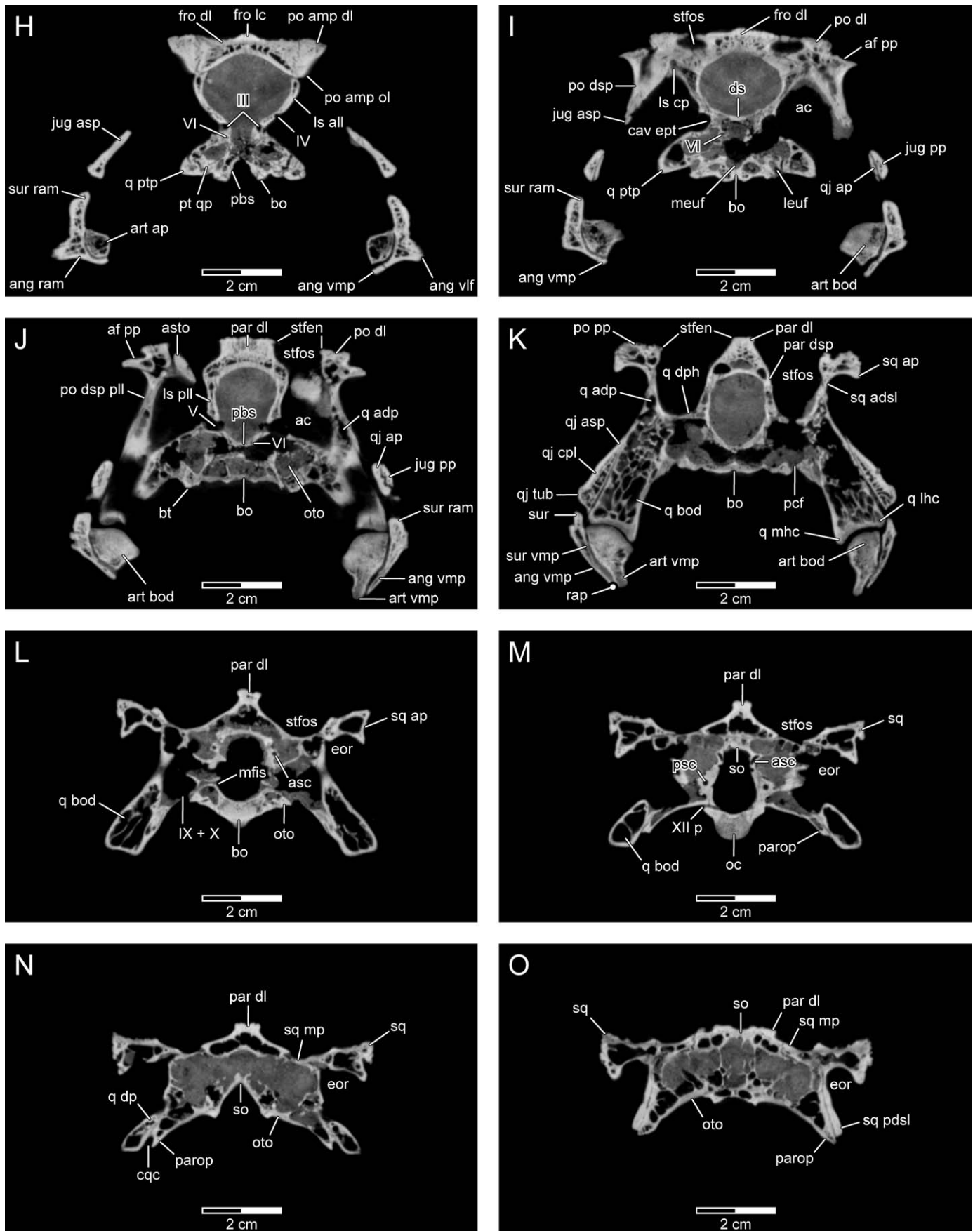


FIGURE 9. Continued.

trabeculae (Figs. 7B, 8C, D). This space is continuous with that which lies between the dorsal and ventral laminae of the palatal process.

Viewed from above, the slightly flattened dorsal terminus of the dorsomedial process is fully exposed and has the shape of a right triangle, with its hypotenuse angled posteromedially toward the midline (Fig. 2). This fits into a complementarily shaped emargination of the anteromedial corner of the nasal. Thus, the dorsomedial processes of the premaxillae separate the anterior-most tips of the nasals from one another (Figs. 2, 5, 8C, 10). These conditions represent autapomorphies of *Simosuchus clarki*.

Extending posteriorly, dorsally, and very slightly laterally from the lateral half of the alveolar process is the dorsolateral process (posterior process sensu Mook, 1921b; ascending process sensu Iordansky, 1973; posterolateral process sensu Turner, 2006; posterodorsal process sensu Pol and Apesteguía, 2005, and Zaher et al., 2006) of the premaxilla (Figs. 2, 4, 5, 11). At its dorsal-most extent, it articulates posterolaterally with the anterodorsal edge of the ascending process of the maxilla, posteromedially with the lateral edge of the nasal, and directly posteriorly with the anterior-most tip of the anterior process of the facial lamina of the lacrimal (Figs. 2, 4, 5). Further ventrally, it establishes a relatively broad lateral contact with the anteromedial edge of the ascending process of the maxilla. In dorsal view, the dorsolateral process can be seen to be strongly triangular in frontal section, with its anterodorsally directed apex forming a prominent crest along the posterolateral margin of the external narial fenestra, thereby mirroring the well-developed anteromedial narial crest formed at the junction of the anterior and posterolateral laminae of the dorsomedial process (Fig. 2). Lateral to this crest, the dorsolateral process is distinctly concave anterolaterally. This concavity extends laterally to the level of the premaxillomaxillary suture and forms the medial half of a relatively large perinarial fossa, which contains a prominent foramen just dorsal to its ventral margin (i.e., where the dorsolateral and alveolar processes of the premaxilla meet) (Figs. 2, 4, 5, 11). Given that this foramen is centered on the premaxillomaxillary suture, it is likely homologous to those foramina straddling this same suture in most other notosuchian taxa; thus, it is likely not homologous to those foramina present within the smaller perinarial fossae of *Marilyasuchus*, *Notosuchus*, *Baurusuchus*, *Mahajangasuchus*, and *Hamadasuchus*. Like the palatal and dorsomedial processes, the dorsolateral process of the premaxilla is heavily pneumatized and contains numerous bony trabeculae (Figs. 7D, 8C, D, 9A, B).

The contact between the dorsolateral process of the premaxilla and the anterior process of the facial lamina of the lacrimal is unique to *Simosuchus clarki* among crocodylomorphs. This character state is clearly correlated with the great reduction in the length of the rostrum in *Simosuchus*.

Maxillae—The maxillae (Figs. 1A–E, 2–5) form nearly the entire lateral surface of the snout, as well as a large portion of the bony palate. Each bears three distinct processes: an alveolar process, a palatal process, and an ascending process.

The ventrally directed alveolar process of the maxilla consists of two nearly parallel laminae of bone, one lateral (labial) and one medial (lingual) (Figs. 8E, F, 9A–C). Contained between these two laminae are 11 alveoli to accommodate the maxillary teeth. Like those in the premaxilla, the alveoli within the maxilla are complete only dorsally; ventrally, their mesial and distal walls are lost. Consequently, the lower portions of the roots of the maxillary teeth, like those of the premaxillary teeth, are contained together within a common alveolar groove (Fig. 9A–C). This groove is partially subdivided by interdental ridges, but these ridges are relatively weakly developed, especially throughout the posterior portion of the groove, where they are almost completely absent from the lateral surface of the medial lamina of the process (Fig. 8F). The alveolar groove is shallowest posteriorly, reflecting the relative shortness of the roots of the posterior maxillary teeth; anteriorly, it is significantly deeper

to accommodate the much taller roots of the anterior-most maxillary teeth (Fig. 12).

As in all other non-baurusuchid ziphosuchians (sensu Turner and Sertich, this volume), the external surface of the alveolar process of the maxilla consists of smooth, unsculptured bone (Figs. 2, 4, 5, 11). However, it is perforated by numerous neurovascular foramina, which are particularly abundant anteriorly. It is laterally convex in both dorsal and anterior views (Figs. 2, 5). These convexities, although slightly greater in magnitude than those seen along the alveolar process of the premaxilla, are nevertheless relatively subtle, and serve in general only to gently round the margins of the otherwise blunt and nearly rectangular snout. In anterolateral view (Fig. 11), the ventral margin of the lateral lamina of the alveolar process can be seen to be distinctly scalloped, in a manner similar to that described above for the anterior lamina of the alveolar process of the premaxilla. (And as for that seen along the latter, this scalloping of the alveolar process of the maxilla represents an autapomorphic character state for *Simosuchus clarki*.) However, this scalloping is associated only with the anterior seven maxillary teeth; posterior to the seventh alveolus, the ventrolateral margin of the maxilla is nearly straight (Fig. 4). There are no significant thickenings of the medial lamina of the alveolar process adjacent to the lingual sides of the maxillary teeth, and thus no scalloping is seen in ventral view, as it is along the posterior lamina of the premaxillary alveolar process (Fig. 3).

Anteromedially, the alveolar process of the maxilla broadly contacts the alveolar process of the ipsilateral premaxilla, thereby establishing the anterior-most portion of the premaxillomaxillary suture (Figs. 2–5, 11). Posteriorly, it tapers abruptly behind the 11th alveolus to terminate in a narrow, posteriorly directed projection that is embraced between the ventromedial edge of the anterior terminus of the anterior process of the jugal, the ventrolateral edge of the ventral portion of the descending process of the lacrimal, and the dorsolateral edge of the anterior portion of the posterior process of the ectopterygoid (Fig. 9E). Along most of its length, the alveolar process of the maxilla is oriented nearly parallel to the longitudinal axis of the skull. At its anterior end, however, it curves medially toward the lateral border of the alveolar process of the premaxilla (Figs. 2–5). Consequently, the major axes of the two anterior-most maxillary tooth crowns are oriented more or less transversely, whereas the more posteriorly positioned tooth crowns are oriented nearly longitudinally.

Extending medially from the alveolar process is the palatal process of the maxilla. It is significantly larger than the palatal process of the premaxilla, forming most of the bony palate (Fig. 3). It exhibits a prominent anterolaterally oriented ventral convexity—most pronounced posteromedially and somewhat less distinct anterolaterally—which is not known to be present in any other crocodylomorph. The palatal process of the maxilla, like that of the premaxilla, exhibits distinct dorsal and ventral laminae and, also as in the premaxilla, the intervening space is pneumatized, although to a somewhat lesser degree; this pneumatization is most extensive posteromedially (Figs. 7C–E, 8F, G, 9A–C).

The palatal processes of the left and right maxillae do not meet at the ventral midline; rather, they are separated by other bones along their entire lengths (Fig. 3). Anteriorly, their medial edges terminate dorsal to the lateral two-thirds of the palatal processes of the premaxillae (Fig. 9A). Near the anteroposterior center of the bony palate, they are separated by the palatal processes of the vomers, which they dorsally overlap anteriorly (Fig. 9B) and laterally abut posteriorly. Posteriorly, the medial margins of the palatal processes terminate by abutting the ventrolateral edges of the ventral lamina of the anterior process of the pterygoid (Figs. 8G, 9C). As noted originally by Buckley et al. (2000), the lack of contact between the palatal processes of the left and right maxillae in *Simosuchus* represents a unique condition among crocodyliforms.

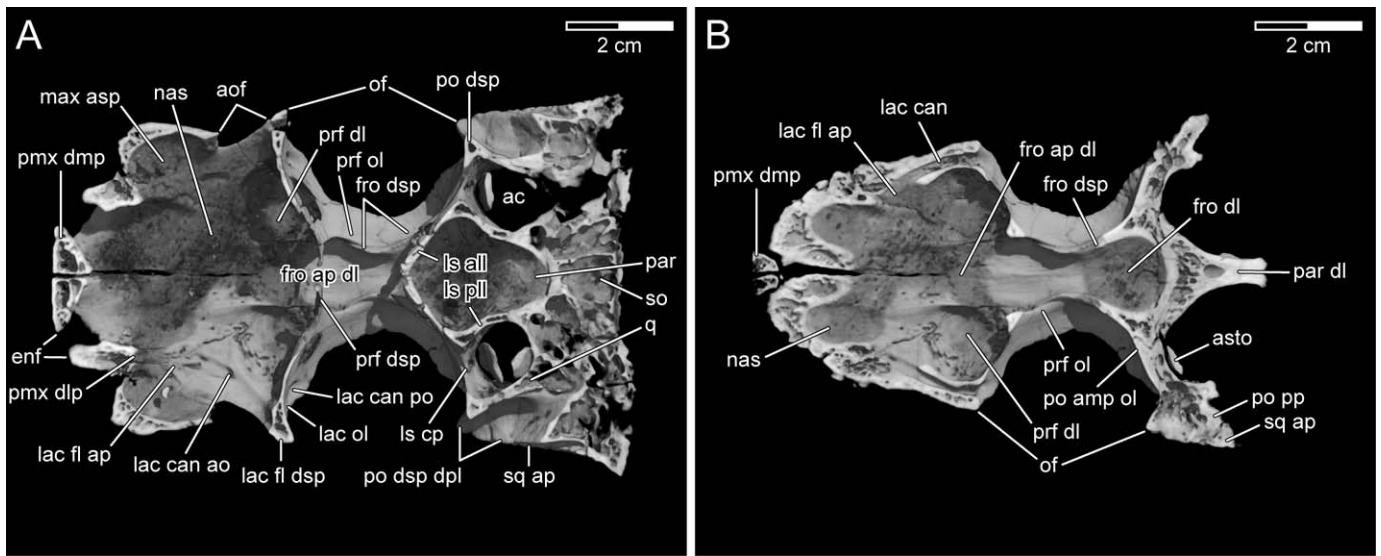


FIGURE 10. Ventral cutaway views through a three-dimensional digital reconstruction of the skull of the holotype (UA 8679) of *Simosuchus clarki* generated from HRXCT scans, as seen from frontal planes passing through the center of the antorbital fenestrae (A) and lacrimal canals (B). In this reconstruction, remaining matrix has been removed digitally so as to provide unobstructed views of unprepared internal regions of the skull. See Appendix 1 for anatomical abbreviations.

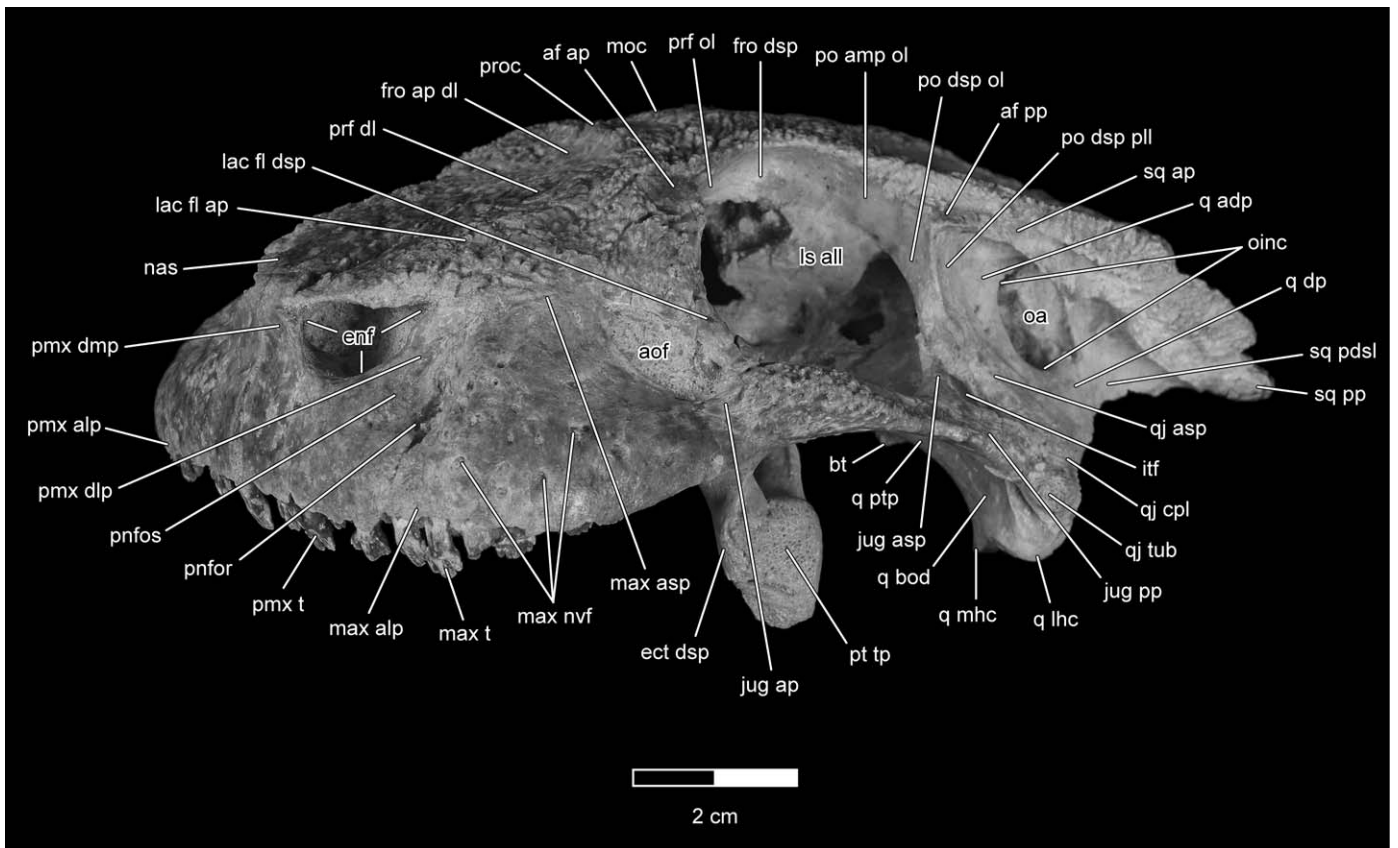


FIGURE 11. Photograph of the skull of the holotype (UA 8679) of *Simosuchus clarki* in left anterolateral (and slightly dorsal) view. See Appendix 1 for anatomical abbreviations.

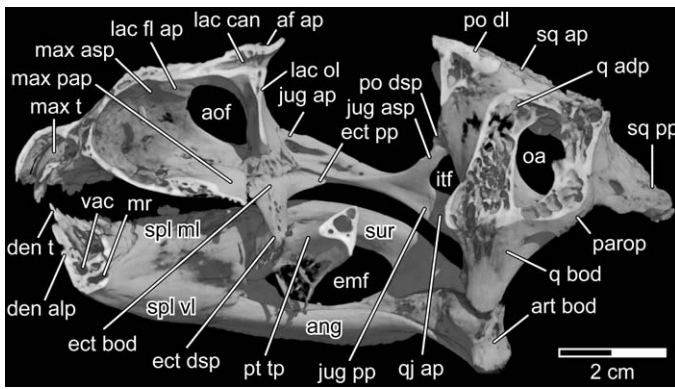


FIGURE 12. Medial cutaway view through a three-dimensional digital reconstruction of the skull and lower jaw of the holotype (UA 8679) of *Simosuchus clarki* generated from HRXCT scans, as seen from a parasagittal plane passing through the right lacrimal canal. In this reconstruction, remaining matrix has been removed digitally so as to provide an unobstructed view of unprepared internal regions of the head skeleton. See Appendix 1 for anatomical abbreviations.

Anteriorly, there is a prominent anterolaterally concave emargination of the palatal process of the maxilla, immediately posterior to the anterior part of the palatal portion of the premaxillomaxillary suture. This notch, closed off anterolaterally by the medial lamina of the alveolar processes of the maxilla, contributes to the formation of a relatively large anterior palatal foramen (Fig. 3), which lies directly dorsal to the fifth dentary tooth, and directly ventral to the foramen contained within the perinarial fossa described above. The anterior palatal foramen is positioned in the anterolateral corner of a subtriangular, dorsally elaborated region of the lateral-most part of the anterior palatal trough, termed here the anterior palatal fossa. Although projecting further dorsally than medially adjacent (i.e., premaxillary) portions of the anterior palatal trough, the paired (left and right) anterior palatal fossae are not as deep as is the unpaired, centrally placed incisive fossa. *Simosuchus clarki* is unique among crocodyliforms in possessing these prominent anterior palatal fossae.

Posteriorly, the lateral portion of the palatal process of the maxilla contacts the anterior margin of the body of the ectopterygoid, whereas the medial portion contacts both the anterior and lateral margins of the palatal process of the palatine. Between these articulations is a narrow zone of exposure of the free posterior margin of the process, which thus contributes to the lateral portion of the anterior border of the suborbital fenestra (Fig. 3).

Where the palatal and alveolar processes of the maxilla meet, a longitudinally oriented, ventrally concave trough is formed along the lateral margin of the bony palate (Fig. 3). This lateral palatal trough is continuous with the transversely oriented one along the anterior border of the palate and serves to accommodate the posterior dentary teeth when the mouth is closed. However, it is significantly shallower than the anterior palatal trough, a reflection of the relative shortness of the posterior dentary teeth relative to the anterior ones. Like the anterior palatal trough, the lateral palatal trough is a feature that appears to be unique to *S. clarki* among crocodyliforms.

Piercing the medial wall of the lateral palatal trough are several palatal foramina (Fig. 3). Although all of these are significantly smaller than the anterior palatal foramen described above, three are particularly prominent: one directed anteromedially, positioned ~13 mm medial to the posterior edge of the fourth maxillary alveolus; another directed anterolaterally, located ~13 mm medial to the interdental ridge separating the

sixth and seventh maxillary alveoli; and a posteriorly positioned one, directed anteriorly, located immediately anterior to the suture between the anterior edge of the body of the ectopterygoid and the posterior edge of the maxillary palatal process. All of these palatal foramina ultimately communicate with the dorsal alveolar neurovascular canal, and thus they likely transmitted mucosal branches of the dorsal alveolar nerve, artery, and vein.

Extending dorsally and medially from the alveolar process is the ascending (facial) process of the maxilla (Figs. 2, 4, 5, 11). It is perforated externally near its base by several neurovascular foramina, but it is predominantly smooth along most of its outer surface. However, some light sculpturing is present at its dorsal margin where it overlaps the dorsolateral surface of the anterior process of the facial lamina of the lacrimal. The posterior margin of the ascending process sweeps ventrally and posteriorly to meet the posterior-most portion of the alveolar process. This produces a posterodorsally concave emargination of the maxilla that serves as the anteroventral border of the antorbital fenestra (Figs. 2, 4, 11). The anterior margin of the ascending process curves strongly medially, presenting a relatively broad area of contact for articulation with the posterolateral surface of the dorsolateral process of the premaxilla, thereby forming the dorsal portion of the premaxillomaxillary suture (Figs. 2, 4, 5, 11). The lower part of this anteromedially curving portion of the process forms the lateral half of the perinarial fossa (the medial half being formed by the adjacent anterolateral surface of the dorsolateral process of the premaxilla).

Uniquely among crocodylomorphs, the ascending process of the maxilla does not contact the nasal in *S. clarki*; rather, it is separated from the latter by the extensive anterior process of the facial lamina of the lacrimal.

Nasals—The paired nasals (Figs. 1A, C, D, 2, 4, 5, 11) are relatively broad, extending as far laterally as the posterolateral corners of the widely spaced, anterolaterally directed external narial fenestrae. They are relatively flat and exhibit a moderate degree of sculpturing along their dorsal surfaces. The two nasals meet at the midline along most of their lengths in a long and relatively straight internasal suture. At their anterior ends, however, the medial margins of the nasals diverge from one another to accommodate the wedge-shaped dorsal termini of the dorsomedial processes of the premaxillae (Figs. 2, 5, 8C, 10, 11); this represents a unique condition among known mesoeucrocodylians. Posteromedially, the nasals contact the anterior margin of the dorsal lamina of the anterior process of the frontal, slightly overlapping the latter for a short distance, thereby forming a relatively short scarf joint (Fig. 7A, B). Both in frontal HRXCT slices (Fig. 8A) and in ventral views of the dermal skull roof generated from 3-D HRXCT reconstructions (Fig. 10), this nasofrontal suture can be seen to be posteriorly concave. However, in dorsal view (Fig. 2), the suture is so tightly closed that it is somewhat difficult to visualize macroscopically; this likely accounts for the slight misinterpretation of the shape and position of the nasofrontal suture in the original description of *Simosuchus clarki* (see Buckley et al., 2000:fig. 1b), which was published before UA 8679 had been HRXCT scanned. Posterolaterally, each nasal contacts the anteromedial margin of the dorsal lamina of the prefrontal (Figs. 2, 5). Laterally, extensive contact is made with the dorsomedial margin of the facial lamina of the lacrimal (Figs. 2, 4, 5, 8B, 10). This contact extends anteriorly almost to the posterolateral corner of the external narial fenestra, where the dorsolateral process of the premaxilla contacts the lateral margin of the nasal (Figs. 2, 4, 5, 9B, 10A). From this point anteriorly, the lateral margin of the nasal angles strongly toward the midline, where it meets the posterolateral edge of the dorsomedial process of the premaxilla (Figs. 2, 5, 10, 11). This anterolateral margin of the nasal forms the dorsal border of the external narial fenestra.

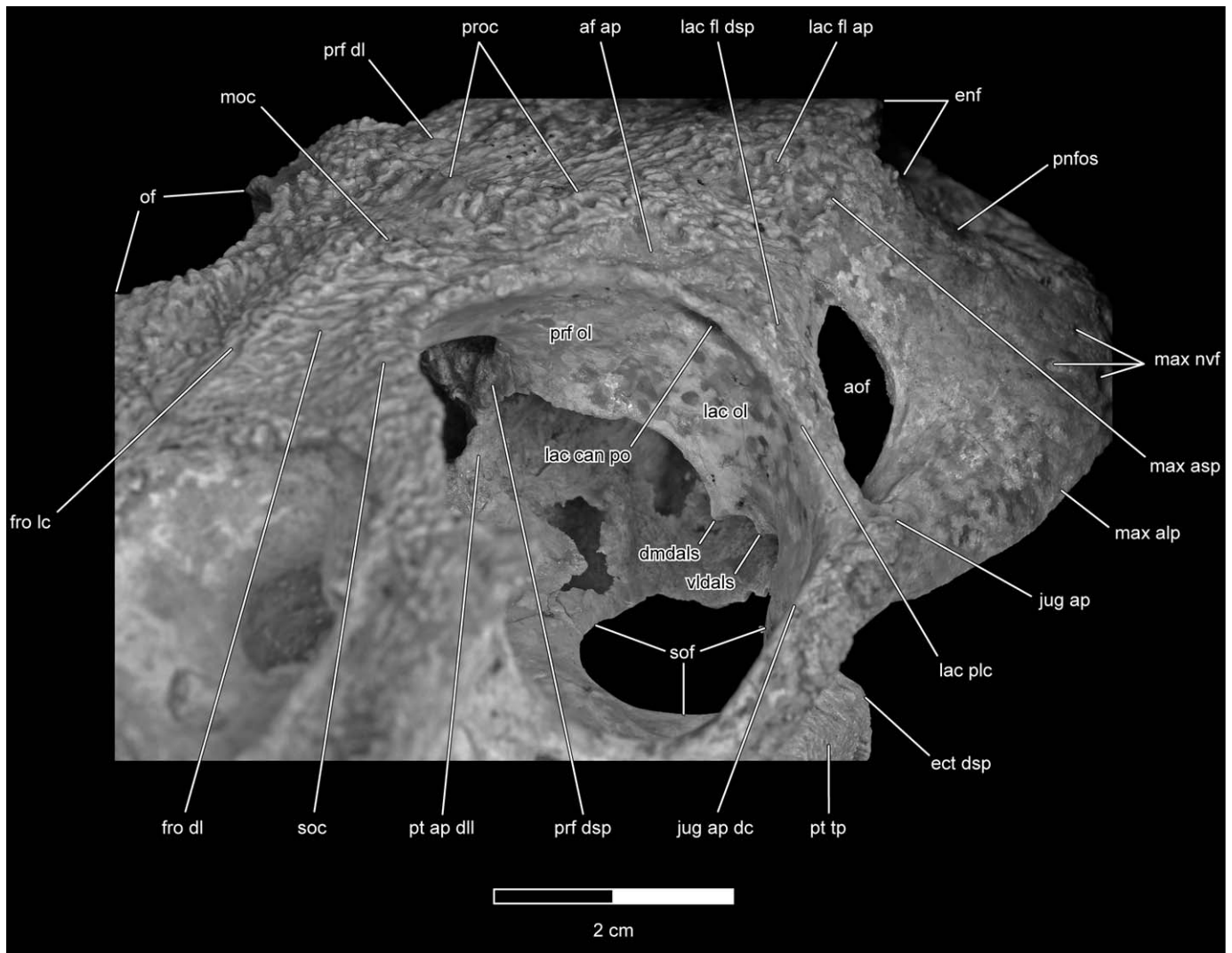


FIGURE 13. Photograph of the anterior wall of the right orbit of the holotype (UA 8679) of *Simosuchus clarki* in oblique posterodorsolateral view. See Appendix 1 for anatomical abbreviations.

Lacrimal—The lacrimals (Figs. 1A, C, D, 2–5, 11, 13) are relatively large and contribute significantly to the preorbital portion of the dermatocranium. Each lacrimal consists of a dorsolaterally oriented facial lamina and a posteriorly oriented orbital lamina. The left lacrimal of UA 8679 is broken in several places and both lacrimals are relatively poorly preserved in both FMNH PR 2596 and FMNH PR 2597. Thus, the following description is based primarily on the right lacrimal of UA 8679.

The facial lamina of the lacrimal (Figs. 2, 4, 5, 11, 13) forms nearly the entire lateral surface and much of the dorsolateral surface of the face in the region immediately anterior to the orbit. It consists of a relatively large anterior process and a much smaller descending process. The anterior process is shaped much like a relatively long isosceles triangle with an anteriorly directed apex. Its base is posteriorly concave and forms the anterior margin of the orbital fenestra. Its ventrolateral edge curves slightly dorsomedially as it sweeps anteriorly toward its apex. The posterior half of this ventrolateral edge is exposed in lateral view and forms the anterior half of the posterodorsal margin of the antorbital fenestra (Figs. 2, 4, 11, 13), whereas the anterior half passes medial to the ascending process of the maxilla; it is thus

hidden in lateral view and can only be visualized through the use of X-ray computed tomography (Figs. 8B, C, 9C, 10A). Like the ventrolateral edge, the dorsomedial edge of the anterior process also curves slightly dorsomedially as it extends anteriorly toward the apex, although it again curves slightly ventrolaterally near the apex itself. The posterior half of this dorsomedial edge is in sutural contact with the lateral margin of the dorsal lamina of the prefrontal, whereas its anterior half is in sutural contact with the lateral margin of the nasal (Figs. 2, 5). Although contact between the lacrimal and nasal is relatively common among mesoeucrocodylians—including nearly all ziphosuchians (sensu Turner and Sertich, this volume)—this contact is particularly extensive in *Simosuchus*. The apex of the anterior process of the facial lamina of the lacrimal terminates several millimeters posterior to the posterolateral corner of the external narial fenestra, where it is embraced medially by the anterolateral corner of the nasal, laterally by the anterodorsal corner of the ascending process of the maxilla, and anterolaterally by the posterodorsal terminus of the dorsolateral process of the premaxilla (Figs. 2, 4, 5, 10A). The anterior process of the facial lamina is slightly convex dorsolaterally and exhibits light to moderate sculpturing

along most of its external surface. One particularly heavy patch of surface sculpturing is present, however, at the extreme posteromedial corner of the facial lamina; this represents the most anterolateral portion of the preorbital crest, which continues posteromedially across the dorsal laminae of both the prefrontal and the frontal.

The descending process of the facial lamina of the lacrimal essentially represents a continuation and elaboration of the posteroventral corner of the anterior process. It extends ventrally, posteriorly, and slightly laterally to contact the anterodorsal edge of the anterior process of the jugal, just posterior to where the latter tapers to a blunt point (Figs. 2, 4, 5, 11, 13). In doing so, it forms a preorbital bar separating the ipsilateral orbital and antorbital fenestrae. More specifically, its posterodorsal edge forms the anteroventral margin of the orbital fenestra, and its anteroventral edge forms the posterior half of the posterodorsal margin of the antorbital fenestra. The descending process is relatively narrow in lateral view (i.e., anteroposteriorly) and exhibits only light sculpturing along its external surface.

The orbital lamina of the lacrimal (Figs. 2–4, 10A, 12, 13) forms the anterior and anteroventral walls of the orbit. It is predominantly posteriorly concave, thus contributing significantly to the smoothly rounded contours of the orbit. At its ventral end, however, where it articulates with the anterior process of the jugal and the posterior process of the ectopterygoid, it becomes almost flat and twists slightly inward to face posteromedially (Fig. 13). The lateral margin of the orbital lamina is continuous with the posterior margin of the facial lamina, with the two laminae meeting at an acute angle and thus forming a prominent posterolateral crest along the anterior and anteroventral margins of the orbital fenestra. Dorsally, this crest is continuous with a somewhat less prominent one formed at the junction of the orbital and dorsal laminae of the prefrontal. Ventrally, it is continuous with the dorsal crest of the anterior process of the jugal. The free-ending medial margin of the orbital lamina presents a more complex morphology. Along its dorsal three-fifths, it is ventromedially concave and approximately sickle-shaped, running nearly parallel with the lateral margin of the bone. Ventral to this smoothly curving portion, however, the medial margin of the orbital lamina forms two sharp triangular spines that project ventrally, medially, and slightly posteriorly (Fig. 13). Between these two spines a small but sharply delimited dorsolateral notch is formed. Immediately ventrolateral to this, between the more ventrolateral of the two spines and the ventromedial corner of the orbital lamina, a second notch is formed, similar in size to the first, but oriented more directly laterally. These notches likely transmitted branches of the maxillary nerve (CN V₂), along with associated vasculature, to supply the upper teeth, gums, and palate, and appear to represent autapomorphies of *Simosuchus clarki*.

The relationships among the orbital lamina of the lacrimal and its surrounding bones are rather complex. Its dorsomedial edge broadly contacts the ventrolateral edge of the orbital lamina of the prefrontal, thereby forming an oblique suture extending from dorsolateral to ventromedial across the entire width of the anterior wall of the orbit (Figs. 4, 13). Its ventral edge meets the dorsomedial margin of the posterior process of the ectopterygoid in a relatively straight suture, but one that angles laterally and slightly dorsally as it extends posteriorly (Fig. 2). Extending anterodorsally at an angle of $\sim 90^\circ$ from the posterior end of this ventral suture with the ectopterygoid is the ventromedial portion of the jugolacrimal suture (Fig. 2). Here the lateral edge of the somewhat flattened ventral portion of the orbital lamina contacts the anteroventral edge of the dorsomedial face of the anterior process of the jugal. Finally, the anterolateral (i.e., non-orbital) surface of the ventral portion of the orbital lamina is strongly buttressed by the posteromedial corner of the maxilla (Fig. 12).

The lacrimal canal (Figs. 8B, 9D, 10, 12, 13) is contained entirely within the lacrimal bone. The posterior opening of the canal, located in the extreme dorsolateral corner of the orbital lamina, is elliptical in shape and measures ~ 2 mm across its minor axis and ~ 3 mm along its major axis. The latter is oriented at an angle of $\sim 25^\circ$ relative to the median sagittal plane such that it slants slightly from dorsomedial to ventrolateral. The canal itself extends anteromedially within the anterior process of the facial lamina of the lacrimal (thus following the dorsolaterally convex contours of the latter) for a distance of ~ 15 mm before emptying into the nasal cavity. The anterior opening of the lacrimal canal lies medially adjacent to the externally visible posterodorsal corner of the ascending process of the maxilla, with only the outermost layer of the anterior process of the facial lamina separating the two.

The lacrimal is extensively pneumatized (Figs. 7D, E, 8A–F, 9D, E, 10, 12).

Prefrontals—The prefrontals (Figs. 1A–D, 2–5, 10, 11, 13) are rather extensive, forming a significant portion of the dermal skull roof directly medial and anteromedial to the orbital fenestrae, as well as the anterodorsal walls of the orbits themselves. Each prefrontal consists of a dorsal lamina and an orbital lamina, with a prominent descending process (prefrontal pillar) projecting ventromedially from the latter.

The dorsal lamina of the prefrontal is relatively long, extending from the mid-orbital region anteriorly to a point lying in a transverse plane coinciding with the anterodorsal apex of the antorbital fenestra (Fig. 2). As it extends anteriorly, it also slants somewhat ventrally, only moderately so along its posterior half, but more markedly along its anterior half due to the prominent preorbital ventroflexion of the entire rostrum. The dorsal lamina exhibits moderate to heavy sculpturing across its entire external surface. This is especially evident adjacent to the anterodorsal margin of the orbital fenestra, where the sculpturing is greatly elaborated to form part of a prominent preorbital crest. This crest continues medially onto the dorsal lamina of the anterior process of the frontal (at the center of which it becomes continuous with its contralateral partner) and anterolaterally onto the posterodorsal corner of the facial lamina of the lacrimal; thus, the left and right halves of this crest together form a conspicuous, transversely broad, U-shaped ridge that separates the dorsal surface of the mid-orbital portion of the skull roof from the flat anterodorsal surface of the rostrum. Although comparable preorbital crests are not known to be present in any other basal mesoeucrocodylians, very similar U-shaped crests are seen in some species of extant caimans (e.g., *Caiman crocodilus*, *Melanosuchus niger*).

The dorsal lamina of the prefrontal is rather complex in both its shape and its relations to surrounding elements (Fig. 2). Its posterior border is oriented nearly transversely, extending medially and very slightly posteriorly from the mid-dorsal part of the rim of the orbital fenestra toward the lateral edge of the dorsal lamina of the anterior process of the frontal. Along this course, it is in sutural contact with the anterior edge of the laterally expanded posterior portion of the dorsal lamina of the frontal. The medial border of the dorsal lamina of the prefrontal is oriented approximately longitudinally, although it exhibits a slight medial concavity where it skirts around the laterally bulging portion of the dorsal lamina of the frontal in the region of the preorbital crest. The posterior two-thirds of this medial border is in sutural contact with the lateral edge of the dorsal lamina of the anterior process of the frontal, with the latter bearing a lateral groove that receives a corresponding ridge projecting medially from the former (Fig. 9D–F); the result of this arrangement is a shallow tongue and groove joint. The anterior one-third of the medial border, which curves anterolaterally toward the nasolacrimal suture, is in sutural contact with the posterolateral edge of the nasal (Figs. 2, 5). From its somewhat blunted anterior-most point, the

dorsal lamina of the prefrontal curves strongly posterolaterally, where it forms a suture with the posterior half of the dorsomedial edge of the facial lamina of the lacrimal (Figs. 2, 5). This lateral border of the dorsal lamina roughly parallels the medial border along the anterior one-third of the prefrontal. However, slightly less than 1 cm anterior to the anterodorsal margin of the orbital fenestra, the prefrontolacrimal suture abruptly changes direction, extending laterally for a distance of ~8 mm before once again changing direction and extending posteriorly for a distance of ~6 mm, to the rim of the orbital fenestra. This results in the formation of a prominent, subtriangular, laterally projecting shelf, which is nearly devoid of surface sculpturing, and which is slightly recessed below the raised, sculptured surface of the anteromedially adjacent preorbital crest (Figs. 2, 5). This shelf serves as an articular facet for the anterior palpebral. The remaining posterior part of the lateral border of the dorsal lamina of the prefrontal is posterolaterally concave and contributes to the formation of the anterodorsal margin of the orbital fenestra (Figs. 2, 4, 11, 13).

The orbital lamina of the prefrontal presents a smooth, posteroventrolaterally concave surface that forms the anterodorsal portion of the orbital wall (Figs. 4, 13). Posterodorsally, it laterally overlaps the anterior-most part of the ipsilateral descending process of the frontal (i.e., the crista cranii frontalis) (Figs. 4, 8B, 9G). This part of the orbital lamina is relatively narrow and extends posteriorly to the midpoint of the orbit. Here its ventral half is drawn out posteriorly into a prominent triangular process, with its apex directed posteriorly. In UA 8679, its dorsal half is also drawn out posteriorly, producing a V-shaped emargination along the posterior border of the orbital lamina between these adjacent dorsal and ventral processes (Figs. 4, 10). However, in FMNH PR 2597, a distinct dorsal process is absent. Anteroventrally, the orbital lamina of the prefrontal widens significantly to establish a broad suture with the obliquely oriented dorsomedial edge of the orbital lamina of the lacrimal (Figs. 4, 13).

Extending ventrally and strongly medially from the widened anteroventral part of the orbital lamina is the descending process of the prefrontal (prefrontal pillar) (Figs. 7B, 8D, 9F, 13). This process is most completely preserved on the right side of the holotype specimen (UA 8679), where it can be seen to closely approach the dorsal surface of the anterior process of the pterygoid near the midline. Although the precise point of contact is not preserved in this specimen (or in either FMNH PR 2596 or FMNH PR 2597), it appears clear that the prefrontal pillar did not contact (or even closely approach) the palatine as it typically does in most other mesoeucrocodylian taxa. It remains unclear, however, whether or not the prefrontal pillars actually contacted one another at the midline, or if they bore medial processes distinct from those that contact the palate.

The dorsal and orbital laminae of the prefrontal are continuous laterally, where they meet at an acute angle to form the anterodorsal margin of the orbital fenestra (Figs. 4, 13). However, somewhat in contrast to the condition described above for the lacrimal, a sharp crest is not formed at the junction of the two laminae; rather, a shallow groove is formed here to accommodate the thin anteromedial edge of the anterior palpebral.

The dorsal lamina of the prefrontal is extensively pneumatized along its relatively thick posterior two-thirds (Figs. 7C, 8A, 9F). Pneumatization is less extensive, however, throughout the thinner orbital lamina and descending process.

Frontal—The frontal (Figs. 1A–D, 2–5, 10, 11, 13, 14) is unpaired, its left and right halves being fully fused. It is relatively simple in its overall morphology, consisting primarily of a dorsoventrally thick, horizontally oriented dorsal lamina from which two thinner, laterally placed descending processes project ventrally. Anteriorly, the frontal is drawn out into a long, narrow anterior process (Figs. 2, 5, 8A, 10).

The dorsal lamina of the frontal is relatively broad posteriorly and heavily sculptured across its entire external surface. In

several areas, this sculpturing is elaborated into low but distinct bony crests. One longitudinal crest is present along the dorsal midline, where the left and right halves of the bone have become fused (Figs. 2, 9H, 13). Two laterally concave supraorbital crests are present along the posterodorsal margins of the orbits (Figs. 2, 13). Finally, three transverse crests extend across the width of the frontal: one preorbital (~7 mm posterior to the anterior edge of the nasofrontal suture), one mid-orbital (~5 mm anterior to the posterior portion of the prefrontofrontal sutures), and one postorbital (immediately anterior to the frontoparietal suture) (Figs. 2, 4, 5, 7A–C, 11, 13). As stated above in the description of the prefrontal, the preorbital crest is a uniquely derived feature of *Simosuchus clarki* among basal mesoeucrocodylians; the similarly prominent mid-orbital crest also represents an autapomorphy of this taxon. Except at its anterior-most tip, the dorsal lamina of the frontal is relatively thick, consisting of well-defined inner (endocranial) and outer (pericranial) layers of compact bone separated by a dense network of bony trabeculae (Figs. 7A, B, 9D–I).

The dorsal lamina of the frontal meets that of the parietal in a posteriorly convex suture (Figs. 2, 8A, 14). Immediately anterior to this frontoparietal suture, the posterodorsal margin of the frontal is raised up into a transversely oriented postorbital crest that is prominent medially but fades as it extends laterally (Figs. 2, 7B). Posterolaterally, the frontal abuts the anteromedial edge of the anteromedial process of the postorbital (Figs. 2, 8A, B, 14). Between these two articulations, however, a small portion of the posterior edge of the frontal remains free, forming the central portion of the anterior margin of the supratemporal fenestra (Figs. 2, 14). At its anterior end, the dorsal lamina of the frontal thins dorsoventrally and terminates by underlapping the posterior edges of the nasals for a short distance, thereby forming a relatively short scarf joint (Fig. 7A, B). In dorsal view, the nasofrontal suture is anteriorly convex (Figs. 2, 8A). From the anterior-most part of the dorsal lamina of the frontal, a thin crest of bone projects dorsally into the posterior-most portion of the internasal suture. The entire anterior process of the frontal is bordered laterally by the prefrontal (Figs. 2, 10).

The ventrally directed descending processes of the frontal are well developed throughout the posterior three-fifths of the length of the bone. The posterior edge of each process contacts the anteromedial edge of the orbital lamina of the postorbital in a nearly vertical suture (Fig. 11). Along its posterior half, the ventral margin of the descending process is in broad contact with the dorsal edge of the anterior two-thirds of the laterosphenoid (Figs. 4, 11). However, anterior to its articulation with the laterosphenoid, the ventral margin of the descending process terminates freely as a sharp crest, the crista cranii frontalis (Figs. 4, 10, 11). The descending processes taper dorsally rather abruptly anterior to the point at which they pass medial to the orbital laminae of the prefrontals. Thus, the anterior half of the anterior process of the frontal consists only of a relatively narrow dorsal lamina.

The lateral margin of the posterior half of the frontal is concave anterolaterally (Figs. 2, 10, 11) and the descending process is concave ventrolaterally (Figs. 4, 10, 11). These concavities contribute significantly to the rounded contours of the dorsal portion of the orbit.

Parietal—The parietal (Figs. 1A, C, E, 2, 4, 6, 14) is unpaired and forms a large proportion of the roof of the braincase. Like the frontal, it exhibits a relatively simple morphology, consisting of a horizontally oriented dorsal lamina from which two prominent descending processes extend ventrolaterally.

The dorsal lamina of the parietal forms the central part of the cranial table (Figs. 2, 4, 6, 14). Like the dorsal lamina of the frontal, it exhibits distinct inner (endocranial) and outer (pericranial) layers of compact bone with an intervening meshwork of bony trabeculae (Figs. 7A, B, 9J–N). However, it differs from the dorsal lamina of the frontal in that these

trabeculae are replaced posteroventrally by a large mid-sagittal sinus (Figs. 7A, 8C, 9M), which communicates with the extensive pneumatized space within the supraoccipital via a pair of large, laterally placed pneumatic foramina. The dorsal laminae of the frontal and parietal differ further in their overall robusticity, with the latter being significantly thicker dorsoventrally than the former, due primarily to a marked thickening of the outer layer of compact bone (Fig. 7A; compare also Fig. 9H with Fig. 9J). This latter difference notwithstanding, the dorsal lamina of the parietal exhibits only moderate surface sculpturing, in contrast to the more heavily sculptured dorsal lamina of the frontal (Figs. 2, 14).

Along most of its length, the dorsal lamina of the parietal is relatively narrow, but it widens abruptly at both its anterior and posterior ends, giving it an I-shaped appearance in dorsal view (Figs. 2, 14). Its widened anterior end meets the posterior edge of the dorsal lamina of the frontal in a relatively broad frontoparietal suture that is anteriorly concave both in dorsal view and in sagittal section (Figs. 2, 7A, B, 8A, 14). Its widened posterior end exhibits more complex relations, however. Directly posteriorly, it meets the anterodorsal margin of the supraoccipital in a broad and largely transversely oriented suture near the posterodorsal edge of the skull. This suture exhibits a slight posterior concavity in dorsal view (Figs. 2, 14), and is beveled strongly (from anteroventral to posterodorsal) in sagittal section, such that the anterior part of the supraoccipital slopes beneath the posterior part of the parietal (Fig. 7A, B). Posterolaterally, the dorsal lamina of the parietal abuts the medial edge of the medial process of the squamosal (Figs. 2, 9N, O, 14). Finally, the free concave lateral edge of the dorsal lamina of the parietal forms the anteromedial, medial, and posteromedial margins of the supratemporal fenestrae, as well as the corresponding surfaces immediately ventral to these margins along the uppermost portions of the supratemporal fossae (Figs. 2, 14).

The descending processes of the parietal (cristae cranii parietales), which are laterally concave in dorsal view and laterally convex in transverse section, form all but the uppermost portions of the medial walls of the supratemporal fossae (Figs. 2, 8C, 9K, 14). They mirror the dorsal lamina in flaring laterally at both anterior and posterior ends, each ultimately forming an anterior overlapping contact with the posteromedial corner of the anteromedial process of the ipsilateral postorbital, and a posterior overlapping contact with the dorsomedial corner (i.e., dorsal primary head) of the ipsilateral quadrate (Fig. 14). In the latter region of overlap, the posterolateral border of the descending process of the parietal exhibits a prominent triangular emargination that exposes a portion of the dorsal primary head of the ipsilateral quadrate along the posterior portion of the floor of the ipsilateral supratemporal fossa, just medial to the temporo-orbital foramen; this represents an autapomorphy of *Simosuchus clarki*. The posterior half of the nearly horizontally oriented ventral edge of the descending process extends anteriorly from the aforementioned overlapping contact with the dorsomedial portion of the quadrate up to the anterior border of that bone. Anterior to this, the ventral edge of the descending process directly abuts the dorsal edge of the posterolateral lamina of the laterosphenoid (Figs. 9J, 14).

Squamosals—The squamosals (Figs. 1A–E, 2–6, 11, 14) are triadate in their general form, with each exhibiting distinct anterior, medial, and posterior processes. In addition, two descending laminae, one anterior and one posterior, project ventrally from the three primary processes. The dorsal surfaces of both the anterior and medial processes form a continuous dorsal lamina that makes up the posterolateral portion of the cranial table, bounding much of the posterior and lateral margins of the supratemporal fenestrae. The posterior process is markedly deflected both ventrally and (to a lesser degree) laterally, and projects well beyond the posterior-most extent of the occiput and the adjacent

quadrates. Laterally, the anterior and posterior processes overhang the otic aperture and all but the lateral half of the distal portion of the body of the quadrate. HRXCT scans of the holotype specimen (UA 8679) reveal that, like many other dermal roofing bones in *Simosuchus*, the squamosals are extensively pneumatized with an intervening meshwork of bony trabeculae (Figs. 7D, E, 8C–F, 9L–O).

The anterior process of the squamosal is mediolaterally wide, its smooth medial third contributing to the ventromedially inclined lateral floor of the supratemporal fossa (Figs. 2, 14). A lightly sculptured raised ridge demarcates the boundary between the smooth surface of the supratemporal fossa and the moderately to heavily sculptured dorsal lamina of the anterior process (Fig. 2). The dorsal lamina is slightly inclined such that its lateral margin is elevated dorsally above its medial margin before the former abruptly angles ventrally, thereby producing a sharp crest along the dorsolateral edge of the process (Figs. 4–6, 9L, M, 11). The anterior process extends anteriorly to form a sutural contact with the posterior process of the postorbital. In dorsal view, this suture is oriented obliquely along an anterolateral-posteromedial axis at approximately the anteroposterior midpoint of the supratemporal fenestra (Figs. 2, 14). Laterally, the posterior process of the postorbital broadly overlaps the anterior process of the squamosal in a strongly beveled contact that extends to the dorsal plate of the descending process of the postorbital (Figs. 4, 7E). Here the anterior process of the squamosal is underlapped by the posterior projection of this dorsal plate (Fig. 10A).

Projecting ventrally from the anterior process of the squamosal is a robust anterior descending lamina, visible medially along the lateral wall of the supratemporal fossa (Figs. 2, 14), and laterally within the external otic recess (Fig. 4). Beginning from the ventral surface of the anterior process dorsal to the otic aperture, the anterior descending lamina flares anteriorly and ventrally to broadly contact the posterior edge of the descending process of the postorbital anteriorly and the anterodorsal process of the quadrate ventrally (Figs. 8D, 9K). Medially, the anterior descending lamina of the squamosal contacts the anterodorsal process of the quadrate within the supratemporal fossa, forming a rather irregular suture (Figs. 2, 14).

The medial process of the squamosal is short, contributing to the posterior margin of the cranial table, the lateral half of the posterior margin of the supratemporal fenestra, and the lateral half of the posterior floor of the supratemporal fossa (Figs. 2, 14). Anteriorly, within the supratemporal fossa, the medial process is smooth, descending anteroventrally to the dorsal margin of the anterior opening of the orbitotemporal passage (temporo-orbital foramen), located at the junction between the anterior and medial processes. The orbitotemporal passage extends ventral to the medial process, opening posteriorly through the posttemporal fenestra, located between the medial process of the squamosal and the postoccipital processes of the otoccipital (Fig. 6). The posterior portion of the medial process is elevated dorsally and heavily sculptured, with its anterodorsal margin slightly overhanging the posterolateral part of the supratemporal fossa (Figs. 2, 14). This dorsal expansion of the medial process is notably elevated above the laterally adjacent dorsal laminae of the anterior and posterior processes of the squamosal, but approximately coplanar with the medially adjacent dorsal laminae of the parietal and supraoccipital (Fig. 6). The medial process of the squamosal extends medially to contact the ipsilateral descending process of the parietal within the supratemporal fossa and the dorsal laminae of the parietal and supraoccipital along the posterior-most part of the cranial table (Figs. 2, 14).

The posterior process of the squamosal is heavily sculptured and exceptionally large, projecting far posteriorly beyond the occipital surface of the skull (Figs. 2–4, 14). Anteriorly, it meets the anterior process at an elevated, transversely oriented ridge that is continuous medially with the posterior margin of the cranial

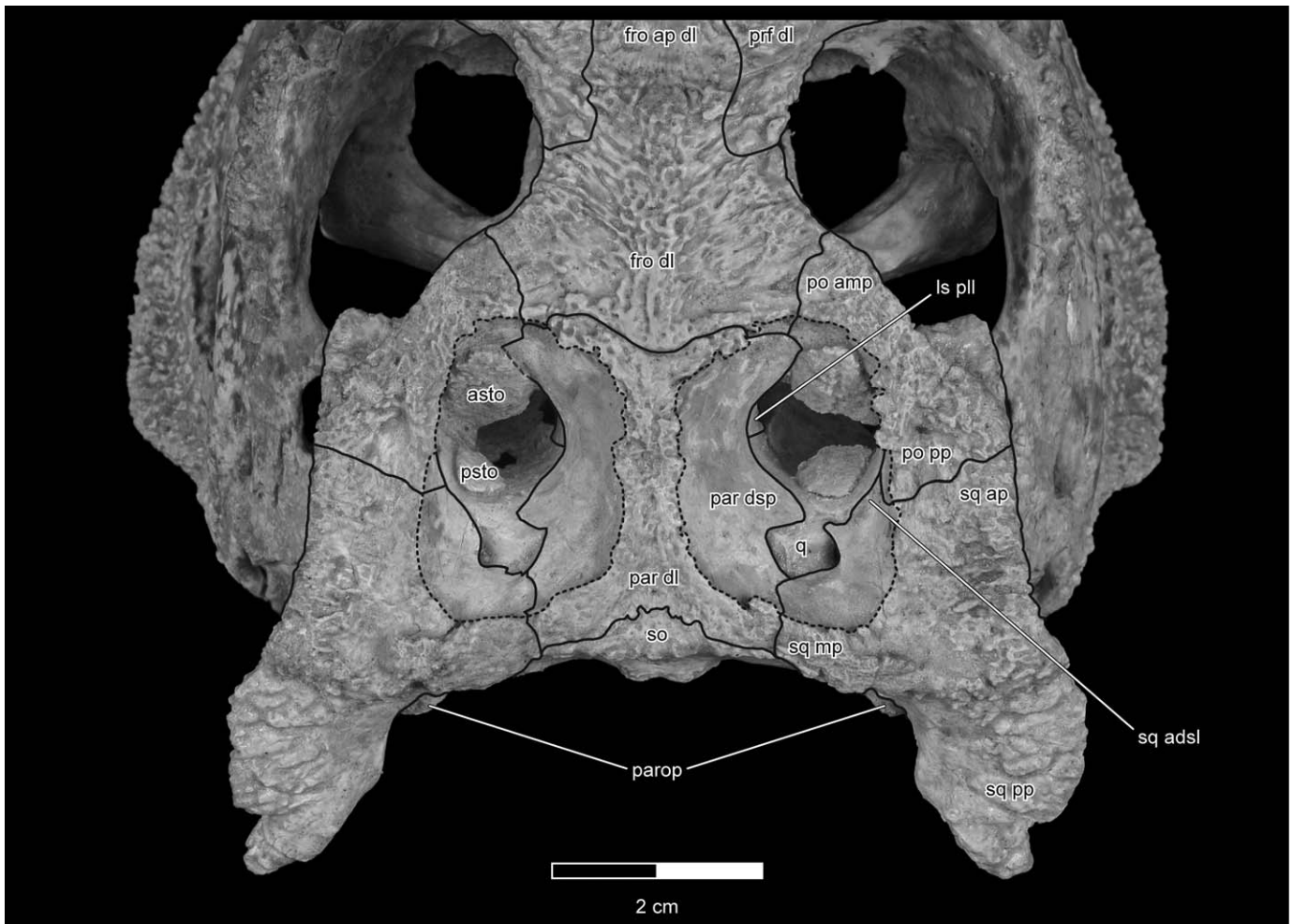


FIGURE 14. Photograph of the orbitotemporal region of the skull of the holotype (UA 8679) of *Simosuchus clarki* in dorsal view, showing relationships between bones within and around the supratemporal fossae and along the dorsal aspect of the orbital fenestrae. Sutures between elements of the skull roof are indicated by solid lines. The relatively short segment of the left postorbitoparietal suture that is obstructed by the overlying anterior supratemporal ossification is indicated by a dashed line. Margins of the supratemporal fenestrae are indicated by dotted lines. See Appendix 1 for anatomical abbreviations.

table in UA 8679 (Figs. 2, 4, 6). Conversely, in FMNH PR 2597, this boundary is present as a shallow transverse sulcus. In both specimens, the dorsal lamina of the posterior process is inclined dorsolaterally (Fig. 6) and extends posteroventrally from the corner of the cranial table (Fig. 4). The medial third of the dorsal lamina in UA 8679 is smooth, with moderate to heavy sculpturing extending laterally (Figs. 2, 14). However, FMNH PR 2597 lacks this smooth medial portion, exhibiting heavy sculpturing across the entire dorsal lamina of the squamosal. Laterally, the dorsal and ventrolateral surfaces of the posterior process meet at an acute angle to form a sharp lateral crest (Figs. 2, 3, 6). This crest terminates posteriorly at a distinct lateral notch, with the posterior process terminating distally in a rugose, subconical, posterolaterally directed tubercle in UA 8679 (Figs. 2–4, 6, 14), and in a somewhat less distinct rounded projection in FMNH PR 2597. Such terminal projections of the posterior processes of the squamosals represent autapomorphies of *Simosuchus clarki*.

As in other crocodyliforms, the posterior descending lamina of the squamosal projects ventrally from the posterior surface of the medial process and the medial margin of the posterior process to contact the quadrate and otoccipital. Beginning lateral to

the posterior opening of the orbitotemporal canal (posttemporal fenestra), it expands both ventrally and laterally, contacting the otoccipital posteriorly in a suture that extends ventrolaterally to the paroccipital process (Figs. 6, 8G, 9O). Further laterally, the posterior descending lamina curves strongly posteriorly at the intersection between the medial and posterior processes, becoming oriented nearly perpendicular to the occipital surface and thus forming a free ventral edge of the squamosal (Figs. 3, 4). The posterior descending lamina of the squamosal forms the medial wall of the external otic recess posterior to the otic aperture. Ventrally, it is in broad sutural contact with the dorsal process of the quadrate, beginning at the dorsoventral midpoint of the posterior rim of the otic aperture and extending posteroventrally to the posterior margin of the body of the quadrate (Fig. 4).

Laterally, the anterior and posterior processes of the squamosal strongly overhang the otic aperture, thereby forming the roof of the external otic recess (Figs. 4, 7E, 8E, F, 9L–O). Dorsal to this recess, the lateral surface of the squamosal is slanted strongly ventromedially, especially along the posterior process (Figs. 3, 5, 11), and is divided nearly equally along its length into a

dorsal portion exhibiting heavy sculpturing and a ventral portion bearing no sculpturing (Fig. 4). The sculptured dorsal portion of this lateral surface meets the dorsal laminae of the anterior and posterior processes at an acute angle to form a distinct lateral crest of the squamosal (Figs. 3–6, 11). In contrast, the smooth ventral portion of this lateral surface is recessed medially and thus moderately overhung by the dorsal sculpturing itself (Fig. 9M, N). The smooth ventral portion of this surface forms a sharp lip overhanging the external otic recess (Fig. 9L–O), with the ventral edge arching dorsally beginning at a point just posterior to the otic aperture to form a distinct semicircular notch (Fig. 4), similar to the condition exhibited by *Mariliasuchus amarali* (see Zaher et al., 2006:fig. 5). Medial to this notch and lateral to the otic aperture itself, the ventral surfaces of the anterior and posterior processes of the squamosal are strongly vaulted to form a dome-like ventral concavity (Fig. 9O). A similar but shallower concavity is present in *Mahajangasuchus insignis* lateral to the otic aperture. A small rugosity is present on the anterior margin of this ventral concavity in UA 8679. Extending posteriorly from this dome-like ventral concavity is a longitudinally oriented, ventrally concave trough that runs the length of the ventral surface of the posterior process (Fig. 3). This hemitubular trough is similar to, but more prominent than, the condition observed in other mesoeucrocodylians, including *Hamadasuchus rebouli* (see Larson and Sues, 2007:fig. 2) and *Mariliasuchus amarali* (see Zaher et al., 2006:fig. 5).

Postorbitals—The postorbitals (Figs. 1A–D, 2–5, 11, 14) are triradiate in their general form, with each exhibiting relatively short but distinct anteromedial, posterior, and descending processes, the three trifurcating from a central point near the posterodorsal corner of the orbit.

The dorsal portions of the anteromedial and posterior processes of the postorbital together form a continuous dorsal lamina that makes up the anterolateral part of the cranial table (Figs. 2, 14). It is moderately thick dorsoventrally, but somewhat less so than the more robust dorsal laminae of the frontal and parietal (Fig. 9I–K). The portion of the dorsal lamina formed by the anteromedial process of the postorbital is relatively narrow, approximately equal in width to the elevated central portion of the dorsal lamina of the parietal, and exhibits a moderate degree of sculpturing across its dorsal surface. At its anteromedial end, it is in sutural contact with the posterolateral corner of the dorsal lamina of the frontal. HRXCT scans of UA 8679 (and, to a lesser degree, CT scans of FMNH PR 2597) reveal that this postorbitofrontal suture is somewhat complex in its internal structure, with a moderate degree of interdigitation occurring between the two bones (Figs. 8B, 9H, I). The dorsal lamina of the anteromedial process of the postorbital serves to separate the orbital and supratemporal fenestrae, thereby contributing to the posterodorsal margin of the former and the anterolateral margin of the latter (Figs. 2, 14).

The portion of the dorsal lamina formed by the posterior process of the postorbital is relatively wide, measuring approximately twice the width of the anteromedial portion, and exhibits moderate to heavy sculpturing across its dorsal surface (Figs. 2, 14). In UA 8679, this sculpturing is markedly elaborated near the posterior end of the process, where two short crests are formed, one extending directly posteriorly along the anterolateral margin of the supratemporal fenestra, the other diverging posterolaterally toward the anterolateral corner of the anterior process of the squamosal. Similar but less distinct crests can be seen on the right postorbital of FMNH PR 2596, but in FMNH PR 2597 they appear to be almost completely absent. At its posterior end, the dorsal lamina of the postorbital is in sutural contact with the anterior edge of the anterior process of the squamosal. In dorsal view, this postorbitosquamosal suture is seen to be oriented somewhat obliquely, extending along an anterolateral-posteromedial axis (Figs. 2, 14). In addition, serial sagittal HRXCT and CT slices

through the skulls of UA 8679 and FMNH PR 2597, respectively, demonstrate an obliquely overlapping arrangement in the internal structure of this joint, with the posterior process of the postorbital tapering dorsally as it extends posteriorly, and the anterior process of the squamosal tapering ventrally as it extends anteriorly. This arrangement results in a relatively broad and strongly beveled contact between the two processes, with the posterior process of the postorbital dorsally overlapping the anterior process of the squamosal (Fig. 7E). However, it does not represent a simple scarf joint, because the expanded dorsal plate of the descending process of the postorbital (see below) extends posteriorly by ventrally underlapping the anterior-most tip of the anterior process of the squamosal, thereby creating a single, but very robust, interdigitation between the two bones, one that can be seen externally in lateral views of both UA 8679 (Fig. 4) and FMNH PR 2597.

The descending process of the postorbital forms the dorsal half of the postorbital bar (Fig. 4). It consists, in part, of an expanded, horizontally oriented dorsal plate and a relatively flat posterolateral lamina. It also contributes, along with the anteromedial process, to a relatively extensive orbital lamina (Fig. 11).

The dorsal plate of the descending process is essentially semi-elliptical in shape, with its free curved edge directed posterolaterally and its major axis running from anterolateral to posteromedial (Fig. 10A). As described above, the posterior part of the dorsal plate underlaps the anterior terminus of the anterior process of the squamosal (Fig. 4). In contrast, however, the anterolateral third of the plate is not overlain by other bones of the skull; rather, it projects strongly anteriorly as a triangular shelf of bone from beneath the anterolateral corner of the cranial table, recessed ventrally relative to the latter by ~3.5 mm (Fig. 4). The nearly flat dorsal surface of this triangular projection of the dorsal plate serves as an articular facet for the posterior palpebral (Figs. 2, 4, 5, 9I, J, 11). Near the base of this projection, the ventrolateral surface of the dorsal plate is perforated by a small foramen. Preserved in association with this foramen in UA 8679 is a Y-shaped network of shallow canals, consisting of one very short canal extending anterolaterally from the foramen itself, and two much longer canals that branch off from the shorter one and then gradually diverge from one another as they extend toward the lateral margin of the dorsal plate (Fig. 10A).

The posterolateral lamina of the descending process of the postorbital is preserved completely without displacement, distortion, or breakage only on the right side of UA 8679, which therefore serves as the primary basis for this description. It exists as a relatively simple, flat sheet of bone that extends ventrolaterally from the dorsal plate, with its medial surface applied directly against the anterior-most part of the lateral surface of the quadrate, along the dorsal two-fifths of the latter (i.e., along the anterodorsal process) (Figs. 4, 9J, 11). It tapers slightly as it descends, ultimately terminating ~3 mm above the dorsal corner of the infratemporal fenestra. (It encroaches directly upon the dorsal corner of the infratemporal fenestra on the left side of UA 8679, but this appears to be the result of slight dorsoventral compression of the entire left side of the skull in this specimen.) At its ventral terminus, the posterolateral lamina of the postorbital contacts the ascending process of the quadratojugal (Fig. 4). More specifically, the W-shaped ventral edge of the former is embraced by the dorsal edge of the latter, which is shaped much like a trident; this forms a strongly interdigitating articulation between the two bones, both of which are relatively thin in this area of contact. The external surface of the posterolateral lamina of the postorbital is entirely smooth.

The remaining component of the postorbital is its orbital lamina, which is formed by portions of both the anteromedial and descending processes. It consists of a thin, smooth, and anteroventrally concave sheet of bone that forms the relatively narrow posterodorsal portion of the orbital wall (Figs. 7D, E, 8C, D, 11,

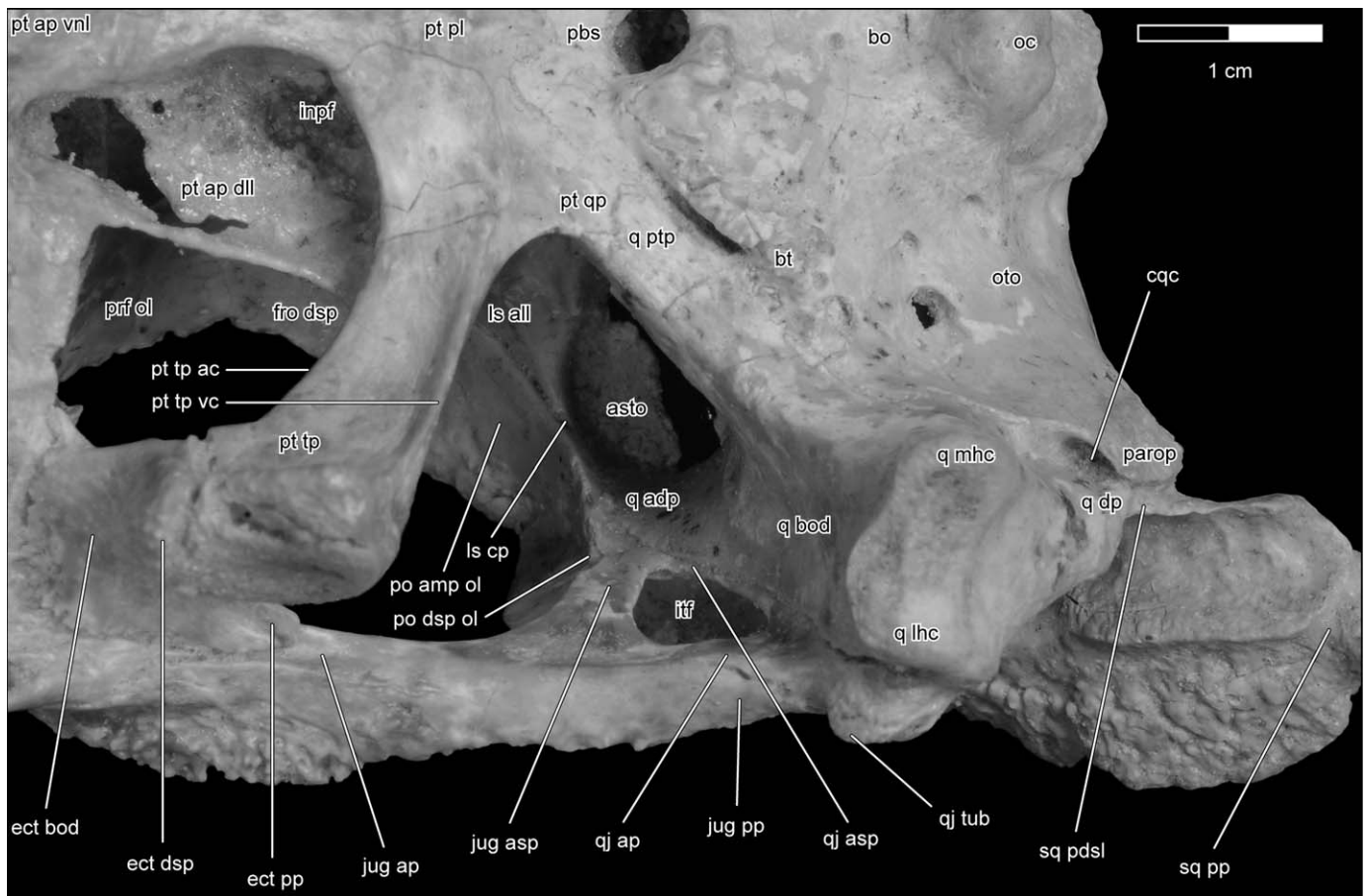


FIGURE 15. Photograph of the right orbitotemporal region of the skull of the holotype (UA 8679) of *Simosuchus clarki* in oblique right anteroventrolateral view, showing details of the structure of the infratemporal fenestra and the morphology and relationships of the capitata process of the laterosphenoid. See Appendix 1 for anatomical abbreviations.

15). Dorsally, the anteromedial edge of the portion of the orbital lamina formed by the anteromedial process is in sutural contact with the posterolateral edge of the ipsilateral descending process of the frontal (Figs. 4, 11). HRXCT scans of UA 8679 show numerous small interdigitations between the opposing articular surfaces throughout this ventral portion of the postorbitofrontal suture (Figs. 8B, 9H, 10B). The ventral edge of the part of the orbital lamina formed by the anteromedial process very closely approaches the dorsal edge of the anterolateral lamina of the laterosphenoid along the posterolateral two-fifths of the latter (Fig. 11); however, no suture is formed here, and the ventral edge of the orbital lamina of the postorbital actually slightly overhangs the dorsal edge of this portion of the laterosphenoid (Figs. 9H, 10A, 15). The latter bone ultimately terminates laterally in a mediolaterally elongate and anteroposteriorly slender capitata process (Fig. 15), the distal tip of which is received by a notch on the posterior surface of the orbital lamina of the postorbital, at a point near the junction of the anteromedial and descending processes (Figs. 7D, 8C, 9I, 10A). Ventrally, the portion of the orbital lamina formed by the descending process of the postorbital tapers to a blunt point along the anterolateral aspect of the dorsal terminus of the ascending process of the jugal (Figs. 4, 9I, 11, 12, 15).

On both the left and right sides of UA 8679, there is a prominent foramen lying within a sulcus between the lateral margin of the orbital lamina of the postorbital and the wedge-shaped an-

terior extension of the dorsal plate of the descending process of this bone. The foramen on the left side of this specimen is slightly larger and more dorsally placed than the one on the right. In FMNH PR 2597, a similarly placed foramen is clearly visible on the left postorbital; however, due to a large crack running across the corresponding portion of the right postorbital in this specimen, the presence or absence of a foramen here cannot be determined with certainty.

HRXCT scans of UA 8679 (and, to a lesser degree, CT scans of FMNH PR 2597) reveal that the postorbitals are largely hollow, with the central core of each bone being nearly devoid of internal trabeculae, but with the posterior processes exhibiting numerous trabeculae (Figs. 7E, 8C, 9J, K, 10B, 12).

Quadratojugals—The quadratojugals (Figs. 1A–E, 2–4, 6, 11, 15) form the posterodorsal margins of the infratemporal fenestrae and contribute (along with the jugals) to the formation of the infratemporal bars. Each quadratojugal consists of an expanded central plate, an ascending process, and an anterior process.

The expanded central portion of the quadratojugal is approximately semi-elliptical in shape (Figs. 2, 4, 6). Its medial surface is nearly flat and is applied directly against the similarly flat lateral surface of the ventral half of the body of the quadrate (Fig. 9K). Its lateral surface is lightly sculptured and bears a prominent anteroventrolaterally directed tubercle near its ventral end (Figs. 4, 6); the presence of this distinct quadratojugal tubercle represents an autapomorphy of *Simosuchus clarki*. Immediately medial to

this tubercle, the central plate becomes extremely thin, forming a semicircular flange around the posteroventral half of the base of the tubercle (Fig. 4). This flange lies directly against the lateral surface of the lateral hemicondyle of the quadrate.

The ascending process of the quadratojugal extends dorsally, anteriorly, and slightly medially along the anterior third of the lateral margin of the anterodorsal process of the quadrate (Figs. 4, 6, 9K, 11, 15). It terminates anterodorsally by contacting the ventral edge of the posterolateral lamina of the descending process of the postorbital in a complex, interdigitating suture (Figs. 4, 11). The ascending process of the quadratojugal is strongly laterally compressed (Figs. 9K, 15), with its narrow anteroventral edge forming the posterodorsal margin of infratemporal fenestra (Figs. 4, 11, 15). In contrast to the central plate of the quadratojugal, the ascending process is almost entirely devoid of surface sculpturing (Fig. 4).

The anterior (infratemporal) process of the quadratojugal forms the posteromedial part of the infratemporal bar (Figs. 3, 9I, J, 15). It can be seen in ventral view to have a distinctly beveled lateral face that gradually tapers medially as the process extends anteriorly (Figs. 3, 8G, 15). This mirrors the condition seen along the laterally adjacent posterior process of the jugal, which exhibits a beveled medial face that gradually tapers laterally as it extends posteriorly. One consequence of this arrangement is that these two processes meet in a relatively long, tall, and obliquely oriented suture that extends nearly the entire length of the infratemporal bar. Another is that anterior process of the quadratojugal is obscured almost completely in lateral view by the posterior process of the jugal (Fig. 4).

Jugals—The jugals (Figs. 1A–E, 2–6, 11–13, 15) form the ventral and posteroventral margins of the orbital fenestrae as well as the ventral and anterior margins of the infratemporal fenestrae. They are triradial in their general form, with each having distinct ascending, anterior, and posterior processes.

The ascending process of the jugal forms the ventral half of the postorbital bar, which separates the orbital fenestra from the infratemporal fenestra (Figs. 2–4, 11, 12, 15). It extends dorsally, medially, and slightly posteriorly from the point at which the three processes of the jugal trifurcate. At its dorsal end, it passes medial to the anteroventral corner of the descending process of the postorbital before tapering and ultimately terminating in the narrow, anteriorly facing fissure between the lateral surface of the anterodorsal process of the quadrate and the medial surface of the ascending process of the quadratojugal (Figs. 8F, 9I, 12, 15); these relations of the dorsal terminus of the ascending process of the jugal are unique to *Simosuchus clarki* among crocodylomorphs. The ascending process is distinctly laterally compressed, having an anteroposterior length approximately twice its medio-lateral width (Figs. 8F, 9H). It is devoid of sculpturing and thus completely smooth along all of its surfaces.

As in several other notosuchian taxa, such as *Adamantina-suchus navae*, *Mariliasuchus amarali*, and *Araripesuchus tsangatsangana*, the anterior (suborbital) process of the jugal in *Simosuchus* is subtriangular in cross-section (Fig. 9G), bearing distinct dorsal, ventromedial, and ventrolateral crests (Figs. 2, 3, 5, 6, 9G, 13). The dorsal crest originates posteriorly along the anterolateral surface of the base of the ascending process and then extends anteriorly along the dorsal aspect of the anterior process up to the jugolacrimal suture; there it is continuous with the posterolateral crest formed at the junction of the orbital and facial laminae of the lacrimal (Fig. 2). Together, the dorsal crest of the anterior process of the jugal and the posterolateral crest of the lacrimal form a prominent circumorbital crest that serves to define the ventral and anterior margins of the orbital fenestra. The ventromedial crest of the anterior process of the jugal represents a continuation of the sharp anterior edge of the ascending process. It passes close to the root of the dorsal crest as it begins to curve anteriorly, but then sweeps ventrally and medially toward

the suture between the ventral margin of the orbital lamina of the lacrimal and the dorsomedial margin of the posterior process of the ectopterygoid (Fig. 2). Finally, the ventrolateral crest of the anterior process (jugal ridge sensu Turner, 2006) represents a continuation and elaboration of a less distinct ventrolateral crest present along the anterior half of the posterior process (Fig. 2). It exhibits sculpturing along its entire length, but this is especially pronounced anteriorly, where the process approaches the posteroventral corner of the antorbital fenestra (Figs. 2–5, 8E, F, 9E, F, 11, 15). This great elaboration of the sculpturing along the lateral edge of the anterior process of the jugal bears a strong resemblance to the ‘jugal prong’ recently described by Novas et al. (2009) for *Yacarerani boliviensis*, both in its general appearance and in its superjacent position relative to the contact between the ramus of the surangular and the posterodorsal process of the dentary in the articulated lower jaw; however, the ‘jugal prong’ of *Yacarerani* lies close to the point of trifurcation of the three processes of the jugal, whereas the comparable region of heavy sculpturing in *Simosuchus* is restricted to the anterior two-thirds of the anterior process. Elaboration of the sculpturing along the anterior process of the jugal has also been reported in *M. amarali* (Zaher et al., 2006), but the degree of elaboration in this taxon is considerably less than that exhibited by either *S. clarki* or *Y. boliviensis*.

The anterior process of the jugal curves gently medially toward its anterior end. This, combined with the heavy sculpturing along the anterior portion of the ventrolateral crest, produces a gentle, yet distinct, lateral convexity along this portion of the bone, making the jugal appear to be markedly ‘bowed out’ laterally (Figs. 2, 3, 5, 6, 15).

At its anterior end, the anterior process of the jugal articulates with the maxilla, lacrimal, and ectopterygoid (Figs. 2–5, 8E, F, 9D–F, 11–13, 15). Laterally, immediately anterior to the dorsolateral portion of the jugolacrimal suture, the process abruptly tapers dorsoventrally to terminate as a slightly blunted, anteriorly directed spike of bone just below the antorbital fenestra (Figs. 2, 4, 5, 11, 13). This anterolateral projection of the anterior process extends along the lateral surface of the posterior-most part of the alveolar process of the maxilla. Dorsally, immediately anterior to the termination of the dorsal crest, a relatively short and nearly horizontally oriented sutural contact is established with the ventral edge of the descending process of the facial lamina of the lacrimal (Figs. 2, 4, 12, 13). Medial to this dorsolateral contact, the anteromedial edge of the anterior process, between the dorsal and ventromedial crests, contacts the ventrolateral edge of the orbital lamina of the lacrimal, thereby forming the relatively tall and obliquely oriented ventromedial portion of the jugolacrimal suture. Finally, along the ventral surface of the anterior process, immediately lateral to the ventromedial crest, there is a deep V-shaped notch to accommodate the dorsal edge of the posterior process of the ectopterygoid (Figs. 3, 9F, 15). This notch extends posteriorly to the mid-orbital level.

The anterior process of the jugal is pierced by numerous foramina. The most conspicuous of these are three relatively large foramina along the smooth, flat, dorsomedially facing surface of the process (i.e., that extending between the dorsal and ventromedial crests). These are positioned nearly identically on both left and right jugals of UA 8679: the largest of these three foramina is positioned immediately posterolateral to the dorsoventral midpoint of the vertically oriented portion of the jugolacrimal suture, whereas the two smaller ones are located along the posterior part of the anterior process, separated anteroposteriorly by a distance of ~4 mm. Similarly, the ventral surface of the process bears at least one prominent foramen just posterior to its anteroposterior midpoint; one of these is present on both jugals in UA 8679, but multiple foramina are present in both (damaged) jugals of FMNH PR 2597. Finally, numerous small foramina pierce the heavily sculptured anterior portion of the ventrolateral crest of

the anterior process. These lateral foramina, which number approximately nine on each side of UA 8679, are best visualized in HRXCT scans of this specimen, as they are very small and well concealed amidst the surrounding sculpturing.

Like the ascending process, the posterior process of the jugal is laterally compressed, giving it a somewhat flattened appearance in lateral view (Fig. 4). However, due to the presence of moderately developed ventromedial and ventrolateral crests, it is actually slightly subtriangular in cross-section, especially anteriorly, in the region subjacent to the anterior portion of the infratemporal fenestra (Fig. 9I). Its dorsal edge is rather sharp and is continuous with the equally sharp posterior edge of the ascending process, the two meeting at an angle of slightly less than 90° (Figs. 4, 12). Due to the somewhat tilted orientation of the posterior half of the jugal, which mirrors that of the lateral surface of the quadratojugal (and thus the quadrate), this dorsal edge of the posterior process slants slightly medially (Figs. 2, 9I, J, 11). The ventrolateral crest of the posterior process is continuous with that of the anterior process. It is only faintly developed posteriorly, but becomes more pronounced anteriorly, where it bears light sculpturing along its surface. In contrast, the ventromedial crest is well developed along the entire length of the posterior process (Fig. 3). In fact, it extends anteriorly onto the ventral surface of the proximal part of the anterior process before terminating completely near the posterior apex of the V-shaped notch accommodating the posterior process of the ectopterygoid. It bears emphasis that the ventromedial crest of the posterior process is not continuous with that of the anterior process; the latter represents an anterior extension of the anterior edge of the ascending process. The posterior process of the jugal laterally overlaps the anterior process of the quadratojugal, the two processes together forming the infratemporal bar (Figs. 3, 9I, J, 12, 15).

Due to the large size of the orbital fenestra, the point at which the three processes of the jugal trifurcate is located relatively far posteriorly. Consequently, the anterior process is more than twice the length of the posterior process (Figs. 2–4, 15). Moreover, although both the anterior and posterior processes are slightly concave ventrally, this is somewhat more pronounced along the longer anterior process, especially near its posterior origin. Together, these concavities produce a subtle curvature that extends along nearly the entire length of the jugal (Figs. 4, 12).

Ectopterygoids—The ectopterygoids (Figs. 1A–C, E, 2–4, 11, 12, 15) are short and robust, each consisting of a relatively large, wedge-shaped anterodorsal portion, the body, from which two processes project: a well-developed and somewhat twisted descending (pterygoid) process and a strongly tapered posterior process.

The body of the ectopterygoid, together with its relatively long, tapering posterior process, is subtriangular in ventral view (Fig. 3), its somewhat rounded anterolateral corner situated ventrally and medially adjacent to the convergence between the posterior end of the alveolar process of the maxilla, the anterior terminus of the anterior process of the jugal, and ventral edge of the descending process of the lacrimal (Figs. 2–4, 9D, 12). Anteriorly, the body of the ectopterygoid meets the palatal process of the maxilla in a broad transverse suture approximately even with the posterior margin of the posterior-most maxillary alveolus (Fig. 3); in contrast to the condition exhibited by other crocodyliforms, a distinct anterior process is lacking in *Simosuchus* (a trait that likely evolved in correlation with the anterior rotation of the transverse processes of the pterygoid [see below]). Dorsolaterally, the body of the ectopterygoid contacts the tapered posterior end of the alveolar process of the maxilla (Fig. 9D). Dorsomedially, it contacts the ventral margin of the orbital lamina of the lacrimal (Figs. 2, 12).

The posterior process of the ectopterygoid is subtriangular in cross-section (its corners being somewhat rounded) (Fig. 9F) and

is received posteriorly by a V-shaped notch that extends along the ventromedial edge of the anterior process of the jugal (Figs. 3, 9F, 12, 15). The posterior process projects posteriorly to a point coinciding with a transverse plane passing through the center of the orbit (Figs. 3, 4); thus, unlike the condition exhibited by most derived neosuchians, it does not contact (or even closely approach) the postorbital bar.

The descending process of the ectopterygoid projects ventrally from the body to meet the anterodorsal part of the expanded lateral terminus of the transverse process of the pterygoid (Figs. 2–4, 8H, 9E, 11, 12, 15). Here the laterally exposed portion of the descending process of the ectopterygoid, like that of the posteriorly adjacent transverse process of the pterygoid, is heavily pitted (Figs. 4, 11). A distinct ridge extending along the lateral surface of the descending process, gently curving from posterodorsal to anteroventral, is formed by an anteroventral continuation of the medial edge of the posterior process; this prominent ridge gives the descending process of the ectopterygoid a conspicuously twisted appearance in lateral view (Figs. 4, 11). This condition represents an autapomorphy of *Simosuchus clarki*. Finally, in at least some individuals, the anterior surface of the descending process of the ectopterygoid is pierced by several small foramina; these are visible on both ectopterygoids in UA 8679 and on the preserved right ectopterygoid in FMNH PR 2597, but appear to be absent from the right ectopterygoid found in association with UA 9754.

Pterygoid—The pterygoid (Figs. 1A–E, 2–6, 11–13, 15–17) is unpaired, its left and right halves being fully fused together. It is very large, forming a significant portion of the ventral part of the skull, and serves to bridge together the braincase, palate, and lateral portions of the dermatocranium. Near the midline, the internal nares (choanae) are contained almost completely within the pterygoid (Figs. 3, 7B, C, 8G, 9D–F, 15). The pterygoid consists of four primary processes: a relatively short dorsal (ascending) process, a pair of prominent and robust transverse processes, and a relatively long and complex anterior (palatal) process. Centrally, in the vicinity of the common origin of these four primary processes, a distinctly broad and dorsoventrally flattened region is formed, constituting the pterygoid plate.

The dorsal process of the pterygoid emanates anteriorly from the posterior part of the pterygoid plate, its origin from the latter being marked by a somewhat subtle V-shaped ridge, the apex of which is directed posteriorly (Figs. 3, 6). From this anterior origin, the process extends posterodorsally for a relatively short distance before establishing a broad contact centrally with the parabasisphenoid. HRXCT scans of the head skeleton of UA 8679 reveal that this contact is relatively extensive along the median sagittal plane, with the prominent rostrum (cultriform process) of the parabasisphenoid arching anterodorsally over the center of the dorsal process of the pterygoid for a distance of ~14 mm (Fig. 7A). However, the extent of this contact diminishes significantly to either side of the midline (Fig. 7B). Lateral to its central contact with the parabasisphenoid, the dorsal process is somewhat elaborated on each side to form a distinct posterolaterally projecting quadrate process, which articulates with the anteromedially projecting pterygoid process of the quadrate (Figs. 3, 8G, 15, 16, 17D).

Beginning from the anterior-most portion of the pterygoid plate and extending posteriorly, the line of fusion between the left and right halves of the pterygoid is demarcated by a mid-ventral longitudinal crest (Fig. 3). This crest is somewhat indistinct near its anterior end, but posteriorly, after it intersects the apex of the V-shaped ridge marking the anterior origin of the dorsal process, it becomes significantly more prominent, remaining strongly developed until it contacts the parabasisphenoid. This longitudinal crest, which bears strong similarity to one present in *Uruguaysuchus*, effectively divides the relatively broad

posteroventral surface of the dorsal process into two ventral concavities, each partially invaded by underlapping projections of the parabasisphenoid.

The dorsally exposed surfaces of the dorsal process of the pterygoid, including those of its posterolaterally projecting quadrate processes, are oriented predominantly dorsolaterally and are continuous anteriorly with the similarly oriented dorsal surfaces of the transverse processes and the anterior process (Figs. 4, 16, 17D). These combined dorsolateral surfaces formed along each side of the pterygoid converge at the midline, where they form a shallow mid-sagittal groove to receive the ventral margin of the anteriorly projecting parabasisphenoid rostrum (Fig. 9G).

Posterolaterally, the area of contact between the quadrate process of the pterygoid and the pterygoid process of the quadrate is relatively large, extending from the ventral surface of the skull dorsally to the trigeminal (CN V) foramen (Figs. 3, 8G, 15, 16, 17D). In the vicinity of the latter, the dorsal surface of the quadrate process of the pterygoid forms the floor of the trigeminal fossa, which is bounded posterolaterally by the quadrate and anteromedially by the laterosphenoid; further anterolaterally, the trigeminal fossa is continuous with a well-developed maxillo-mandibular groove, through which passed the combined maxillary and mandibular divisions of the trigeminal nerve (CN $V_2 + V_3$) (Fig. 16). The anterolateral orientation of the trigeminal foramen (and that of the associated trigeminal fossa and maxillo-mandibular groove) represents a uniquely derived condition in *Simosuchus clarki* among crocodyliforms.

Immediately lateral to its contact with the laterosphenoid, the dorsal process of the pterygoid forms a distinct dorsally directed pedicel for articulation with the ventral end of the slender, columnar epipterygoid (Fig. 16). Just medially adjacent to this articular pedicel, the pterygoid-laterosphenoid suture extends anteroventrally for a short distance before curving medially toward the parabasisphenoid rostrum (Fig. 4).

The transverse processes of the pterygoid are extraordinarily robust and approximately subtriangular in shape in sagittal section (Figs. 7E, 12); in these respects, they are somewhat similar to those exhibited by *Mariliasuchus*, *Notosuchus*, and *Baurusuchus*. Each originates centrally from the middle of the pterygoid plate and projects strongly laterally as well as anteroventrally (Figs. 3, 4, 6, 9G, 11, 15, 17D)—again bearing similarity to the condition seen in *Mariliasuchus*—before ultimately terminating distally in an expanded facet that is highly rugose, gently concave laterally, and, in lateral view, approximately amygdaloid in shape (Figs. 4, 11, 16). The anterodorsal margin of this expanded distal facet articulates with the posterior surface of the descending process of the ectopterygoid (Figs. 3, 4, 8H, 11, 12, 15, 16). From the center of this articulation, a well-defined but low crest extends posteriorly, medially, and slightly dorsally along the anterior margin of the transverse process (Figs. 7D, E, 9F, 15). This anterior crest ultimately forms the posterior margin of the internal narial fenestra and the anterolateral margin of the pterygoid plate before turning anteromedially to join the lateral margin of the ventral lamina of the anterior process. At this latter junction, on both sides of the pterygoid, a ventrally projecting tubercle is formed (Figs. 3, 6).

In addition to the well-developed crest that runs along the anterior margin of each transverse process, an even more sharply defined crest extends along the ventral margin of each of these processes (Figs. 3, 6, 7D, E, 8H, 9G, 12, 15). On each side, this ventral crest originates from—and in large part defines—the posterior border of the pterygoid plate (Figs. 3, 6). From this central origin, it extends laterally, anteriorly, and ventrally along a gently curvilinear path, ultimately terminating laterally near the ventral apex of the expanded distal facet of the transverse process (Figs. 3, 15). We interpret this ventral crest in *Simosuchus* as being homologous with the posterior edge of the transverse process of the

pterygoid in other crocodyliforms. Between the anterior and ventral crests of each transverse process is a relatively long but shallow anteroventromedially directed trough that merges medially with the flattened posteroventral surface of the pterygoid plate (Figs. 3, 15).

The dorsal surfaces of the transverse processes of the pterygoid are posterodorsally convex, and are continuous medially with the dorsal surfaces of the dorsal process and the anterior process (Figs. 2, 17D). Running along this convex dorsal surface of each transverse process is a distinct elongate tuberosity, extending laterally approximately one-half the length of the process (Figs. 2, 6, 7E). In posteroventral view, the central portion of this dorsal tuberosity is seen to be raised into a relatively prominent triangular projection, the apex of which is directed posterodorsally. Further medially, the thin dorsolateral lamina of the anterior process, which forms a continuous roof over the internal nares, is seen to arise from the anterodorsal surfaces of the proximal portions of the transverse processes (i.e., where they converge toward the midline) (Figs. 9G, 17D). On each side, a sulcus formed between the proximal-most part of this dorsolateral lamina of the anterior process and the anterior crest of the transverse process expands posteromedially, with this expansion ultimately creating a relatively deep, cup-like, posterior fossa within each internal naris (Figs. 7A, 9G, 15).

The anterior process of the pterygoid contributes to the formation of the central portion of the posterior part of the bony palate, as well as to the nasopharyngeal canals and their posterior openings, the internal nares (secondary choanae sensu Witmer, 1995) (Figs. 3, 17). The process therefore presents a relatively complex morphology, and one that is not fully preserved in any known specimen of *S. clarki*. The anterior process is most completely preserved in UA 8679, and most of the following description is based predominantly on the morphology exhibited by this specimen, as interpreted through both direct visual observations and careful scrutiny of serial HRXCT slices and three-dimensional digital reconstructions generated from those slices. However, we supplement our description with observations made on the skull of FMNH PR 2597, in which the anterior process of the pterygoid is broken but partially preserved.

The anterior process of the pterygoid consists of three distinct laminae: a thin dorsolateral lamina, which forms the roof and lateral walls of the internal nares and nasopharyngeal canals; a much thicker ventral lamina, which contributes to the formation of the internarial (choanal) septum posteriorly and to the central portion of the posterior part of the bony palate anteriorly; and a very thin vertical lamina, which forms a median septum between the left and right internal nares and nasopharyngeal canals.

As described above, the dorsolateral lamina of the anterior process of the pterygoid originates from the dorsal margins of the proximal-most portions of the paired transverse processes (Figs. 9G, 17D). From this posterior origin, it extends anteriorly, forming a thin, dorsolaterally convex roof over the internal nares (Figs. 3, 9D–F, 15). Along the dorsal surface of this roof, the left and right halves of the lamina converge at the midline to form a distinctly angulated longitudinal ridge that is contacted dorsally by the ventral ends of the descending processes of the prefrontals (i.e., prefrontal pillars) (Figs. 9F, 13). Through the creation of this roof overlying the internal nares, the dorsolateral lamina also comes to define the free lateral margin of each internal narial fenestra (Figs. 3, 15).

Near the anterior ends of the internal nares, the lateral margin of each half of the dorsolateral lamina of the anterior process of the pterygoid contacts the ascending process of the ipsilateral palatine in a ventrally concave suture (Figs. 3, 9C, 17B, D). Immediately anterior to this, the lateral margin of the dorsolateral lamina descends further ventrally to contact the dorsal surface of the palatal process of the ipsilateral maxilla (Fig. 17A, D). This

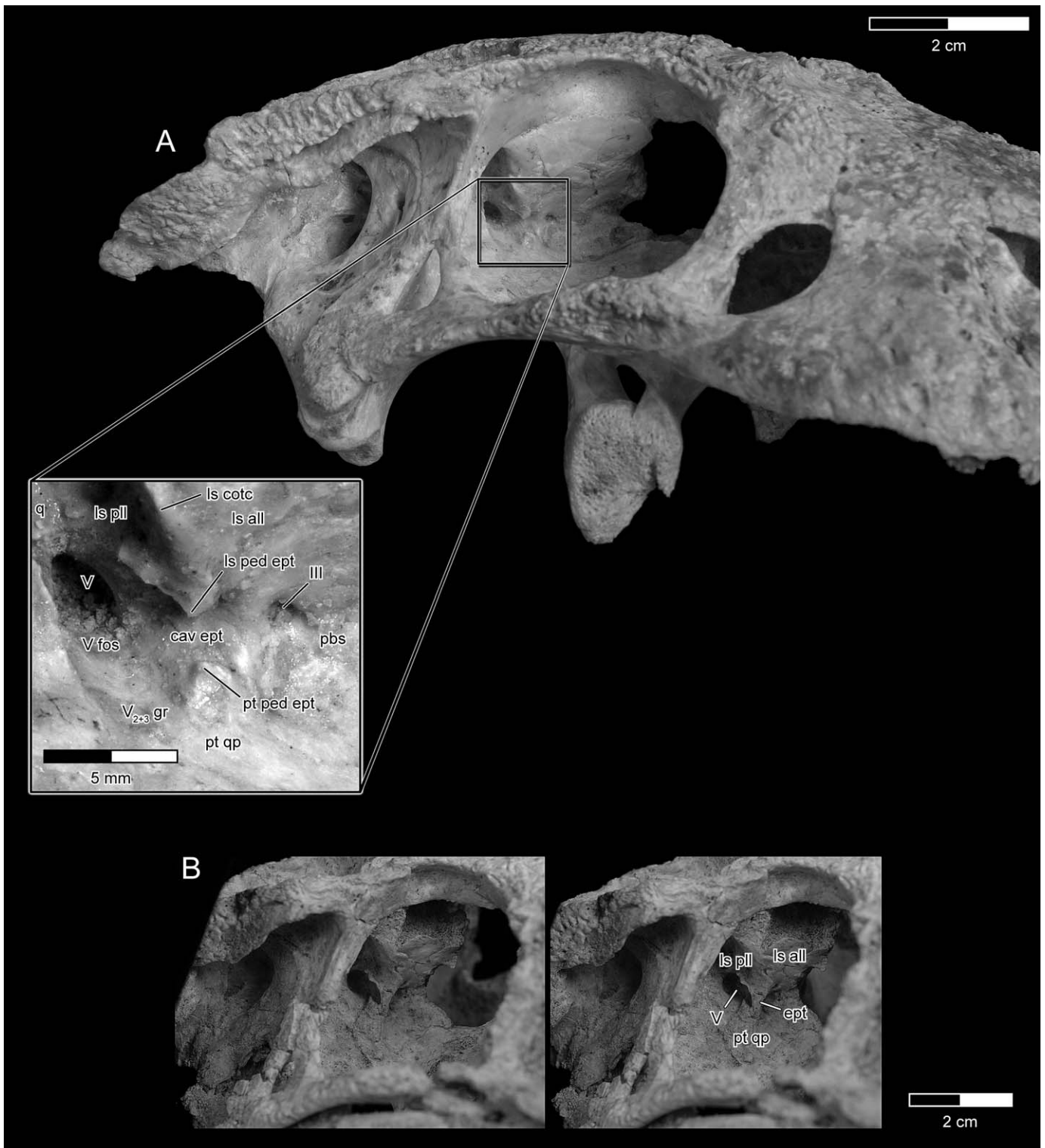


FIGURE 16. The epipterygoid and associated structures in *Simosuchus clarki*. **A**, photograph in oblique anterodorsolateral view of the right orbitotemporal region of the holotype, UA 8679 (upper right), with high-magnification inset (lower left), showing the distinct pedicels on the laterosphenoid and pterygoid for articulation with the epipterygoid (missing in this specimen). **B**, stereophotographic oblique anterodorsolateral views of the right orbitotemporal region of FMNH PR 2597, showing the largely intact, columnar epipterygoid preserved in this specimen. See Appendix 1 for anatomical abbreviations.

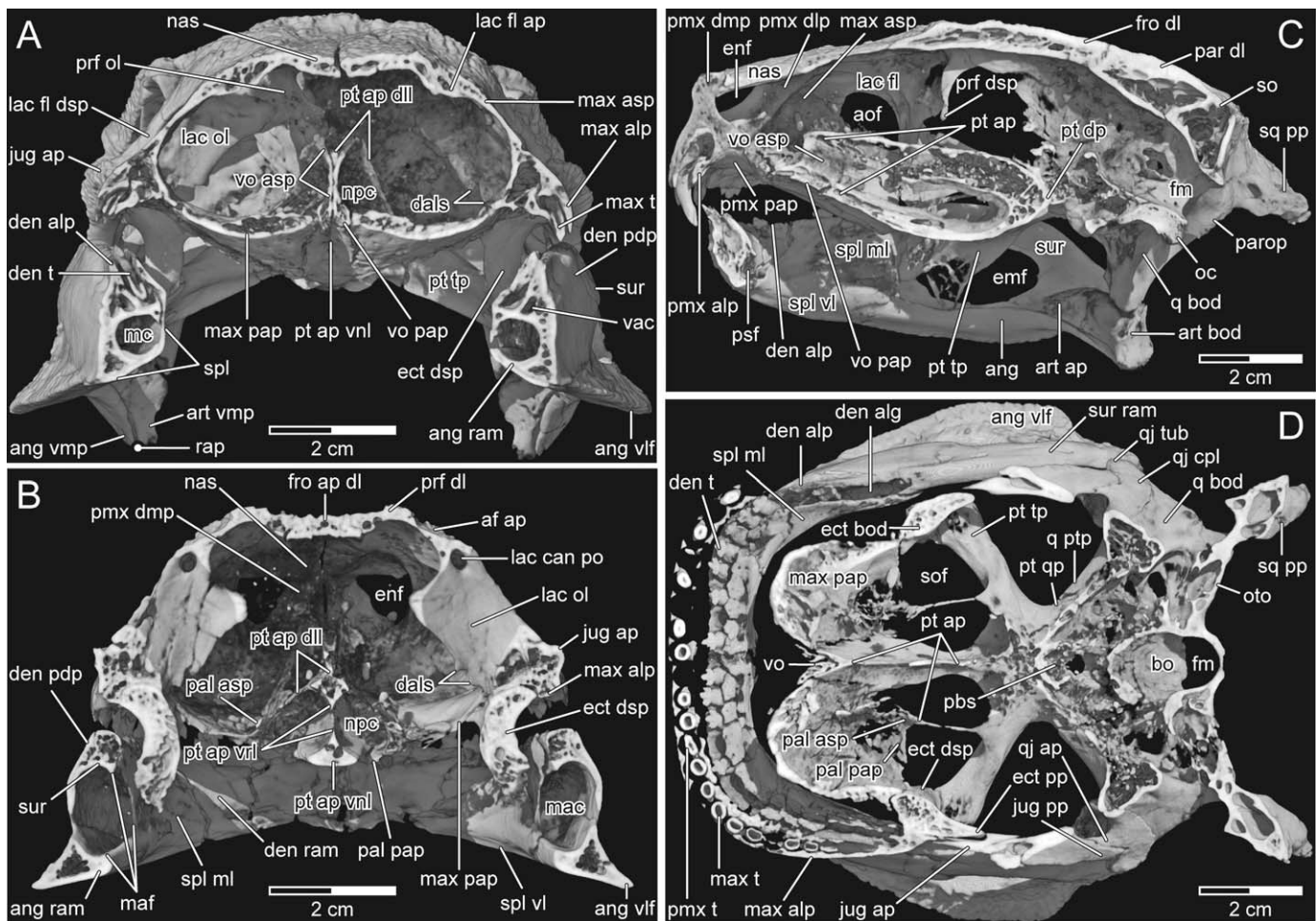


FIGURE 17. Morphology of the bony palate, nasal cavities, and nasopharyngeal canals of *Simosuchus clarki*, as seen in cutaway views through a three-dimensional digital reconstruction of the skull and lower jaw of the holotype (UA 8679) generated from HRXCT scans. In this reconstruction, remaining matrix has been removed digitally so as to provide unobstructed views of unprepared internal regions of the head skeleton. **A**, anterior view from a transverse plane passing through the anterior ends of the nasopharyngeal canals (i.e., primary choanae sensu Witmer, 1995). **B**, posterior view from a transverse plane passing through the posterior ends of the nasopharyngeal canals (i.e., internal nares, or secondary choanae sensu Witmer, 1995). **C**, medial view from the median sagittal plane. **D**, dorsal view from a frontal plane passing through the internal nares. (Note: ‘virtual preparation’ of this specimen has resulted in the digital deletion of portions of the thinnest laminae of bone throughout the head skeleton, such as those that surround the nasopharyngeal canals and internal nares; these thin laminae of bone are in actuality better preserved in this specimen than is depicted in this computer-generated reconstruction.) See Appendix 1 for anatomical abbreviations.

creates a relatively flat, ventrolaterally sloping surface that forms the dorsolateral wall of the nasopharyngeal canal (Figs. 9C, 17A, B). Finally, from the anterior-most point along this ventrolateral contact with the palatal process of the maxilla, the lateral margin of the dorsolateral lamina sweeps abruptly anteriorly, medially, and dorsally to contact the dorsolateral terminus of the ascending process of the ipsilateral vomer. This creates a subtriangular anterior opening to each nasopharyngeal canal (primary choana sensu Witmer, 1995), bounded medially and dorsomedially by the ascending process of the vomer and dorsolaterally by the anterior process of the pterygoid (Figs. 9C, 17A).

Also extending to the transverse level of the anterior openings of the nasopharyngeal canals, but not participating in their formation, is a median projection of the dorsolateral lamina (Fig. 7A) that terminates anteriorly by insinuating itself between the two divergent ascending processes of the vomers (Figs. 8E, 17A, C). This sharply tapered midline projection represents an anterior continuation of the prominent ridge that extends along the mid-dorsal surface of the lamina where it arches over the inter-

nal nares. This ridge becomes independent of the remainder of the dorsolateral lamina just posterior to the anterior origin of the nasopharyngeal canals, where the lateral portions of each half of the lamina diverge laterally toward the palatal process of the maxilla.

The ventral lamina of the anterior process of the pterygoid originates from the anterior part of the pterygoid plate, its lateral margins being continuous with the anterior crests of the transverse processes (Figs. 3, 15). It is relatively narrow at its posterior end, measuring ~5 mm mediolaterally. However, near the anteroposterior midpoint of the internal narial fenestrae, the lamina begins to gradually widen, ultimately reaching a maximum mediolateral width of ~10 mm adjacent to the anterior margins of the fenestrae. Throughout this posterior portion of its course, the ventral lamina of the anterior process contributes (along with the vertical lamina) to the formation of an extensive internarial (choanal) septum (Figs. 3, 9D–F, 15, 17D). Throughout all but the anterior-most part of this posterior portion of the lamina, it presents a smooth and nearly flat ventral surface.

Anterior to the internal narial fenestrae, the ventral lamina of the anterior process of the pterygoid remains moderately wide (relative to its much narrower posterior root) and extends anteriorly along the midline of the posterior part of the bony palate (Fig. 3). In doing so, it insinuates itself between the palatal processes of the left and right palatines (Figs. 9C, 17B, D), and between the posterior halves of the palatal processes of the left and right maxillae (Figs. 8G, 17A, D), before ultimately contacting the palatal processes of the vomers anteriorly (Figs. 7A, B, 17A, C, D). In contrast to the several overlapping articulations established between the palatal processes of neighboring bones throughout the anterior part of the palate, the ventral lamina of the anterior process of the pterygoid meets all of its neighboring palatal elements in simple end-to-end contacts. Along its anterior (palatal) portion, the ventral lamina is prominently concave ventrally, thereby contributing to, along with the vomer, a longitudinally oriented mid-ventral trough along the posterior part of the bony palate (Figs. 3, 9C, 17A). At least four foramina pierce the ventral lamina of the anterior process along its length; two of these are located adjacent to the anterior margins of the internal narial fenestrae, whereas two others are located near the anterior terminus of the lamina. One of these four foramina, located in the ventral midline immediately posterior to the posterior terminus of the intervomerine suture, is significantly larger than the other three.

Finally, extending between the dorsolateral and ventral laminae of the anterior process of the pterygoid, and intersecting both perpendicularly, is an extremely thin vertical lamina (Fig. 4). It originates posteriorly from the anterodorsal surface of the pterygoid plate and extends anteriorly within the median sagittal plane to contact the ascending processes of the vomers. In so doing, the vertical lamina of the anterior process of the pterygoid creates a midline septum that divides the left and right internal nares posteriorly, and the left and right nasopharyngeal canals anteriorly (Figs. 9E, F, 17B).

HRXCT scans of the head skeleton of UA 8679 demonstrate that nearly the entire pterygoid is heavily pneumatized, with particularly large vacuities in the transverse processes, and extensively reinforced internally by numerous bony trabeculae (Figs. 7A–E, 8G–I, 9D–G, 12, 17B–D). However, one noteworthy exception to this generalization is the extremely thin dorsolateral lamina of the anterior process that arches over the internal nares and nasopharyngeal canals; this region of the bone remains non-pneumatized.

Palatines—The palatines (Figs. 1B, C, E, 3, 4) are preserved on both sides of the skull of the holotype (UA 8679) of *Simosuchus clarki*. In this specimen, the right element is better preserved than the left; however, both exhibit damage in certain places. In addition, both palatines are partially preserved with the head skeleton of FMNH PR 2597, but significant portions of each are missing.

The palatines are relatively small, but nevertheless contribute to the formation of the bony palate, the internal narial fenestrae, and the suborbital fenestrae. Each consists of a horizontally oriented palatal process and a vertically oriented ascending process.

The overall shape of the palatal process of the palatine is best preserved on the right side of the skull of UA 8679, despite the posteromedial corner of the element being broken off (Fig. 3). In general, the shape of the process approximates that of a square, but one with a short rectangular extension that projects medially from its anterior half. This rectangular anteromedial extension contacts the lateral margin of the ventral lamina of the anterior process of the pterygoid (Figs. 3, 9C). However, the palatal process of the palatine shares its most extensive contact along its lateral and anterior borders with the palatal process of the maxilla (Figs. 3, 4, 7C, D, 8G, 9C, 17B, D). The posterior border of the square (main) portion of the palatal process of the palatine forms the medial half of the anterior border of the suborbital fenestra, whereas the posterior border of the rectangular medial projection

off of the palatal process forms the anterior margin of the internal narial fenestra (Fig. 3). The palatal process exhibits a smooth, gently convex ventral surface. In addition, a small, rounded, ventrally directed tubercle is located on its ventral surface just anteriorly adjacent to the center of its main posterior border (i.e., near the anteromedial corner of the suborbital fenestra).

The ascending process of the palatine arises from the dorsal surface of the palatal process and projects dorsomedially toward the anterior process of the pterygoid. It ultimately contacts the lateral margin of the ipsilateral half of the dorsolateral lamina of the latter, thereby forming an anterodorsally directed suture that extends along the lateral walls of the internal naris (posteriorly) and nasopharyngeal canal (anteriorly) (Figs. 3, 9C, 17B, D).

Like other neighboring elements of the palate, the palatines are pneumatized (Figs. 7C, D, 8G, 9C). This pneumatization is most extensive throughout the posterior portions of the palatal processes. However, the relatively broad bases of the ascending processes are also pneumatized.

It bears emphasis that the most peculiar feature of the palatines in *S. clarki* relates not to the morphology of these bones themselves, but rather to the separation between them. The palatal processes of the left and right palatines are separated at the posterior end of the bony palate by the strongly developed ventral lamina of the anterior process of the pterygoid (Fig. 3). This condition is unique among crocodyliforms.

Vomers—The paired vomers (Figs. 1B, 3) are rather small in size and relatively simple in their overall morphology. Each consists of a nearly horizontally oriented palatal process and a vertically oriented ascending process.

The palatal process of each vomer is fully exposed in ventral view and is approximately semi-elliptical in shape, with its major axis positioned immediately adjacent to the median sagittal plane of the skull (Fig. 3). This portion of the bone contacts the posteromedial edge of the palatal process of the premaxilla anteriorly, the central portion of the medial edge of the palatal process of the maxilla laterally, and the anterior edge of the anterior process of the pterygoid posteriorly. Medially, the left and right palatal processes meet at the midline in a relatively straight intervomerine suture (Figs. 3, 9B, 17A). The palatal processes are slightly concave ventrally, thus forming a shallow vomerine fossa anterior to the center of the bony palate (Figs. 3, 7A, 9B). Like the palatal processes of the premaxillae and maxillae, those of the vomers are pneumatized (Figs. 7B, 9B, 17A, C, D). In addition, each palatal process is pierced by a relatively large foramen; that on the right vomer is positioned posteriorly, whereas that on the left vomer is positioned anteriorly.

Although a palatal exposure of the vomers appears to have been relatively widespread among basal crocodylomorphs (e.g., *Sphenosuchus acutus*, *Dibothrosuchus elaphros*, *Litargosuchus leptorhynchus*), this condition is unique to *Simosuchus clarki* among known basal mesoeucrocodylians. As pointed out by Buckley et al. (2000), the exposure of the palatal processes of the vomers in this taxon, as well as their general shape and position between the palatal processes of the premaxillae and maxillae, most closely approximates (among crocodyliforms) that exhibited by the extant crocodylian *Melanosuchus niger*. Much narrower and far more posterior palatal exposures of the vomers are also seen in the goniopholidid *Calsoyasuchus valliceps* and in the extant crocodylian *Tomistoma schlegelii* among neosuchians.

From the medial edge of the palatal process of each vomer arises a vertically oriented ascending process. Along the anterior half of the vomer, the ascending process exists as little more than a relatively short, dorsally projecting crest (Fig. 9B). Throughout this anterior region, the left and right ascending processes are in direct sutural contact with one another. Approximately midway along the length of the vomer, however, the ascending process abruptly increases in height (Figs. 9C, 17C). It first rises directly vertically, but as it approaches the anterior-most tip of the

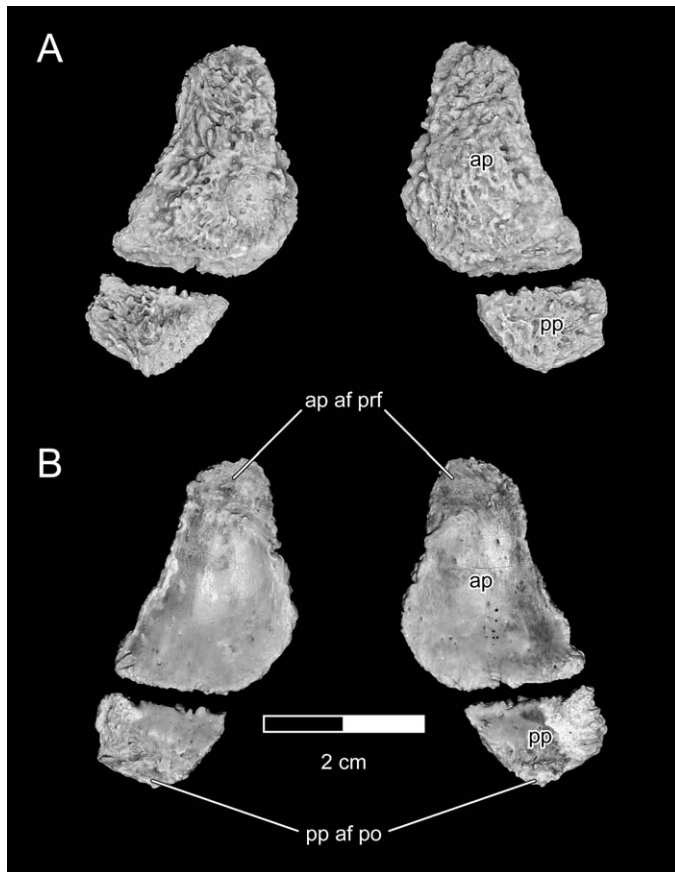


FIGURE 18. Disarticulated anterior and posterior palpebrals from the holotype (UA 8679) of *Simosuchus clarki*. Photographs in **A**, dorsal; and **B**, ventral views. Anterior to top and lateral to sides in both views. See Appendix 1 for anatomical abbreviations.

anterior process of the pterygoid, it curves gently laterally (Fig. 8E), ultimately contacting the dorsomedial edge of the dorsolateral lamina of the anterior process of the pterygoid (Fig. 17A). Thus, the ascending process of the vomer forms the medial and dorsomedial margins of the anterior opening of the nasopharyngeal canal (primary choana sensu Witmer, 1995), as well as the medial and dorsomedial walls of the anterior half of the canal itself.

Other Dermal Ossifications Associated with the Skull

Palpebrals—The palpebrals (Figs. 1A, B, D, 2, 3, 5, 18) are dermal ossifications, extrinsic to the skull proper, that develop within the fixed upper eyelids (Romer, 1956). In *Simosuchus clarki*, there are two on each side, one anterior and one posterior, with the anterior one being the much larger of the two. Together, the anterior and posterior palpebrals form a relatively expansive bony roof overhanging the orbit that extends laterally 1–2 cm from the true dorsal margin of the orbital fenestra (Fig. 2). Owing to the relatively large size and dorsal position of the palpebrals, the effective orientation of the orbits in *S. clarki* is almost purely lateral.

The anterior palpebral has the shape of a slightly non-planar (ventrally concave) irregular pentagon, but one with slightly rounded corners (Fig. 18). At its anteromedial corner, it bears a relatively large triangular facet on its ventral surface (Fig. 18B). This corresponds with a similarly shaped dorsally facing facet located on the lateral-most part of the dorsal lamina of the pre-

frontal, immediately anterior to the anterodorsal corner of the orbital fenestra (Figs. 2, 4, 5, 7D, 9E, 11–13). With these two facets in articulation with one another, the relatively narrow anterior edge of the anterior palpebral is oriented almost transversely (although it does angle slightly from anteromedial to posterolateral) and is positioned directly against the posterior edge of the lateral-most portion of the preorbital crest (Fig. 2). The anteromedial and posteromedial edges of the anterior palpebral very closely parallel the dorsal margins of the orbital fenestra (Fig. 2). The former extends posteromedially along the posterolateral edge of the prefrontal; it is relatively long and straight. The latter extends posterolaterally along the anterolateral edge of the main portion of the frontal; it is relatively short and slightly convex posteromedially. The obtuse angle between these two edges lies immediately adjacent to the posterior, transverse portion of the prefrontofrontal suture. Similarly, the angle between the posteromedial and posterior edges lies closely adjacent to the postorbifrontal suture. From this point of intersection, the posterior edge extends almost directly laterally (though very slightly anteriorly as well); it is relatively wide and straight, and closely parallels the anterior edge of the posterior palpebral. The posterior edge of the anterior palpebral is distinctly beveled (from anterodorsal to posteroventral) along its entire width (Fig. 18A). Finally, the free lateral edge of the anterior palpebral extends posterolaterally over the anterior three-quarters of the orbit (Fig. 2); it is the longest of the five sides of the bone and is slightly concave anterolaterally.

The anterior palpebral exhibits a moderate amount of sculpturing across its gently convex dorsal surface (Figs. 2, 18A), but is smooth across its concave ventral (orbital) surface (Fig. 18B). However, the latter surface is pierced by numerous small foramina. In addition, despite being relatively thin (dorsoventrally), it exhibits a distinctly trilaminar structure; CT scans of FMNH PR 2597 taken when its left anterior palpebral was still in place reveal a central layer of cancellous bone sandwiched between dorsal and ventral layers of compact bone.

The posterior palpebral is approximately trapezoidal in shape, having two nearly parallel edges (anterior and posterior) and two distinctly non-parallel edges (medial and lateral) (Figs. 2, 18). The anterior edge is the longest of the four and is oriented nearly transversely, closely paralleling the posterior edge of the anterior palpebral. The medial edge is gently convex, curving posterolaterally along the anterolateral edge of the anteromedial process of the postorbital. The posterior and lateral edges are both relatively short and straight, with neither contacting other bones.

The posterior palpebral is supported by a prominent triangular shelf that projects anterolaterally from the central part of the postorbital (Figs. 2, 4, 5, 7E, 9I, J, 11). Correspondingly, the posterior palpebral bears a dorsal recess along the posterior half of its ventral surface (Fig. 18B), into which the anterior half of the postorbital shelf projects. However, the roof of this recess is rather rugose, in contrast to the smooth ventral articular facet at the anteromedial corner of the anterior palpebral. Similarly, the dorsal (articular) surface of the postorbital shelf is somewhat rugose as well.

Like the anterior palpebral, the posterior palpebral exhibits sculpturing across its dorsal surface (Figs. 2, 18A), but is comparatively smooth along the anterior half of its ventral (orbital) surface (i.e., anterior to its dorsal recess) (Fig. 18B), with the latter surface bearing only a small number of foramina.

Supratemporal Ossifications—In the holotype specimen (UA 8679) of *Simosuchus clarki*, two relatively small and very flat bones are preserved within each supratemporal fossa. These supratemporal ossifications (Figs. 1A, 2, 14) are interpreted as osteoderms that were, in life, embedded within the skin overlying each supratemporal fenestra. As preserved, the larger anterior ossification is positioned with its deep surface facing anteroventrally against the posteromedial surface of the anteromedial

process of the postorbital. The smaller posterior ossification is positioned with its deep surface facing posteroventrally against the anterior surface of the dorsal part of the quadrate (i.e., where the dorsal primary head and anterodorsal process of the latter curve to meet one another along the posterior wall of the adductor chamber). Neither of these ossifications is known to be present in any other crocodyliform taxa.

Each anterior supratemporal ossification in UA 8679 exhibits a nearly straight lateral edge but a distinctly convex medial edge, the latter curving toward the former at its anterior end, thus producing a bluntly rounded anterolateral apex (slightly notched or broken on the left side) (Figs. 2, 14). The proximity of this rounded apex to the similarly rounded anterolateral corner of the supratemporal fenestra, taken together with the correspondence in shape between the lateral margins of both the ossification and fenestra, suggests that the anterior supratemporal ossification was positioned in life at the anterolateral corner of the fenestra, presumably in an approximately horizontal orientation. However, as preserved, the ossification is inclined strongly vertically, with its anterolateral apex projecting both dorsally and anteriorly from the supratemporal fossa.

The posterior part of the anterior supratemporal ossification is preserved only on the left side of UA 8679. Here the posterior half of the bone rather closely mirrors the anterior half in its general morphology. This gives the ossification a nearly semilunar overall shape.

The anterior supratemporal ossifications are marked by numerous rugosities across their superficial surfaces and along their edges. They are significantly larger than the posterior ossifications (Figs. 2, 14), with the most complete one (left side of UA 8679) measuring ~12 mm in maximum length and ~8 mm in maximum width.

The most completely preserved of the two posterior supratemporal ossifications in UA 8679 is the right one. It approximates the shape of an equilateral triangle, but one with slightly rounded corners (Figs. 2, 14). Each of its three sides measures ~7.5 mm in length. It is faintly rugose both across its superficial surface and along its sides. Its anterior edge, which faces anteroventrally and slightly medially as preserved, bears a prominent central tubercle and two smaller lateral tubercles. The left posterior supratemporal ossification in UA 8679 is similar in shape to the right one, but is slightly smaller. Its sides and corners are more rounded, and it is significantly smoother across its superficial surface and along its sides.

Supratemporal ossifications were not preserved in either FMNH PR 2596 or FMNH PR 2597.

Bones of the Chondrocranium

Laterosphenoids—The laterosphenoids (Figs. 1C, 4, 11, 14–16) form the anterolateral walls of the braincase. In the holotype specimen (UA 8679) of *Simosuchus clarki*, the right laterosphenoid is better preserved than the left one. In FMNH PR 2597, the left and right laterosphenoids exhibit similar levels of preservation relative to one another. Each laterosphenoid is sharply angled to form a broad, anterolaterally facing lamina and a narrower, posterolaterally facing lamina (Figs. 8C–E, 10A, 16). Thus, *S. clarki* possesses a well-developed cotylar crest (sensu Clark et al., 1993) separating the anterolateral and posterolateral laminae of the laterosphenoid at an approximately right angle.

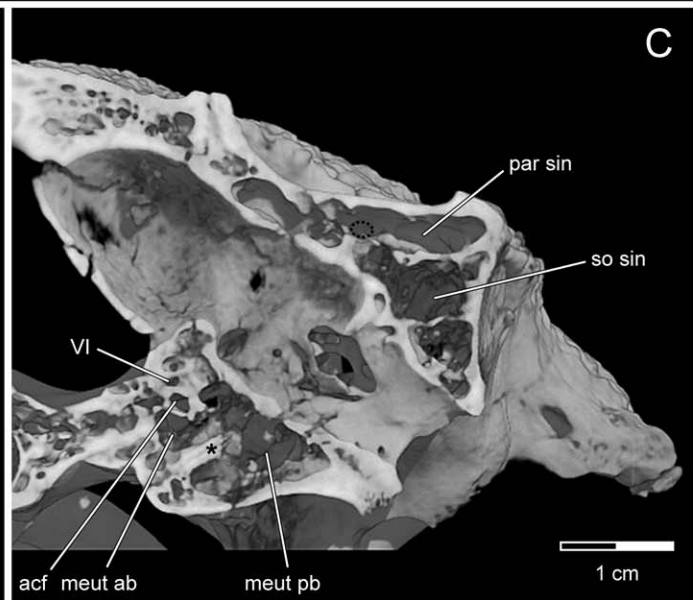
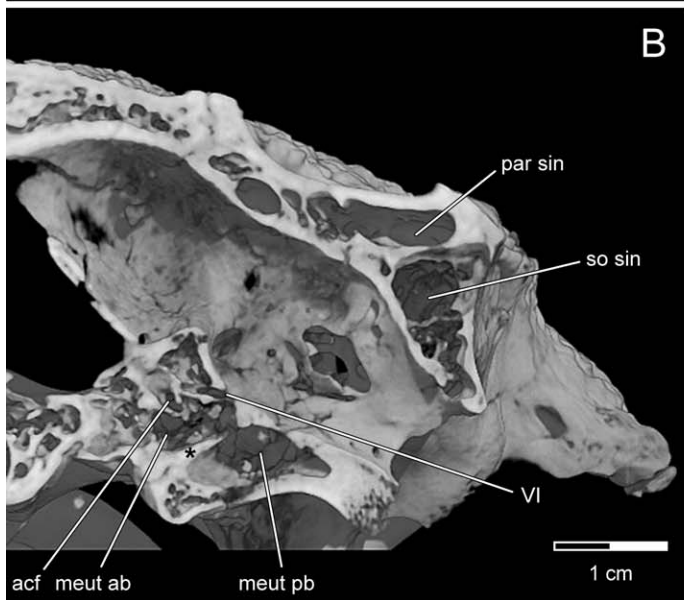
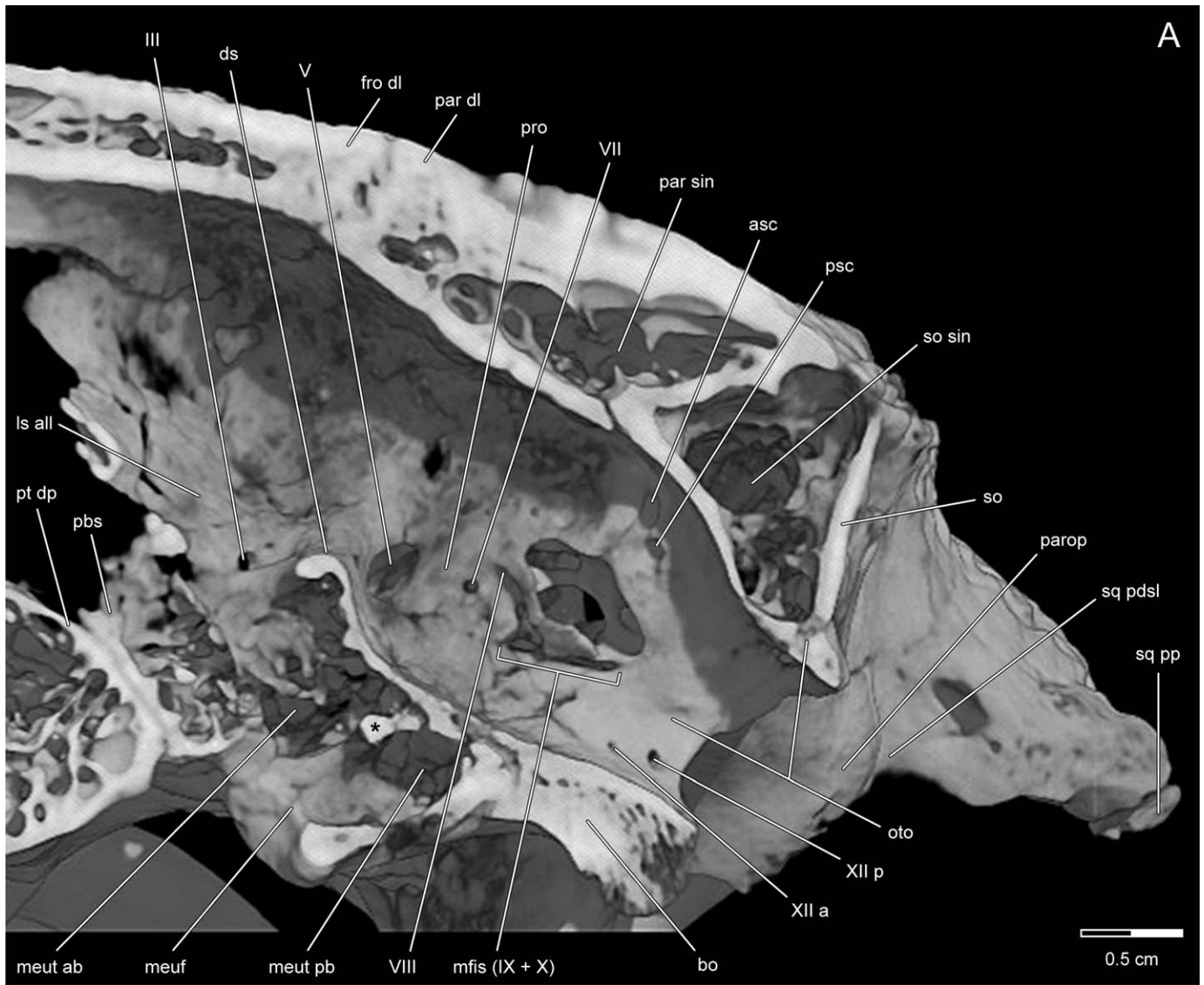
The anterolateral laminae of the left and right laterosphenoids contact the descending processes of the frontal dorsally and approach one another as they near the median sagittal plane, briefly making contact just dorsal to the parabasisphenoid rostrum (Figs. 4, 8D, E, 9H, 10A, 11, 16). The dorsal margin of the posterolateral lamina shares a short contact with the descending process of the parietal before curving anterolaterally toward the capitata process (Fig. 9J). The latter process is anteroposteriorly thin

in *S. clarki* and, in contrast to the condition exhibited by most other mesoeucrocodylians, it is not a rounded articular process, nor does it fill a corresponding depression on the ventral surface of the laterosphenoid. Rather, it projects into a shallow slot on the posterior surface of the orbital lamina of the postorbital, near the intersection of its anteromedial and descending processes (Figs. 8C, 9I, 10A, 15). The posterior margin of the posterolateral lamina of the laterosphenoid meets the quadrate broadly in a vertically oriented suture dorsal to the trigeminal foramen (Fig. 16).

A very distinct tensor crest is located on the ventral half of the cotylar crest just dorsal to the laterosphenoid contact with the epipterygoid (Fig. 16). The tensor crest serves as the attachment site for the *M. tensor periorbitae*, a component of the constrictor internus dorsalis (CID) muscle group (Holliday, 2006). Dorsal to this, the laterosphenoid of *Simosuchus* lacks a distinct impression or crest ('longitudinal oblique crest' of Iordansky [1964] or 'cotylar crest' of Busbey [1989]), corresponding to the attachment site for a muscle identified by Iordansky (1964) and Busbey (1989) as the *M. adductor mandibulae externus profundus*, but more recently by Holliday (2006, 2009) as the *M. pseudotemporalis superficialis*.

In UA 8679, the epipterygoid is missing, thereby exposing the cavum epiptericum and the ventral contact of the laterosphenoid with the parabasisphenoid and pterygoid (Figs. 4, 7B, C, 9H–J, 16). The contact between the laterosphenoid and parabasisphenoid is narrow, with the laterosphenoid forming a mediolaterally narrow pedicle ('body' of the laterosphenoid sensu Holliday, 2006), an ossified derivative of the embryonic *pila antotica*. It is on this pedicle that the remainder of the laterosphenoid rests (Fig. 16). Medial to the pedicle, a ventrolaterally facing foramen, which transmitted the oculomotor nerve (CN III), is present (Figs. 9H, 16). Dorsolateral to the oculomotor foramen, a very small foramen pierces the anterior surface of the laterosphenoid roughly at the midpoint of the tensor crest; this foramen represents the exit for the trochlear nerve (CN IV) (Figs. 8D, 9H). Ventral to the oculomotor foramen there is yet another even smaller foramen that itself sits within a shallow depression on the parabasisphenoid and transmitted the abducens nerve (CN VI) (Fig. 9H). A shallow groove extends anterodorsally from the trochlear foramen along the lateral part of the anterolateral lamina of the laterosphenoid.

The trigeminal foramen exits into a deep fossa that the trigeminal (Gasserian) ganglion would have occupied (Fig. 16). This fossa is bordered posterolaterally by the dorsal primary head of the quadrate, dorsomedially by the laterosphenoid and prootic, and anteriorly by the epipterygoid and a small portion of the dorsal process of the pterygoid. In UA 8679, the epipterygoid is missing, thus exposing the small, dorsally directed pedicel on the dorsal process of the pterygoid for articulation with the epipterygoid, and the corresponding ventrally directed articular pedicel on the laterosphenoid (Fig. 16). With the epipterygoid in articulation with these small pedicels, as it is on both sides of FMNH PR 2597 (Fig. 16), it forms the lateral wall of the cavum epiptericum and serves to subdivide the deep fossa around the trigeminal foramen into a large, anterolaterally directed maxillomandibular foramen and a smaller ophthalmic foramen directed anteriorly and hidden from view laterally by the epipterygoid itself. There is a small notch in the dorsal surface of the rim of the maxillomandibular foramen in UA 8679 and FMNH PR 2597 (Fig. 16) that likely corresponds to the path of the supraorbital nerve (Holliday, 2006). A very small flange of bone from the laterosphenoid is associated with this notch. This small flange may be homologous with the 'caudal bridge,' a novel structure of the laterosphenoid recently described by Holliday (2006). Conversely, this flange in *S. clarki* may simply be the result of a prominent rim to the maxillomandibular foramen and the notch formed by the path of the supraorbital nerve.



Prootics—The prootics are not exposed externally. However, their internal structure, which is relatively well preserved in the holotype (UA 8679) of *Simosuchus clarki*, is readily visualized in HRXCT scans (Fig. 19).

The prootic of *S. clarki* is typically crocodyliform in its overall shape. It shares a posteriorly inclined contact with the opisthotic portion of the otoccipital and forms the anterior half of the tympanic bulla. The anterior semicircular canal can be seen arching anterolaterally, through the prootic, and then terminating in the region that would have been occupied by the anterior ampulla. The metotic fissure incises the posteroventral margin of the prootic below the tympanic bulla. At the anterior end of the metotic fissure, a small foramen corresponding to that for the glossopharyngeal nerve (CN IX) pierces the prootic. Dorsal to this foramen, a larger one, for the vestibulocochlear nerve (CN VIII), is present at the base of the tympanic bulla. Anterior to these two foramina, the facial nerve (CN VII) exits through the prootic. Finally, the prootic forms the posterolateral boundary of the foramen for the trigeminal nerve (CN V). Dorsal to the trigeminal foramen, the prootic shares a long, posteriorly slanted contact with the laterosphenoid, with the dorsal-most surface of the prootic contacting the parietal.

Parabasisphenoid—As in other crocodyliforms, the endochondral basisphenoid is fused together with the dermal parasphenoid in *Simosuchus clarki*. Thus, here and throughout our description, we recognize the compound nature of this element by referring to it as the parabasisphenoid.

The parabasisphenoid (Figs. 1B, C, 3, 4, 15, 20) has almost no exposure along the floor of the braincase. In both lateral and posterior views of the latter, it is not visible (Figs. 4, 6). Only in ventral view is the contribution of the parabasisphenoid to the floor of the braincase evident, in which it is visible as a small strip of bone measuring ~20 mm transversely and ~6 mm anteroposteriorly between the basioccipital and the dorsal process of the pterygoid (Fig. 3). This contrasts with the broad ventral exposure of the parabasisphenoid exhibited by many other basal mesoeucrocodylians (e.g., *Araripesuchus tsangatsangana*, *Hamadasuchus rebouli*, *Mariliasuchus amarali*, *Sphagesaurus huenei*). However, it is common among notosuchians for the parabasisphenoid to be visible only in ventral view due to the strong anteroventral inclination of the occipital surface. This is particularly evident in taxa such as *Malawisuchus mwakasyungutiensis*, *Mariliasuchus amarali*, and *Notosuchus terrestris*.

The anterior contact between the parabasisphenoid and the dorsal process of the pterygoid is M-shaped in ventral view due to a thin, posteriorly directed crest running along the ventral midline of the dorsal process of the pterygoid; this crest serves to subdivide the parabasisphenoid into two discrete lobes as it extends toward its anterior border (Fig. 3). The exoccipital portions of the otoccipital do not contact the parabasisphenoid and the pterygoid process of the quadrate shares only a much abbreviated contact with it anteromedial to the lateral Eustachian foramen (Figs. 3, 8G, 9H, I, 15). The entire ventral exposure of the parabasisphenoid is anteroposteriorly narrower than that of the basioccipital (Fig. 3), and it rests in a raised area anterior to the median Eustachian opening (foramen intertympanicum) (Figs. 3, 7A, B, 17C, 19). The median and lateral Eustachian

foramina are situated completely between the parabasisphenoid and basioccipital (Figs. 3, 7A, B, 9I, 15, 19, 20), as in all mesoeucrocodylians except *Mariliasuchus amarali* and *Sphagesaurus huenei*.

The parabasisphenoid rostrum (cultriform process) is medio-laterally compressed and dorsoventrally short (Figs. 4, 8F). On either side of the rostrum, the contact between the parabasisphenoid and laterosphenoid is relatively short. Ventral to the oculomotor foramen in the superjacent laterosphenoid, a foramen for the abducens nerve (CN VI) pierces the parabasisphenoid (Fig. 9H); it is very small and is surrounded by a shallow depression. As in extant crocodylians, the path of CN VI begins ventral to the trigeminal foramen on the internal surface of the cranial cavity. Specifically, it enters posteriorly into the parabasisphenoid near the lateral margin of the dorsum sellae and proceeds anteriorly lateral to, and paralleling, the path of the internal carotid artery (Fig. 19B, C). The abducens canal shifts laterally prior to exiting the parabasisphenoid in the shallow depression described above.

On the dorsal surface of the dorsal process of the pterygoid, lateral to the parabasisphenoid rostrum, a flange of bone from the pterygoid extends posteriorly up onto the braincase, contacting the dorsal surface of the pterygoid process of the quadrate laterally and overlying the parabasisphenoid dorsally. Near the intersection between the parabasisphenoid, the body of the laterosphenoid, and the dorsal process of the pterygoid, a small pedicel is formed on the dorsal surface of the latter for articulation with the epipterygoid (Fig. 16).

Basioccipital—The basioccipital (Figs. 1B, E, 3, 6, 15, 20A, B) is subtriangular in shape and forms nearly all of the posteroventrally directed occipital condyle. The neck of the occipital condyle is not constricted, thus rendering it indistinct, and the posterior surface of the condyle exhibits a shallow, mid-sagittal apical depression (Figs. 3, 6, 20A, B).

The median Eustachian (intertympanic) foramen is relatively large, as is common among basal mesoeucrocodylians, and is situated between the basioccipital and parabasisphenoid, centered at the base of the basioccipital (Figs. 3, 7A, B, 15, 19A, 20A, B). In ventral view, the lateral Eustachian foramina are partially obscured by the basal tubera and anterolateral extensions of the basioccipital plate (Fig. 3). The actual openings are oval in shape, with their long axes oriented from anteromedial to posterolateral (Fig. 20B). Because the foramina are deeply recessed, a canal incises the parabasisphenoid as the Eustachian tubes are transmitted to the pharynx. Due to asymmetry in the parabasisphenoid, it appears on the right side of UA 8679 that the pterygoid process of the quadrate forms the lateral margin of the lateral Eustachian foramen. However, HRXCT scans clarify this peculiar morphology, demonstrating that indeed a small projection of bone from the parabasisphenoid projects dorsally, separating the pterygoid process of the quadrate from the margin of the foramen.

The ventrolateral corners of the basioccipital form the medial one-quarter of the small but moderately developed basal tubera (Figs. 3, 6, 9J, 15, 20A, B). These are marked by extensive surface rugosity, which is continuous with that present along the ridge formed by the ventral edge of the basioccipital plate. This

← FIGURE 19. Internal structures within the braincase of *Simosuchus clarki*, as seen in medial cutaway views through a three-dimensional digital reconstruction of the skull and lower jaw of the holotype (UA 8679) generated from HRXCT scans, as seen from the median sagittal plane (A) and from two parasagittal planes passing through the posterior (B) and anterior (C) portions of the abducens canal. In this reconstruction, remaining matrix has been removed digitally so as to provide unobstructed views of unprepared internal regions of the skull. Note the bony partition between the anterior and posterior branches of the median Eustachian tube (asterisk in A, B, and C) and the foramen through which the parietal and supraoccipital sinuses communicate (dotted oval in C). The relatively large subrhomboidal aperture in the wall of the braincase dorsal to the metotic fissure does not represent a natural fenestra. See Appendix 1 for anatomical abbreviations.

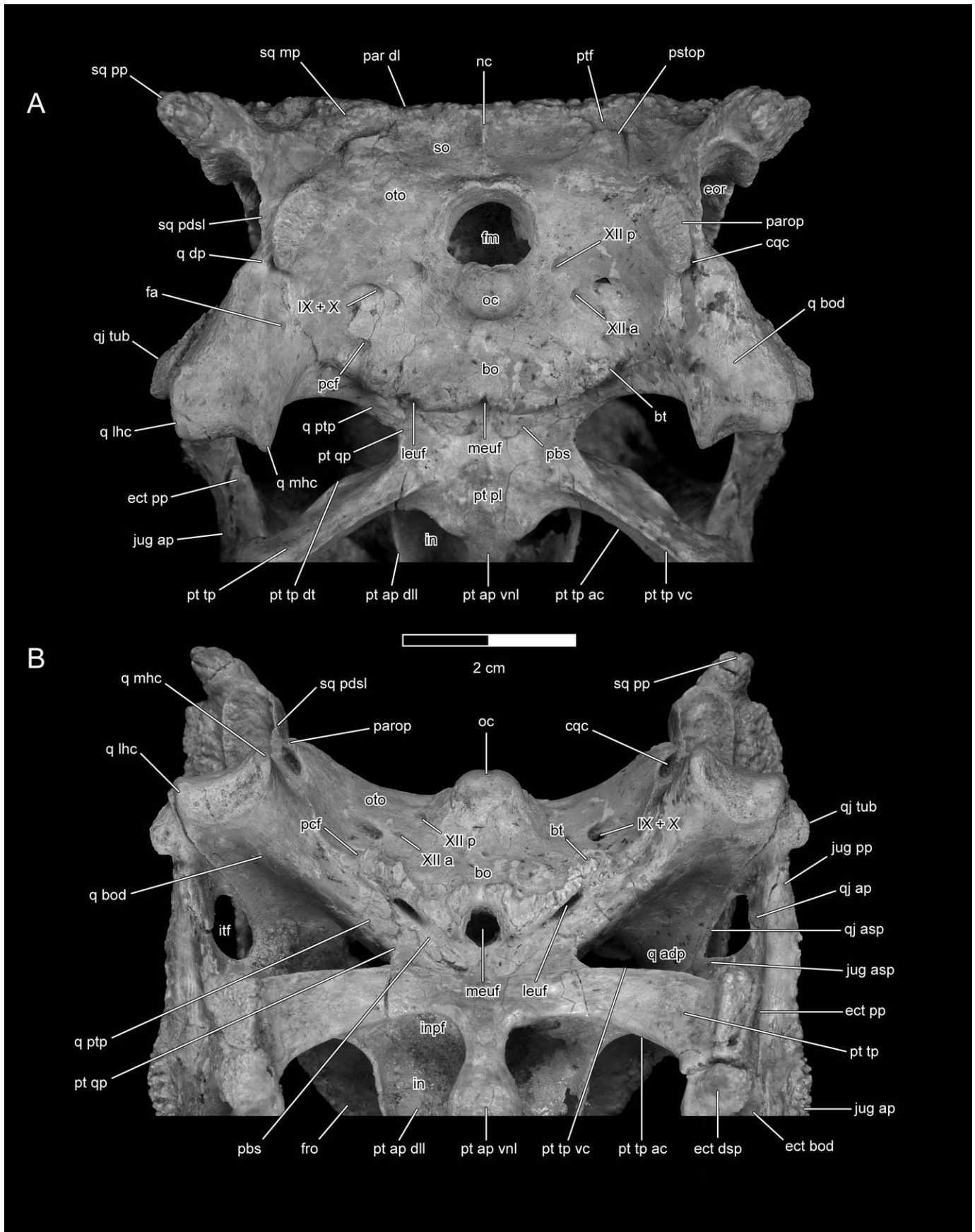


FIGURE 20. Basicranium of the holotype (UA 8679) of *Simosuchus clarki*, showing the occiput and its foramina, as well as the median and lateral Eustachian foramina. Photographs in **A**, posteroventral; and **B**, anteroventral views. See Appendix 1 for anatomical abbreviations.

ridge is most highly rugose just posteroventral to the median Eustachian foramen, where it is elaborated into two small ventrally projecting processes divided by a shallow divot (Figs. 3, 6, 20A, B). Running posterodorsally from each of these processes is a low, rounded ridge extending to the base of the occipital condyle (Fig. 3). Between these two (left and right) parallel ridges, the surface of the basioccipital is weakly excavated to form a shallow, longitudinally oriented sulcus. Near the anteroposterior midpoint of this sulcus, but slightly nearer to the occipital condyle than to the median Eustachian foramen, there is a small but distinct foramen (Figs. 3, 20) that may correspond to the remnant of the craniopharyngeal duct. However, HRXCT scans of the skull of UA 8679 show this foramen leading to a channel in the basioccipital that opens on the internal surface of the braincase well posterior to the hypophyseal fossa (Fig. 19A), the structure from which the duct should be traveling if it were indeed the craniopharyngeal duct. This raises the possibility that this foramen and its associated canal served to transmit an emissary vein, perhaps one associated with the ventral longitudinal dural venous sinus (see 'Cranial Endocast' [below]). Laterally adjacent to the anterior end of each of the two longitudinal ridges mentioned above, and bordered laterally by the ipsilateral basal tuber, is a shallow triangular depression (Fig. 3). Extending posterodorsomedially from each basal tuber for a distance of ~5 mm along the basioccipital-otoccipital suture is a low ridge, itself bordered medially by a small amygdaloid depression.

Owen (1850) was the first to describe the complex Eustachian system present in living crocodylians. Complementing this description was Colbert's (1946) brief discussion of the system and illustration of a cast of the system in *Crocodylus acutus*. These two descriptions will serve as the basis for interpreting the spaces within the parabasisphenoid and basioccipital of *Simosuchus clarki* (as visualized in HRXCT scans of the skull of UA 8679), which are so highly pneumatized as to be nearly hollow.

At the ventral midline, the median Eustachian foramen is extraordinarily large, and served to transmit what is assumed to have been an equally large median Eustachian tube. The median Eustachian tube would have immediately divided into anterior and posterior divisions, as evidenced by a thin sheet of bone separating an anterior recess housed in the parabasisphenoid from a posterior recess housed in the basioccipital (Fig. 19A). The bony division between the anterior and posterior chambers becomes progressively better developed laterally (Fig. 19B, C). The suture between the parabasisphenoid and basioccipital is evident laterally in this bony wall between the chambers. The anterior chamber would have accommodated the lateral branches of the anterior division of the median Eustachian tube and the posterior chamber would have accommodated the posterior division. The two chambers remain divided until the level of the lateral Eustachian foramen, at which point they connect to form the rhomboidal sinus. The canal for the lateral tube passes down from the rhomboidal sinus, between the parabasisphenoid and basioccipital, connecting the sinus to the pharynx.

One of the primary structures passing through the rhomboidal sinus would have been the internal carotid artery, as it extended anteriorly toward the hypophyseal fossa. The internal carotid artery would have entered the skull through the posterior carotid foramen, passed through the bony cranial carotid canal, and then entered the rhomboidal sinus and/or the ventral-most region of the tympanic cavity. As it moved toward the midline, it would have entered the anterior chamber within the parabasisphenoid prior to exiting the cranial cavity. Here no osteological correlates of the path of the artery are observed because it passed through the pneumatic space of the skull. At the approximate level of exit of the abducens nerve (CN VI) from the cranial cavity, the internal carotid artery re-entered the portion of the parabasisphenoid that forms the base of the dorsum sellae. The bony canal for this portion of the internal carotid artery can be seen in HRXCT

scans passing ventromedial to the path of CN VI through the parabasisphenoid before entering into the hypophyseal fossa.

Otoccipital—The otoccipital (Figs. 1B, C, E, 3, 4, 6, 15, 20A, B) is a large, unpaired element that is derived through the complete fusion of the left and right exoccipitals and opisthotics. It forms a large portion of the occiput, which in *Simosuchus clarki* is subdivided into two distinct surfaces with differing orientations: a posteriorly facing surface, formed dorsally by the supraoccipital and the dorsal-most portions of the otoccipital, comprising approximately one-third of the occipital surface; and a posteroventrally facing surface, formed ventrally by the remainder of the otoccipital and also the basioccipital, comprising approximately two-thirds of the occipital surface (Figs. 3, 6, 7A–D, 19A–C, 20A, B). The orientation and composition of this latter surface resembles those seen in many notosuchians (e.g., *Malawisuchus*, *Notosuchus*).

Dorsally, the left and right halves of the otoccipital meet above the foramen magnum, thus excluding the supraoccipital from the margins of the latter (Figs. 6, 7A, B, 17D, 19A, 20A). The portion of the otoccipital above the foramen magnum is very constricted dorsoventrally, unlike the broader contact in taxa such as *Araripesuchus tsangatsangana*, *Baurusuchus salgadoensis*, and *Notosuchus terrestris*. In addition, it is slightly rugose and projects posteriorly beyond the posterior margin of the occipital condyle (Figs. 6, 7A, 19A). The otoccipital contacts the supraoccipital in a wide V-shaped suture (Figs. 6, 20A). The descending pillars of the otoccipital form the ventrolateral margins of the foramen magnum and terminate at the dorsolateral margins of the occipital condyle (Figs. 6, 19A, 20A). Laterally, the otoccipital contacts the squamosal and the quadrate (Figs. 3, 6, 8G, 9L–O, 15, 17D, 19A, 20A, B). The anteroventrolateral portions of the otoccipital are extraordinarily thin and, on each side, wedge between the quadrate and basioccipital (Figs. 3, 8G, 15, 20A, B). There is not an externally exposed contact between the otoccipital and the parabasisphenoid. Consequently, the pterygoid process of the quadrate contacts the anterolateral margin of the basioccipital along the ventral margin of the braincase (Figs. 3, 20B). This morphology is present to a varying extent in *Martialisuchus amarali*, *Mahajangasuchus insignis*, and *Zosuchus davidsoni*. The ventral end of the otoccipital lacks the enlarged ventrolateral process that is present in most basal crocodyliforms and thalattosuchians (Clark, 1986).

On each side of the otoccipital, where the lateral edge of the paroccipital process contacts the dorsal process of the ipsilateral quadrate and the posterior descending lamina of the ipsilateral squamosal, the otoccipital plays a major role in the formation of the cranioquadrate canal (Figs. 3, 6, 7E, 8G, 9N, 20A, B), through which the hyomandibular branch of the facial nerve (CN VII) and lateral cephalic vein exited and the orbitotemporal artery entered. As in many basal mesoeucrocodylians, the opening for the cranioquadrate canal is located close to the lateral margin of the skull, with only a small portion of the dorsal process of the quadrate and posterior descending lamina of the squamosal forming its lateral wall.

On each side of the occiput, the dorsal extremity of the otoccipital forms a short, dorsally projecting postoccipital process that makes up the ventral edge of the ipsilateral posttemporal fenestra (Figs. 6, 20A). From this process, the dorsolateral margin of the otoccipital curves ventrolaterally along its broad contact with the squamosal. The lateral margin of the otoccipital forms a relatively short paroccipital process, which does not extend laterally beyond the posterior opening of the cranioquadrate passage (Figs. 3, 6, 8G, 9M–O, 14, 15, 20A, B). Similarly reduced paroccipital processes are present in derived neosuchians (e.g., *Goniopholis stovalli*, *Shamosuchus djadochaensis*, *Isisfordia duncani*, *Hylaeochampsa vectiana*, *Iharkutosuchus makadii*). As in most mesoeucrocodylians, the paroccipital process in *Simosuchus*

clarki is semi-ellipsoidal in shape and relatively blunt. Its exposed posteroventromedial surface is slightly rugose, bearing numerous subtle striations that radiate distally toward its curved posterolateral margin (Figs. 3, 6, 20A).

The ventromedial margin of each half of the otoccipital contacts the ipsilateral dorsolateral margin of the basioccipital along an anterolaterally slanting suture (Figs. 3, 6, 8G, 20A). At its anterolateral terminus, the former makes up the lateral three-quarters of a moderately well-developed and rugose basal tuber (Figs. 3, 6, 7D, 9J, 15, 20A, B). The portion of the otoccipital along this suture is weakly concave posteroventrally (due to its conformation to the contours of the portion of the quadrate that lies deep to it) and is pierced by four foramina (Figs. 3, 6, 20A, B). The most medial and posterior of these foramina is large, located just anterolateral to where the descending pillar contacts the base of the occipital condyle; it served as the primary exit for the hypoglossal nerve (CN XII) (Figs. 7C, 9M). Lateral and slightly anterior to this posterior hypoglossal foramen, the otoccipital bears two additional foramina. The more medial of these, the anterior hypoglossal foramen, is smaller; it served as the exit for two of the roots of CN XII (see description of internal path below). The larger and more laterally placed of these two foramina served as the exit for the vagal and glossopharyngeal nerves (CNs X and IX) (Figs. 7D, 8G, 9L), as well as the sympathetic contributions to CNs VII and IX (Iordansky, 1973). Both the vagal and anterior hypoglossal foramina are surrounded by small, shallow, laterally directed fossae (Figs. 3, 6, 20A, B). Lastly, the anteroventrolateral corner of the otoccipital, immediately posterodorsolateral to the basal tuber, is pierced by the foramen for the entrance of the internal carotid artery (posterior carotid foramen) (Figs. 7D, 9K).

Internally, the otoccipital forms the posterior half of the lateral wall of the braincase and tympanic bulla (Fig. 19A). Three small foramina pierce the otoccipital along the ventral-most portion of the braincase wall. These correspond to the intracranial exits for the roots of CN XII. The posterior-most is the largest of these three foramina and it re-emerges through the external surface of the skull via the posterior hypoglossal foramen discussed above. The anterior two foramina (of which only the more posterior is visible in Fig. 19A) form separate canals through the otoccipital, entering into the rhomboidal sinus before re-entering the otoccipital bone through separate foramina. Within the otoccipital these canals can be seen in HRXCT scans of the skull of UA 8679 to extend anterolaterally, nearly in parallel with one another, toward the anterior hypoglossal foramen, into which they open.

Both left and right tympanic bullae are damaged in UA 8679. Nevertheless, many important aspects of the morphology of this region are preserved in this specimen. Ventral to each tympanic bulla, the metotic fissure incises the anterolateral part of the otoccipital (Fig. 19A). Dorsal to this, and visible just posterodorsal to the damaged area of the tympanic bulla on each side of the skull, a strikingly angular common crus of the anterior and posterior semicircular canals is visible in HRXCT scans, in which it appears to extend into the opisthotic portion of the otoccipital. Within the otoccipital, the posterolateral arch of the posterior semicircular canal is apparent on its path toward the posterior ampulla (Figs. 7C, 8F, 9M). Although nearly obliterated, the sutural contact between the prootic and the opisthotic portion of the otoccipital is seen in HRXCT scans of UA 8679 to divide the tympanic bulla into nearly equal anterior and posterior portions (Fig. 19A).

Supraoccipital—The supraoccipital (Figs. 1A, B, E, 2, 6, 14, 20A) is a wedge-shaped element that projects anteriorly to underlie the posterior part of the parietal and laterally to contact the otoccipital. It has only a very limited exposure along the dorsal surface of the skull roof, appearing as a small but relatively wide wedge of bone (~5 mm in mid-sagittal anteroposterior length and ~22 mm in transverse width) along the posterior margin of the dorsal lamina of the parietal (Fig. 2). However, its occipital surface is more broadly exposed and resembles a wide, inverted

triangle (albeit one with a somewhat rounded base) in posterior view (Figs. 6, 20A). This occipital surface is weakly concave posteriorly but possesses a distinct nuchal crest, similar to those seen in *Anatosuchus minor*, *Comahuesuchus brachybuccalis*, and *Notosuchus terrestris*. Laterally, the supraoccipital forms a small portion of the medial wall of the rudiments of the posttemporal fenestra (Figs. 6, 20A). It does not, however, form any portion of the small, dorsally directed postoccipital process (Figs. 6, 20A), unlike the condition in most other mesoeucrocodylians (e.g., *Araripesuchus gomesii*, *Lomasuchus palpebrosus*, *Mahajangasuchus insignis*).

Internally, the supraoccipital forms the posterior portion of the cerebral cavity (Figs. 7A, B, 8D–F, 9M, N, 17C) but does not contribute to the formation of the tympanic bullae (Fig. 19A–C); this is similar to the condition in *Araripesuchus*, but unlike that in *Alligator* and other crocodylians. Sagittal HRXCT slices through the skull of the holotype specimen (UA 8679) reveal that the supraoccipital projects strongly anteroventrally beneath the posterior half of the parietal (Figs. 7A, B, 17C, 19A–C), and that this wedge-shaped portion of the bone is relatively taller dorsoventrally, and less acutely tapered, than in derived crocodylians (e.g., Iordansky, 1973; Brochu, 1999). Nevertheless, the supraoccipital of *Simosuchus clarki* exhibits the typically high level of pneumatization seen in most mesoeucrocodylians (Fig. 19A–C). Notably, *S. clarki* possesses a large transverse canal through the supraoccipital, which connects the mastoid antra (peritympanic cavities) on either side of the skull. This canal communicates posterolaterally through a second set of bilateral openings that lead back into the otoccipital and the peritympanic space/Eustachian system. Anteriorly, the pneumatic space of the supraoccipital communicates with a very large sinus within the parietal by way of a pair of widely spaced openings (Fig. 19C). Similar openings are present in the supraoccipital of crocodylians, but these appear to be closer to the midline than in *Simosuchus*.

Semicircular Canals

Anterior Semicircular Canal—The anterior semicircular canal (Figs. 7C, 8E, 9L, M, 19A), which lies at an angle of 49° relative to the sagittal plane, is more triangular in shape than the typical ovoid shape exhibited by extant crocodylians. This difference results primarily from two factors: (1) the boundary between the dorsal wall of the vestibular cavity and the base of the common crus (i.e., the junction between the anterior and posterior semicircular canals) is sharply angular in *Simosuchus clarki*, in contrast to the more gradual interface in extant crocodylians; and (2) the course of the anterior canal as it arises from the common crus continues higher in *S. clarki* than in extant crocodylians, and therefore must also turn ventrally more sharply and run a straighter, more direct course toward the anterior ampulla. These differences not only result in a more triangular anterior semicircular canal path in *Simosuchus*, but also render the canal taller relative to its width than in extant crocodylians. Although divergent from extant crocodylians, this morphology is consistent with that found in some other fossil crocodylomorphs, such as *Junggarsuchus sloani* and *Araripesuchus gomesii*.

Posterior Semicircular Canal—The posterior semicircular canal (Figs. 7C, 8F, 9M, 19A), which lies at an angle of 44° relative to the sagittal plane, 91° relative to the ipsilateral anterior semicircular canal, and 19° relative to the contralateral anterior semicircular canal, also shows a different shape than that of the typical extant crocodylian posterior canal. Whereas the crocodylian posterior semicircular canal is ellipsoidal in shape, that of *Simosuchus clarki* is, again, taller relative to the width of the canal and, because this difference in height is most prominent at the end of the canal near the common crus, the overall shape is ovoid. This difference in shape is further emphasized, as in the anterior canal, by a more angular distinction between the

common crus and the dorsal wall of the vestibular cavity. As for the anterior semicircular canal, this morphology, although not found in extant crocodylians, is seen in both *Junggarsuchus sloani* and *Araripesuchus gomesii*.

Lateral Semicircular Canal—In contrast to the vertical semicircular canals, the lateral (horizontal) semicircular canal, which lies at an angle of 95° relative to the sagittal plane (angled ventrolaterally), 99° relative to the anterior semicircular canal, and 104° relative to the posterior semicircular canal, is unusual among crocodylomorphs due to its particularly circular appearance. Laterally, this circular shape results from increased curvature of the canal (relative to that seen in extant crocodylians) as it runs from the lateral ampulla toward the posterior utricle. More medially, however, this circular shape is due primarily to the reduced influence of the wall of the vestibular cavity on the course of the bony canal. In extant crocodylians, the dorsal portion of the vestibular cavity (i.e., the portion that passes through the plane of the lateral semicircular canal) is more bulbous and therefore partially obliterates the medial aspect of the lateral canal circuit; this is not the case in *Simosuchus clarki*. This points to a likely difference in the vertical position of the bulbous saccule within the vestibular cavity. However, the inner and middle ear regions ventral to the plane of the lateral canal are poorly preserved in all available specimens of *S. clarki*, and thus the exact difference cannot be determined with certainty. It is interesting to note that, in this morphology, *S. clarki* does not resemble other crocodylomorphs, and that, for example, *Junggarsuchus sloani* and *Araripesuchus gomesii* more closely resemble the extant crocodylian condition.

Bones of the Splanchnocranium

Ceratobranchialia—One partial element of the hyobranchial apparatus was preserved with the holotype specimen (UA 8679) of *Simosuchus clarki* (Fig. 21). Such preservation, although incomplete, is significant because the morphology of the hyobranchial apparatus remains unknown for the vast majority of non-crocodylian crocodylomorphs. Although ossified hyobranchial cornua have been reported for a small number of basal crocodylomorphs (e.g., *Dromicosuchus grallator*, *Hesperosuchus agilis*, *Litargosuchus leptorhynchus*), basal crocodylians (e.g., *Protosuchus richardsoni*), and basal mesocrocodylians (e.g., *Araripesuchus gomesii*, *A. tsangatsangana*), these elements have been described in detail only very rarely.

In extant crocodylians, the hyobranchial apparatus is relatively simple in its overall morphology, consisting of a broad, unpaired cartilaginous plate, generally identified as the basihyoid or corpus hyoideum, and a pair of ossified cornua, generally identified as ceratobranchialia I (e.g., Fürbringer, 1922; Edgeworth, 1935; Gnanamuthu, 1937; Romer, 1956; Sondhi, 1958; Schumacher, 1973; Tanner and Avery, 1982; Cleuren and De Vree, 2000). Preserved hyobranchial cornua in fossil crocodylomorphs have been identified alternatively as representing either ceratobranchialia I (e.g., Clark and Sues, 2002; Sues et al., 2003) or ceratohyalia (e.g., Clark et al., 2000; Turner, 2006). With respect to the preserved element in question in *Simosuchus*, we accept the consensus hypothesis of homology that has arisen through broadly comparative neontological investigations (e.g., Fürbringer, 1922; Tanner and Avery, 1982), because these have involved extensive studies of not only the hyobranchial skeleton itself, but also the musculature that attaches to the constituent elements of this skeleton. Thus, we identify this element in *Simosuchus* as a first ceratobranchial. More specifically, based on comparisons made with other crocodylomorphs, both extant and extinct, we interpret this preserved portion of bone as representing a nearly complete right ceratobranchial I.

The portion of the first ceratobranchial preserved with UA 8679 is distinctively sickle-shaped; it is strongly curved in the dorsoventral (i.e., sagittal) plane (Fig. 21A, B), and whereas its



FIGURE 21. Partial right first ceratobranchial of the holotype (UA 8679) of *Simosuchus clarki*. Photographs in (approximately) **A**, lateral; **B**, medial; **C**, dorsal; and **D**, ventral views.

ventral margin is relatively blunt (Fig. 21D), measuring 2.3 mm in mediolateral width at its thickest point, its dorsal margin is very strongly tapered, thereby forming a relatively sharp edge along the inner curvature of the element (Fig. 21C). The preserved portion of bone exhibits a straight-line (i.e., chord) length of 28.7 mm, but measures ~ 34.2 mm along its outer curvature and ~ 27.7 mm along its inner curvature. It reaches its maximum dorsoventral height near its center, where it is more than twice as tall as it is wide, measuring 5.1 mm between its inner and outer margins. However, it tapers significantly as it extends posterodorsally (Fig. 21A, B). Although the cornu is most strongly curved dorsoventrally, it also exhibits a more gentle mediolateral curvature as well (Fig. 21C, D). Together, these two curvatures render the element with an overall shape that mirrors very closely the curved ventromedial margin of the posterior part of the right mandibular

ramus (i.e., the portion of the lower jaw formed anteroventrally by the medial edge of the central portion of the angular, and posterodorsally by the anterior process and body of the articular) (see below).

In addition to its general shape and size, several surface features of the first ceratobranchial merit special emphasis. First, near the center of the outer curvature of the cornu (i.e., where the anteroventral half of the bone curves to meet its posterodorsal half), there is a prominent tubercle that bears conspicuous muscle scarring (Fig. 21A, B, D). Second, two even more prominent areas of scarring are evident toward the anterior end of the cornu. The first of these occurs in a narrow recess along the ventromedial margin of the anterior two-fifths of the preserved portion of the bone (Fig. 21B). The second, more or less continuous with the first, extends broadly across the medial surface of the element, nearly reaching its dorsal margin; however, although this second area of scarring is more expansive than the first, it appears not to extend as far posteriorly. Finally, near the center of the medial surface of this element, between the thickened portion of its outer curvature (i.e., in the vicinity of the enlarged tubercle described above) and its sharply tapered inner curvature, there is a prominent fossa (Fig. 21C). Although the bony surface within this depressed area appears relatively smooth when examined macroscopically, microscopic examination reveals subtle yet extensive muscle scarring throughout the floor of this fossa.

Stapedes—Stapedes are not preserved in any known specimens of *Simosuchus clarki*.

Epipterygoids—Recent work by Holliday (2006) and Holliday and Witmer (2009) examining the orbitotemporal region in crocodyliforms has revealed the apparent persistence of an epipterygoid ossification long into the evolutionary history of Crocodyliformes. These authors, based on their examination of the skull of the holotype (UA 8679) of *Simosuchus clarki*, posited the presence of an (unpreserved) epipterygoid bridging the narrow gap present in this specimen between the laterosphenoid and the dorsal process of the pterygoid along the anterior margin of the maxillomandibular foramen (CN V_2+V_3) (Figs. 4, 7C, 16). Complete preparation of the orbitotemporal region of the head skeleton in a more recently discovered referred specimen confirms this prediction.

The epipterygoids in this newly prepared specimen (FMNH PR 2597) are relatively narrow and columnar in their general shape (Fig. 16); in these respects, the epipterygoids of *S. clarki* appear to be unique among the basal mesoeucrocodylians that retain these elements (Holliday and Witmer, 2009). Each epipterygoid spans the gap between two distinct articular pedicels—one near the ventral terminus of the cotylar crest of the laterosphenoid and one on the dorsal process of the pterygoid—and in so doing, forms the lateral wall of the cavum epiptericum. Each is widest dorsally and tapers slightly toward its ventral contact with the pterygoid. In addition, each epipterygoid exhibits slight mediolateral compression. On both the right and left sides of FMNH PR 2597, the lateral surface of the epipterygoid is relatively smooth; there is no apparent impression of the maxillary division of the trigeminal nerve (CN V_2) that would have passed nearby.

The shape of the contact between the epipterygoid and laterosphenoid is variable between the right and left sides of FMNH PR 2597. On the right side it is weakly sinusoidal, with a zone of poor ossification at the area of contact (Fig. 16). On the left side the contact is ventrally convex, and no such zone of diminished ossification is evident. On both sides, however, a thin projection of bone extends posteriorly along the ventral edge of the laterosphenoid-formed anteromedial rim of the trigeminal foramen. The articular pedicel for the epipterygoid on the dorsal process of the pterygoid is wider on the right side than it is on the left. The epipterygoid-ptyerygoid contact is slightly damaged on

the left side. The contact on the right side is an anteroventrally sloping suture with no signs of interdigitation.

Quadrates—The quadrates (Figs. 1A–C, E, 2–4, 6, 11, 14–16, 20A, B) are relatively well preserved in the holotype (UA 8679) of *Simosuchus clarki*, and HRXCT scans of the skull of this specimen reveal these elements to be nearly completely hollow (Figs. 7D, E, 8E–I, 9H–N, 10A, 12, 17D). As in other crocodyliforms, the anterodorsal region of the quadrate is divided into a medially inclined dorsal primary head and an anterodorsal process. The dorsal primary head contacts the posterolateral lamina of the laterosphenoid and the lateral surface of the prootic dorsomedially, before ultimately becoming continuous posteriorly with the anterodorsal process by smoothly curving into the latter within the temporal adductor chamber (Figs. 8E, 9K). The anterodorsal process is sutured along the anterior portion of its lateral face to the medial surfaces of the anterior descending process of the squamosal and the descending process of the postorbital (Figs. 4, 8E, 9J, K, 15). However, much of the anterodorsal process remains exposed laterally, revealing a smooth external surface and a free posterior margin that contributes greatly to the formation of the otic aperture (Figs. 4, 11). This aperture is subelliptical in shape in *S. clarki*, with its anteroventral margin more smoothly rounded than its posterodorsal margin. The former is delineated entirely by a semilunar emargination of the posterior margin of the anterodorsal process of the quadrate (i.e., the otic incisure). In contrast, the latter is formed dorsally by the anteroventral margin of the posterior descending process of the squamosal, and ventrally by the anterodorsal margin of the dorsal process of the quadrate, the latter of which is oriented posterodorsally in *S. clarki* (Figs. 4, 11). The dorsal process of the quadrate is robust and similar to corresponding processes present in other basal mesoeucrocodylians such as *Comahuesuchus*, *Notosuchus*, and *Araripesuchus* (*A. tsangatsangana*, *A. gomesii*). It is anteroposteriorly short (Figs. 3, 4, 7E, 8G, 15), resulting in the otic aperture being positioned near the posterior margin of the skull. In this respect, *Simosuchus* is more similar to *Comahuesuchus*, which also has a very robust but anteroposteriorly short dorsal process. In *Araripesuchus gomesii*, *Malawisuchus*, and *Notosuchus*, the dorsal process is anteroposteriorly longer and broadly separates the otic aperture from the posterior margin of the skull.

The contact between the dorsal process of the quadrate and the posterior descending lamina of the squamosal is oblique, sloping steeply from anterodorsal to posteroventral along the length of the suture (Fig. 4). This contact delimits the dorsal and lateral borders of the anteroventral end of the cranioquadrate passage (Figs. 3, 6, 7E, 8G, 9N, 15, 20A). A small preotic siphoneal foramen is located anterior to the otic aperture (Fig. 4). The lateral surface of the quadrate bears a slightly depressed semilunar area, demarcated by a subtle ridge immediately anteroventral to the otic incisure, that surrounds the ventral margins of the otic aperture and the siphoneal foramen (Figs. 4, 8F). This depressed area, and the ridge that delineates it, terminates posteriorly, anterior to the contact between the posterior descending lamina of the squamosal and the dorsal process of the quadrate, near where the latter diverges from the root of the anterodorsal process.

The distal portion of the body of the quadrate is short, robust, and directed anteroventrally (Figs. 3, 4, 6, 9K, 11, 12, 20A, B). In most respects, it is similar to those of other basal mesoeucrocodylians (e.g., *Araripesuchus gomesii*, *Anatosuchus*, *Comahuesuchus*). It is more strongly developed than in basal crocodyliforms (e.g., *Protosuchus*), but less so than in some derived notosuchians (e.g., *Notosuchus*, *Baurusuchus salgadoensis*), or in derived neosuchians (e.g., *Alligator mississippiensis*, *Goniopholis stovalli*, *Rhabdogathus*). The distal portion of the body of the quadrate is subrectangular in frontal section (Fig. 8I), resembling that of most other notosuchians and some more basal taxa as well, such as *Zosuchus*. The medial hemicondyle extends further ventrally than does the lateral hemicondyle and is separated

from the latter by a relatively deep groove (Figs. 3, 4, 6, 9K, 20A, B). The lateral hemicondyle is the larger of the two quadratic hemicondyles in its mediolateral width. In posterior view, with the skull held such that the cranial table is oriented horizontally, the articular surface of the lateral hemicondyle is also oriented horizontally (Fig. 6). The articular surface of this hemicondyle is weakly convex (Fig. 20A, B). The medial hemicondyle is mediolaterally compressed and terminates ventrally in an acute angle (Figs. 3, 6, 9K, 20A, B). The articular surface of the medial hemicondyle is even less convex than that of the lateral hemicondyle, and is indeed nearly flat (Fig. 20A, B). Dorsal to the medial hemicondyle, a subtle rounded ridge emerges along the posterior surface of the body of the quadrate and becomes more prominent as it ascends toward the zone of contact between the paroccipital process of the otoccipital and the posterior descending lamina of the squamosal (Figs. 3, 6, 20A). Ultimately, this ridge becomes continuous dorsally with the posterior margin of the dorsal process, and thus effectively subdivides the posterior aspect of the distal portion of the body of the quadrate. Lateral to this ridge, the quadrate is weakly concave posteriorly, relatively wide, and posteriorly facing. Medial to the ridge, however, the quadrate is narrow and curves anteromedially to establish a dorsal contact with the ventrolateral edge of the otoccipital; immediately ventrolateral to this contact, a foramen aereum pierces the quadrate (Fig. 20A). Thus, the distal portion of the body of the quadrate has two distinct faces in posterior view: a posterior one and a medial one bearing the foramen aereum (Figs. 6, 20A). A posterior quadrate ridge similar in size and position to the one described above for *Simosuchus* is present in several other basal mesoeucrocodylians, such as *Malawisuchus*, *Mariliasuchus*, and *Araripesuchus tsangatsangana*.

The dorsomedial portion of the body of the quadrate contacts the very thin ventrolateral portion of the otoccipital in a relatively long suture (Figs. 3, 6, 8G, 15, 20A, B). The contact begins anteroventral to the cranioquadrate passage and extends anteroventromedially toward the small basal tuber. Dorsal, lateral, and posterior to the posterior origin of this suture, the dorsal process of the quadrate is bordered by a short paroccipital process, which forms the posterior and medial walls of the cranioquadrate passage (Figs. 3, 6, 7E, 8G, 9N, 15, 20A, B). Due to the close proximity between the external otic recess and the occipital surface, the cranioquadrate passage is very short and the course it traverses is almost entirely vertical.

Projecting anteromedially from the body of the quadrate is a robust pterygoid process (Figs. 3, 6, 11, 15, 17D, 20A, B). At its distal (anteromedial) end, it forms a mediolaterally wide interdigitating suture with the posterolateral end of the quadrate process of the pterygoid (Figs. 3, 8G, 9H, 20B). It also establishes a far less extensive contact with the small, ventrally exposed portion of the parabasisphenoid (Figs. 3, 8G, 20B).

The anterior surface of the quadrate is concavo-convex, in that it is anteriorly convex along its major axis (i.e., its dorsoventral height) and anteriorly concave across its minor axis (i.e., its mediolateral width). Its long-axis convexity effectively divides this surface into a dorsal half, consisting of the region of continuity between the dorsal primary head and anterodorsal process, and a ventral half, comprised of the body of the quadrate and, to a much lesser degree, the pterygoid process; the dorsal half faces almost directly anteriorly, whereas the ventral half faces slightly ventrally as well. Both the dorsal and ventral halves of this anterior surface are predominantly smooth. However, the lateral half of the latter is marked distinctly by a well-developed curvilinear rugosity. This rugosity begins ~5 mm medial to the dorsal apex of the infratemporal fenestra and curves ventrally and gently laterally for a distance of ~10 mm before ending at a point ~3 mm medial to the posteroventral corner of the infratemporal fenestra. Immediately distal to the ventral terminus of this raised rugosity is a roughened, elongate depression that extends

~3 mm further along this same trajectory (i.e., parallel to the syndesmosis between the lateral surface of the quadrate and the medial surface of the ascending process of the quadratojugal). Collectively, this curvilinear array of roughened bone corresponds to 'crest A' of Iordansky (1964), which is present in most, but not all, broad-snouted species of extant crocodylians (Iordansky, 1964:table 2); it represents the area of attachment for the lateral lamina of the cranial adductor tendon (i.e., 'A-tendon' of Iordansky, 1964; CATII of Busbey, 1989), which serves as a major site of origin for both the *M. adductor mandibulae externus medius* (MAMEM) and the *M. adductor mandibulae posterior* (MAMP) (Iordansky, 1964; Schumacher, 1973; Busbey, 1989). Furthermore, as noted by Iordansky (1964, 1973), this crest (and other ones associated with the origins of various other portions of the *M. adductor mandibulae* complex) is generally well developed only in relatively large adult crocodylians, and often absent or very poorly developed in juvenile specimens. Thus, the presence of these crests in both UA 8679 and FMNH PR 2597 suggests that both of these specimens represent adult individuals (see also 'Variation in Overall Size, Relative Proportions, and Ontogenetic Maturity' [below]).

Articulars—The articulars (Figs. 1C–E, 4, 6, 12, 17A, C, 22–28) are well preserved on both sides of the lower jaw of the holotype (UA 8679) of *Simosuchus clarki*. Both articulars are also preserved nearly completely and intact in the otherwise badly crushed head skeleton of FMNH PR 2596 (although they are fully visible only in CT scans, because both left and right elements remain partially surrounded by matrix in this specimen). However, only fragments of the left articular are preserved with FMNH PR 2597.

Each articular, which represents the ossified and expanded posterior-most portion of the embryonic Meckelian cartilage, consists of a bulbous central portion, the body, from which two prominent processes project: a strongly tapered anterior process, and a broad, flat ventromedial process (Figs. 22–28). By far the most conspicuous and functionally significant external feature of the body of the articular is its broad, dorsally and dorsomedially oriented articular surface, the glenoid fossa (Figs. 22, 25, 27, 28), which receives the condyle of the quadrate to form the craniomandibular joint. When viewed from a dorsal perspective, the glenoid exhibits a nearly oval outline, with its major axis oriented approximately perpendicular to the long axis of the skull and lower jaw (Fig. 22). However, its three-dimensional shape is far more complex.

Each glenoid fossa is effectively divided into two distinct facets by a ~45° angulation of its articular surface (Figs. 22, 25, 27, 28). This strong angulation creates a prominent yet bluntly rounded ridge that runs anteroposteriorly through the mediolateral center of the fossa, thereby partitioning the glenoid approximately equally into a dorsally facing lateral articular facet and a dorsomedially facing medial articular facet. The articular surface of the former is very slightly convex dorsally, whereas that of the latter exhibits a subtle dorsomedial concavity (Fig. 9J, K); however, both are similar in being extremely smooth (except for several small, isolated areas of erosion). The medioventrally slanting medial articular facet, which receives the medial hemicondyle of the quadrate, extends medially well beyond the remainder of the body of the articular, thereby creating a conspicuous overhang above the ventromedially projecting retroarticular process (Figs. 6, 9I–K, 22, 23, 25–28). A similar but more slender expansion of the glenoid beyond the main portion of the body of the articular is also associated with the lateral articular facet, which receives the lateral hemicondyle of the quadrate; however, this expansion projects posteriorly rather than medially and emanates only from the lateral half of the lateral facet (Figs. 22, 25, 28). As in many other basal mesoeucrocodylian taxa (e.g., *Anatosuchus*, *Araripesuchus*, *Malawisuchus*, *Mariliasuchus*, *Notosuchus*), the glenoid fossa of *Simosuchus* lacks a transversely oriented pos-



FIGURE 22. Lower jaw of the holotype (UA 8679) of *Simosuchus clarki* in dorsal view. **A**, photograph; **B**, interpretive drawing. See Appendix 1 for anatomical abbreviations.

terior buttress, which in extant crocodylians is well developed (Iordansky, 1973) and contributes significantly to the overall stabilization of the craniomandibular joint by preventing anterior translation of the lower jaw relative to the overlying skull and thus effectively limiting motion at the jaw joint to simple rotation within a sagittal plane (e.g., Cleuren and De Vree, 2000).

HRXCT scans of the holotype specimen (UA 8679) reveal that the body of the articular is remarkably robust in its construction, exhibiting an exceptionally dense packing of trabeculae, especially in the region immediately beneath the cortical bone forming the articular surface of the glenoid fossa (Fig. 9J, K). In fact, the only other region of the head skeleton exhibiting a similar level of trabecular bone density is the occipital condyle (Figs. 7A, B, 9M). (Such extensive internal reinforcement may explain the surprisingly good level of preservation of both articulars in the otherwise severely crushed head skeleton of FMNH PR 2596.)

Nevertheless, isolated regions within the body of the articular are less densely trabeculated; these regions, concentrated primarily medioventrally (Fig. 9K), are pneumatized, ultimately communicating with a small foramen aereum (Fig. 28). The foramen aereum is located on the posterior aspect of the articular body, ~3 mm ventral to the articular surface of the glenoid fossa, in association with a sharp, posterodorsally projecting postglenoid spine (Figs. 27, 28).

The anterior process of the articular projects anterolaterally from the body (Figs. 12, 17C, 22, 23, 25, 28) and is far less densely trabeculated than the latter (Fig. 9H). It exhibits a relatively evenly rounded ventrolateral surface, which is received by a complementarily shaped groove—the posterior extension of Meckel's groove—that runs along the ventromedial aspect of the angular (Figs. 9H, 25, 28). In contrast, the exposed dorsolateral portion of the anterior process is strongly angulated, bear-

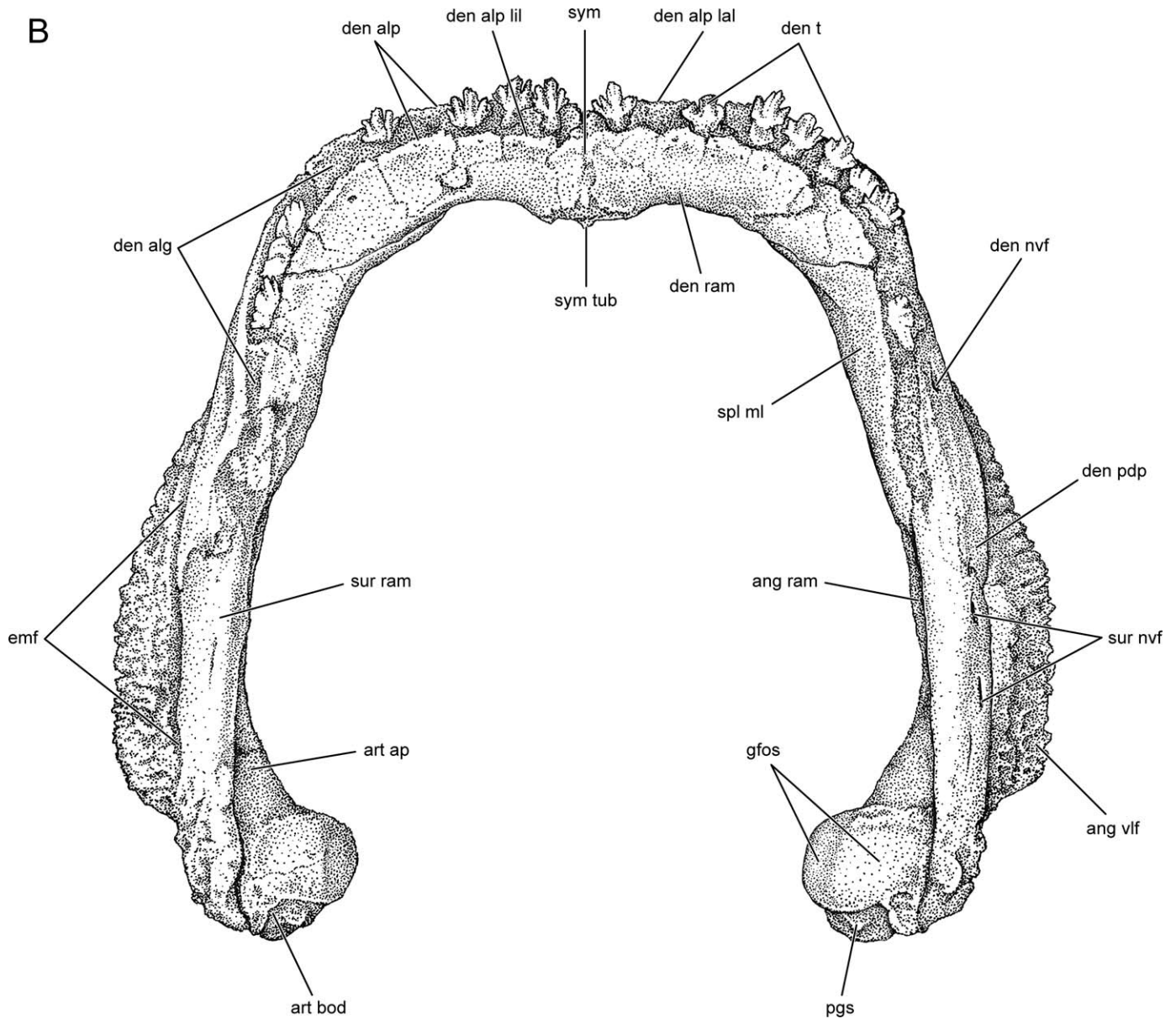


FIGURE 22. Continued.

ing a prominent medial longitudinal ridge running along the long axis of the process, with the latter dividing this visible portion of the process into distinct ventromedial and dorsomedial surfaces that diverge from one another at an angle of $\sim 100^\circ$ (Figs. 9H, 25, 28). The anterior process tapers strongly as it passes anterolaterally, but it terminates abruptly without tapering to a sharp point; rather, the anterior-most tip of the process is squared off (Fig. 25), leaving a small, roughened, subtriangular facet that, in life, would have contacted the posterior end of Meckel's cartilage.

Although well visualized only microscopically under oblique lighting, both the ventromedial and dorsomedial surfaces of the anterior process of the articular exhibit subtle but relatively extensive areas of muscle scarring. Based on comparisons with extant crocodylians, we interpret the scarring along these two surfaces as representing areas of attachment for portions of the *M. pterygoideus posterior* and *M. adductor mandibulae posterior*,

respectively (Iordansky, 1964; Schumacher, 1973; Busbey, 1989). In addition, the longitudinal ridge that divides these ventromedial and dorsomedial surfaces is itself conspicuously rugose, especially along its posterior half. Again by comparison with the condition exhibited by extant crocodylians, we interpret the rugosity along this longitudinal ridge as representing the area of attachment for a portion of the mandibular adductor tendon (i.e., 'X-tendon' of Iordansky, 1964; lamina posterior [MATlp] of Schumacher, 1973, and Busbey, 1989) that serves as the main site of insertion for the deepest fibers of the *M. adductor mandibulae posterior*.

Finally, extending ventromedially and somewhat posteriorly from the body of the articular is the robust ventromedial process (Figs. 6, 9J, K, 17A, 23–28). It is approximately semidiscoidal in shape and forms the innermost, and by far the thickest, lamina of a highly flattened, trilaminar retroarticular process (the middle and outer laminae being formed by the ventromedial processes of



FIGURE 23. Lower jaw of the holotype (UA 8679) of *Simosuchus clarki* in ventral view. **A**, photograph; **B**, interpretive drawing. See Appendix 1 for anatomical abbreviations.

the surangular and angular, respectively) (Figs. 6, 24, 27, 28). The semicircular free posteroventral margin of the ventromedial process of the articular is bluntly rounded, with the ventral portion in particular being somewhat thickened and roughened (visible on both sides of UA 8679 and on the exposed portion of the left articular in FMNH PR 2596) (Figs. 6, 23, 26–28). However, no such thickened or roughened areas are present along the anterior edge of the process, which is nearly vertical in its orientation, but with a slight anteromedially concave emargination (Figs. 23, 25, 26, 28).

The exposed face of the ventromedial process of the articular is oriented primarily medially, but also somewhat posterodorsally (Figs. 6, 25, 27, 28). It exhibits two distinct areas of muscle scarring. The first, which is clearly visible macroscopically, is located along its anteromedial margin (Figs. 25, 28). This area of scarring extends dorsally to the junction between the ventrome-

dial process and the body of the articular, where it becomes most strongly developed; here it even extends slightly anterodorsally onto the ventral surface of the articular body. This pronounced anteromedial scarring almost certainly represents the area of attachment for one of the major tendons of the *M. pterygoideus posterior* (i.e., semi-ring tendon of Iordansky, 1964; aponeurosis six of posterior pterygoideus tendon of Schumacher, 1973; lamina superior of posterior pterygoideus tendon [PPTIs] of Busbey, 1989). In addition to this heavily scarred area anteriorly, a second, less conspicuous but more expansive, area of scarring is evident posteriorly, with microscopically visible striae fanning out along the posterior one-third of the process toward its semicircular free posteroventral margin. These more subtle muscle scars likely correspond to the area of insertion of the *M. depressor mandibulae* (Iordansky, 1964; Schumacher, 1973; Busbey, 1989).

B

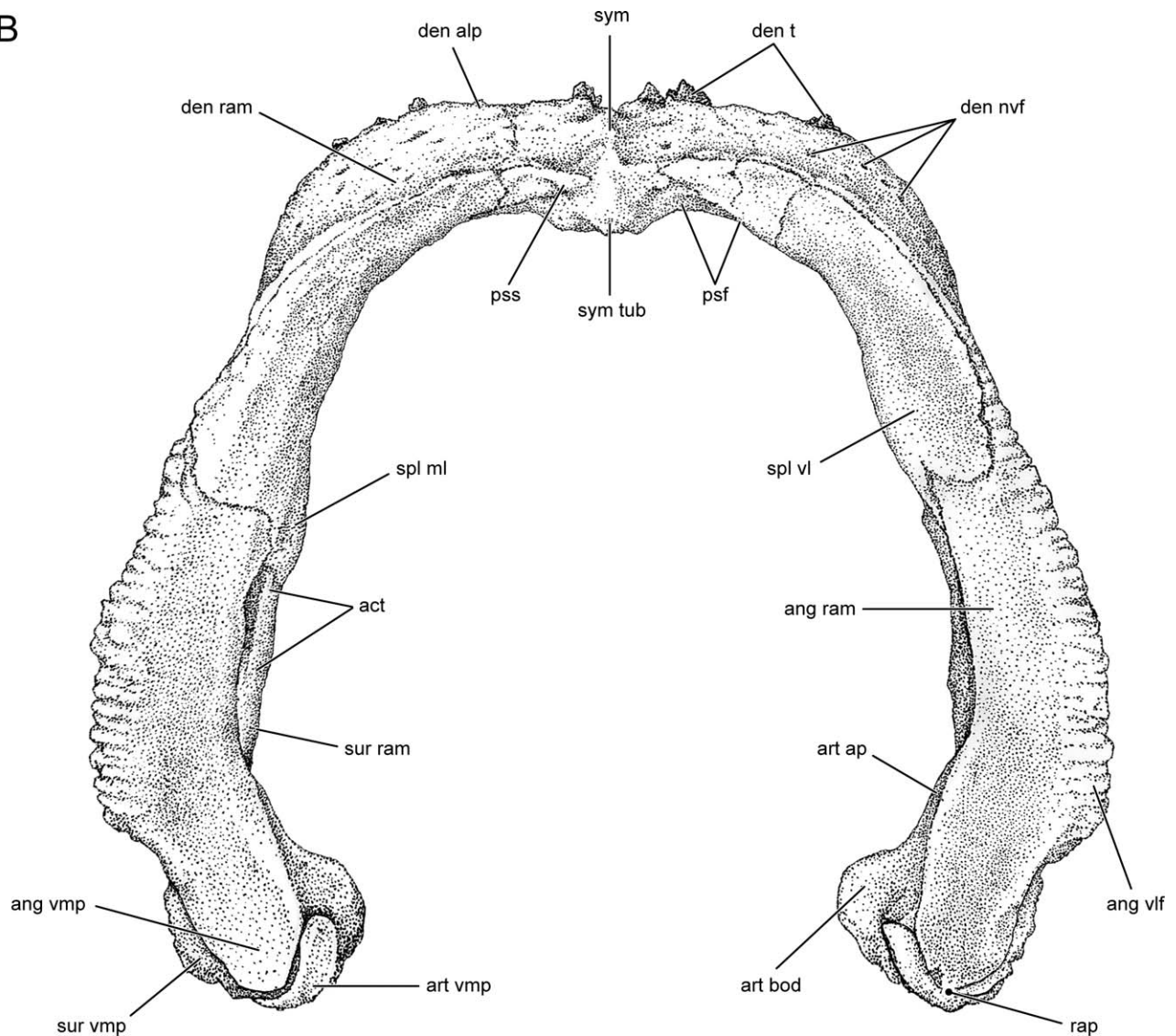


FIGURE 23. Continued.

Dermal Bones of the Lower Jaw

Surangulars—The surangulars (Figs. 1A, C–E, 2, 4, 6, 12, 17, 22–29) exhibit a relatively simple gross morphology, with each consisting of a relatively long, arched ramus anteriorly and a much shorter, flattened ventromedial process posteriorly. However, detailed examination of this bone reveals a remarkable level of fine-scale anatomical complexity.

The posterior origin of the ramus of the surangular lies at a level approximately coincident with a transverse plane passing through the posterior margin of the glenoid fossa of the articular (Figs. 6, 22, 25, 27, 28). From this point, it extends anteriorly, gently arching dorsally above the angular, to ultimately insinuate itself between the posterodorsal process of the dentary (laterally) and the medial lamina of the splenial (medially) (Figs. 9E, 17, 22–28). Throughout most of this course, the overall cross-sectional shape of the ramus is roughly ovoid (Fig. 9G). However, as it ascends anterodorsally toward its highest point (i.e., ‘coronoid process’), located above the approximate anteroposterior midpoint of the external mandibular fenestra, it becomes

deeply grooved along its ventral surface (Figs. 9E, F, 17B, 29A). This groove, which almost certainly accommodated the mandibular nerve (CN V₃) posteriorly as it descended into the mandibular adductor fossa (Poglayen-Neuwall, 1953; Schumacher, 1973), and then the entire ventral alveolar neurovascular bundle more anteriorly (Sedlmayr, 2002), effectively creates a pair of roughly parallel, sharp-edged, ventrally projecting flanges that descend from the concave ventral surface of the ramus (Fig. 29A). The ventral margin of the lateral one of these two descending flanges forms the central portion of the dorsal margin of the external mandibular fenestra.

In addition to its dorsal curvature, the surangular ramus exhibits two additional changes in shape as it extends anteriorly. First, along its posterior half, it arches gently laterally, whereas along its anterior half, it arches gently medially. The conspicuous lateral curvature that results from this contributes significantly to the overall ‘bowed-out’ appearance of the lower jaw in dorsal view (Fig. 22). (However, the surangular ramus does not bow outward nearly as far as does the prominent ventrolateral flange of the angular. [See below.]) Among other notosuchians, similar

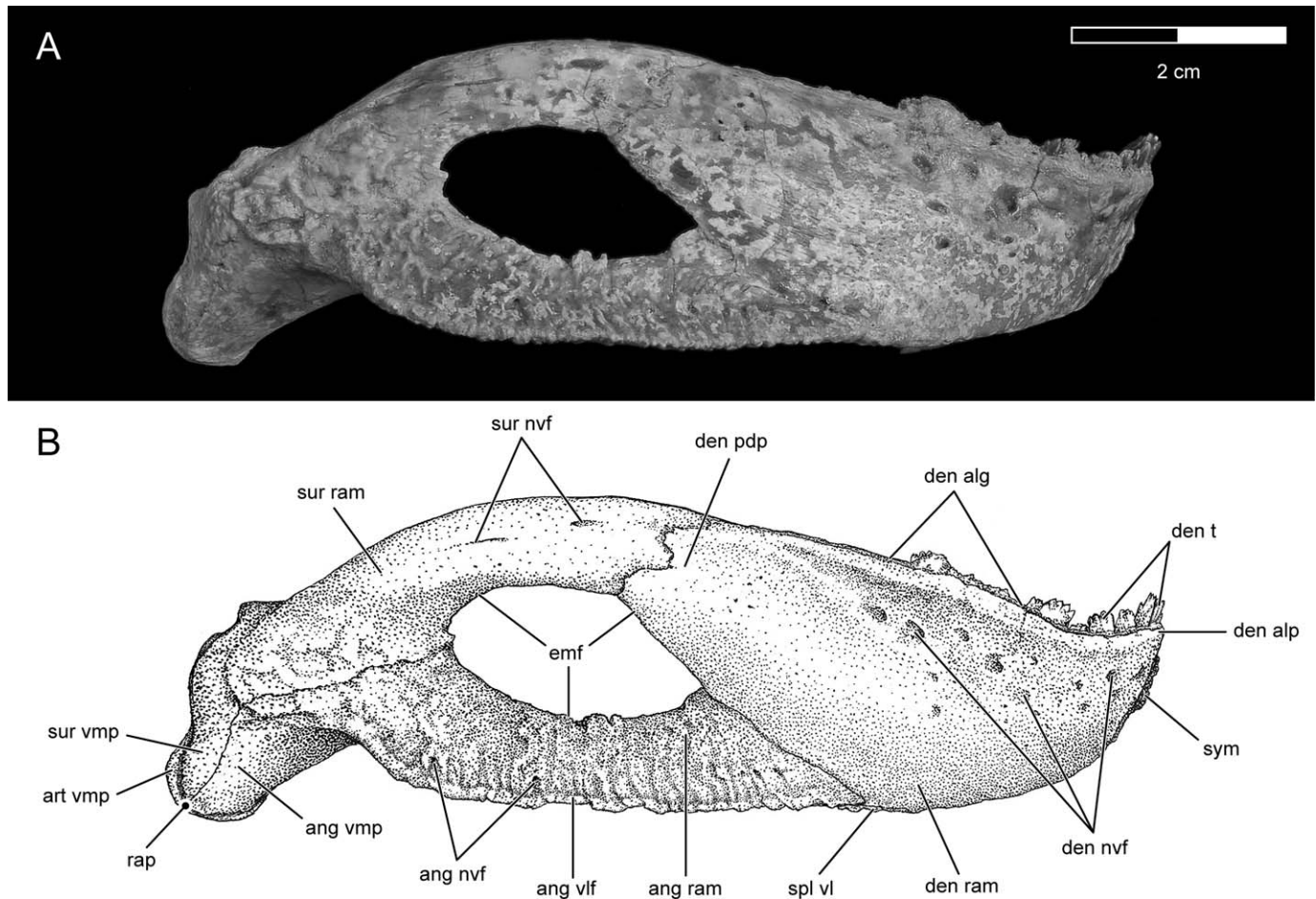


FIGURE 24. Lower jaw of the holotype (UA 8679) of *Simosuchus clarki* in right lateral view. **A**, photograph; **B**, interpretive drawing. See Appendix 1 for anatomical abbreviations.

lateral arching of the surangular is seen in *Libycosuchus*, *Marilia-suchus*, and *Notosuchus*. Second, immediately anterior to its posterior origin, as the ramus begins its anterodorsal ascension, it undergoes a moderate degree of torsion along its longitudinal axis such that its bluntly rounded dorsal margin rotates slightly medially. Consequently, the lateral surface of the ramus is inclined somewhat so as to face slightly dorsally as well (Figs. 9E–J, 17A, B, D, 22, 26–28).

Except near its posterior-most end, where some light sculpturing is present, the lateral surface of the surangular ramus consists of unsculptured bone (Fig. 24). However, this smooth lateral surface is perforated by numerous small-diameter neurovascular foramina along its length (Figs. 22, 24, 28). These lateral surangular foramina number three per side in the holotype specimen (UA 8679), but cannot be counted fully in FMNH PR 2596 (although at least one foramen is visible on the preserved and exposed posterior portion of the right surangular ramus), FMNH PR 2597 (although at least two foramina are visible on the unbroken right surangular ramus), or in the incomplete right surangular ramus preserved with FMNH PR 2598. The latter fragment does, however, preserve nearly the entire anterior end of the ramus—hidden from external view in the fully prepared articulated specimens (UA 8679 and FMNH PR 2597)—thereby revealing the presence of a well-developed dorsolateral recess to accommodate the dorsal prong of the bluntly forked posterodorsal process of the dentary. HRXCT scans of UA 8679 clearly

confirm the presence of a similar dorsolateral recess at the anterior end of each surangular ramus in this specimen (Fig. 9E), and lower-resolution CT scans of FMNH PR 2597 confirm a similar morphology on the relatively well-preserved right surangular in this specimen. (Indeed, slight displacement and/or breakage of the posterodorsal process of the right dentary in this latter specimen renders a small portion of this recess visible externally.)

The medial surface of the surangular ramus exhibits two prominent and functionally significant features. First, near its posterior-most end, it bears a small but relatively well-developed fossa (fully visible on both sides of the lower jaw of UA 8679 [Figs. 22, 25, 27, 28] and partially visible on the right side of FMNH PR 2597, in which the lower jaw remains in articulation with the skull). This fossa serves to accommodate the lateral surface of the lateral hemicondyle of the quadrate (Figs. 6, 9K), thus augmenting the already relatively extensive articular surface area of the primary craniomandibular joint, formed between the quadrate and articular, as well as providing resistance against medial displacement of the latter relative to the former. Second, further anteriorly, as the surangular ramus approaches its highest elevation, a much more conspicuous feature begins to develop along its medial surface, one that extends anteriorly to where the ramus is overlapped medially by the medial lamina of the splenial, and ventrally to the free edge of the medial descending flange formed by the groove for the mandibular nerve. Here an extensive and elongate area of conspicuous longitudinal stria-

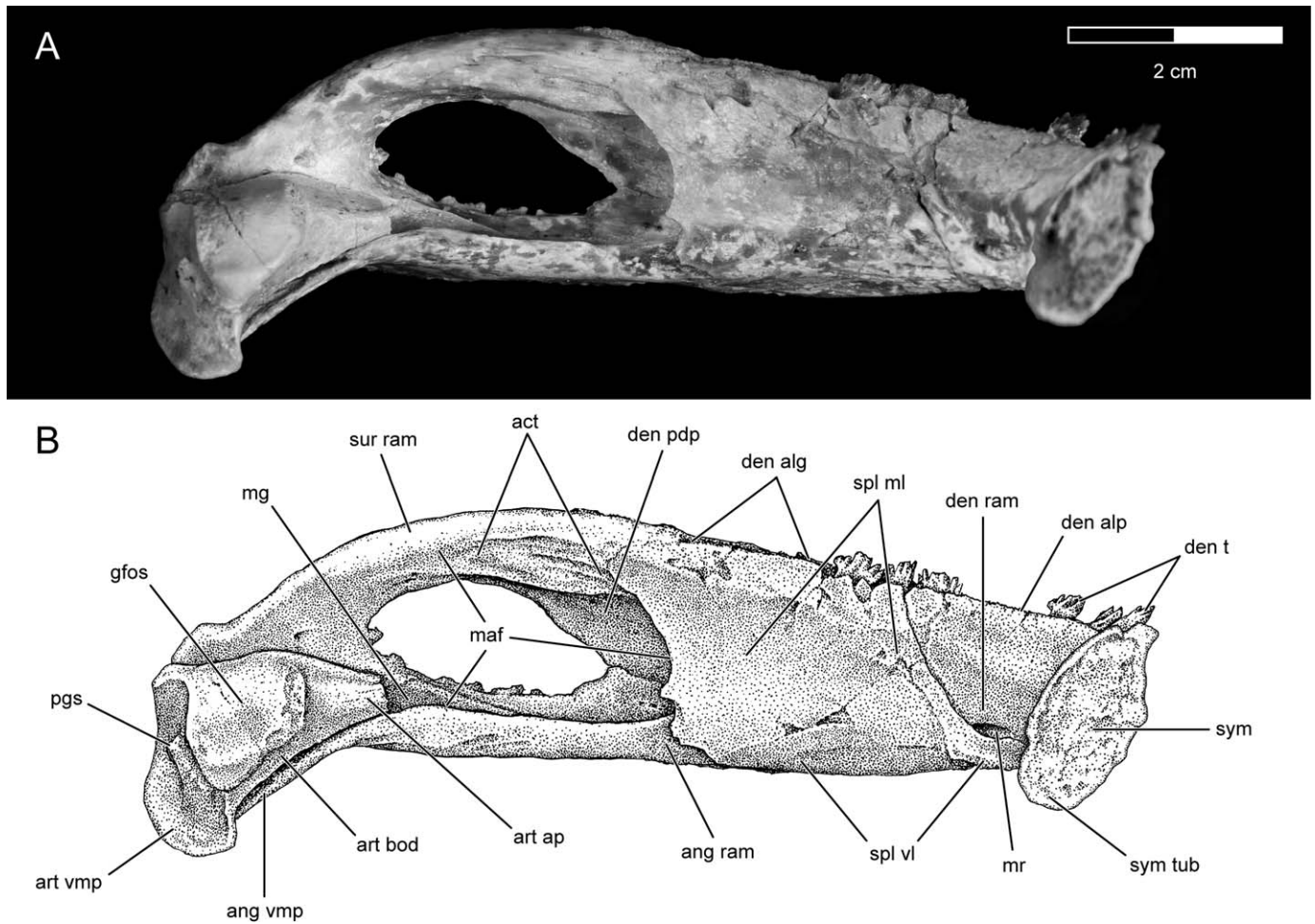


FIGURE 25. Left mandibular ramus of the holotype (UA 8679) of *Simosuchus clarki* in medial view. **A**, photograph; **B**, interpretive drawing. The mandibular symphysis in **A** is digitally simulated from a median sagittal HRXCT slice through the lower jaw of this specimen. See Appendix 1 for anatomical abbreviations.

tions forms a roughened and well-demarcated facet, or ‘coronoid tuberosity’ (Schumacher, 1973) (Figs. 23, 25, 27, 28). In living crocodylians, this represents an area of contact for the cartilago transiliens (Fig. 9F), a functional ensemble of two loosely connected cartilaginous disks surrounded by a thick layer of fibrous connective tissue (fibrous ‘pillow’ or ‘cushion’ of Iordansky, 1964, 1973), which collectively serves as the common site of insertion for several major tendons of the *M. adductor mandibulae* complex (Iordansky, 1964; Schumacher, 1973; Busbey, 1989; Cleuren and De Vree, 2000). This contact area measures nearly 19 mm anteroposteriorly by ~5.5 mm dorsoventrally on both sides of the lower jaw of UA 8679. Comparable measurements could not be made on FMNH PR 2597 because the lower jaw remains articulated with the skull in this specimen; however, a similar area of comparable size is partially exposed on the unbroken right surangular of this specimen, with the remainder of the facet being hidden by the expanded distal end of the right transverse process of the pterygoid. Similarly, this contact area is well preserved in the fragmentary right anterior surangular ramus preserved with FMNH PR 2598, but it cannot be measured accurately due to breakage. On both sides of the lower jaw of UA 8679, and on the surangular fragment preserved with FMNH PR 2598, the contact area for the cartilago transiliens is bounded dorsally by a well-developed longitudinal crest (Figs. 25, 27, 28). Based on the con-

dition(s) exhibited by extant crocodylians, this prominent crest likely represents an area of attachment for anterolateral fibers of the mandibular adductor (‘stem’) tendon and/or lateral fibers of the fibrous capsule (‘pillow’ or ‘cushion’) of the cartilago transiliens ensemble (Iordansky, 1964, 1973; Schumacher, 1973).

Immediately dorsal to the contact area for the cartilago transiliens is a relatively well-demarcated area of muscle scarring that extends for more than 20 mm anteroposteriorly along the dorsal and dorsomedial surfaces of the gently arched dorsal-most portion of the surangular ramus (i.e., ‘coronoid process’). This area of muscle attachment is divided into somewhat distinct lateral and medial portions of approximately similar mediolateral widths by a subtle angulation—best visualized microscopically under oblique lighting, but also discernible in HRXCT scans of UA 8679 (Fig. 9F)—extending longitudinally along the dorsomedial margin of this portion of the ramus. Again by comparison with living crocodylians, we interpret these lateral and medial areas of muscle scarring as representing the areas of insertion for the *M. adductor mandibulae externus superficialis* and *M. adductor mandibulae externus medius*, respectively (Iordansky, 1964; Schumacher, 1973; Busbey, 1989; Cleuren and De Vree, 2000).

In addition to the lateral surangular foramina described above, numerous foramina are also present along the ventral and me-

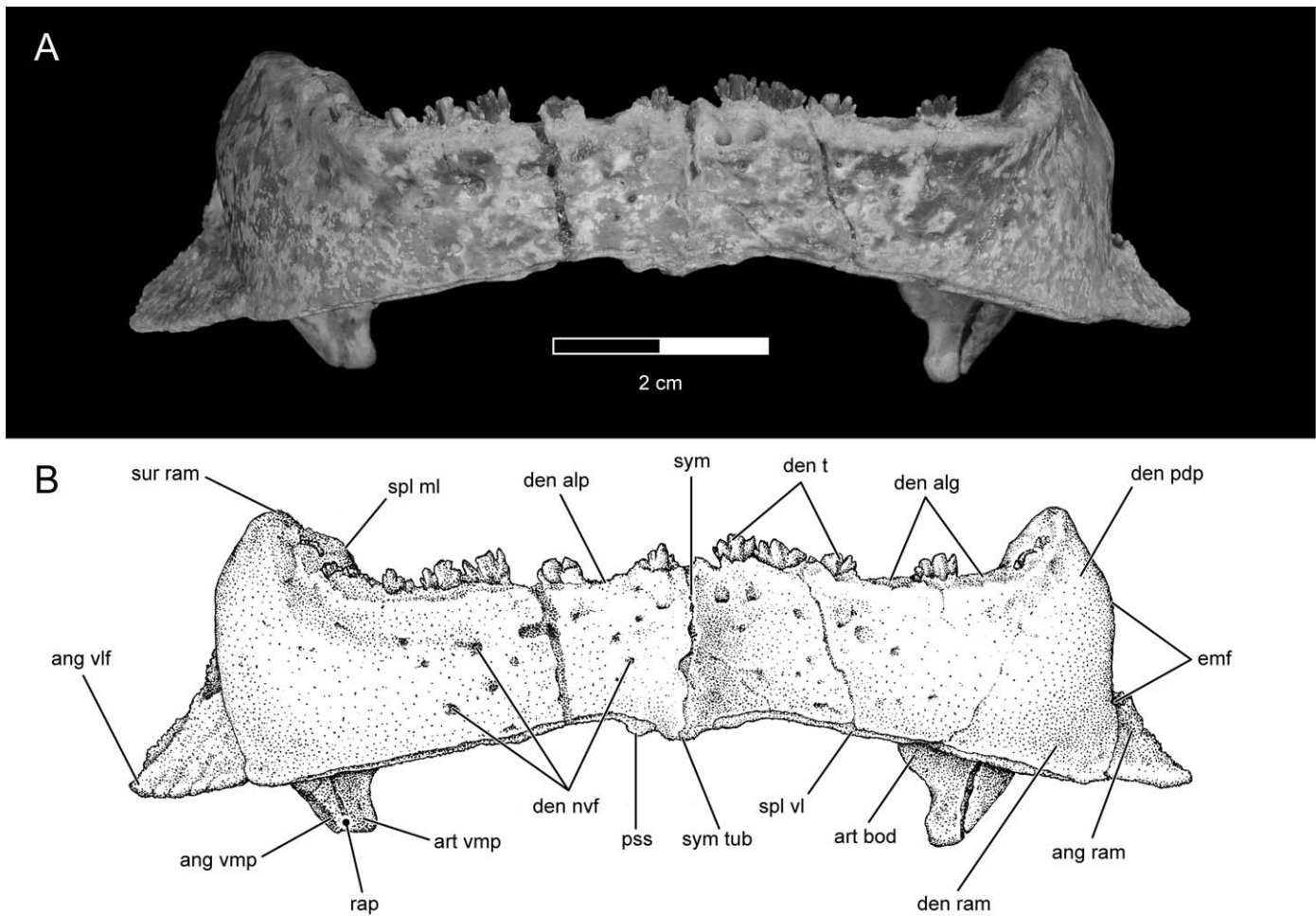


FIGURE 26. Lower jaw of the holotype (UA 8679) of *Simosuchus clarki* in anterior view. **A**, photograph; **B**, interpretive drawing. See Appendix 1 for anatomical abbreviations.

dial aspects of the surangular ramus. On the ventral surface of the ramus, in the roof of the prominent groove for the mandibular nerve, there is a single relatively large foramen leading into a posteriorly directed canal, which can be seen on both sides of the lower jaw of UA 8679 (Fig. 29A), on the unbroken right surangular of FMNH PR 2597, and on the surangular fragment preserved with FMNH PR 2598. In HRXCT slices through the head skeleton of UA 8679, the canal into which this foramen leads can be traced far posteriorly within both surangular rami; on both sides, the canal can be seen to be confluent with numerous smaller canals, emanating from the three dorsally placed lateral surangular foramina, as well as from two small medial foramina located very close to the posterodorsal margin of the external mandibular fenestra. Thus, we interpret the large dorsal foramen and its associated canal as having transmitted an early afferent trunk of the mandibular division of the trigeminal nerve, one which branched off immediately after the latter entered into its groove, and one which provided sensory innervation to (at least in part) the skin along the dorsolateral surface of the posterior half of the lower jaw. However, in addition to the small medial foramina described above, one significantly larger medial foramen is found further posteriorly, ~1 mm dorsal to the posterior part of the anterior process of the articular (Fig. 25). This foramen, also confluent with the main surangular canal described above, may have transmitted

sensory fibers innervating the capsule of the craniomandibular joint.

Finally, projecting posteriorly, ventrally, and medially from the posterior-most part of the surangular ramus is the ventromedial process of the surangular (Figs. 6, 9K, 23, 24, 27, 28). It contributes to the formation of the highly modified, trilaminar retroarticular process of *Simosuchus* by insinuating itself between the medially placed ventromedial process of the articular and the laterally placed ventromedial process of the angular. This portion of the surangular, preserved only in the holotype specimen (UA 8679), is largely hidden from external view, being visible only along its ventromedially slanting posterolateral edge. Near the root of this process, on the lateral aspect of the posterior-most part of the ramus, is one additional lateral surangular foramen, significantly larger in diameter than the three smaller ones described above; like the latter, however, it is confluent with the main surangular canal, and likely transmitted small cutaneous branches of the mandibular nerve that innervated the skin overlying the area surrounding the jaw joint.

Angulars—The angulars (Figs. 1A, C–E, 2, 4–6, 12, 17, 22–29), like the surangulars, each consist of a relatively long ramus anteriorly and a much shorter, flattened ventromedial process posteriorly. In fact, the angulars mirror the surangulars in several aspects of their morphology, including their somewhat deceptively

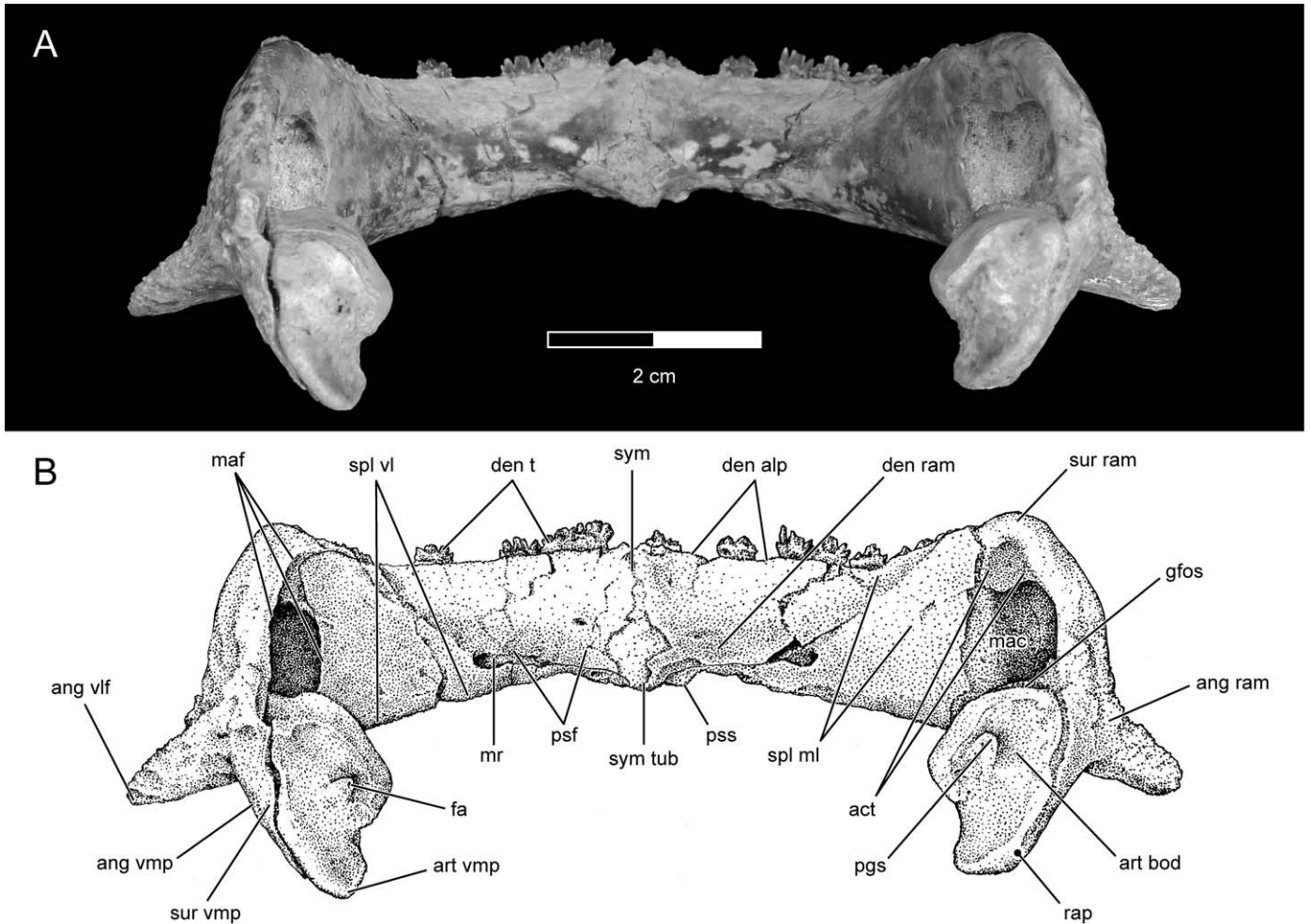


FIGURE 27. Lower jaw of the holotype (UA 8679) of *Simosuchus clarki* in posterior view. **A**, photograph; **B**, interpretive drawing. See Appendix 1 for anatomical abbreviations.

simple gross appearance. However, the angulars do differ significantly from the surangulars in one very conspicuous way: each bears a robust, sharp-edged flange that projects strongly ventrolaterally from the ramus along its entire length, a prominent anatomical feature that adds considerably to the overall width of the lower jaw, and indeed, to that of the entire head skeleton (Figs. 2, 5, 6, 9C–H, 17A, B, D, 22, 23, 26–28, 29B, C).

The ramus of the angular originates posteriorly where it meets the ventromedial process, an intersection that is oriented somewhat obliquely, beginning medially subjacent to the tip of the anterior process of the articular and extending laterally to the posterior terminus of the ventrolateral flange (Figs. 6, 23–25, 27, 28). From this posterior origin, the ramus extends anteriorly, forming the ventral margin of the external mandibular fenestra laterally (Figs. 5, 9E–G, 22, 24, 26, 28) and that of the mandibular adductor fossa medially (Figs. 9G, 25, 28), before ultimately becoming embraced between the dentary (laterally) and the splenial (medially and ventrally) (Figs. 5, 6, 9C, D, 12, 17A–C, 23–26, 28, 29B, C). However, HRXCT scans of the head skeleton of UA 8679 reveal that the angular ramus continues anteriorly well beyond these initial points of contact for a distance of more than 20 mm, hidden from external view by—and maintaining continued syndesmoti contact with—the surrounding dentary and splenial (Figs. 9C, 17A, B, 29B, C). (A similar anterior extension of the angular can

be seen within the left mandibular ramus in CT scans of the head skeleton of FMNH PR 2597 as well.) Along this entire course, including that portion anteriorly that is hidden from external view, the angular ramus presents a prominently concave dorsal surface with distinctly raised medial and lateral walls. The trough that is formed by this dorsal concavity accommodated Meckel's cartilage. Indeed, it is continuous posteriorly with a dorsomedially facing groove that extends along the internal surface of the ventromedial process of the angular to accommodate the anterior process of the articular (Figs. 9C–H, 25, 28, 29B, C), which represents an endochondral derivative of the posterior portion of the embryonic Meckelian cartilage. Thus, the ramus of the angular forms the floor of Meckel's groove throughout the mandibular adductor fossa (Figs. 9E–G, 25, 28, 29B, C), and the floor of Meckel's canal more anteriorly (Figs. 17A, 29C), with the walls of the latter being formed by the ramus of the dentary laterally and by the medial lamina of the splenial medially.

The angular ramus exhibits virtually no sagittal curvature whatsoever, such as that seen in the dorsally arching surangular ramus. Rather, it is almost perfectly straight when viewed medially (Figs. 12, 17C, 25). However, dorsal and ventral views reveal a conspicuous yet relatively gentle lateral curvature of the ramus (Figs. 22, 23, 29B, C). This curvature gives the ramus of the angular a distinctive 'bowed-out' appearance, similar to that seen in

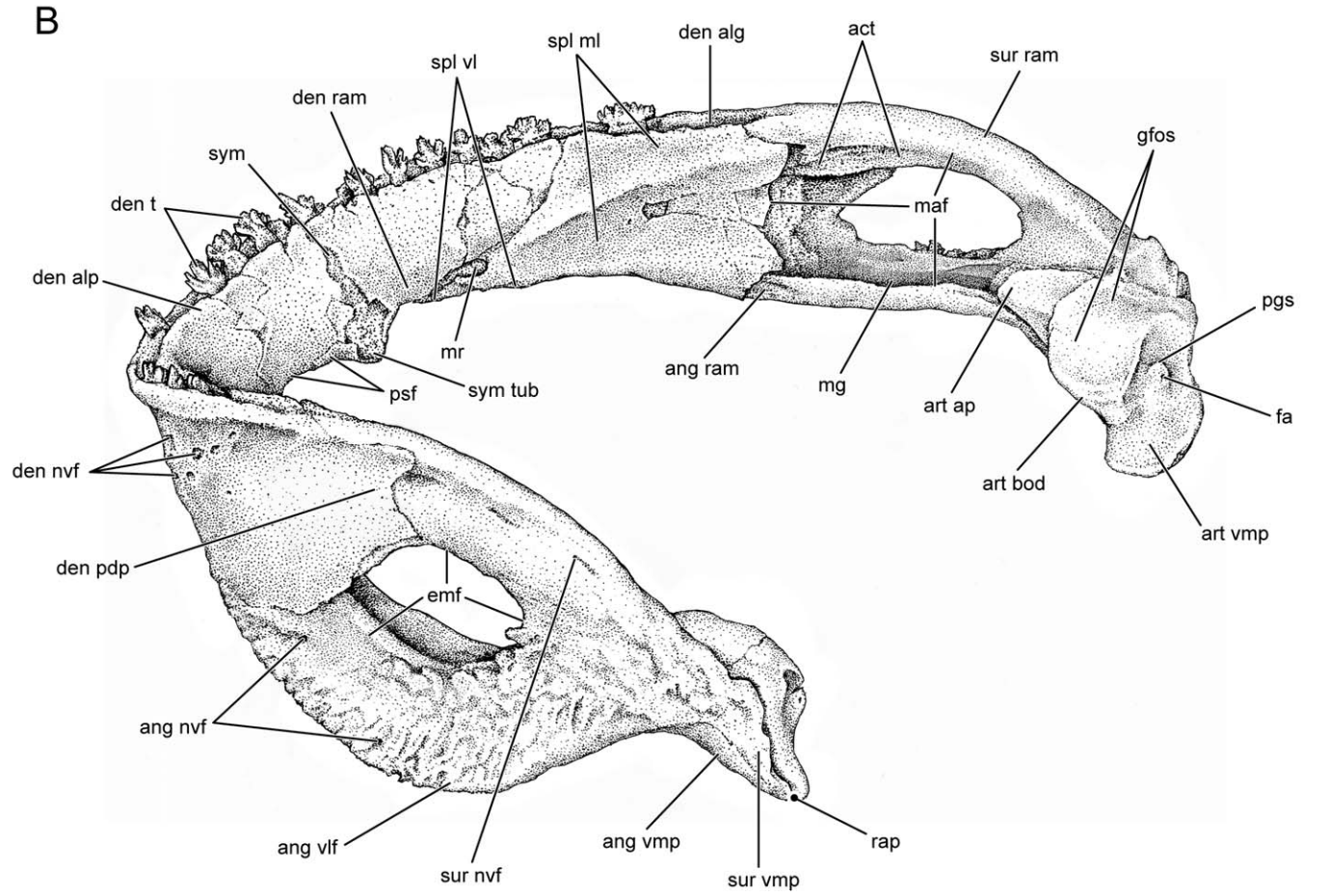
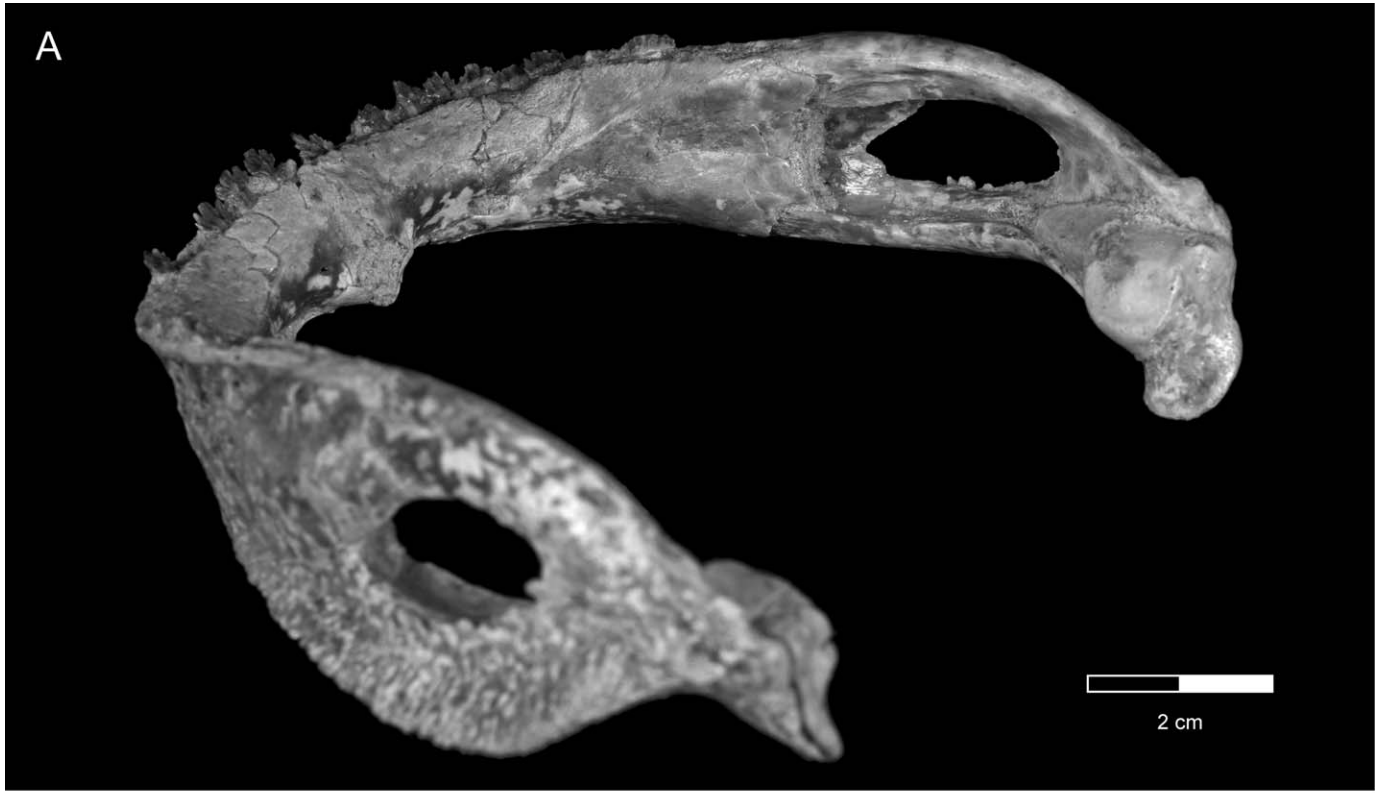


FIGURE 28. Lower jaw of the holotype (UA 8679) of *Simosuchus clarki* in oblique posterodorsal view. **A**, photograph; **B**, interpretive drawing. See Appendix 1 for anatomical abbreviations.

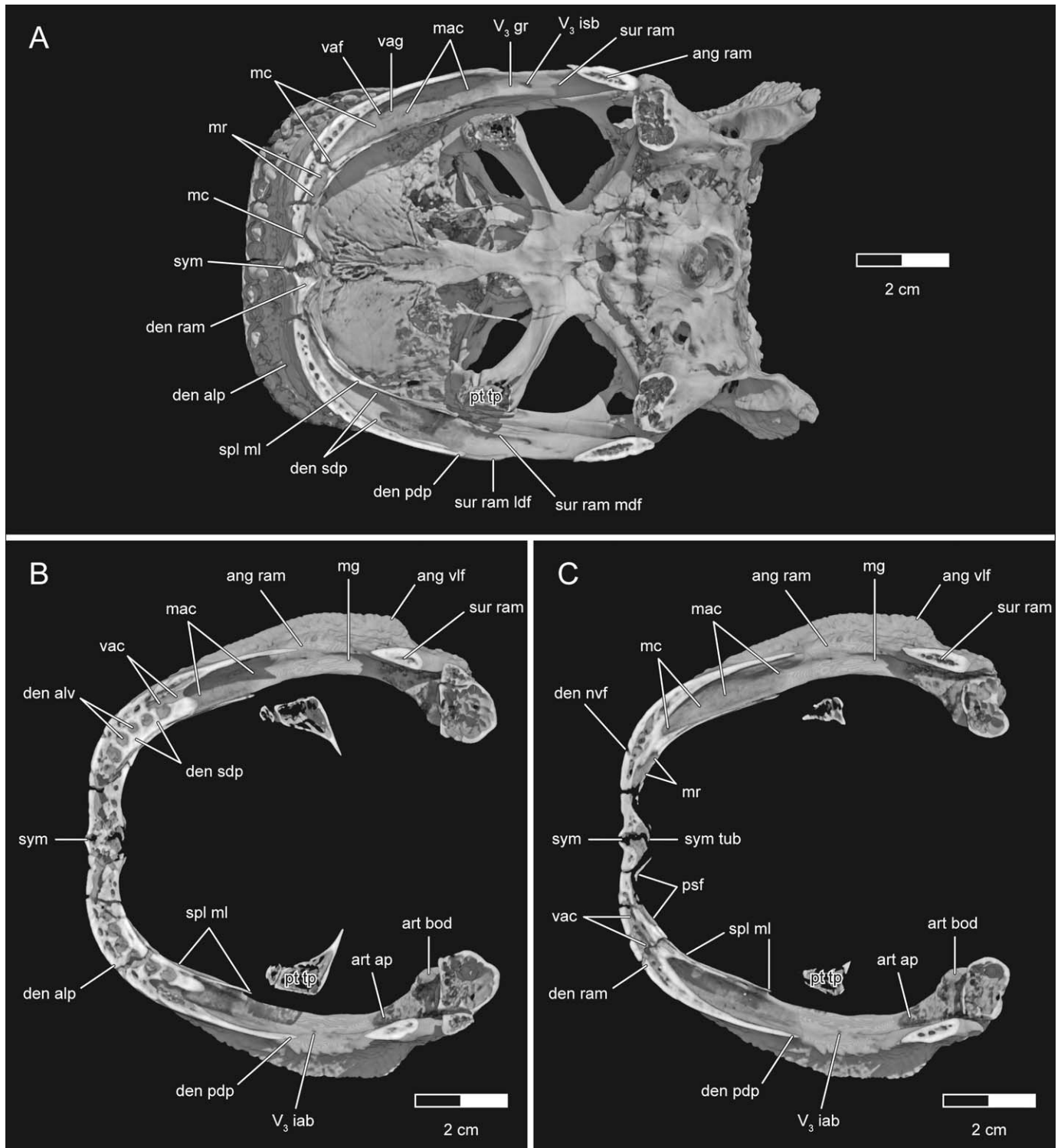


FIGURE 29. Morphology of the lower jaw of *Simosuchus clarki*, as seen in frontal (horizontal) cutaway views through a three-dimensional digital reconstruction of the head skeleton of the holotype (UA 8679) generated from HRXCT scans. In this reconstruction, remaining matrix has been removed digitally so as to provide unobstructed views of unprepared internal regions of the lower jaw. **A**, ventral view from a frontal plane passing through Meckel's canal. **B**, dorsal view from a frontal plane passing through the posterior portion of the ventral alveolar canal. **C**, dorsal view from a frontal plane passing through Meckel's canal. (Note: 'virtual preparation' of this specimen has resulted in the digital deletion of portions of the thinnest laminae of bone throughout the head skeleton, such as those that surround the nasopharyngeal canals and internal nares; these thin laminae of bone are in actuality better preserved in this specimen than is depicted in this computer-generated reconstruction.) See Appendix 1 for anatomical abbreviations.

the surangular ramus. However, this effect is amplified greatly in the contours of the angular due to its widely flaring ventrolateral flange.

In general, the ventrolateral flange of the angular is one of the most characteristic features of the head skeleton of *Simosuchus clarki*, due in large part to the extent to which it flares laterally beyond the remaining margins of the skull and lower jaw, especially posteriorly (Figs. 2, 5, 6, 9C–H, 17A, B, D, 22, 23, 26–28, 29B, C). Adding further to its highly conspicuous nature is the heavy sculpturing that it exhibits along its entire external surface, both dorsolaterally (Figs. 5, 22, 24, 26, 28) and along the lateral margin of its ventral surface (Figs. 6, 23); this contrasts markedly with the surfaces along the remainder of the angular ramus, which are completely devoid of sculpturing (Figs. 6, 12, 17C, 23, 25, 28).

The ventrolateral flange essentially represents a highly elaborated expansion of the ventrolateral portion of the angular ramus. It originates posteriorly from a point located laterally adjacent to the proximal part of the anterior process of the articular (Figs. 9H, 12, 17C, 22, 23, 28, 29B, C), and it extends anteriorly to the posterior end of the syndesmosis between the ventral margin of the ramus of the dentary and the lateral margin of the ventral lamina of the splenial (Figs. 5, 9C, 17A, 23, 24, 26, 28). Along this relatively long anteroposterior course (extending nearly 5 cm both in UA 8679 and on the articulated left side of the mandible in FMNH PR 2597), the shape and extent of the ventrolateral flange vary considerably. Immediately anterior to its posterior origin it abruptly flares laterally (and to a lesser extent ventrally), very nearly reaching its maximum mediolateral width within the first few millimeters of its length. This abrupt ventrolateral flaring renders the flange with a strongly angled and nearly straight posteroventrolateral border (Figs. 22, 23, 29B, C). Upon achieving its near-maximum width, the ventrolateral flange extends anteriorly for a distance of nearly 2 cm without its width changing significantly; thus, this segment of the flange appears to have a nearly straight lateral margin in dorsal or ventral view, and one that meets the strongly flared posterolateroventral margin at a distinct angle (Figs. 22, 23, 29B, C). Finally, anterior to this relatively straight segment, beginning at a point lying in a transverse plane coinciding with the posterior tip of the ventral prong of the dorsolateral process of the dentary, the lateral margin of the ventrolateral flange begins to deviate medially toward the main part of the ramus. This tapering of the anterior 2.5 cm of the flange creates a second angulation along its lateral margin, but one that is considerably more subtle than the strong posteroventrolateral angulation described above (Figs. 5, 22, 23, 29B, C).

The dorsolateral surface of the ventrolateral flange of the angular is subtly concave, except along its tapered anterior end (Fig. 26). Nevertheless, the flange as a whole exhibits a cross-sectional shape closely approximating that of an obtuse triangle, with its obtuse angle formed between its ventromedial and medial sides (the latter being the junction between the flange and the main portion of the ramus, a ‘side’ that is, of course, not freely exposed) (Figs. 9D–G, 17B). In the holotype specimen (UA 8679) of *S. clarki*, this medial ‘side’ of the ventrolateral flange—effectively representing its basal height—measures 7–8 mm dorsoventrally along most of its anteroposterior length, giving the flange a tall, robust appearance (Figs. 17A, 26, 27). However, it tapers rapidly as it extends ventrolaterally, thereby forming a relatively sharp lateral edge (Figs. 5, 17A, 26). It bears emphasis that, because this sharp lateral edge is created through the acute intersection of two surfaces that are heavily sculptured, so too is the edge itself; it is rough and irregular along nearly its entire length (Figs. 22–24), having the texture of a finely serrated (though relatively dull) knife blade.

Although both the dorsolateral and ventromedial surfaces of the ventrolateral flange of the angular bear heavy sculpturing, the morphology of this sculpturing differs markedly between these two surfaces. That which covers the dorsolateral surface of the

flange is relatively similar to the sculpturing seen along the external surfaces of several of the more heavily ornamented dermal roofing bones, such as the squamosal and prefrontal, consisting of a seemingly near-random pattern of reticulating ridges of variable shape with relatively deep pits and grooves interspersed between them (Figs. 22, 24, 28). In contrast, the sculpturing present along the lateral edge of the ventromedial surface of the flange is highly regular, consisting of an array of relatively straight and roughly parallel (and thus non-reticulating) ridges running approximately perpendicular to the lateral margin of the flange, with similarly straight grooves passing between these ridges (Fig. 23).

Scattered across the dorsolateral surface of the ventrolateral flange of the angular, and largely recessed within the pits and grooves created between the sculptured ridges that ornament this surface, are numerous relatively small neurovascular foramina (Figs. 24, 28). Although several of these can be readily seen externally, especially with the aid of a microscope, they are most easily visualized (and counted) in HRXCT scans of the head skeleton of UA 8679; in this specimen, at least 10 of these foramina are present on each angular. Each of these foramina is associated with a straight, posteromedially oriented canal that ultimately enters into a larger central canal running throughout the length of the angular ramus. Moreover, and further mirroring the condition exhibited within the surangular, this main angular canal communicates with the mandibular adductor fossa via a relatively prominent foramen on the dorsal surface of the ramus (Fig. 29B, C), located almost directly ventral to the somewhat larger corresponding foramen on the ventral surface of the surangular ramus (Fig. 29A). As for the neurovascular network running throughout the surangular ramus, we interpret this system of foramina and canals within the angular ramus and its associated ventrolateral flange as having transmitted sensory fibers from the skin overlying the lateral surface of the lower jaw to the mandibular division of the trigeminal nerve, most likely along with small accompanying arteries and veins.

Within the region of the mandibular adductor fossa, two additional features of the angular ramus warrant description. The first of these is a sharp but low, dorsally projecting crest that originates posteriorly near the root of the angular ramus and that extends anteriorly along the lateral half of the floor of the adductor fossa for a distance of ~1 cm before terminating immediately posterior to the prominent foramen described above (Figs. 9G, 25, 28, 29B, C). Along this relatively short anterior course, the crest also arcs gently medially, thereby largely following the overall curvature of the entire mandibular ramus in this region. This crest represents the raised lateral wall of the posterior-most portion of Meckel’s groove. It is seen on both sides of the lower jaw of UA 8679, and on the disarticulated right angular of FMNH PR 2597. A second conspicuous feature in this region, located just 3–4 mm medial to the lateral crest just described, is a marked elaboration of the dorsomedial margin of the angular ramus. Here, along the ventral margin of the mandibular adductor fossa, the dorsomedial edge of the ramus is moderately elevated, greatly thickened, and marked by extensive muscle scarring along its surface (Figs. 9G, 12, 17C, 25, 28, 29B, C). This thickened area of the ramus, which is well preserved only in UA 8679 (both sides), is most well developed throughout the posterior one-third of the adductor fossa; however, it does extend somewhat further anteriorly, gradually tapering throughout the middle one-third of the fossa before disappearing altogether. Based on comparisons with extant crocodylians, this tuberosity along the dorsomedial margin of the angular ramus likely represents an area of insertion for portions of the *M. pterygoideus* anterior (referred to as the *M. pterygoideus dorsalis* by some authors; e.g., Lakjer [1926], Witmer [1995], Holliday [2009]), as well as those portions of the highly complex mandibular adductor tendon that arise within this muscle (Iordansky, 1964; Schumacher, 1973; Busbey, 1989).

The ventromedial process of the angular contributes the outermost layer to the peculiar trilaminar retroarticular process of *Simosuchus* (Figs. 6, 9K, 17A, 23–28). Although it is indeed relatively long, and more extensively exposed than the ventromedial processes of either the surangular or articular, it is by far the thinnest (mediolaterally) of the three processes that make up the retroarticular process. Its externally exposed surface, which faces laterally, ventrally, and anteriorly, bears a relatively large central concavity near its junction with the angular ramus, but then becomes flat toward its rounded ventromedial end (Figs. 9H–K, 17A, 23, 24, 26). It appears smooth, both macroscopically and microscopically, along much of this exposed surface. However, its anteroventromedial margin exhibits a rather distinctive area of muscle scarring, characterized by relatively low but thick parallel striae. These largely longitudinally oriented striae fan out somewhat toward the flattened distal end of the ventromedial process of the angular, where it approaches the thickened, roughened, and rounded posteroventral margin of the ventromedial process of the articular. Based on comparisons with modern crocodylians, this area of scarring almost certainly served as a site of insertion for a portion of the *M. pterygoideus posterior* (referred to as the *M. pterygoideus ventralis* by some authors; e.g., Lakjer [1926], Witmer [1995], Holliday [2009]) (Iordansky, 1964; Schumacher, 1973; Busbey, 1989).

Coronoids—Coronoids are not preserved in any known specimens of *Simosuchus clarki*. Moreover, no apparent bony signatures are present anywhere along the surfaces of the dermal bones circumscribing the mandibular adductor fossa (i.e., splenial, surangular, angular) in any of the known specimens of this species—including the exquisitely preserved holotype specimen (UA 8679)—to suggest that coronoids were present in this taxon. Indeed, among crocodylians, the presence of coronoids has only been documented definitively within Crocodylia.

Splenials—The splenials (Figs. 1D, E, 5, 6, 12, 17, 22–28) are well preserved only in the holotype (UA 8679) of *Simosuchus clarki*, and even in this exquisitely preserved specimen, both of these very thin bones show small, isolated areas of breakage. CT scans of the head skeleton of FMNH PR 2596 reveal both splenials to be badly crushed in this specimen, and only part of the ventral portion of the left splenial is preserved in FMNH PR 2597.

The splenials are extraordinarily thin, sheet-like bones that contribute to the formation of the mandibular/Meckelian canals and to the delineation of the mandibular adductor fossae (Figs. 6, 7E, 8H, I, 9A–D, 12, 17A–C, 25, 27–29). Although they closely approach the mandibular symphysis, they do not participate in its formation (Figs. 6, 7A, 23, 26, 27). Each consists posteriorly of relatively expansive medial and ventral laminae that meet one another at a slightly obtuse angle along the ventromedial margin of the mandibular ramus (Figs. 6, 9C, 12, 17A–C, 23, 25, 27). Anteriorly, however, both laminae taper significantly. The medial lamina tapers more abruptly, disappearing altogether near where the mandibular ramus angles sharply medially (Figs. 12, 17C, 22, 25, 27, 28). In contrast, the narrowed ventral lamina continues beyond this angulation, extending medially along the ventral aspect of the transversely oriented anterior portion of the mandibular ramus before tapering to a blunted point on the ventrolateral edge of the enlarged symphyseal tubercle formed by the dentaries (Figs. 6, 23, 26–28).

Viewing the mandibular ramus from an oblique posterodorsomedial perspective, the thin sheet of bone that constitutes the medial lamina of the splenial can be seen to exhibit a subtrapezoidal outline, being slightly longer than it is tall, having a gentle semilunar emargination along its posterior edge, and having an anterior edge that slants steeply anteroventrally (Fig. 28). However, a pronounced lateral flaring of the anterodorsal corner of the lamina renders this sheet of bone non-planar, and the angulation created through this flaring effectively divides the medial lamina into two

subtriangular regions of unequal size: a relatively large medially facing one and a smaller dorsomedially facing one, with the latter having an area approximately one-third that of the former (Figs. 25, 28). Both of these subtriangular surfaces are smooth and subtly concave, and neither appears to be pierced by any foramina.

In addition to occupying two different planes, the two well-delineated subtriangular areas of the medial lamina of the splenial described above contribute to the overall structure of the lower jaw in entirely different ways. The slightly emarginated posterior edge of the medially facing surface of the lamina forms the anterior margin of the mandibular adductor fossa (Figs. 17B, 25, 27, 28). Immediately anterior to this, the tall posterior portion of this medial face forms the medial wall of the mandibular canal (Figs. 8H, I, 9C, D, 17B, 27, 29), which transmitted both Meckel's cartilage (ventrally) and the ventral alveolar neurovascular bundle (dorsolaterally). Further anteriorly, however, the ventral alveolar neurovascular bundle separated from this common canal, passing into its own dorsolaterally placed canal within the dentary at the anteroposterior level of the 11th mandibular alveolus, and thus near the approximate anteroposterior midpoint of the medial lamina of the splenial (Figs. 8H, 9C, 29). Therefore, along the sharply tapered anterior portion of the medially directed face of the medial lamina, this portion of the splenial contributes only to the medial wall of Meckel's canal (Figs. 8I, 9B, 17A, 29A, C). At its anterior terminus, this larger of the two subtriangular surfaces of the medial lamina does not taper to a sharp point; rather, its anterior apex exhibits a slight, anteromedially concave emargination that forms the posterolateral margin of a well-developed notch for the anteromedial continuation of Meckel's cartilage (Figs. 17C, 25, 27, 28).

The dorsomedially facing subtriangular portion of the medial lamina of the splenial does not contribute in any way to the formation of either the mandibular canal or the Meckelian canal. Instead, it flares laterally to form the medial wall of the posterior, longitudinally oriented portion of the mandibular alveolar groove, from the center of the ninth mandibular alveolus posteriorly (Figs. 5, 8H, 9C, D, 12, 17, 22, 25, 27, 28, 29B). Anteroventromedially, this dorsomedially facing portion of the lamina terminates in a sharply tapered point immediately dorsal to the prominent emargination at the anterior terminus of the medially directed face of the lamina (Figs. 12, 17C, D, 22, 25, 28).

The ventral lamina of the splenial is approximately sickle-shaped in ventral view, gradually tapering as it gently curves anteromedially toward the symphyseal region (Figs. 6, 23). This relatively gentle curvature contrasts markedly with the sharp angulation seen along the dorsal margin of the alveolar process of the dentary (Figs. 5, 8H, 17D, 22–24, 26, 28). Near its posterior end, immediately anterior to the mandibular adductor fossa, the ventral lamina effectively forms a 'subfloor' of the mandibular canal; from its junction with the medial lamina along the ventromedial margin of the mandibular ramus, it extends laterally, overlapping the true floor of the canal (formed by the anterior-most portion of the angular ramus), before ultimately reaching the ventrolateral margin of the mandibular ramus, where it establishes a syndesmotomic contact with the ventral edge of the ramus of the dentary (Figs. 9C, 17A, 23, 24, 26). Further anteriorly, however, beyond the anterior terminus of the angular ramus (and the origin of the ventral alveolar canal), the ventral lamina of the splenial does contribute (along with a prominent process projecting medially from the ramus of the dentary) to the formation of the true floor of Meckel's canal (Fig. 9B).

Along its wide posterior part, the exposed surface of the ventral lamina of the splenial is smooth and relatively featureless, bearing only a shallow, longitudinally oriented concavity (Figs. 6, 23, 25). However, this shallow groove is continuous anteriorly with a somewhat more prominent and well-defined fossa located directly subjacent to the fourth through sixth mandibular alveoli (and thus in the region of angulation of the alveolar process of

the dentary) (Figs. 6, 23, 25, 27). This fossa is delineated in part by the anterolateral edge of the ventral lamina, which is significantly thickened in this region to form a distinct curvilinear ridge. In addition, however, a similarly well-developed ridge serves to define the posteromedial border of the fossa. Both of these surrounding ridges present distinctly irregular, undulating margins indicative of muscle and/or tendon scarring. Immediately posterior to the posterolateral portion of this fossa is a very small, round foramen. Slightly further posterolaterally is a relatively deep groove, also associated with a foramen, that extends longitudinally along the ventral lamina for a distance of nearly 3 mm.

The ventral lamina of the splenial tapers rapidly as it extends medially beyond the fossa just described (Fig. 23). As it does so, it follows the dorsoventrally curved contours of a relatively wide but shallow emargination that extends along the ventral edge of the dentary in this region (Figs. 6, 9A, 26, 27). Ultimately, the ventral lamina terminates in a slightly blunted point along the ventrolateral edge of the expanded symphyseal tubercle formed at the junction of the left and right dentaries (Fig. 23). Projecting ventrolaterally from this terminal point is a relatively small but distinct parasymphyseal spine (preserved only in UA 8679, and distinctly larger on the right side of this specimen) (Figs. 7C, 23, 26, 27). Although the ventral lamina of the splenial does encroach upon the ventrolateral margin of the symphyseal tubercle, it does not contribute in any way to the formation of the mandibular symphysis itself.

The extraordinarily broad ventral exposure of the splenial—in particular, that of the posterior part of the ventral lamina, which extends across the entire mediolateral width of the anterior portion of the mandibular ramus—represents an autapomorphy of *S. clarki*.

Dentaries—The dentaries (Figs. 1A, C–E, 2, 4–6, 17, 22–28) are relatively well preserved on both sides of the lower jaw of the holotype (UA 8679) of *Simosuchus clarki*, although both right and left elements in this specimen exhibit numerous cracks. Both dentaries are also preserved in FMNH PR 2596 and FMNH PR 2597; however, both elements are partially crushed and remain largely surrounded by matrix in the former specimen, and those of the latter specimen, although largely free of surrounding matrix, exhibit considerable distortion and breakage, especially on the right side. Nevertheless, due to its missing right splenial and incomplete left splenial, FMNH PR 2597 offers many informative views of the internal morphology of the dentaries.

The dentaries are the largest bones of the lower jaw, measuring (in UA 8679) ~73 mm mesiodistally along their dorsal margins (i.e., including both their transversely and longitudinally oriented segments) and ~22 mm in maximum dorsoventral height. Each consists of three primary parts: a strongly curved basal portion, the ramus; a sharply angulated and dentigerous dorsal extension of the ramus, the alveolar process; and a dorsoventrally tall and bluntly forked posterodorsal process (Figs. 5, 6, 22–28). No posterioventral process is present in *S. clarki*. The left and right dentaries are sutured tightly together at the anterior midline, forming a relatively firm and tall mandibular symphysis (Figs. 5, 6, 7B, 8H, I, 22–29).

The ramus of the dentary constitutes the basal portion of this complex element, from which both the alveolar and posterodorsal processes project (Figs. 5, 6, 22–28, 29A, C). Its ventral margin extends from the anterior terminus of the ventrolateral flange of the angular to the mandibular symphysis. Along nearly this entire course—except at the symphysis itself—it meets the anterolateral margin of the ventral lamina of the splenial in a tight syndesmotomic connection (Figs. 9B, C, 23, 26). Consequently, the ramus of the dentary mirrors the splenial in exhibiting a strong but relatively smooth anteromedial curvature (Figs. 8I, 23, 24, 26, 29A, C), rather than the more abrupt angulation seen dorsally along the margins of the overlying alveolar process (Figs. 5, 8H, 17D, 22–24, 26, 28).

Although the ramus of the dentary is conspicuously expanded at the symphysis to participate (along with its contralateral partner) in the formation of a prominent ventroposteriorly directed tubercle, it is shortest in dorsoventral height just laterally adjacent to this tubercle. This is due in part to a gentle dorsal emargination of the ventral surface of the ramus in this region (Figs. 5, 6, 23, 26–28). Perhaps more so, however, it reflects the great height of the superjacent alveolar process in the parasymphyseal region required to accommodate the relatively long roots of the anterior dentary teeth (Fig. 7A, C, D). Further laterally, and especially posteriorly along the largely longitudinally oriented portion of the dentary, where the roots of the teeth gradually shorten somewhat, the dorsoventral height of the ramus increases considerably. This gradual increase in the height of the ramus (and correlated decrease in the height of the alveolar process) may be visualized to some degree in the course of a prominent sulcus that slants (from anteroventral to posterodorsal) across the lateral surface of the longitudinal segment of the dentary (Figs. 24, 28). Although this sulcus is located slightly dorsal to the junction between the ramus and alveolar process, it rather closely parallels this junction along most of its length (as does the prominent angulation along the medial lamina of the splenial [Figs. 27, 28], albeit slightly less faithfully). Also clear when viewing the lower jaw in lateral view is that, as the ramus of the dentary increases in height posteriorly, its dorsal portion extends posteriorly beyond its ventral portion (the latter terminating where it contacts the anterior end of the ventrolateral flange of the angular) (Fig. 24); thus, even the posterior-most part of the alveolar process of the dentary is supported by the ramus.

Although pierced by numerous neurovascular foramina (Figs. 5, 8H, 23, 24, 26, 28, 29C), the labial surface of the ramus of the dentary is relatively smooth. However, two exceptions to this generalization are seen in the symphyseal region. First, where the left and right dentaries meet at the midline, the anteromedial edge of each ramus (and that of its superjacent alveolar process) is drawn sharply anteriorly to form (together with its contralateral partner) a distinct, vertically oriented crest that extends nearly the entire dorsoventral height of the symphysis (Figs. 5, 8H, 17C, 23, 24, 26, 29). Second, immediately adjacent to this symphyseal crest, the anteroventral surface of each ramus (and that of its superjacent alveolar process) is subtly corrugated, exhibiting several relatively low, horizontally oriented ridges that extend laterally from the symphysis for a distance of several millimeters (Figs. 17C, 23, 24, 26, 29A). These corrugations, which appear most strongly developed on the right side of the symphysis in UA 8679, are particularly evident in lateral view.

Across the predominantly transversely oriented anterior portion of the lower jaw, the lingual surface of the ramus of the dentary is broadly exposed in posterior view (Figs. 6, 17B, 27, 28). By far the most conspicuous feature seen in this area is the large, bulbous symphyseal tubercle, which is formed by ventroposterior expansions of the left and right dentary rami where they are sutured united at the mandibular symphysis (Figs. 6, 7B, 8I, 9A, 22, 23, 25–28, 29C). This prominent protuberance is preserved only in the lower jaw of the holotype (UA 8679), and even in this specimen it is slightly damaged, with the bone that constituted the central portion of its posterior surface having broken away. However, the bony surfaces of the dentary rami on either side of the symphyseal tubercle remain relatively well intact, revealing the presence of several additional morphological features in these areas. First, toward the ventral part of each ramus, immediately adjacent to the symphyseal tubercle, is a shallow but distinct parasymphyseal fossa (Figs. 6, 8I, 17C, 23, 27, 28, 29C). Based on comparisons with living crocodylians, this fossa almost certainly served as the primary site of origin for the *M. genioglossus* (Gnanamuthu, 1937; Sondhi, 1958; Schumacher, 1973). Second, lateral to the fossa just described, the ventroposterior portion of the ramus forms a horizontally oriented recess that

extends mediolaterally for a distance of several millimeters immediately dorsal to the medial extension of the ventral lamina of the splenial (Figs. 6, 9A, 12, 25, 27, 28, 29A, C). This recess, together with the underlying portion of the splenial, effectively represents an anteromedial continuation of Meckel's canal, which becomes incompletely enclosed in this region due to the abrupt anterior termination of the medial lamina of the splenial; thus, Meckel's cartilage was left partially exposed here along its posterior surface for a distance of several millimeters before it once again became fully encircled by bone as it more closely approached the mandibular symphysis. Finally, laterally adjacent to the symphyseal tubercle, several small foramina are preserved (Figs. 6, 27, 28). On both the left and right dentary rami of UA 8679, these parasymphyseal foramina include a larger, medially placed foramen, positioned ~7 mm lateral to the midline, as well as a smaller, more laterally (and dorsally) placed foramen, located ~11 mm from the midline. However, the foramina on the left ramus are positioned slightly further dorsally than those on the right ramus, with the latter actually being contained within the dorsal part of the right parasymphyseal fossa. In addition, on the left ramus only, a third foramen is present ~1.5 mm medial and ~1.0 mm ventral to the smaller, more dorsolaterally placed one of the two foramina just described.

HRXCT scans of the head skeleton of UA 8679 reveal the presence of a well-developed process that projects strongly lingually (and slightly dorsally) from the ventral edge of the labial surface of the ramus of the dentary. Posteriorly, this process insinuates itself between the lateral half of the anterior end of the angular ramus (dorsally) and the lateral half of the ventral lamina of the splenial (ventrally) (Fig. 9C). In doing so, it contributes (along with the ventral lamina of the splenial) to the formation of a 'subfloor' along the posterior-most part of Meckel's canal (the actual floor of the canal being formed by the dorsally concave anterior extension of the angular ramus). Further anteriorly, however, beyond the anterior terminus of the angular ramus, the dorsal surface of this submeckelian process of the dentary comes to form much of the true floor of Meckel's canal, with only a relatively small portion of the floor along the lingual side of the canal being formed by the dorsal surface of the ventral lamina of the splenial (Figs. 7E, 9A, B).

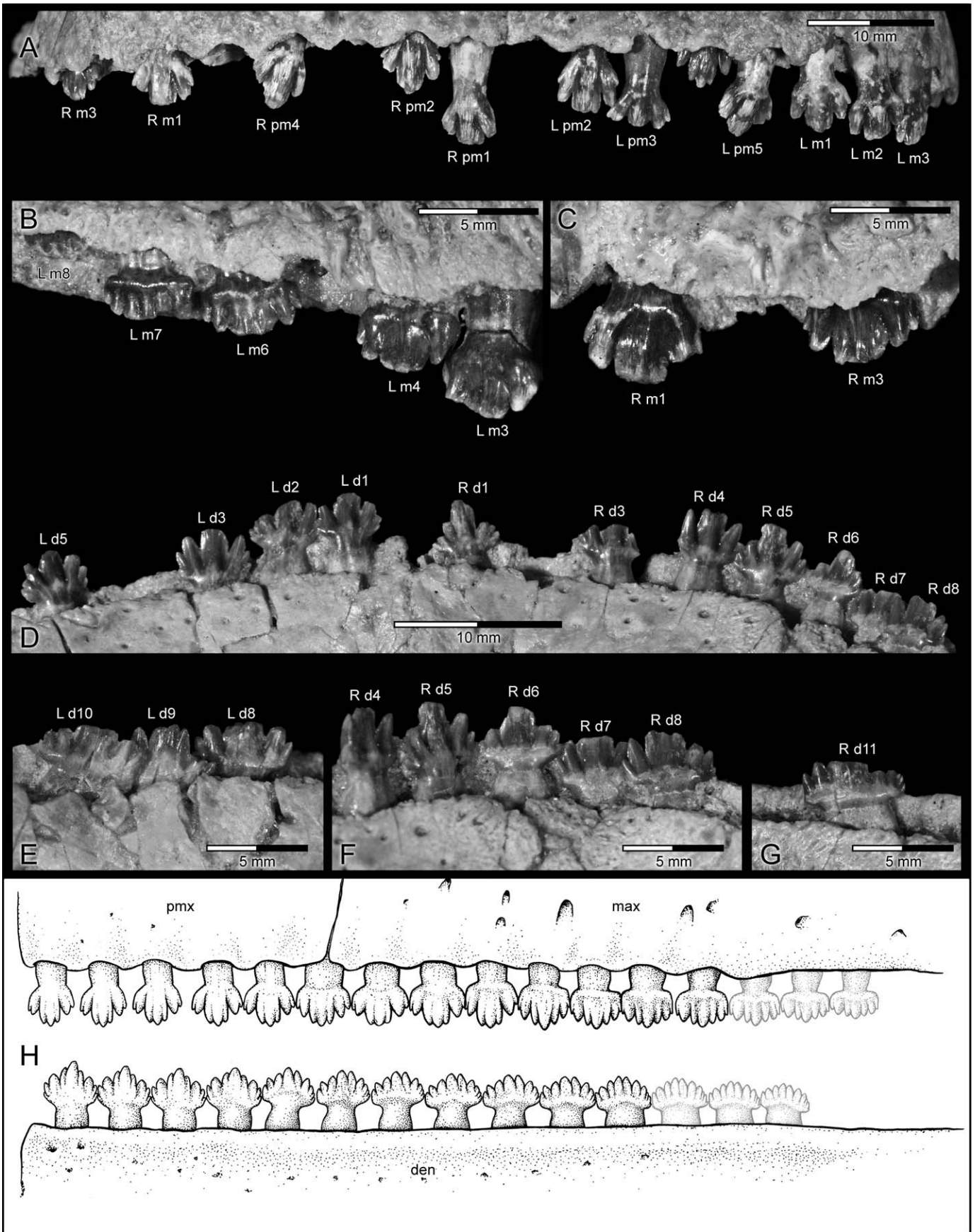
The alveolar process of the dentary projects predominantly dorsally from the underlying ramus (Figs. 5, 6, 22–28, 29A). However, along the largely transversely oriented anterior portion of the bone, the alveolar process also flares somewhat anteriorly, increasingly so as it extends laterally (Figs. 5–7, 12, 17D, 22–25, 28). In contrast, along the largely longitudinally oriented posterior portion of the bone, the alveolar process also flares somewhat laterally, increasingly so as it extends anteriorly (Figs. 5, 9B, C, 17A, 22, 23, 26, 28). As a consequence of these differing orientations, the alveolar process as a whole appears strongly angulated in dorsal view, with the complete mandibular dental arcade describing three sides of an only very slightly rounded rectangle having a mediolateral width nearly twice its anteroposterior length (Figs. 17D, 22, 28). This complete dental arcade consisted of 28 functional teeth, with 14 having been accommodated by the alveolar process of each dentary (Fig. 17D).

As in many other notosuchians, the roots of the teeth of each dentary are accommodated largely within a continuous alveolar groove (Figs. 5, 7C, 8H, 9A–D, 12, 17A, D, 22, 24–26, 28), with only their bases being set into discrete and complete (though extraordinarily shallow) alveoli (Figs. 8H, 29B). This mirrors the conditions seen within the alveolar processes of both the premaxilla and, to an even greater degree, the maxilla. Along the anterior and predominantly transversely oriented part of the dentary, the alveolar groove is situated between two nearly parallel, anterodorsally inclined laminae of the alveolar process: an anterior one, termed here the labial lamina, and a posterior one, termed here the lingual lamina (Fig. 22). This arrangement continues dis-

tally along the alveolar process, throughout the angulation at its anterolateral 'corner,' up to the level of the ninth alveolus. Here the lingual lamina—now positioned along the medial aspect of the longitudinal segment of the alveolar process rather than along the posterior aspect of its transverse segment—abruptly terminates, and the medial lamina of the splenial abruptly ascends to form the lingual wall of the remaining posterior portion of the alveolar groove (Figs. 5, 8H, 9C, D, 12, 17, 22, 25–28). In contrast, the labial lamina—now positioned along the lateral aspect of the longitudinal segment of the alveolar process rather than along the anterior aspect of its transverse segment—continues to extend posteriorly until it contacts the anterolateral edge of the surangular ramus. As a consequence of this arrangement, the distal four dentary teeth are surrounded laterally by the labial lamina of the alveolar process of the dentary, but medially by the anterodorsal part of the medial lamina of the splenial.

Like its walls, the floor of the mandibular alveolar groove also varies somewhat in overall morphology and composition along its mesiodistal course. Mesially, and indeed throughout the entire transversely oriented anterior portion of the dentary, the floor of the groove is formed by the labial and lingual laminae of the alveolar process simply curving gently to meet one another near their bases, thus forming an anterodorsally concave region of continuity between the two laminae (Figs. 7A, C–E, 9A, 12, 17C). Shallow alveoli along the concave surface of this intervening sheet of bone serve to accommodate the bases of the roots of the first through eighth dentary teeth (Figs. 8H, 29B). As described above, however, the lingual lamina of the alveolar process of the dentary is lost further distally, abruptly terminating immediately after passing lateral to the anterior margin of the medial lamina of the splenial (Fig. 8H). Thus, from this point posteriorly, the floor of the alveolar groove is formed entirely by a free-ending subdental process that extends ventromedially from the basal-most part of the labial lamina of the alveolar process of the dentary to ultimately terminate in a simple abutting contact with the lateral surface of the medial lamina of the splenial (Figs. 9C, D, 17A). The concave dorsal surface of this subdental process bears six shallow alveoli to accommodate the bases of the roots of the ninth through 14th dentary teeth.

The floor of the mandibular alveolar groove effectively represents the junction between the alveolar process and the ramus of the dentary. As such, it serves not only as a floor into which the bases of the dentary teeth are implanted, but also as part of the roof that overlaid Meckel's cartilage. More specifically, along the posterior part of its course, the ventral surface of this bony partition forms much of the roof of the mandibular canal (Figs. 9C, D, 29A), a common passageway through which both Meckel's cartilage and the ventral alveolar neurovascular bundle would have passed. Further anteriorly, however, it forms the roof of Meckel's canal (Figs. 7, 9B, 12, 17A, 29A), which transmitted the anterior portion of Meckel's cartilage in isolation. The confluence between the mandibular canal and Meckel's canal is located at the approximate anteroposterior level of the 11th alveolus, where a groove running along the ventrolateral aspect of the subdental process leads into a fully formed independent canal for transmission of the ventral alveolar neurovascular bundle (Figs. 8H, 9C, 29A, B). Anterior to this point, the ventral alveolar canal follows a course along the labial aspect of the dentary, near the junction between the ramus and the alveolar process (Figs. 7, 9B, 12, 17A, 29C). Along this entire course, the ventral alveolar canal gives rise to numerous smaller canals. Some of these extend in a labial direction to communicate with the prominent neurovascular foramina along the external surfaces of both the ramus and alveolar process of the dentary (Figs. 5, 8H, 22–24, 26, 28, 29C); these canals clearly transmitted cutaneous branches of the ventral alveolar nerve, artery, and vein for distribution to the labial gingivae and the skin overlying the anterior portion of the lower jaw. Others of these small canals extend in a lingual direction to



empty into the alveolar groove through its labial wall; these likely transmitted dental and gingival branches of the ventral alveolar nerve, artery, and vein to (partially) supply the lower teeth and lingual gingivae. However, the latter structures also appear to have been supplied in part by neurovasculature emanating from a relatively prominent canal running throughout the lingual margin of the floor of the alveolar groove (Figs. 9B, 12, 17A).

Finally, arising from the posterior-most part of the ramus of the dentary (i.e., that portion which lies ventral to the posterior terminus of the alveolar process) is the posterodorsal process (Figs. 5, 22, 24–26, 28). From this anteroventral origin, it extends posterodorsally for a distance of ~10 mm along the lateral surface of the anterior part of the surangular ramus, its posteroventral edge thereby forming the anterior two-fifths of the dorsal margin of the external mandibular fenestra. The process terminates in two short (2–3 mm) and somewhat blunt prongs—one dorsal and one ventral—separated by a relatively wide V-shaped emargination. Most of the mediolateral width of the dorsal prong is accommodated within a well-developed recess along the lateral surface of the anterior end of the surangular ramus (Fig. 9E). The lateral surface of the posterodorsal process is entirely smooth and, unlike both the ramus and alveolar process of the dentary, it lacks neurovascular foramina (Fig. 24).

Dentition

Partial dentitions and associated teeth preserved with UA 8679, FMNH PR 2596, and FMNH PR 2597 collectively represent nearly the complete dentition of *Simosuchus clarki* (Figs. 1B–E, 3–6, 11, 12, 17A, C, D, 22–28, 30, 31), consisting of 16 teeth in each upper quadrant (five premaxillary and 11 maxillary) and 14 in each dentary, for a total of 30 teeth on each side (expressed according to the dental formula $5/11/14 = 30$). As such, *Simosuchus* has more teeth (in some cases, many more) than do most other notosuchians for which complete or nearly complete dentitions are known: *Adamantinasuchus* ($3/7/7+ = 17+$), *Armadillosuchus* ($2/4+/6+ = 12+$), *Baurusuchus salgadoensis* ($4/5/10 = 19$), *Chimaerasuchus* ($2/4/? = ?$), *Malawisuchus* ($4/6/8 = 18$), *Martiliasuchus* ($4/5/9 = 18$), *Notosuchus* ($4/7/10 = 21$), *Sphagesaurus huenei* ($2/6/9 = 17$), *Sphagesaurus montealtensis* ($1/7/9 = 17$), and *Yacarerani* ($4/6/10 = 20$). The only clear exceptions to this generalization are *Anatosuchus* ($6/19/21 = 46$), *Araripesuchus tsangatsangana* ($5/11+/18 = 34+$), *Araripesuchus wegneri* ($5/14/16 = 35$), and *Uruguaysuchus* ($4/12$ or $13/17 = 33$ or 34). In addition to the three specimens of *Simosuchus clarki* that preserve teeth in their jaws, 14 isolated teeth (UA nos. 9755–9761, 9854; FMNH nos. PR 2591–PR 2595, PR 2600) from various parts of the dentition have been collected and referred to this species (see complete list in Krause et al., this volume).

Tooth crowns are expanded mesiodistally, each with a slight lingual concavity and labial convexity, and multiple cusps of variable size arranged in a single longitudinal row (Figs. 30, 31). In these respects, the crowns of *Simosuchus* somewhat resemble those of *Uruguaysuchus* and *Araripesuchus wegneri*, both of which have mesiodistally expanded ‘spatulate’ crowns, each with a prominent central portion (i.e., an incipient tripartite crown morphology), on their posterior-most teeth. Most of the tooth

crowns of *Simosuchus* are generally tripartite, with each portion, referred to here as ‘prongs,’ divided into variable numbers of cusps, though partitioning of the crowns becomes less distinct in the posterior (distal) dentition. Generally, there are seven cusps on each crown of the upper dentition and eight or nine cusps on each crown of the lower dentition, although in some cases an accessory cusp may be absent or additional small accessory cusps are developed near the bases of some crowns. The cervical region supporting the crown of each tooth is strongly constricted (as in many other basal mesoeucrocodylians), but then widens into a labiolingually compressed and elongate root, with a height two to three times greater than that of the crown.

The dentition is moderately heterodont, with considerable regionalization related to the specific position of teeth within the jaws; however, the degree of heterodonty in *Simosuchus* is significantly less than that exhibited by nearly all other notosuchians. The subrectangular snout of *Simosuchus* differentiates upper and lower tooth rows into two general regions: a wide, straight, transverse portion at the front of the snout, and a short parasagittal portion on each side of the snout. The transverse portion of the upper tooth row consists of teeth from both premaxillae and the first two teeth of each maxilla, for a potential total of 14 teeth (if all are erupted and in place) across the anterior surface of the snout. In the lower jaw, the corresponding transverse portion consists of the first six teeth of each dentary, for a potential total of 12 teeth. Crowns on both the upper and lower teeth from this transverse region are strongly tripartite, with tall, centrally positioned primary cusps. The transition between the transverse tooth row and the parasagittal tooth row is rounded, but abruptly so, such that it incorporates two alveoli in each corner of both the upper and lower jaws. Tooth crowns from the laterally positioned distal tooth row are generally shorter and mesiodistally longer, with greater uniformity in cusp size. A pattern of imbrication is preserved in these distal teeth, with the distal cusp of each crown overlapping the lateral (labial) surface of the mesial cusp of the following tooth. This ‘en echelon’ arrangement could conceivably be an artifact of preservation, but the frequency with which it occurs suggests rather strongly that it represents the true orientation of these teeth.

Premaxillary Dentition—Each premaxilla contains alveoli to accommodate five teeth (Figs. 3–6, 11, 30A, H). (However, as in both *Martiliasuchus* and *Notosuchus*, the premaxilla also contributes to the mesial portion of the alveolus that accommodates the first maxillary tooth.) In UA 8679, functional teeth are preserved in all positions but the first one in the left premaxilla, but in only the first, second, and fourth positions in the right premaxilla (though a developing tooth crown is preserved, sitting askew, in the fifth position as well). The right premaxilla of FMNH PR 2596 preserves all but the second tooth; no teeth are preserved in the left premaxilla. No premaxillary teeth are preserved on either side of FMNH PR 2597.

The premaxillary teeth are symmetrically tripartite, with a total of seven cusps: three on the tall central prong and two each on the shorter mesial and distal prongs (Fig. 30A, H). Although the labial (anterior) and lingual (posterior) bases of the crowns are both gently convex in occlusal view, the shape of the crown changes at the bases of the prongs to convex labially but slightly

← FIGURE 30. Dentition of the holotype (UA 8679) of *Simosuchus clarki*. **A**, labial (anterior) view of left and right premaxillary and mesial-most maxillary teeth. **B**, lingual view of left mesial and middle maxillary teeth. **C**, lingual view of right mesial maxillary teeth. **D**, lingual view of left and right mesial dentary teeth. **E**, lingual view of left middle dentary teeth. **F**, lingual view of right mesial and middle dentary teeth. **G**, lingual view of 11th right dentary tooth. **H**, composite interpretive drawing of labial views of premaxillary and maxillary teeth (above) and dentary teeth (below) preserved in UA 8679, supplemented by those in FMNH PR 2596; transversely oriented premaxillary and mesial dentary teeth and longitudinally oriented distal maxillary and dentary teeth are depicted as a continuous linear row projected onto a single plane. The three most distal maxillary and dentary teeth are unknown and are here reconstructed. See Appendix 1 for anatomical abbreviations. **Additional abbreviations:** **L**, left; **R**, right; **d**, dentary tooth; **m**, maxillary tooth; **pm**, premaxillary tooth.

concave lingually. Deep vertical sulci separate the three prongs of each crown on both the labial and lingual surfaces; these sulci are generally deeper on the labial surface. The tall central prong of each crown consists of a tall, centrally positioned, primary apical cusp flanked on each side (mesially and distally) by a smaller accessory cusp expressed near the apex. Mesial and distal to this central tricuspid prong are two bicuspid prongs. The mesial prong has a dominant distal cusp, which, although large, does not extend ventrally even to the level of the accessory cusps on the central prong, and a minuscule mesial accessory cusp. Conversely, the distal prong has a large mesial cusp and a relatively tiny distal accessory cusp.

Maxillary Dentition—Each maxilla contains alveoli to accommodate 11 teeth (Figs. 3–6, 11, 30A–C, H). In UA 8679, functional teeth are preserved in the first through fourth, sixth, and seventh alveoli of the left maxilla, with visible unerupted teeth present in the fifth and eighth alveoli. In the right maxilla, functional teeth are present in only the first and third alveoli, with visible unerupted teeth present in the seventh and eighth alveoli. A number of additional maxillary teeth are unerupted and remain obscured by matrix in UA 8679; these are visible only in HRXCT scans of this specimen. In FMNH PR 2596, the first five teeth are preserved in the right maxilla. No teeth are exposed in the left maxilla of FMNH PR 2596. A single poorly preserved tooth is present in the fourth alveolus of the left maxilla of FMNH PR 2597; no teeth are present in the right maxilla. The bases of each root are implanted in discrete alveoli, which merge to form a continuous alveolar groove along the ventral margin of the maxilla. The first maxillary tooth (the sixth tooth distal to the midline) is located at the contact between the maxilla and premaxilla, with the medial half (or slightly less) of the first alveolus formed by the premaxilla. As such, it is somewhat arbitrary whether to refer to this tooth as the first maxillary tooth or the sixth premaxillary tooth; we choose the former.

The first and second maxillary teeth are similar in shape to the premaxillary teeth, being convex both labially and lingually at their coronal bases but convex labially and concave lingually at the bases of the separate prongs (Fig. 30A, C, H, 31A). Like the premaxillary teeth, these first two maxillary teeth have strongly tripartite crowns with tall central tricuspid prongs and mesially and distally adjacent lower prongs (the only slight difference being that the mesial prong appears to be unicuspid, rather than bicuspid, on the left first and second maxillary teeth). This similar morphology between the premaxillary teeth and the mesial maxillary teeth renders the entire transverse dental series nearly homodont. The third maxillary tooth is also morphologically similar to the premaxillary teeth, although the lingual side of its coronal base is flat to slightly concave in occlusal view, and the central prong of the crown has decreased in size relative to the mesial and distal prongs (Fig. 30A–C, H). Furthermore, the accessory cusps on each prong have increased in size relative to the primary cusp. The combined effect of these features, relative to those on the first and second maxillary teeth, results in overall greater uniformity in cusp height and size along the crown. The tricuspid central prong continues to decrease in relative height in the fourth position, with the apical cusp and its two accessory cusps becoming nearly equal in size (Fig. 30B, H). The mesial accessory cusp of the mesial prong of the left fourth maxillary tooth, as for the first and second, is absent. The shape of the base of the fourth maxillary tooth crown is distinctly concave lingually and convex labially in occlusal view. The central prong of the fifth and sixth crowns is mesiodistally long and low, with an apical cusp only slightly taller than its two accessory cusps (Fig. 30B, H). The mesial and distal bicuspid prongs of these crowns are similarly mesiodistally long, with the most mesial and distal cusps increasing in relative size. The seventh and eighth maxillary crowns are mesiodistally long and low, with a mesiodistal length approximately twice their height. The shape of the tooth in

occlusal view, at the level of the bases of the prongs, is labiolingually symmetrical, in contrast to the lingually concave shape of more mesial teeth. Each cusp is approximately equal in size, separated by shallow sulci both labially and lingually, and can no longer be grouped into distinct prongs as in the more mesial parts of the dentition.

The pattern in the maxillary dentition is one in which the crowns, beginning with a morphology similar to the premaxillary crowns, become progressively longer (relative to width), lower, and more homogenized, with each of the seven (or six) cusps eventually becoming nearly equal in size (Fig. 30H). The missing distal-most three maxillary teeth can therefore perhaps be inferred to have been similar to the eighth tooth in general morphology.

Dentary Dentition—Each dentary contains alveoli to accommodate 14 teeth (Figs. 4–6, 22–28, 30D–H). Intact functional teeth are present in the first, third through eighth, and 11th positions of the right dentary and first through third, fifth, and eighth through 10th positions of the left dentary. The bases of each root are implanted in discrete alveoli, which merge to form a continuous alveolar groove along the dorsal margin of the dentary. The pattern of crown morphology is similar to that seen in the upper dentition, although each crown of the lower dentition typically has nine, rather than seven, cusps, although some have only eight (Figs. 30D–H, 31D–F).

The first six dentary teeth are morphologically similar, with symmetrically tripartite, spatulate crowns with weakly crenulated carinae (Fig. 30D, F, H). The bases of the crowns are, in occlusal view, strongly convex labially and moderately convex lingually. The central prong on each of the first six crowns consists of a tall semiconical apical cusp flanked on each side by two small, labiolingually compressed, ridge-like accessory cusps. Mesial and distal to this central prong, each separated from the latter by deep labial and lingual sulci, are the other two tricuspid prongs of the crown. Each of these prongs consists of a large semiconical cusp flanked by two small accessory cusps positioned at the base of the crown (mesially on the mesial prong and distally on the distal prong). There is some variability in this pattern in that the right fourth and sixth dentary teeth appear to have had only a single accessory cusp on the mesial prong. The tall central prong on the seventh and eighth dentary crowns is decreased in height and is more elongate relative to those of the mesial and distal prongs, compared to those on the more mesial teeth; the result is longer, lower teeth with cusps of more nearly equal size (Fig. 30D–F, H). The mesial prong of the eighth dentary tooth, on both sides, has only two cusps whereas the distal prong has three. The ninth, 10th, and 11th crowns are nearly symmetrical labiolingually and are still weakly separated into three separate prongs (Fig. 30E, G, H). The mesial prong of each crown is bicuspid whereas the central prongs remain tricuspid, with cusps of nearly equal size. The distal prongs of each crown have three cusps that decrease in height and size from mesial to distal. The 11th tooth on the right side differs from this pattern in having a tiny fourth accessory cusp developed distally on the distal prong.

The overall pattern of the lower dentition mirrors that of the upper dentition, with the teeth becoming mesiodistally longer (relative to their labiolingual widths) and lower distally and, correspondingly, the cusps becoming more homogenized in size and height (Fig. 30H). The three missing distal tooth positions can therefore be inferred to have been similar in morphology to the 11th tooth but perhaps still more elongate, lower, and with greater homogenization of cusps.

Replacement Teeth—HRXCT scans and both macroscopic and microscopic examination of the head skeleton of UA 8679 reveal a number of replacement teeth at varying stages of development (Figs. 7B, 8F, H, 9B, 17D). Replacement teeth are present in the second through fourth alveoli of the left premaxilla and the first, third, and fifth alveoli of the right premaxilla.

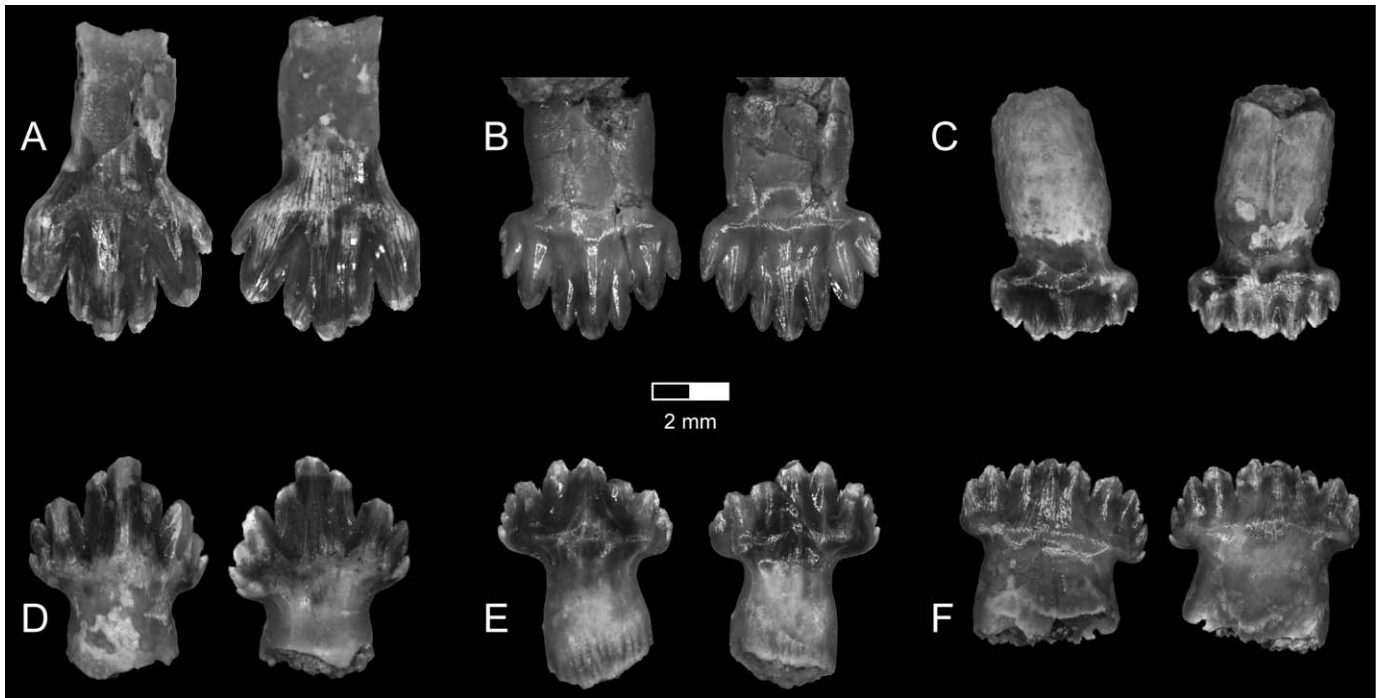


FIGURE 31. Isolated teeth associated with the holotype (UA 8679) of *Simosuchus clarki*. **A**, mesial maxillary tooth in labial (left) and lingual (right) views; **B**, mesial-middle maxillary tooth in labial and lingual views; **C**, distal maxillary tooth in labial and lingual views; **D**, mesial dentary tooth in labial and lingual views; **E**, middle dentary tooth in labial and lingual views; **F**, distal dentary tooth in labial and lingual views.

Replacement teeth are only present in the second alveolus of the left maxilla and the second and third alveoli of the right maxilla. Within the lower jaw, developing replacement teeth are present in the first, third, fifth, seventh, and 10th alveoli of the right dentary and only the fifth and seventh alveoli of the left dentary. As in crocodylians (Poole, 1961), the crowns develop first and are positioned within the hollow root cavities of the functional teeth. No organized pattern of tooth replacement can be discerned from the teeth preserved in UA 8679.

Associated Teeth—A total of 25 isolated teeth were recovered in association with UA 8679 (see Fig. 31). Based on the morphology of the intact dentition, 13 of these isolated teeth appear consistent with the upper dentition and seven are consistent with the lower dentition. Two small isolated tooth crowns with only three cusps are not morphologically consistent with any known tooth position; if they pertain to *Simosuchus clarki*, which seems likely based on their size, cusp morphology, and provenance, they may represent unerupted crowns or may have been from the distal-most portions of the upper and/or lower tooth rows. Several other teeth are too badly damaged to allow placement. An isolated tooth associated with FMNH PR 2597 can be attributed to the upper dentition, likely the second or third maxillary position, on the basis of its morphology.

Tooth Wear—Although the apices of cusps, particularly those on the central prong, on many of the teeth in UA 8679 appear to be worn or abraded, discrete wear facets indicating tooth-tooth contact can be recognized only on the lingual surfaces of the first tooth of the right premaxilla and the second tooth of the left premaxilla. The wear facets are small and restricted to only the central prong of each tooth. No corresponding facets can be seen on the complementary lower dentition or on any other in situ tooth crowns. Similarly, no wear facets can be discerned on the few teeth exposed on FMNH PR 2596 or on the single, damaged tooth preserved in FMNH PR 2597.

Cranial Endocast

High resolution X-ray computed tomography (HRXCT) of the skull of the holotype (UA 8679) of *Simosuchus clarki* allows for a detailed description of the space once occupied by the brain, brainstem, membranous labyrinth, cranial nerves, and craniocerebral vascular elements. In some cases, these structures can be characterized nearly completely, highlighting specific morphology, such as the position, orientation, and general organization of cranial nerve trunks relative to elements of the chondrocranium. In other cases, however, relatively superficial structures within the cranial cavity—most notably, the dural venous sinuses—overlie and obscure the morphology of deeper endocranial structures (e.g., brainstem and cerebellum), but are themselves able to be visualized and approximated relative to the endocranial surfaces of the bones of the skull and the central nervous system more generally.

As discussed previously by numerous other workers (e.g., Jerison, 1973; Hopson, 1979; Sampson and Witmer, 2007; Witmer et al., 2008), endocranial casts in sauropsids typically do not reflect the actual morphology of the brain and brainstem, but more closely represent contours of the external surface of the surrounding dura mater (i.e., endocranium) where it was once in contact with the internal surface of constituent bones of the braincase. Moreover, due to the intimate relationship between the dura mater and underlying soft tissues (e.g., the cerebral hemispheres), many soft-tissue features impart their position on the internal surface of the braincase through the dural interface. Finally, many intrinsic features of the dura mater itself, including a variety of dural venous sinuses, represent some of the most easily reconstructed anatomical elements in endocranial casts. Here we aim to describe the general organization of the constituent regions of the brain and brainstem in *S. clarki* and, where possible, comment on other endocranial structures through either their representation in the endocranial cast or via their associ-

ated fossae, foramina, sulci, or canals, as identified in bony elements of the chondrocranium described above. Our intent is to provide an overview of endocranial organization in *Simosuchus* to facilitate basic comparisons with extant Crocodylia, and to provide perspective for an ongoing comparative study of endocranial anatomy among the morphologically and ecologically diverse basal mesoeucrocodylians.

Due to its exquisite preservation, the holotype (UA 8679) of *S. clarki* provides the best potential for reconstructing endocranial anatomy. However, certain portions of this specimen—in particular the anteroventral end of the cranial cavity and the ventral portions of the inner and middle ear—are inadequately preserved, thus precluding a full characterization of the morphology of these areas. Specifically, incomplete preservation of the anterior portion of the chondrocranium, which would have defined the anteroventral boundaries of the cranial cavity, limits our ability to comment on specific characteristics of the olfactory system, such as the volume of the olfactory bulbs. Moreover, breakage near the ventral portion of the inner and middle ear (i.e., structures occupying positions ventral to the lateral semicircular canal; see Fig. 19) renders the analysis incapable of characterizing structures such as the vestibule and cochlea of the inner ear.

The general shape of the cranial endocast (Fig. 32) is similar in several aspects to those of extant crocodylians (e.g., *Gavialis gangeticus* [see Wharton, 2000], *Crocodylus johnstoni* [see Witmer et al., 2008]), including the presence of broad cerebral hemispheres that taper anteriorly and posteriorly, a significant midline expansion on the ventral aspect of the forebrain that delimits the location of the hypophyseal fossa, and rather indistinct neural morphology in the postcerebral portions of the endocast. One notable difference, however, relates to the extremely truncated olfactory apparatus in *Simosuchus* (Fig. 32), no doubt a reflection of the greatly abbreviated rostrum in this taxon. Although the dorsal aspect of the olfactory tracts and bulbs (Fig. 32A; see also Fig. 8A) is constrained in the cranial endocast based on the internal surface of the preserved frontal (Fig. 10), the ventral and lateral extent of these structures remains unknown due to poor preservation (see hatched areas in Fig. 32B, C).

Another distinctive feature of the cranial endocast of *Simosuchus* pertains to the morphology of its dorsal surface. Specifically, the dorsal contour of the endocast (Fig. 32C) is marked by three distinct linear surfaces: an anterior segment coincident with the position of telencephalic structures (e.g., olfactory apparatus and cerebral hemispheres), a middle segment represented solely by the dorsal longitudinal dural venous sinus presumably overlying tectal and cerebellar structures, and a gently sloping posterior segment represented by the occipital dural venous sinus complex overlying the dorsal aspect of the medulla. This organization is in marked contrast to that in at least some extant crocodylians (e.g., *Crocodylus johnstoni* [see Witmer et al., 2008:fig. 6.3]), in which the dorsal contour of the endocranial cast is generally curvilinear. The distinctive dorsal contour of the endocast in *Simosuchus* likely reflects the planar organization of the major components of the head skeleton as described above. However, endocranial organization appears generally similar to that of other mesoeucrocodylians (e.g., *Anatosuchus minor*, *Araripesuchus wegneri*; Sereno and Larsson, 2009) in having a spade-shaped cerebrum that tapers both anteriorly and posteriorly. *Simosuchus clarki* differs significantly from both of these taxa, however, in having a dorsoventrally expanded cerebrum (Fig. 32C). As endocasts of the olfactory apparatus were not prepared for either *Anatosuchus minor* or *Araripesuchus wegneri*, it is unclear to what degree they differ from those of either *S. clarki* or extant crocodylians.

The dorsal midline of the endocranial reconstruction illustrates components of the dural venous sinus system (Fig. 32A). The dorsal longitudinal sinus occupies the anterodorsal two-thirds of the reconstruction, overlying the cerebrum and olfactory

apparatus, even though these regions are clearly demarcated based on their parasagittal anatomy. The occipital dural venous sinus overlies the tectum, cerebellum, and medulla. It is so prominent as to completely obscure any detailed morphology of the posterior portion of the brainstem (see Sedlmayr, 2002, as noted in Sampson and Witmer, 2007). A pineal prominence on the dorsal midline just posterior to the cerebrum is not apparent (Fig. 32C), consistent with the condition exhibited by extant crocodylians in general (Witmer et al., 2008). This is in stark contrast to the morphology in bird-line archosaurs (e.g., theropod dinosaurs), in which a dorsally projecting flap of dura mater marks the junction of the fore- and midbrain, emphasizing the position of the pineal body (e.g., Rogers, 1999; Larsson, 2001; Sampson and Witmer, 2007). The ventral midline of the endocranial cast (Fig. 32B) is characterized by the presence of a large hypophyseal fossa (and its associated paired cavernous dural venous sinuses) immediately posteroventral to the cerebral hemispheres, a distinct postpituitary notch, and a ventral longitudinal sinus adjacent to and underlying the hindbrain.

Other endocranial vascular structures of note include (1) the transversely oriented sphenoparietal dural venous sinus that occupied the postcerebral constriction (see Witmer et al., 2008) and connected the dorsal longitudinal sinus to the cavernous sinus and other ventrally positioned sinuses; and (2) the transverse dural venous sinus that typically occupies the tectal-otic sulcus and continues extracranially as the middle cerebral vein. Note that, whereas the sphenoparietal dural venous sinus in *Simosuchus* can be identified based on the position of the postcerebral constriction, the transverse sinus is less well constrained. It is likely that it occupied the shallow sulcus along the anterior edge of the flocculus (Fig. 32C).

Similar to the conditions exhibited by other sauropsids (see Sampson and Witmer, 2007), most components of the cerebellar apparatus are obscured in endocranial cast reconstructions due to the well-developed occipital dural venous sinus system. However, one exception to this generalization (and similar to the condition exhibited by most other sauropsids) is that the flocculus, or cerebellar auricle, is apparent just anterior to the anterior semicircular canal (Fig. 32C). Although the relative size of the flocculus has been used as a proxy for modeling cervicocephalic, whole-body, and reflexive ocular-stabilization kinematics in a variety of extinct archosaurs (see Witmer et al., 2003; Sampson and Witmer, 2007), comparative data among crocodyliforms in general and notosuchians specifically are sparse to non-existent. Ongoing work characterizing the morphology and precise dimensions of these and other structures (e.g., elements of the endosseous labyrinth) in notosuchians will provide novel comparative perspectives for examining the role of differential body size, dietary regime, and inferred habitus (e.g., terrestrial vs. aquatic) characteristic for this diverse group of bizarre crocodyliforms.

DISCUSSION

Intraspecific Variability

Since the initial discovery of the exquisitely preserved holotype specimen (UA 8679) of *Simosuchus clarki* more than a decade ago, five additional specimens that preserve portions of the skull and/or lower jaw have been recovered and referred to this taxon (see Krause et al., this volume). Although two of these newly referred specimens include relatively complete head skeletons that remain largely articulated, one is severely crushed and remains partially surrounded by matrix (FMNH PR 2596), and the other, although much better preserved, exhibits considerable distortion and some associated breakage (FMNH PR 2597) (see 'Specimens of *Simosuchus clarki*' in the Materials and Methods section above). The other three newly referred specimens include only isolated elements (UA 9754) or fragments of elements (UA 9762 and FMNH PR 2598) from the skull or lower jaw. Thus, the lim-

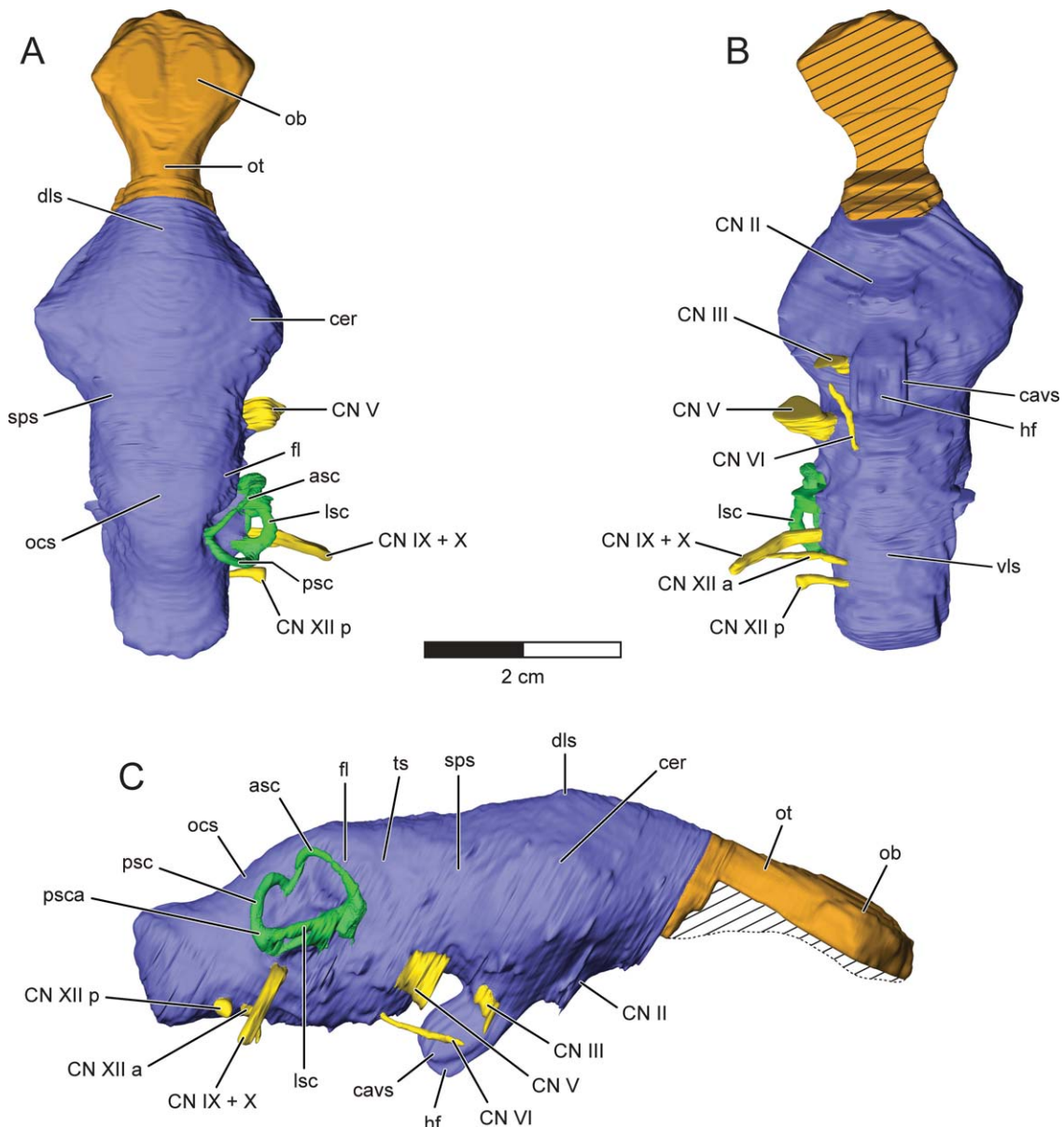


FIGURE 32. Reconstruction of the cranial cavity of *Simosuchus clarki*. Digital endocast in dorsal (A), ventral (B), and right lateral (C) views, generated from HRXCT scans of the holotype (UA 8679). The right side of the endocast depicts selected cranial nerve trunks and the endosseous labyrinth in yellow and green, respectively. The anterior region indicated in tan is an estimated reconstruction of the olfactory tracts and bulbs; uncertainty in this reconstruction (hatched area) results from incomplete preservation of the anteroventral-most floor of the cranial cavity in this specimen. See Appendix 1 for anatomical abbreviations.

ited number, nature, and condition of these available specimens clearly preclude a thorough assessment of intraspecific variability within the craniofacial skeleton of *S. clarki* at this time. Nevertheless, each of these specimens preserves morphological features that are clearly homologous to features exhibited by the holotype specimen, thereby permitting at least some preliminary qualitative and quantitative comparisons.

Variation in Shape—Of the five newly referred specimens of *Simosuchus clarki* that preserve portions of the head skeleton, FMNH PR 2597 is by far the most complete and well preserved (Figs. 33–35). Although both the skull and lower jaw of this specimen exhibit some distortion and breakage, both preserve numerous features that remain relatively undisturbed and that

can be compared directly with corresponding features in the holotype specimen (UA 8679). Indeed, it is only through comparisons made between FMNH PR 2597 and UA 8679 that discrete, qualitative differences in craniofacial shape have been identified among the known individuals of *S. clarki*; the relatively poor condition and/or fragmentary nature of the remaining four referred specimens have obscured any such differences that may have existed among these individuals.

Detailed scrutiny of FMNH PR 2597 reveals that this specimen exhibits the following discrete shape-related character states that differ from those found in UA 8679 [character states for UA 8679 given in brackets]: (1) posterior margin of orbital lamina of prefrontal without [with] pronounced V-shaped emargina-

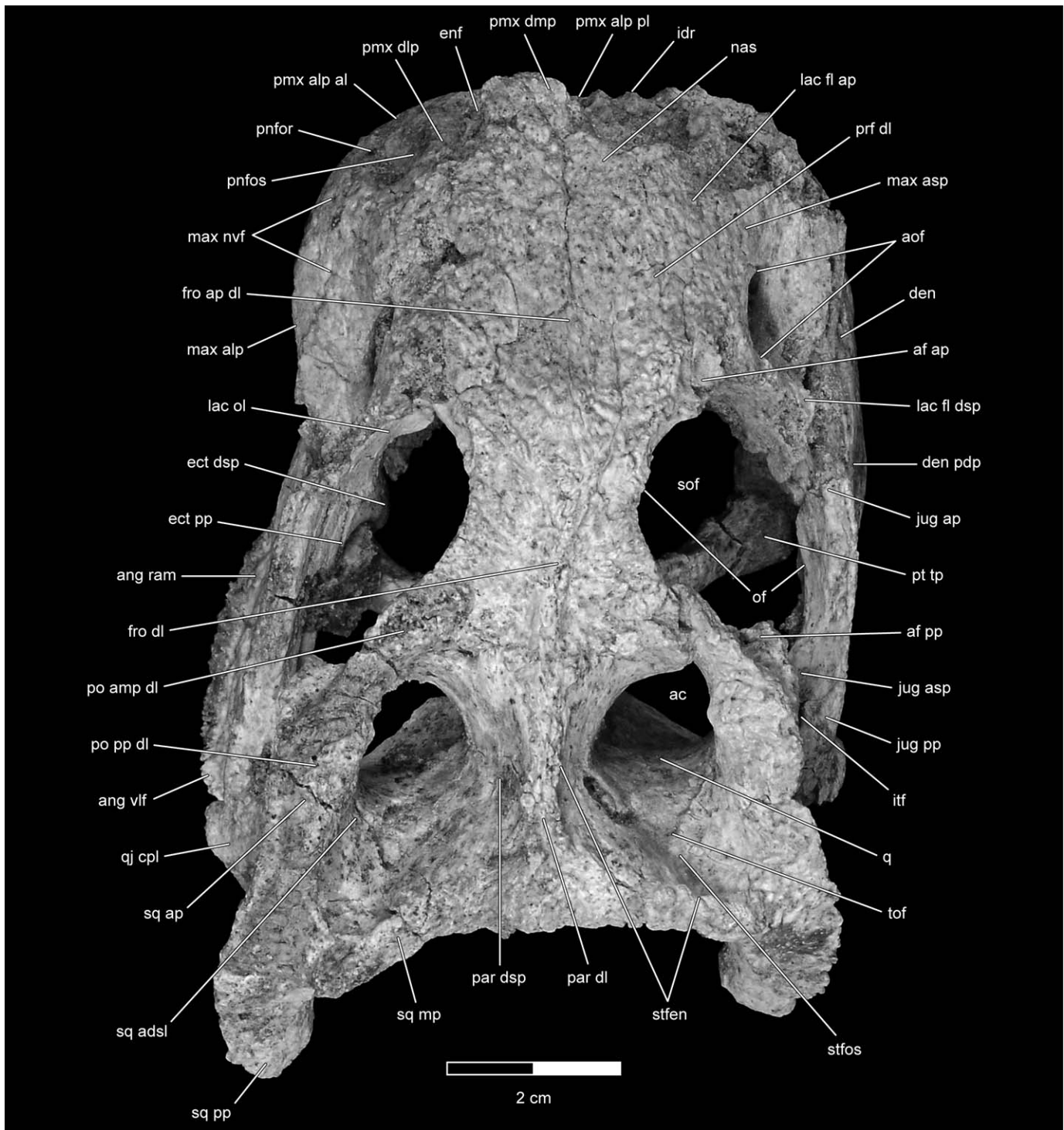


FIGURE 33. Skull and partial lower jaw of one of the referred specimens (FMNH PR 2597) of *Simosuchus clarki*. Photograph in dorsal view. Compare with similar view of the holotype (UA 8679) in Figure 2. See Appendix 1 for anatomical abbreviations.

tion; (2) frontoparietal suture nearly straight [anteriorly concave] in dorsal view; (3) posterior margin of dorsal lamina of frontal without [with] raised postorbital crest anterior to frontoparietal suture; (4) anterior end of dorsal lamina of parietal without [with] significant lateral expansion; (5) dorsal lamina of parietal strongly [weakly] convex; (6) dorsal laminae of anterior

and posterior processes of squamosal strongly convex [nearly flat, but intersecting one another at a distinct angle]; (7) posterior process of squamosal terminates in relatively short, weakly developed protuberance [relatively long, well-developed protuberance that projects strongly posteroventrolaterally]; (8) lateral margin of dorsal lamina of posterior process of squamosal only weakly

appearance in dorsal view]; (12) anteromedial surface of transverse process of pterygoid gently convex [strongly concave]; (13) dorsolateral surface of ventrolateral flange of angular nearly flat and oriented steeply vertically [distinctly concave, separating surface into steeply sloping basal portion and laterally flaring distal portion]; and (14) dorsolateral surface of ventrolateral flange of angular with only moderate sculpturing concentrated primarily along its distal margin [heavy sculpturing across its entire surface].

Clearly evident from the preceding list of discrete morphological characters that vary between FMNH PR 2597 and UA 8679 is that these characters are strikingly non-random in both their anatomical distribution and their cumulative effects on the overall shape of the head skeleton in these specimens. Nine of these characters (2–10) relate to the morphology of the four bones—frontal, parietal, postorbital, and squamosal—that contribute to the formation of the posterior portion of the dermal skull roof (i.e., the ‘cranial table’), and 11 (3–11, 13, 14) relate to the relative prominence of various projections, angulations, and/or areas of ornamentation distributed throughout the posterior two-thirds of the skull and lower jaw. The collective effect of differences in the second group of characters between FMNH PR 2597 and UA 8679 is that the bony processes, crests, and flanges that project most strongly laterally and posteriorly beyond the remaining margins of the skull and lower jaw are more prominent, distinctly angulated, and heavily ornamented in the latter specimen.

Variation in Overall Size, Relative Proportions, and Ontogenetic Maturity—As for the discrete qualitative differences in craniofacial shape discussed above, the most extensive quantitative comparisons that can be drawn among the known specimens of *Simosuchus clarki* that preserve portions of the skull and/or lower jaw pertain to the two most complete, fully articulated, and well-preserved specimens, UA 8679 and FMNH PR 2597. However, isolated measurements of specific craniofacial features preserved in FMNH PR 2596, FMNH PR 2598, UA 9754, and UA 9762 provide at least some limited context for interpreting the overall size of these specimens relative to that of UA 8679 (and FMNH PR 2597).

A summary of the quantitative (i.e., morphometric) comparisons made between the head skeletons of UA 8679 and FMNH PR 2597 is provided in Tables 1 and 2. In general, these data demonstrate that the skull and lower jaw of FMNH PR 2597 are somewhat smaller than those of UA 8679. More specifically, a global mean of 37 pairwise morphometric comparisons that could be made between these two specimens (see Table 2) suggests that the overall size of the head skeleton of FMNH PR 2597 is approximately 93.1% that of UA 8679. However, although this overall estimate of the relative sizes of these two specimens is fully consistent with the general impression that one gets when examining them side-by-side (i.e., that the head skeleton of the referred specimen is clearly smaller than that of the holotype), it also conceals significant proportional and regional differences.

In its three primary orthogonal dimensions, the head skeleton of FMNH PR 2597 compares with that of UA 8679 as follows: it is 90.8% as long (115.5 mm vs. 127.2 mm HSTL), 79.2% as wide (82.2 mm vs. 103.8 mm HSTW), and 108.4% as tall (70.0 mm vs. 64.6 mm HSTH). Although these comparisons reveal striking proportional differences between these two specimens as preserved, these differences must be considered carefully within the context of the postmortem distortion that is clearly evident throughout portions of the skull and lower jaw of FMNH PR 2597 (see ‘Specimens of *Simosuchus clarki*’ in the Materials and Methods section above for a detailed description of this distortion). For instance, the sagittal shearing that has distorted the head skeleton of this specimen would have necessarily rendered it both longer and narrower than it actually was in life, and the effects of this proportional change would be expected

to be strongest toward the periphery of the skeleton and weakest near its center. Thus, measurements defined at least in part by peripherally placed landmarks—such as total length, width, and height of the head skeleton (HSTL, HSTW, and HSTH, respectively; see Table 1)—must be interpreted with particular caution. For this reason, we also calculated global means of multiple pairwise comparisons made between these two specimens grouped by measurements of length ($n = 8$; HSTL, SLMD, SLMV, SRLPRO, SRLMO, SRLPOO, SQPOL[L], SQPOL[R]), width ($n = 19$; HSTW, SNWA, SNWP, AOIFD, OIFD, SWMO, CTAW, CTCW, CTPW, SWP, SWT, OCW, OCTTW, TOJW, TQW, QICD, LJWPF, ANGW[L], ANGW[R]), and height ($n = 6$; HSTH, SHMS, SHPO[L], SHPO[R], BCH, OCVH) (see Table 1 for definitions of these measurements), with each mean incorporating measurements taken from as many different regions of the skull and lower jaw as possible. The results of this analysis suggest that the head skeleton of FMNH PR 2597 is 93.1% as long, 88.8% as wide, and 102.5% as tall as that of UA 8679. We consider these estimates to be somewhat more reflective of the true proportional differences between these two specimens, because they are mathematically ‘buffered’ against individual measurements that might be disproportionately affected by the postmortem distortion evident in FMNH PR 2597. Consistent with this interpretation is our pairwise comparison between these two specimens in the width of the frontal bone, which is positioned at the very center of the skull roof in *S. clarki*, and which consequently appears to be nearly completely undistorted in FMNH PR 2597; the magnitude of this width measurement (see orbital interfenestral distance [OIFD] in Tables 1 and 2) in FMNH PR 2597 is 86.6% of that recorded for UA 8679, which agrees very closely with the 88.8% difference in overall craniofacial width estimated through the analysis described above.

In addition to the differences just described between the primary orthogonal dimensions of FMNH PR 2597 and UA 8679, these specimens also exhibit striking differences in regional craniofacial proportions. For instance, the length of the preorbital portion of the skull roof (SRLPRO) in FMNH PR 2597 is 87.2% of that in UA 8679, and a mean of three pairwise comparisons of preorbital dermatocranial width (SNWA, SNWP, AOIFD) indicates that the preorbital portion of the skull (i.e., the snout) of FMNH PR 2597 is 85.9% as wide as that of UA 8679. Similarly, the length of the mid-orbital portion of the skull roof (SRLMO) in FMNH PR 2597 is 86.0% of that in UA 8679, and a mean of two pairwise comparisons of mid-orbital dermatocranial width (OIFD, SWMO) indicates that the mid-orbital portion of the skull of FMNH PR 2597 is 85.0% as wide as that of UA 8679. In strong contrast to these relative proportions, however, the length of the postorbital portion of the skull roof (SRLPOO) in FMNH PR 2597 is 112.6% of that in UA 8679, and a mean of three pairwise comparisons of postorbital dermatocranial width (CTAW, CTCW, CTPW) indicates that the cranial table of FMNH PR 2597 is 94.1% as wide as that of UA 8679. Moreover, the width of the occiput (OCW) in FMNH PR 2597 is 97.5% of that in UA 8679, and the height of the braincase (BCH) in FMNH PR 2597 is 105.9% of that in UA 8679. Thus, whereas these two specimens share relatively similar dimensions throughout much of the postorbital part of the skull (with the referred specimen actually being slightly larger than the holotype in some of its dimensions throughout this region), the mid- and preorbital portions of the skull differ significantly in their relative dimensions, being both shorter (anteroposteriorly) and narrower (mediolaterally) in FMNH PR 2597 than in UA 8679.

The comparisons presented above demonstrate that FMNH PR 2597 and UA 8679 represent individuals that were generally similar in their overall size but somewhat different in their relative proportions. However, such quantitative comparisons do not directly or unambiguously establish whether these individuals



FIGURE 35. Skull and partial lower jaw of one of the referred specimens (FMNH PR 2597) of *Simosuchus clarki*. Photograph in left lateral view. Compare with similar view of the holotype specimen (UA 8679) in Figure 4. See Appendix I for anatomical abbreviations.

TABLE 1. Measurements taken on the skull and lower jaw in two articulated specimens (UA 8679 [holotype] and FMNH PR 2597) of *Simosuchus clarki*.

Measurement	Abbreviation	Landmarks used for measurement
Total length of head skeleton ^{1,2}	HSTL	pmx alp (anterior surface), sq pp (posterior terminus)
Total width of head skeleton ^{1,3}	HSTW	L ang vlf (lateral edge), R ang vlf (lateral edge)
Total height of head skeleton ^{1,4,5}	HSTH	par dl (center), spl vl (posterolateral margin)
Mid-dorsal skull length ^{6,7}	SLMD	interpremaxillary suture (anterodorsal terminus), so (posterodorsal margin)
Mid-ventral skull length ^{6,7}	SLMV	interpremaxillary suture (anteroventral terminus), oc (posterior surface)
Length of preorbital skull roof ^{6,7}	SRLPRO	interpremaxillary suture (anterodorsal terminus), proc (center)
Length of mid-orbital skull roof ^{6,7}	SRLMO	proc (center), fro dl-par dl suture (center)
Length of postorbital skull roof ^{6,7}	SRLPOO	fro dl-par dl suture (center), so (posterodorsal margin)
Squamosal postoccipital length ^{7,8}	SQPOL	posterolateral corner of cranial table, sq pp (posterior terminus)
Anterior snout width ⁷	SNWA	L pmx alp-max alp suture (ventral terminus), R pmx alp-max alp suture (ventral terminus)
Posterior snout width ^{1,3}	SNWP	L max alp (lateral surface), R max alp (lateral surface)
Antorbital interfenestral distance ⁷	AOIFD	L aof (anterodorsal corner), R aof (anterodorsal corner)
Orbital interfenestral distance ^{3,9}	OIFD	L of (dorsal margin), R of (dorsal margin)
Mid-orbital skull width ^{1,3}	SWMO	L jug ap (lateral margin), R jug ap (lateral margin)
Cranial table anterior width ⁷	CTAW	L fro dl-po dl suture (anterolateral terminus), R fro dl-po dl suture (anterolateral terminus)
Cranial table central width ⁷	CTCW	L po pp-sq ap suture (dorsolateral terminus), R po pp-sq ap suture (dorsolateral terminus)
Cranial table posterior width ⁷	CTPW	L sq (at posterolateral corner of cranial table), R sq (at posterolateral corner of cranial table)
Posterior skull width ^{1,3}	SWP	L sq pp (lateral margin), R sq pp (lateral margin)
Terminal skull width ⁷	SWT	L sq pp (posterolateral terminus), R sq pp (posterolateral terminus)
Occipital width ^{1,3}	OCW	L parop (lateral margin), R parop (lateral margin)
Occipital transtuberous width ^{1,3}	OCTTW	L bt (lateral margin), R bt (lateral margin)
Transquadratojugal width ^{1,3}	TQJW	L qj tub (lateral surface), R qj tub (lateral surface)
Transquadratic width ^{1,3}	TQW	L q lhc (posterolateral margin), R q lhc (posterolateral margin)
Snout height ^{7,8}	SNH	pmx dmp (dorsal terminus), pmx alp (ventromedial margin)
Mid-sagittal skull height ^{6,7}	SHMS	moc (center), pt ap vnl (posteriormost part)
Postorbital skull height ^{7,8}	SHPO	posterolateral corner of cranial table, q lhc (ventral margin)
Braincase height ^{6,7}	BCH	par dl (center), bo (posteroventral margin of meuf)
Vertical occipital surface height ^{6,7}	OCVH	so (posterodorsal margin), fm (dorsal margin)
Hard palate length ^{7,8}	HPL	pmx alp (posteriorly adjacent to idr between 1 st and 2 nd teeth), posteromedial corner of pal pap
Hard palate width ⁷	HPW	L max alp (medially adjacent to 7 th max alv), R max alp (medially adjacent to 7 th max alv)
Pterygoid width ^{1,3}	PTW	L pt tp (lateral surface), R pt tp (lateral surface)
Total length of lower jaw ^{1,2}	LJTL	den alp (anterodorsal margin), rap (posterior margin)
Preglenoid lower jaw length ^{1,2,8}	LJLPG	den alp (anterodorsal margin), gfos (center)
Postsplenial lower jaw length ^{7,8}	LJLPS	spl ml (center of posterior margin), gfos (center)
Retroarticular process length ^{7,8}	RAPL	gfos (center), rap (ventral terminus)
Glenoid fossa length ^{1,7,8,10}	GFL	gfos (anterior margin of articular surface), gfos (posterior margin of articular surface)
Glenoid fossa width ^{1,7,8,11}	GFW	gfos (lateral margin of articular surface), gfos (medial margin of articular surface)
Quadratic condyle length ^{7,8,10}	QCL	q con (anterior margin of articular surface), q con (posterior margin of articular surface)
Quadratic condyle width ^{1,7,8,11}	QCW	q lhc (lateral surface), q mhc (medial surface)
Quadratic intercondylar distance ^{1,3}	QICD	L q mhc (anteromedial margin), R q mhc (anteromedial margin)
Symphyseal height ^{6,7}	SYMH	interdentary suture (dorsal terminus), sym tub (posteroventral tip)
Lower jaw height ^{1,4,8}	LJH	sur ram (dorsal margin adjacent to den pdp dorsal prong), ang (ventral surface at lateral margin)
Postfenestral lower jaw width ^{1,3}	LJWPF	L sur/ang junction (at posterior margin of emf), R sur/ang junction (at posterior margin of emf)
Angular width ^{7,8,12}	ANGW	ang vlf (lateral margin), ang ram (medial margin)

See Appendix 1 for a list of anatomical abbreviations for structures used as landmarks in defining these measurements.

¹Maximum measurement.

²Measurement made along an axis parallel to the median sagittal plane and extending perpendicularly between two transverse planes passing through defining landmarks.

³Measurement made along a horizontal axis extending perpendicularly between two parasagittal planes passing through defining landmarks.

⁴Measurement made along a vertical axis extending perpendicularly between two frontal planes passing through defining landmarks.

⁵Measurement made with skull resting on lower jaw in articulated position, with entire lower jaw resting on flat surface.

⁶Measurement made in median sagittal plane.

⁷Straight-line measurement.

⁸Measurement made on both sides of specimen.

⁹Minimum measurement.

¹⁰Measurement made along minor axis of condyle/glenoid.

¹¹Measurement made along major axis of condyle/glenoid.

¹²Maximum measurement that can be made perpendicular to lateral margin of angular.

were ontogenetically mature adults, or whether they were juveniles. Thus, to infer the ontogenetic status of these specimens, we rely primarily on other characters that have been used by previous workers to discriminate between juvenile and adult specimens of various types of crocodyliforms (e.g., Mook, 1921a; Iordansky, 1964, 1973; Joffe, 1967). Specifically, we point toward five cranial characters in particular that strongly suggest that both FMNH PR 2597 and UA 8679 represent adult individuals: (1) presence of heavy sculpturing across the external surfaces of the bones of the dermal skull roof; (2) closure—and, in some instances, nearly complete obliteration in external view—of sutures between adjacent elements of the dermal skull roof; (3) presence of a well-developed ‘crest A’ on the anterior surface of the body of the quadrate for attachment of the lateral lamina of the cranial adductor tendon; (4) relatively large size of the supratemporal fenestrae; and (5) close spacing of the supratemporal fenestrae near the dorsal midline, with the center of each fenestra positioned directly posterior to the dorsomedial margin of the ipsilateral orbital fenestra. Our inferences regarding the ontogenetic maturity of FMNH PR 2597 and UA 8679 are fully congruent with those made by Georgi and Krause (this volume) on the basis of the complete fusion of neurocentral sutures throughout the postatlantal portions of the vertebral columns preserved with these two specimens. In addition, it is relevant to note in this context that Hill (this volume), based on his paleohistological studies of lines of arrested growth (LAGs) in isolated osteoderms of FMNH PR 2597 and UA 8679, concluded that these two specimens represent individuals that were at least 5 and 3 years old, respectively, and most likely significantly older than this.

Whereas the nearly complete head skeletons of UA 8679 and FMNH PR 2597 invite relatively detailed quantitative comparisons, the incomplete and/or poor preservation of FMNH PR 2596, FMNH PR 2598, UA 9754, and UA 9762 permit far fewer such comparisons, thereby making it more difficult to assess the relative craniofacial dimensions, and thus the general ontogenetic status, of these individuals. Nevertheless, the relatively few measurements that could be taken on elements of the skull and/or lower jaw in these specimens provide valuable, albeit limited, data on the sizes of these individuals relative to those of the adult individuals represented by UA 8679 and FMNH PR 2597. These data are summarized in Table 3.

Available morphometric data indicate that the head skeleton of FMNH PR 2596 is most similar in size to that of UA 8679. A mean of two pairwise comparisons based on measurements of the skull and lower jaw in these specimens suggest that the head skeleton of FMNH PR 2596 is approximately 101.6% the size of that of UA 8679. This close similarity in size, combined with the extensive sculpturing visible externally along the dorsal laminae of the parietal, frontal, and prefrontals, and the fully closed suture that remains intact between the latter two bones on the right side of this very badly crushed specimen, suggests that FMNH PR 2596 represents an adult individual.

Quantitative comparisons between preserved portions of the head skeletons of FMNH PR 2598 and UA 8679 demonstrate that the former specimen represents a significantly smaller individual than does the latter. A mean of three possible pairwise comparisons based on measurements of portions of the skull and lower jaw in these specimens suggest that the craniofacial skeleton of FMNH PR 2598 is approximately 84.6% the size of that of UA 8679. Moreover, in two of the three measurements that could be taken from the few craniofacial fragments preserved with FMNH PR 2598, this specimen was also found to be smaller than FMNH PR 2597. These findings are consistent with those reported by Sertich and Groenke (this volume:tables 1, 2), based on the relative dimensions of elements throughout the appendicular skeleton, and with those reported by Georgi and Krause (this volume:table 1), based on relative vertebral dimensions. The latter authors also noted that the proximal caudal ribs remain unfused

TABLE 2. Measurements of the skull and lower jaw in two articulated specimens (UA 8679 [holotype] and FMNH PR 2597) of *Simosuchus clarki*.

Measurement	UA 8679	FMNH PR 2597
HSTL	127.2 ± 0.1	115.5* ± 0.2 (90.8%)
HSTW	103.8 ± 0.0	82.2* ± 0.3 (79.2%)
HSTH	64.6 ± 0.1	70.0* ± 0.1 (108.4%)
SLMD	106.1 ± 0.1	97.9* ± 0.3 (92.3%)
SLMV	102.3 ± 0.1	93.8* ± 0.1 (91.7%)
SRLPRO	48.3 ± 0.1	42.1* ± 0.2 (87.2%)
SRLMO	33.5 ± 0.1	28.8 ± 0.2 (86.0%)
SRLPOO	28.5 ± 0.1	32.1 ± 0.1 (112.6%)
SQPOL	23.0 ± 0.2 / 23.0 ± 0.1	21.2 ± 0.2 (92.2%) / 21.2 ± 0.1 (92.2%)
SNWA	51.3 ± 0.1	44.6* ± 0.2 (86.9%)
SNWP	76.7 ± 0.1	64.8* ± 0.3 (84.5%)
AOIFD	48.4 ± 0.0	41.8* ± 0.2 (86.4%)
OIFD	21.7 ± 0.0	18.8 ± 0.1 (86.6%)
SWMO	82.4 ± 0.1	68.7* ± 0.3 (83.4%)
CTAW	31.2 ± 0.1	30.4 ± 0.1 (97.4%)
CTCW	64.1 ± 0.1	58.0* ± 0.1 (90.5%)
CTPW	74.7 ± 0.0	70.5 ± 0.0 (94.4%)
SWP	80.1 ± 0.0	71.8* ± 0.0 (89.6%)
SWT	74.5 ± 0.0	64.6* ± 0.1 (86.7%)
OCW	51.0 ± 0.1	49.7* ± 0.1 (97.5%)
OCTTW	32.7 ± 0.3	29.0* ± 0.2 (88.7%)
TQJW	82.3 ± 0.0	76.8* ± 0.1 (93.3%)
TQW	76.6 ± 0.1	68.2* ± 0.1 (89.0%)
SNH	24.5 ± 0.1 / 24.4 ± 0.0	21.4* ± 0.1 (87.3%) / —
SHMS	43.9 ± 0.1	50.6 ± 0.1 (115.3%)
SHPO	43.6 ± 0.1 / 43.6 ± 0.1	41.8* ± 0.1 (95.9%) / 44.5* ± 0.1 (102.1%)
BCH	37.2 ± 0.1	39.4 ± 0.1 (105.9%)
OCVH	14.3 ± 0.1	12.5* ± 0.1 (87.4%)
HPL	40.2 ± 0.1 / 40.1 ± 0.1	— / —
HPW	69.5 ± 0.1	—
PTW	66.3 ± 0.1	—
LJTL	90.7 ± 0.2	—
LJLPG	80.8 ± 0.4 / 80.4 ± 0.5	— / —
LJLPS	42.0 ± 0.2 / 42.1 ± 0.1	— / —
RAPL	17.0 ± 0.2 / 17.0 ± 0.2	— / —
GFL	10.9* ± 0.1 / 10.6* ± 0.1	— / —
GFW	12.3 ± 0.2 / 12.5 ± 0.2	— / —
QCL	5.6 ± 0.2 / 5.8* ± 0.2	— / 5.8 ± 0.2 (100.0%)
QCW	13.4 ± 0.0 / 13.1 ± 0.1	— / 12.5 ± 0.0 (95.4%)
QICD	51.1 ± 0.1	44.3* ± 0.1 (86.7%)
SYMH	18.1 ± 0.0	—
LJH	27.1 ± 0.3 / 27.1 ± 0.3	30.9* ± 0.3 (114.0%) / —
LJWPF	87.4 ± 0.1	69.9* ± 0.1 (80.0%)
ANGW	15.6 ± 0.0 / 15.3 ± 0.1	14.4 ± 0.1 (92.3%) / 14.5 ± 0.2 (94.8%)

For each measurement, the mean ± standard deviation of 10 individual repeated measurements is given. All measurements are rounded to the nearest 0.1 mm. Measurements taken on both sides of the skull or lower jaw are given as left/right. Percentages given in parentheses for FMNH PR 2597 represent the relative magnitudes of measurements taken from this referred specimen expressed as percentages of corresponding measurements recorded from UA 8679.

*Measurement estimated because of slight breakage, erosion, or distortion.

to their corresponding vertebral centra in FMNH PR 2598, further suggesting that this specimen may represent a juvenile individual.

UA 9754 and UA 9762 represent the most incomplete craniofacial specimens of *S. clarki* currently known. UA 9754 includes only an isolated right ectopterygoid, the height of which is 87.6% that of the right ectopterygoid in UA 8679. UA 9762 includes only the fragmentary right posterior portion of an isolated frontal. However, this fragment preserves intact the posterior-most portion of the descending process of the frontal, the height of which was found to be 91.2% of that recorded for UA 8679. Thus, these very incomplete data suggest that both UA 9754 and

TABLE 3. Measurements of portions of the skull and lower jaw in three fragmentary (UA 9754, UA 9762, FMNH PR 2598) and three articulated (UA 8679 [holotype], FMNH PR 2596, FMNH PR 2597) specimens of *Simosuchus clarki* that preserve elements of the head skeleton.

Measurement	UA 8679	UA 9754	UA 9762	FMNH PR 2596	FMNH PR 2597	FMNH PR 2598
PAPW	26.2 ± 0.1 [R]	—	—	26.7* ± 0.1 [R] (101.9%)	22.8* ± 0.0 [R] (87.0%)	—
FDPH	10.2 ± 0.1 [R]	—	9.3* ± 0.0 [R] (91.2%)	—	9.2 ± 0.2 [R] (90.2%)	—
QJTL	8.5 ± 0.0 [R]	—	—	—	7.4* ± 0.0 [L] (87.1%)	7.6 ± 0.1 [R] (89.4%)
ECTH	18.5 ± 0.1 [R]	16.2 ± 0.1 [R] (87.6%)	—	—	—	—
PARW	15.6 ± 0.1 [L]	—	—	15.8* ± 0.1 [L] (101.3%)	13.1 ± 0.1 [R] (84.0%)	—
AVFH	11.5 ± 0.1 [R]	—	—	—	10.2 ± 0.0 [R] (88.7%)	8.9 ± 0.0 [R] (77.4%)
SARW	4.6 ± 0.1 [R]	—	—	—	5.0 ± 0.1 [R] (108.7%)	4.0 ± 0.0 [R] (87.0%)

The following measurements were made where possible, all selected specifically to facilitate estimation of the relative sizes of the highly fragmentary specimens: **PAPW** = width of alveolar process of premaxilla (dorsal portion); **FDPH** = height of descending process of frontal (posterior portion); **QJTL** = length of quadratojugal tubercle; **ECTH** = height of ectopterygoid; **PARW** = width of angular ramus (posterior portion); **AVFH** = height of ventrolateral flange of angular (central portion); **SARW** = width of surangular ramus (central portion). For each measurement, the mean ± standard deviation of 10 individual repeated measurements is given. All measurements are rounded to the nearest 0.1 mm. Letters in brackets indicate whether the measurements were taken on the left [L] or right [R] side of the specimen. Percentages given in parentheses for UA 9754, UA 9762, and FMNH nos. PR 2596–2598 represent the relative magnitudes of measurements taken from these five referred specimens expressed as percentages of corresponding measurements recorded from the fully articulated holotype (UA 8679).

*Measurement estimated because of slight breakage, erosion, or distortion.

UA 9762 were somewhat smaller than UA 8679, and that both of the former specimens may have been closer in size to FMNH PR 2597. If the latter of these inferences is correct, then UA 9754 and UA 9762 both likely represent adult individuals, although perhaps relatively small ones. The adult status of UA 9762 is further suggested by the highly rugose external surface of the dorsal lamina of this fragmentary frontal.

Sexual Dimorphism in *Simosuchus clarki*?—The relatively extensive qualitative and quantitative differences in craniofacial morphology clearly evident in comparisons between the holotype specimen (UA 8679) of *S. clarki* and the most complete and articulated referred specimen (FMNH PR 2597) raise the question of whether this taxon exhibited sexual dimorphism in its skeletal shape and/or proportions. Indeed, in addition to being more heavily ornamented and strongly angulated, the head skeleton of UA 8679 also exhibits a relatively wider snout (SNWA, SNWP, AOIFD; Table 1), more widely spaced orbital fenestrae (OIFD; Table 1), and more widely spaced quadrates (TQW; Table 1) than does FMNH PR 2597, despite the two specimens sharing very similar neurocranial proportions (e.g., OCW, BCH; Table 1); all three of these proportional differences have been documented as being sexually dimorphic in at least some extant species of crocodylians (e.g., *Crocodylus novaeguineae*; see Hall and Portier, 1994), with males exhibiting wider craniofacial skeletons than females.

Regional proportional differences in the skeletons of UA 8679 and FMNH PR 2597 appear not to be limited to the skull and lower jaw. Rather, they also seem to be evident throughout the pectoral girdle and forelimb as well. Based on detailed measurements compiled by Sertich and Groenke (this volume:table 1), we calculated regional means of multiple pairwise comparisons made between these two specimens, grouped by measurements of elements of the pectoral girdle ($n = 3$), stylopodium and zeugopodium ($n = 7$), and autopodium ($n = 14$). This analysis revealed that the relative sizes of appendicular elements varied between specimens along a proximodistal axis, with FMNH PR 2597 being larger than UA 8679 in the relative proportions of its pectoral girdle (118%) and its stylopodia and zeugopodia (109%), but smaller than UA 8679 in the relative proportions of its autopodia (90%).

Collectively, these regional proportional differences between UA 8679 and FMNH PR 2597 in the structure of both the craniofacial and appendicular skeletons are suggestive not only of sexual dimorphism, but perhaps even some degree of niche partitioning as well. Moreover, based on extrapolation from the well-documented sexual dimorphisms known to exist among at least some species of extant crocodylians (e.g., *Crocodylus novaeguineae*; Hall and Portier, 1994), there is at least some reason to believe that UA 8679 may represent a male individual, whereas FMNH PR 2597 may represent a female.

Functional Implications

Habitual Head Posture—Sharing in common with most other tetrapods a well-differentiated neck and a highly specialized atlas-axis complex for articulation with the skull (see Georgi and Krause, this volume), *Simosuchus clarki* doubtless possessed a highly mobile head that could be freely rotated ventrally (i.e., flexed), dorsally (i.e., extended), and side-to-side (i.e., laterally flexed), and also rotated about its own longitudinal axis. Moreover, the complete behavioral repertoire of *S. clarki*—i.e., taking into account all aspects of its feeding and locomotion, as well as its possible stereotyped communicatory behaviors (e.g., Senter, 2008)—almost certainly included all of these potential movements, quite likely to the full extent that each was possible, at least under certain circumstances. Nevertheless, it is equally likely that this species, like most other tetrapods that have been investigated in this regard, also preferred to orient its head in a specific and relatively steady position throughout a wide range of its normal activities, thereby maintaining a characteristic habitual head posture, upon which other behaviors involving the head were superimposed (e.g., de Beer, 1947; Duijm, 1951a, 1951b). Unfortunately, however, the highly unusual shape of the skull of *S. clarki* makes it particularly challenging to infer the habitual head posture of this species relative to those of most other fossil tetrapods.

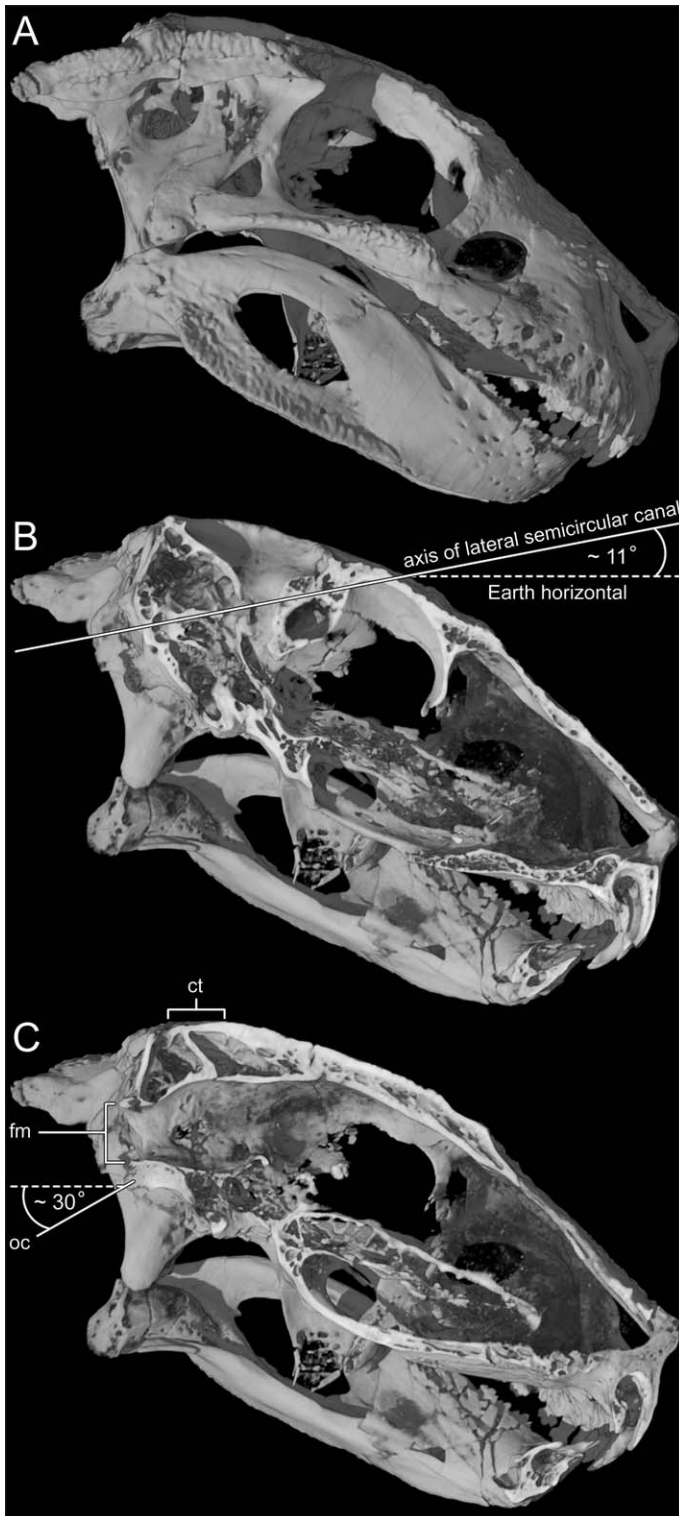
In many species of extinct (and extant) quadrupedal tetrapods, the long axis of the rostrum lies nearly parallel with a horizontal plane passing along the ventral surface of the braincase (i.e., the palate and basicranium are more or less in line with

one another), and the foramen magnum is oriented almost directly posteriorly. In such taxa having relatively ‘straight’ skulls, a natural longitudinal cranial axis can be recognized with relative ease. In contrast, however, the skull of *S. clarki* is far from straight: the preorbital portion of the skull is ventroflexed at an angle of $\sim 20^\circ$ relative to the mid-orbital portion, and both the mid- and postorbital portions exhibit a continuous dorsal convexity along most of their lengths; the ventral two-thirds of the

occiput is anteroflexed at an angle of $\sim 60^\circ$ relative to the more vertically oriented dorsal one-third; the foramen magnum and occipital condyle differ in their orientations by $\sim 30^\circ$, with neither sharing its orientation with that of either of the two primary occipital surfaces; and the basicranium and palate deviate from coplanarity by $\sim 35^\circ$. Thus, different portions of the skull are suggestive of markedly different head orientations. Nevertheless, we note that placing the flat posterior-most dorsal surface of the cranial table in a horizontal position results in the foramen magnum being oriented directly posteriorly, with the relatively short dorsal occipital surface slanting along a steeply inclined anterodorsal-posteroventral axis between the former two features (Fig. 36C); such orientations are fully consistent with the way in which living crocodylians generally hold their heads when alert. We further note that this head posture results in the endocranial surface of the braincase being oriented horizontally and the central portion of the bony palate being oriented nearly horizontally (with only a very slight anterodorsal-posteroventral declination) (Fig. 36C). Perhaps more significantly, however, HRXCT scans of UA 8679 also reveal that, with the skull in this position, the lateral semicircular canals are oriented such that their major axes are inclined anterodorsally at an angle of $\sim 11^\circ$ above horizontal (Fig. 36B).

It has long been hypothesized that terrestrial vertebrates generally hold their heads such that their lateral semicircular canals are oriented horizontally (i.e., parallel to ‘Earth horizontal’) (e.g., Girard, 1923; Ledebkin, 1924; de Beer, 1947; Duijm, 1951a, 1951b), and some recent authors have inferred the habitual head postures of numerous extinct archosaurs based on this assumption (e.g., Witmer et al., 2003; Sereno et al., 2007; Witmer and Ridgely, 2009). However, as noted in recent reviews by Hullar (2006) and Taylor et al. (2009), most available empirical data that have been collected using modern experimental techniques suggest that resting but alert vertebrates generally hold their heads such that their lateral semicircular canals are in fact inclined slightly anterodorsally relative to Earth horizontal (e.g., Mazza and Winterson, 1984; Vidal et al., 1986; Brichta et al., 1988; Erichsen et al., 1989; Graf et al., 1995). The specific magnitude of this inclination appears to vary somewhat among the relatively few species that have been carefully studied in this regard, but the most extensive data set available for any extant archosaur is that for pigeons (*Columba livia*), which have been found to orient their heads at rest such that their lateral semicircular canals are inclined anterodorsally by 5° – 15° ($\bar{x} = 10^\circ$) relative to Earth horizontal (Erichsen et al., 1989). These data are clearly highly concordant with our estimate of a $\sim 11^\circ$ anterodorsal inclination of the lateral semicircular canals in *S. clarki*, thereby providing further corroboration of our inferences regarding the habitual head posture of *Simosuchus*, based initially on external morphological features.

Thus, based on all available external and internal morphological evidence gleaned from the skull of *S. clarki*, and by com-



← FIGURE 36. Inferred habitual head posture of *Simosuchus clarki*, illustrated using a three-dimensional reconstruction of the skull and lower jaw of the holotype (UA 8679) generated from HRXCT scans. In this reconstruction, remaining matrix has been removed digitally so as to provide unobstructed views of unprepared internal regions of the head skeleton. **A**, right lateral view of the entire head skeleton; **B**, lateral cutaway view through the right otic capsule, showing the orientation of the lateral semicircular canal (solid line) relative to Earth horizontal (dashed line); **C**, lateral cutaway view through the median sagittal plane, showing the horizontal orientation of the ‘cranial table’ (ct), the posteriorly directed orientation of the foramen magnum (fm), and the posteroventral orientation of the occipital condyle (oc) relative to Earth horizontal (dashed line).

parison with the habitual head postures of numerous extant tetrapods, we characterize that inferred for *S. clarki* as follows (see Fig. 36): posterior portion of cranial table and endocranial surface of parietal portion of cranial vault oriented horizontally; central portion of bony palate oriented nearly horizontally; pre-orbital (i.e., rostral) portion of dermal skull roof tilted downward at an angle of $\sim 45^\circ$ between horizontal and vertical; foramen magnum oriented directly posteriorly; and occipital condyle oriented posteroventrally at an angle of $\sim 30^\circ$ below horizontal.

Diet and Feeding Mechanics—As is the case for the vast majority of extinct vertebrates, most aspects of the trophic biology of *Simosuchus clarki* can be inferred only indirectly. Nevertheless, numerous aspects of the craniodental morphology of this bizarre crocodyliform provide strong clues, albeit somewhat general ones, about both its diet and feeding mechanics. In this account, we limit our discussion primarily to a re-evaluation and extension of the preliminary functional interpretations presented by Buckley et al. (2000) in their initial description of *S. clarki*, which addressed several of the most salient morphological features of the feeding apparatus of this species. A more detailed and complete analysis of the feeding mechanics of *S. clarki*, taking into account fully the numerous osteological correlates of relevant soft-tissue structures preserved in particular in the holotype specimen (UA 8679)—i.e., various trigeminal, facial, and hypoglossal muscles, the cartilago transiliens, the cranial adductor tendon, etc.—will be presented as a future contribution elsewhere.

As emphasized strongly by Buckley et al. (2000), the highly distinctive multicusped teeth of *Simosuchus* differ radically from the far less elaborate conical teeth exhibited by most other crocodyliform taxa, the vast majority of which are thought to have been (or are known to be) faunivorous. Furthermore, these authors noted that the teeth of *S. clarki* are highly convergent upon those of certain extinct and extant amniotes that are thought to have been, or are known to be, largely or exclusively herbivorous. In particular, they noted a striking similarity between the teeth of *Simosuchus* and those of certain ornithischian dinosaurs, such as ankylosaurs and stegosaurs, which have long been thought to have been dedicated herbivores. Based on these observations, Buckley et al. (2000:941) concluded that *S. clarki* was most likely “predominantly if not exclusively herbivorous.”

Since the initial discovery and description of *S. clarki*, additional information about the structure and implantation of its teeth has emerged, both through further preparation and HRXCT scanning of the head skeleton of the holotype specimen (UA 8679) and through the recent discovery and preparation of an additional articulated specimen (FMNH PR 2596) that retains exceptionally well-preserved premaxillary and maxillary teeth. Our studies of these specimens, in conjunction with additional comparisons made with other herbivorous vertebrates, provide further corroboration of the observations and inferences made by Buckley et al. (2000), and also elucidate additional characters of the dentition that similarly support the hypothesis of herbivory in *Simosuchus*. Specifically, building on those characters first noted by Buckley et al. (2000), we identify a total of five dental characters exhibited by *S. clarki* that are widely recognized as being strongly correlated with herbivory among other vertebrates (e.g., Galton, 1986; Reisz and Sues, 2000): (1) the crowns of all teeth are strongly compressed labiolingually and markedly expanded mesiodistally; (2) the mesiodistally expanded crowns of all teeth bear a linear array of numerous distinct cusps, with each oriented apically at an angle of $\sim 45^\circ$ ($\pm \sim 10^\circ$) relative to the edge (mesial or distal) of the crown; (3) the crowns of all but the most posterior teeth are subtly spatulate in that each exhibits a shallow lingual concavity near its base; (4) the crowns of successive teeth are positioned close together, with little or no gap intervening between them; and (5) the crowns of all teeth are oriented such that their mesiodistal axes are angled somewhat obliquely in ‘occlusal’

view, resulting in an ‘en echelon’ arrangement. These five dental characters, in varying combinations and degrees of expression, have been documented in an extraordinarily wide array of herbivorous vertebrates (Fig. 37), including some teleost fishes (e.g., Purcell and Bellwood, 1993), pareiasaurs (e.g., Lee, 2000), several clades of both ornithischian and saurischian dinosaurs (e.g., Thulborn, 1970; Colbert, 1981; Attridge et al., 1985; Coombs and Maryańska, 1990), iguanine lizards (e.g., Hotton, 1955; Ray, 1965; Montanucci, 1968), and anomodont synapsids (e.g., Rybczynski and Reisz, 2001). Such widespread adaptive convergence in tooth morphology clearly points unambiguously toward *Simosuchus* as having been predominantly herbivorous in its general feeding habits.

In addition to several of the dental characters discussed above, Buckley et al. (2000) also briefly considered the functional implications of several aspects of the morphology of the jaws themselves in *Simosuchus*. Two of these gnathic features—the antero-posterior position of the craniomandibular joint and the length of the lower jaw—are not only correlated with one another, but also strongly interrelated functionally, because they both contribute toward determining the lengths of the in- and out-levers within the jaw apparatus during simple opening and closing movements of the jaws. For this reason, we will consider these two characters together.

In the vast majority of crocodyliforms, the body of the quadrate is oriented such that its distal end projects moderately to strongly posteroventrally, resulting in the condyle of the quadrate, and thus the craniomandibular joint, being positioned at or near the posterior end of the skull. In sharp contrast to this arrangement, the distal end of the body of the quadrate in *Simosuchus* projects ventrally and even slightly anteriorly (Fig. 4), thereby resulting in the craniomandibular joint being positioned unusually far anteriorly relative to the more posterior placement seen in other crocodyliforms. Analyzing the jaws as a simple third-class lever system, it may be readily understood that this anterior shift in the position of the jaw joint in *Simosuchus*, by itself, would have had two effects: (1) shortening of the system’s out-lever, or resistance arm (i.e., the distance between the fulcrum, or pivot point, and the point of resistance), but only to a relatively moderate degree; and (2) shortening of the system’s in-lever, or force arm (i.e., the distance between the fulcrum and the point of applied force), to a proportionately much greater degree. Therefore, assuming that all other aspects of the system remained constant, the net effect of these two changes would have been an overall decrease in the system’s mechanical advantage. That is, in the system under consideration here, the anterior shift in the placement of the craniomandibular joint that occurred in the evolution of *S. clarki* would have, by itself, resulted in a decrease in the force with which the jaws could have been closed, a functional consequence that was noted by Buckley et al. (2000).

However, the anterior shift in the position of the jaw joint discussed above did not evolve by itself; rather, it evolved in conjunction with an overall reduction in the length of the lower jaw, which occurred not only through a shortening of its posterior end, but also through an even greater shortening of its anterior end (the latter being associated primarily with the extreme reduction in the length of the snout of *S. clarki*, but also secondarily with the shortening of the lower jaw relative to the upper jaw in this species). It is significant to note that the latter of these modifications (i.e., shortening of the lower jaw anterior to the mandibular adductor fossa) would have decreased the length of the system’s out-lever without affecting that of its in-lever. Consequently, significant shortening of the anterior portion of the lower jaw would have resulted in a greatly increased mechanical advantage within the system.

Thus, when considered together, the anterior shift in the placement of the craniomandibular joint and the overall reduction in the length of the lower jaw likely had the net effect of an evo-

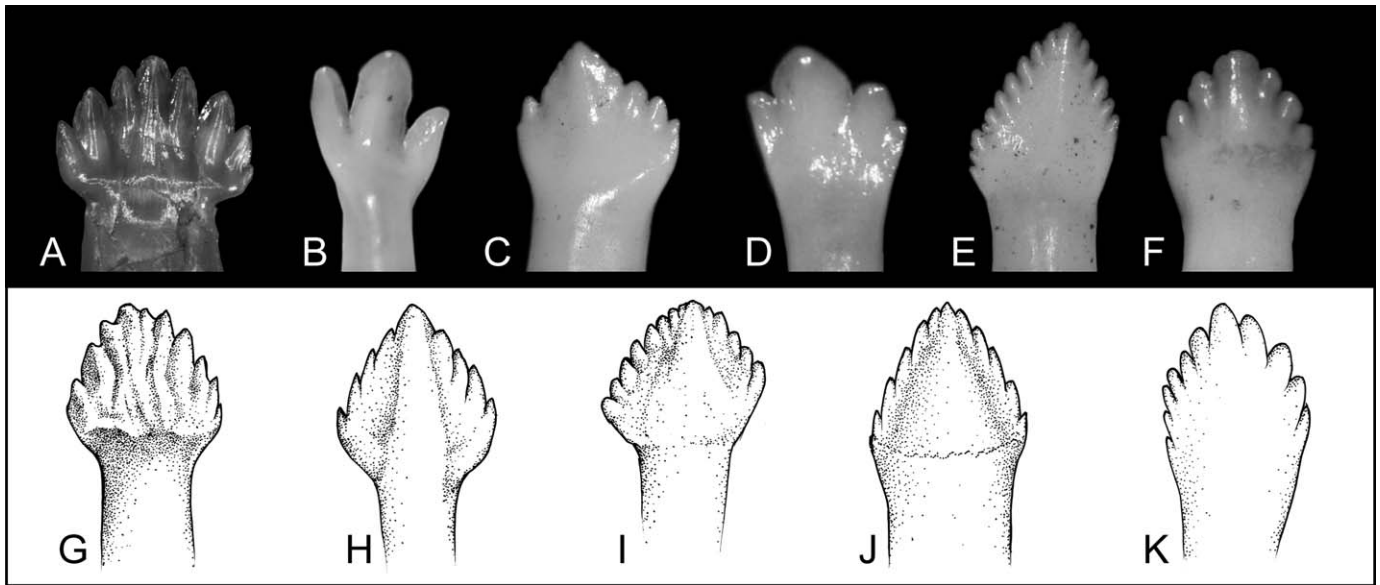


FIGURE 37. Individual teeth from a phylogenetically diverse sample of extant vertebrates known to be herbivorous and extinct vertebrates inferred to have been herbivorous, including the notosuchian crocodyliform *Simosuchus clarki* (A), five iguanine squamates (B–F), three ornithischian dinosaurs (G–I), a pareiasaur (J), and an acanthurid actinopterygian (K). A, *Simosuchus clarki* (holotype, UA 8679), mesial-middle maxillary tooth in lingual view. B, *Amblyrhynchus cristatus* (AMNH 75943), left fifth maxillary tooth in lingual view. C, *Cyclura cornuta* (AMNH 50799), right eighth maxillary tooth in lingual view. D, *Ctenosaura hemilopha* (AMNH 147854), right 14th maxillary tooth in lingual view. E, *Iguana iguana* (AMNH 74631), left 14th maxillary tooth in lingual view. F, *Sauromalus hispidus* (AMNH 73616), 16th left dentary tooth in lingual view. G, *Edmontonia rugosidens*, tooth of unknown placement, position, and orientation (redrawn after Coombs and Maryańska, 1990). H, *Scutellostaurus lawleri*, maxillary tooth in lingual view (redrawn after Colbert, 1981). I, *Lesothosaurus diagnosticus*, maxillary tooth in lingual view (redrawn after Sereno, 1991). J, *Scutosaurus karpinskii*, maxillary tooth in lingual view (redrawn after Lee, 2000). K, *Acanthurus nigrofuscus*, fourth left premaxillary tooth in medial view (redrawn after Purcell and Bellwood, 1993).

lutionary increase in the mechanical advantage of the jaws in *S. clarki*. This notwithstanding, however, *Simosuchus* was likely not able to bite with particularly great force, due primarily to the structure of its glenoid fossa, which lacks transverse buttresses both posteriorly and anteriorly. Stabilization of the craniomandibular joint during jaw closing was therefore presumably almost entirely dependent upon the action of muscles, most likely those that inserted relatively close to the joint itself (e.g., *M. pterygoideus posterior*, *M. adductor mandibulae posterior*).

Although implicit in the preceding analysis, it merits explicit emphasis that, whereas the anterior shift in the placement of the craniomandibular joint and the overall reduction in the length of the lower jaw discussed above would have resulted in a net evolutionary increase in the mechanical advantage of the muscles of the *M. adductor mandibulae* complex during jaw closing, these changes would have had the opposite effect on the velocity with which *Simosuchus* could have closed its jaws. This represents another independent line of evidence that supports the hypothesis of herbivory in *S. clarki*, because it suggests that this species would have been particularly poorly adapted for catching elusive animal prey with its jaws.

It is particularly interesting to note that both the vertical orientation of the body of the quadrate and the relative brevity of the lower jaw, which as discussed above are of great importance in dictating fundamental aspects of the feeding mechanics of *Simosuchus*, are features that are well known to characterize various embryonic stages of extant crocodylians (Parker, 1883; Rieppel, 1993; Peterka et al., 2010). The presence of these and numerous other such characters (e.g., dorsally convex skull roof throughout mid- and postorbital regions of cranium; prominent ventroflexion of preorbital portion of cranium; short, blunt snout; lack of contact between palatal processes of left and right maxillae; large

orbits; long anterior process of jugal) throughout the craniofacial skeleton in adult individuals of *S. clarki* suggests that paedomorphosis may have played a significant role in the evolution of this species.

In addition to the anteroposterior position of the craniomandibular joint and the extreme brevity of the lower jaw, Buckley et al. (2000:942) also commented briefly on the morphology of the glenoid fossa and how it might have influenced feeding mechanics in *S. clarki*, noting that: “The glenoid fossa is narrow anteroposteriorly, suggesting limited propalinal motion. This is in stark contrast to the long jaw articulation in *Notosuchus* (Late Cretaceous, Argentina) and *Malawisuchus* (Early Cretaceous, Malawi).” Although we generally agree with this statement, we emphasize the fact that limited propalinal movements were indeed possible in *S. clarki*, given that (1) the glenoid fossa lacks a transversely oriented posterior buttress that would have prevented forward translation of the articular relative to the condyle of the quadrate; and (2) the main portion of the articular surface of the glenoid fossa is nearly twice the length of the condyle of the corresponding quadrate (see GFL vs. QCL in Tables 1 and 2). Moreover, as described above, projecting from the lateral-most part of the glenoid fossa is a prominent posterior expansion of its articular surface; in the holotype specimen of *S. clarki* (UA 8679), this expansion extends posteriorly for a distance of ~3 mm, thereby effectively increasing the anteroposterior extent of the articular surface for the lateral hemicondyle of the quadrate by more than 25%.

Finally, one additional aspect of the craniomandibular joint not discussed by Buckley et al. (2000), but of potential functional significance in the context of the jaw closing mechanism of *S. clarki*, is the dorsoventral position of the glenoid fossa. In contrast to the condition exhibited by other crocodylians, the glenoid fossa

lies well ventral to the dentary tooth rows in *S. clarki*. This ventral shift in the placement of the glenoid fossa would have had three potentially significant functional consequences: (1) it would have increased the moment arms of many of the muscles of the *M. adductor mandibulae* complex, in particular those whose courses angled most strongly from posterodorsal to anteroventral, such as the *M. pseudotemporalis*; (2) it would have decreased the moment arms of both of the two largest members of the *M. adductor mandibulae internus* group, the *Mm. pterygoideus anterior et posterior*, due to the strongly angled anterodorsal-to-posteroventral course of their fibers; and (3) perhaps most significantly, this ventral position of the glenoid would have resulted in the entire lower tooth row approaching the entire upper tooth row at only a very shallow angle during jaw closing, thereby maximizing the number of teeth that would have simultaneously contacted a given food item contained either partially or fully within the oral cavity. The ventral placement of the glenoid fossa in *S. clarki* represents yet another anatomical feature consistent with the hypothesis that this species was largely or entirely herbivorous, because similar morphologies are well known to have evolved widely among numerous clades of herbivorous dinosaurs (Galton, 1986).

Fossoriality and Burrowing—In their initial description and preliminary functional assessment of *Simosuchus clarki*, Buckley et al. (2000:943) stated that: “Several features suggest that *Simosuchus*, like *Malawisuchus*, may have been an adept head-burrower. These traits, seen in extant head-burrowing vertebrates, include a short, flat, shovel-like snout and deep cranium, a posteroventrally positioned occipital condyle that would orientate the cranium in a more vertical position, a short, underslung lower jaw that would prevent friction from inadvertently opening the jaws during burrowing, and extensive insertion areas for neck musculature (enlarged hypapophyses and elongated neural spines on the cervical vertebrae, expanded squamosal region and occiput).” Although we agree fully that such traits are characteristic of many (but not all) species of head-first burrowing tetrapods, and that similar traits have indeed evolved convergently in *Simosuchus*, numerous lines of evidence cast a significant shadow of doubt over the hypothesis that these traits evolved in *Simosuchus* as specific adaptations for head-first burrowing.

Head-first burrowing represents one of the most highly specialized forms of fossorial locomotion. Simply defined, it entails the construction of patent underground tunnel systems in compact soils using the head as the primary burrowing instrument. In that it involves forceful penetration and compaction of earth in the immediate vicinity of the head against the roof, walls, and/or floor of the tunnel being created, it differs fundamentally from other methods of burrowing that rely on various limb- or jaw-based excavation techniques (e.g., scratch digging, chisel-tooth digging; Hildebrand, 1985) to physically dislodge and remove soil from burrows. Moreover, although head-first subterranean locomotion in loose soils generally requires no significant specializations in craniofacial morphology, true head-first burrowing (i.e., that occurring in relatively densely packed substrates) is generally associated with relatively extreme morphological modifications due to the severe loading regimes imposed on the head skeleton (Gans, 1974; Wake, 1993).

True head-first burrowing has evolved only very rarely among extant quadrupedal tetrapods; this likely testifies to the relative efficiency of even the most generalized of tetrapod limbs as digging instruments (Kley and Kearney, 2007). Rather, this derived form of burrowing is by far most common among fossorial forms of limbless and limb-reduced amphibians and reptiles, which, of course, are unable to rely on limb-based digging techniques for burrowing. Among such limbless and limb-reduced taxa, head-first burrowing is most strongly developed in amphisbaenians (e.g., Gans, 1960, 1968, 1969, 1974; Navas et al., 2004),

uropeltid snakes (e.g., Gans, 1973b, 1976; Gans et al., 1978; Rajendran, 1985), and caecilians (e.g., Gaymer, 1971; Gans, 1973a; Wake, 1993; O’Reilly et al., 1997). These are uniformly slender animals, with most exhibiting head diameters of 0.5–2.5 cm; moreover, nearly all have conspicuously modified snouts of various shapes conducive to burrowing (e.g., round, conical, wedge-shaped, keel-shaped, shovel-shaped). (For detailed discussions regarding the theoretical principles underlying the functional significance of snout size and shape in the context of head-first burrowing mechanics, see Gans, 1960, 1968, 1974.)

In sharp contradistinction to the conditions just described, *Simosuchus*, whose somatotype was decidedly not slender, exhibits a broad and tall snout measuring more than 5 cm in width and nearly 2.5 cm in height. Perhaps of equal or even greater importance, it is not at all shaped like those of extant head-first burrowers; rather, its relatively expansive anterior surface is nearly completely flat. The snout of *Simosuchus* is therefore not “shovel-like” (contra Buckley et al., 2000:943) in that it clearly lacks a dorsoventrally narrowed cutting edge, such as those seen along the snouts of ‘shovel-headed’ amphisbaenians (e.g., *Rhineura* [Gans, 1967a, 1967b], *Leposternon* [Gans, 1971], *Monopeltis* [Gans and Lehman, 1973; Broadley et al., 1976]), and which represents an important morphological component of the soil penetration mechanisms used by these taxa (Gans, 1968, 1974). Furthermore, we suggest more generally that, based on the above considerations (and others, such as the relatively large, dorsally positioned external narial fenestrae and the morphology of the sutures throughout the facial portion of the skull), that the snout of *Simosuchus* exhibits no structural modifications to suggest that this taxon engaged in, or was even capable of, head-first burrowing.

Another craniofacial feature of *S. clarki* cited by Buckley et al. (2000:943) as being suggestive of a head-first burrowing lifestyle is its “underslung lower jaw.” Many extant head-first burrowers do possess short, subterminal lower jaws, and in some taxa they are even ‘countersunk’ such that they fit completely within a dorsal recess created by the margins of the overhanging snout and upper jaws, a characteristic perhaps most strongly expressed among scolecophidian snakes (e.g., Jan and Sordelli, 1860–1866; Boulenger, 1893; McDowell, 1974; Roux-Estève, 1974). As noted by Buckley et al. (2000), this morphology assists in preventing the mouth from being forced open as the overlying snout is rammed forward during burrowing. However, the morphology exhibited by *Simosuchus* in relation to this character differs significantly from that seen among extant head-first burrowers in several ways. First, only a relatively limited portion of the lower jaw would have been ‘shielded’ from substrate reaction forces during burrowing. With the jaws closed and the anterior dentary teeth accommodated within the anterior palatal trough, the dorsal margin of the transverse part of the lower jaw is indeed partially ‘shielded’ anteriorly. However, the ventral portion of this part of the jaw, a strip ~ 1 cm in dorsoventral height, is still left exposed along its anterior surface in this position. Second, and perhaps even more significantly, the structures ‘shielding’ the dorsal margin of the transverse part of the lower jaw when it was closed were the prominent, anteroposteriorly compressed, ventrally projecting premaxillary teeth, features of critical importance to the feeding apparatus of *Simosuchus*, and ones that would likely not have endured the extreme loading regimes associated with head-first burrowing. Finally, although the anterior-most part of the lower jaw of *Simosuchus* is contained within the overhanging margins of the upper jaws, this is not at all true of the posterior part of the jaw. Indeed, the ventrolateral flanges of the angular project well beyond the lateral margins of the overlying skull. Thus, if the cranium was rotated dorsally or forced anteriorly within a compact substrate, associated reaction forces would, in fact, have tended to force the jaws open. For these reasons, we do not believe that the subterminal lower jaw of *Simosuchus* represents an adapta-

tion for head-first burrowing; instead, its utility may have been related to the cropping of low vegetation between the dentary and premaxillary teeth when the head was lowered toward the ground during feeding. In fact, several characters cited by Buckley et al. (2000:943) as evidence of a head-first burrowing lifestyle in *Simosuchus* could be interpreted at least equally as parsimoniously as instead being associated with a grazing lifestyle involving an habitually ventroflexed head that was frequently lowered toward the ground and then raised again (e.g., posteroventrally positioned occipital condyle, extensive insertion areas for neck musculature).

Finally, we point toward the relatively large size of the orbits in *Simosuchus* as being one of the most striking craniofacial features that would appear to be highly inconsistent with a head-first burrowing lifestyle in this taxon. It has long been recognized that there is a strong tendency toward evolutionary reduction (and sometimes even complete loss) of the eyes in fossorial vertebrates, both in taxa that rely predominantly on their heads for burrowing, and in those that rely more heavily on limb- and/or jaw-based excavation techniques (e.g., Walls, 1942; Dubost, 1968; Underwood, 1970). In at least some representatives of the latter category, the risk of mechanical damage to the eyes during burrowing may be relatively small, and ocular reduction in such taxa could be due primarily to a reduced need for vision in a perpetually dark environment. However, in fossorial vertebrates that use their heads as instruments for burrowing, the risk of direct trauma to the eyes is clearly severe. Thus, nearly all head-first burrowers exhibit markedly reduced eyes (relative to their non-burrowing relatives), both in terms of their relative size and in their functional complexity. In contrast, the size of the orbital fenestrae of *Simosuchus*—accounting for approximately one-third of the total mid-dorsal length of the skull—suggests that this taxon retained relatively large eyes (even taking into account the possibility that it possessed somewhat enlarged Harderian glands, as some burrowing tetrapods do). Although the eyes of *Simosuchus* would have been partially protected by some associated hard and soft tissues (e.g., anterior and posterior palpebrals, eyelids, nictitating membranes), it would seem that they would have been very poorly suited for a head-first burrower.

Based on the above considerations, we conclude that the morphology of the head skeleton of *S. clarki* is inconsistent with Buckley et al.'s (2000) hypothesis of a head-first burrowing lifestyle for this taxon. Similarly, the postcranial axial and appendicular components of the skeleton have also failed to reveal distinctive adaptations for burrowing behavior (Georgi and Krause, this volume; Sertich and Groenke, this volume). That said, it nevertheless remains possible that *S. clarki* may have occasionally used its head to augment a limb-based scratch-digging mechanism, much as some living crocodylians have been documented to do (for a recent review, see Kley and Kearney, 2007). Indeed, one extant species, *Alligator sinensis*, is known to construct remarkably extensive and elaborate burrow systems in this way, some extending more than 50 m in length (Huang, 1982; Watanabe and Huang, 1984).

Phylogenetic Implications

The first cladistic treatment of crocodyliform phylogeny was presented in the seminal works of Clark (1986, 1994). Subsequent work by various research groups has led to an expanded set of characters that relate to reconstructing crocodyliform interrelationships (e.g., Wu et al., 1997; Pol, 1999, 2003; Buckley et al., 2000; Larsson and Gado, 2000; Ortega et al., 2000; Sereno et al., 2001, 2003; Tykoski et al., 2002; Carvalho et al., 2004, 2007; Pol et al., 2004, 2009; Pol and Norell, 2004a, 2004b; Turner, 2004, 2006; Pol and Apesteguía, 2005; Turner and Calvo, 2005; Gasparini et al., 2006; Jouve et al., 2006; Andrade and Bertini, 2008a; Turner and Buckley, 2008; Jouve, 2009), with craniofacial morphology

providing the predominant source of phylogenetically informative characters in these analyses. This is understandable given the robust construction and relative ease of preservation of cranial remains among crocodyliforms and the corresponding paucity of well-described postcranial skeletal material. Moreover, the relevance of craniofacial morphology to phylogenetic reconstruction has expanded dramatically over the past 15 years with the discovery of an increasingly diverse assemblage of notosuchian crocodyliforms on Gondwanan landmasses. Collectively, these taxa exhibit a wide diversity of craniofacial morphologies that unquestionably departs from the stereotypical 'crocodyliform' gestalt.

With a few notable exceptions, monographic descriptions of basal mesoeucrocodylians are rare, thus hindering comparisons and the search for new characters and character systems for phylogenetic analysis. This detailed description of the craniofacial morphology of *Simosuchus clarki* places many aspects of notosuchian and basal mesoeucrocodylian cranial anatomy into a comparative context and, due to the exquisite preservation of the head skeleton of the holotype specimen (UA 8679), a number of understudied regions have been given an unprecedented level of attention. The description of the skull and lower jaw of *Simosuchus* presented here allows several additional phylogenetic characters to be identified and defined and also provides an opportunity to reassess existing character sets.

Many of the highly derived craniofacial features discussed here are autapomorphic for *S. clarki*. Indeed, 45 cranial autapomorphies are currently recognized (for a complete list, see Turner and Sertich, this volume), thus providing a rich source of potential character data for future phylogenetic and taxonomic work. Other regions of mesoeucrocodylian craniofacial anatomy offer the possibility of expanded phylogenetic characters that are explored further by Turner and Sertich (this volume). For example, the presence of an epipterygoid has only recently been recognized among crocodyliforms (Holliday and Witmer, 2009). The morphology of the epipterygoid in *Simosuchus* and the gross morphology of the adductor chamber offer a source of phylogenetically informative characters whose potential has not yet been explored. Moreover, the dentitions of most notosuchians, including that of *Simosuchus*, show an enormous degree of morphological disparity in both the elaboration of cusps, denticles, and enamel ridges and the physical record of feeding behavior, including the presence or absence of abrasion surfaces. Expanding the characterization of this dental morphology is crucial for deciphering the phylogenetic interrelationships of notosuchians, including *Simosuchus*. The shape and construction of the internal narial fenestrae of *Simosuchus* appear to be, in many respects, transitional to the derived morphologies exhibited by other notosuchians such as *Notosuchus* and *Marilyasuchus* on the one hand, and *Araripesuchus* and peirosaurids on the other. Similarities between the choanal morphologies of *Simosuchus*, *Uruguaysuchus*, and *Libycosuchus*—all with large, deep internal narial fenestrae bordered almost entirely by the pterygoid—may represent the plesiomorphic condition for Notosuchia.

ACKNOWLEDGMENTS

We thank J. Groenke, V. Heisey, and G. Buckley for their skillful preparation of the head skeletons of UA 8679 and FMNH PR 2597; J. Neville for her expertise in photographing these specimens; L. Betti-Nash for her extreme patience and tireless efforts in executing the illustrations of these specimens; M. Colbert and J. Maisano for μ CT-scanning the skull and lower jaw of UA 8679 and digitally processing the resultant HRXCT data set; members of the Radiology Department at the Stony Brook University Medical Center for their assistance in CT-scanning the head skeletons of FMNH PR 2596 and FMNH PR 2597; D. Sammis for locating and providing numerous obscure papers; C. Holliday for helpful correspondences regarding various aspects of the

morphology of *Simosuchus*; and C. Brochu and J. Clark for their detailed reviews of an earlier draft of the manuscript. We also gratefully acknowledge the extensive financial support to D.W.K. from the National Science Foundation (EAR-9706302, DEB-9904045, EAR-0106477, EAR-0116517, EAR-0446488) and the National Geographic Society (6400-99, 6940-00, and 7645-04) that facilitated the discovery, preparation, and study of all specimens of *Simosuchus clarki* examined throughout the course of this study. The digital reconstruction of the cranial endocast was facilitated by a National Science Foundation grant (EAR-0617561) to P.M.O. Finally, N.J.K. acknowledges a grant from the National Science Foundation (IOS-0749750) that helped to support operations in his laboratory during the preparation of the manuscript.

LITERATURE CITED

- Andrade, M. B. de, and R. J. Bertini. 2008a. A new *Sphagesaurus* (Mesoeucrocodylia: Notosuchia) from the Upper Cretaceous of Monte Alto City (Bauru Group, Brazil), and a revision of the Sphagesauridae. *Historical Biology* 20:101–136.
- Andrade, M. B. de, and R. J. Bertini. 2008b. Morphology of the dental carinae in *Mariliasuchus amarali* (Crocodylomorpha, Notosuchia) and the pattern of tooth serration among basal Mesoeucrocodylia. *Arquivos do Museu Nacional, Rio de Janeiro* 66:63–82.
- Attridge, J., A. W. Crompton, and F. A. Jenkins, Jr. 1985. The southern African Liassic prosauropod *Massospondylus* discovered in North America. *Journal of Vertebrate Paleontology* 5:128–132.
- Baumel, J. J., A. S. King, J. E. Breazile, H. E. Evans, and J. C. Vanden Berge (eds.). 1993. *Handbook of Avian Anatomy: Nomina Anatomica Avium*, 2nd edition. Publications of the Nuttall Ornithological Club, No. 23, Cambridge, Massachusetts, 779 pp.
- Benton, M. J., and J. M. Clark. 1988. Archosaur phylogeny and the relationships of the Crocodylia; pp. 295–338 in M. J. Benton (ed.), *The Phylogeny and Classification of the Tetrapods, Volume 1: Amphibians, Reptiles, Birds*. Clarendon Press, Oxford, U.K.
- Bonaparte, J. F. 1991. Los vertebrados fósiles de la Formación Río Colorado, de la Ciudad de Neuquén y cercanías, Cretácico Superior, Argentina. *Revista del Museo Argentino de Ciencias Naturales "Bernardino Rivadavia"*, Paleontología 4:116–123.
- Boulenger, G. A. 1893. *Catalogue of Snakes in the British Museum (Natural History)*, Volume I. British Museum (Natural History), London, U.K., 448 pp.
- Brichta, A. M., D. L. Acuña, and E. H. Peterson. 1988. Planar relations of semicircular canals in awake, resting turtles, *Pseudemys scripta*. *Brain Behavior and Evolution* 32:236–245.
- Broadley, D. G., C. Gans, and J. Visser. 1976. Studies on amphisbaenians (Amphisbaenia, Reptilia) 6. The genera *Monopeltis* and *Dalophia* in Southern Africa. *Bulletin of the American Museum of Natural History* 157:311–486.
- Brochu, C. A. 1999. Phylogenetics, taxonomy, and historical biogeography of Alligatoroidea; pp. 9–100 in T. Rowe, C. A. Brochu, and K. Kishi (eds.), *Cranial Morphology of Alligator mississippiensis and Phylogeny of Alligatoroidea*. Society of Vertebrate Paleontology Memoir 6. *Journal of Vertebrate Paleontology* 19(2, Supplement).
- Brochu, C. A. 2003. Phylogenetic approaches toward crocodylian history. *Annual Review of Earth and Planetary Sciences* 31:357–397.
- Brochu, C. A., M. L. Bouaré, F. Sissoko, E. M. Roberts, and M. A. O'Leary. 2002. A dyrosaurid crocodyliform braincase from Mali. *Journal of Paleontology* 76:1060–1071.
- Broin, F., and P. Taquet. 1966. Découverte d'un Crocodilien nouveau dans le Crétacé inférieur du Sahara. *Comptes Rendus de l'Académie des Sciences de Paris, Séries D* 262:2326–2329.
- Buckley, G. A., and C. A. Brochu. 1999. An enigmatic new crocodile from the Upper Cretaceous of Madagascar; pp. 149–175 in D. Unwin (ed.), *Cretaceous Fossil Vertebrates. Special Papers in Palaeontology*, No. 60, The Palaeontological Association, London, U.K.
- Buckley, G. A., C. A. Brochu, D. W. Krause, and D. Pol. 2000. A pug-nosed crocodyliform from the Late Cretaceous of Madagascar. *Nature* 405:941–944.
- Buffetaut, E., and P. Taquet. 1979. An early Cretaceous terrestrial crocodylian and the opening of the South Atlantic. *Nature* 280:486–487.
- Busbey, A. B., III. 1989. Form and function of the feeding apparatus of *Alligator mississippiensis*. *Journal of Morphology* 202:99–127.
- Carrano, M. T., M. A. Loewen, and J. J. W. Sertich. In press. New materials of *Masiakasaurus knopfleri* Sampson, Carrano, and Forster, 2001 and implications for the morphology of the Noosauridae (Theropoda: Ceratosauria). *Smithsonian Contributions to Paleobiology*.
- Carrano, M. T., S. D. Sampson, and C. A. Forster. 2002. The osteology of *Masiakasaurus knopfleri*, a small abelisauroid (Dinosauria: Theropoda) from the Late Cretaceous of Madagascar. *Journal of Vertebrate Paleontology* 22:510–534.
- Carvalho, I. S. 1994. *Candidodon*: um crocodilo com heterodontia (Notosuchia, Cretáceo Inferior—Brasil). *Anais da Academia Brasileira de Ciências* 66:331–346.
- Carvalho, I. S., and R. J. Bertini. 1999. *Mariliasuchus*: um novo Crocodylomorpha (Notosuchia) do Cretáceo da Bacia Bauru, Brasil. *Geologia Colombiana* 24:83–105.
- Carvalho, I. S., A. C. A. Campos, and P. H. Nobre. 2005. *Baurusuchus salgadoensis*, a new Crocodylomorpha from the Bauru Basin (Cretaceous), Brazil. *Gondwana Research* 8:11–30.
- Carvalho, I. S., L. C. B. Ribeiro, and L. S. Avilla. 2004. *Uberabasuchus terrificus* sp. nov., a new Crocodylomorpha from the Bauru Basin (Upper Cretaceous), Brazil. *Gondwana Research* 7:975–1002.
- Carvalho, I. S., F. M. Vasconcellos, and S. A. S. Tavares. 2007. *Montealtosuchus arrudacamposi*, a new peirosaurid crocodile (Mesoeucrocodylia) from the Late Cretaceous Adamantina Formation of Brazil. *Zootaxa* 1607:35–46.
- Clark, J. M. 1985. A new crocodylomorph from the Late Jurassic Morrison Formation of western Colorado, with a discussion of the relationships within the "Mesosuchia." M.A. thesis, University of California, Berkeley, Berkeley, California, 102 pp.
- Clark, J. M. 1986. Phylogenetic relationships of the crocodylomorph archosaurs. Ph.D. dissertation, The University of Chicago, Chicago, Illinois, 556 pp.
- Clark, J. M. 1994. Patterns of evolution in Mesozoic Crocodyliformes; pp. 84–97 in N. C. Fraser and H.-D. Sues (eds.), *In the Shadow of Dinosaurs: Early Mesozoic Tetrapods*. Cambridge University Press, Cambridge, U.K.
- Clark, J. M., and M. A. Norell. 1992. The Early Cretaceous crocodylomorph *Hylaeochampsia vectiana* from the Wealden of the Isle of Wight. *American Museum Novitates* 3032:1–19.
- Clark, J. M., and H.-D. Sues. 2002. Two new basal crocodylomorph archosaurs from the Lower Jurassic and the monophyly of the Sphenosuchia. *Zoological Journal of the Linnean Society* 136:77–95.
- Clark, J. M., H.-D. Sues, and D. S. Berman. 2000. A new specimen of *Hesperosuchus agilis* from the Upper Triassic of New Mexico and the interrelationships of basal crocodylomorph archosaurs. *Journal of Vertebrate Paleontology* 20:683–704.
- Clark, J. M., J. Welman, J. A. Gauthier, and J. M. Parrish. 1993. The laterosphenoid bone of early archosauriforms. *Journal of Vertebrate Paleontology* 13:48–57.
- Clark, J. M., X. Xu, C. A. Forster, and Y. Wang. 2004. A Middle Jurassic 'sphenosuchian' from China and the origin of the crocodylian skull. *Nature* 430:1021–1024.
- Cleuren, J., and F. De Vree. 2000. Feeding in crocodylians; pp. 337–358 in K. Schwenk (ed.), *Feeding: Form, Function, and Evolution in Tetrapod Vertebrates*. Academic Press, San Diego, California.
- Colbert, E. H. 1946. The Eustachian tubes in the Crocodylia. *Copeia* 1946:12–14.
- Colbert, E. H. 1981. A primitive ornithischian dinosaur from the Kayenta Formation of Arizona. *Museum of Northern Arizona Bulletin* 53:1–61.
- Colbert, E. H., and C. C. Mook. 1951. The ancestral crocodylian *Protosuchus*. *Bulletin of the American Museum of Natural History* 97:143–182.
- Coombs, W. P., Jr., and T. Maryańska. 1990. Ankylosauria; pp. 456–483 in D. B. Weishampel, P. Dodson, and H. Osmolska (eds.), *The Dinosauria*. University of California Press, Berkeley, California.
- Cope, E. D. 1869. Synopsis of the extinct Batrachia, Reptilia and Aves of North America. *Transactions of the American Philosophical Society, New Series* 14:1–252.
- Curry Rogers, K. A., and C. A. Forster. 2001. The last of the dinosaur titans: a new sauropod from Madagascar. *Nature* 412:530–534.

- Curry Rogers, K. A., and C. A. Forster. 2004. The skull of *Rapetosaurus krausei* (Sauropoda: Titanosauria) from the Late Cretaceous of Madagascar. *Journal of Vertebrate Paleontology* 24:121–144.
- de Beer, G. R. 1947. How animals hold their heads. *Proceedings of the Linnean Society of London* 159:125–139.
- Depéret, C. 1896. Note sur les dinosaures sauroïdes et théropodes du Crétacé supérieur de Madagascar. *Bulletin de la Société géologique de France*, 3^e Série 24:176–194.
- Dubost, G. 1968. Les mammifères souterrains. *Revue d'Écologie et de Biologie du Sol* 5:99–197.
- Duijm, M. 1951a. On the head posture in birds and its relation to some anatomical features. I. *Proceedings of the Koninklijke Nederlandse Akademie van Wetenschappen, Series C* 54:202–211.
- Duijm, M. 1951b. On the head posture in birds and its relation to some anatomical features. II. *Proceedings of the Koninklijke Nederlandse Akademie van Wetenschappen, Series C* 54:260–271.
- Edgeworth, F. H. 1935. *The Cranial Muscles of Vertebrates*. Cambridge University Press, Cambridge, U.K., 493 pp.
- Erichsen, J. T., W. Hodos, C. Evinger, B. B. Bessette, and S. J. Phillips. 1989. Head orientation in pigeons: postural, locomotor and visual determinants. *Brain Behavior and Evolution* 33:268–278.
- Evans, S. E., M. E. H. Jones, and D. W. Krause. 2008. A giant frog with South American affinities from the Late Cretaceous of Madagascar. *Proceedings of the National Academy of Sciences of the United States of America* 105:2951–2956.
- Fiorelli, L., and J. O. Calvo. 2008. New remains of *Notosuchus terrestris* Woodward, 1896 (Crocodyliformes: Mesoeucrocodylia) from Late Cretaceous of Neuquén, Patagonia, Argentina. *Arquivos do Museu Nacional, Rio de Janeiro* 66:83–124.
- Fürbringer, M. 1922. Das Zungenbein der Wirbeltiere insbesondere der Reptilien und Vögel. *Abhandlungen der Heidelberger Akademie der Wissenschaften Mathematisch-Naturwissenschaftliche Klasse, Abteilung B* 11:1–164.
- Gaffney, E. S., D. W. Krause, and I. Zalmout. 2009. *Kinkonychelys*, a new side-necked turtle (Pelomedusoides: Bothremydidae) from the Late Cretaceous of Madagascar. *American Museum Novitates* 3662:1–25.
- Galton, P. M. 1986. Herbivorous adaptations of Late Triassic and Early Jurassic dinosaurs; pp. 203–221 in K. Padian (ed.), *The Beginning of the Age of the Dinosaurs: Faunal Change across the Triassic-Jurassic Boundary*. Cambridge University Press, Cambridge, U.K.
- Gans, C. 1960. Studies on amphisbaenids (Amphisbaenia, Reptilia). 1. A taxonomic revision of the Trogonophinae, and a functional interpretation of the amphisbaenid adaptive pattern. *Bulletin of the American Museum of Natural History* 119:129–204.
- Gans, C. 1967a. *Rhineura*; pp. 42.1–42.2 in H. G. Dowling (ed.), *Catalogue of American Amphibians and Reptiles*. American Society of Ichthyologists and Herpetologists, New York, New York.
- Gans, C. 1967b. *Rhineura floridana*; pp. 43.1–43.2 in H. G. Dowling (ed.), *Catalogue of American Amphibians and Reptiles*. American Society of Ichthyologists and Herpetologists, New York, New York.
- Gans, C. 1968. Relative success of divergent pathways in amphisbaenian specialization. *American Naturalist* 102:345–362.
- Gans, C. 1969. Amphisbaenians—reptiles specialized for a burrowing existence. *Endeavour* 28:146–151.
- Gans, C. 1971. Studies on amphisbaenians (Amphisbaenia, Reptilia). 4. A review of the amphisbaenid genus *Leposternon*. *Bulletin of the American Museum of Natural History* 144:379–464.
- Gans, C. 1973a. Locomotion and burrowing in limbless vertebrates. *Nature* 242:414–415.
- Gans, C. 1973b. Uropeltid snakes—survivors in a changing world. *Endeavour* 32:60–65.
- Gans, C. 1974. *Biomechanics: An Approach to Vertebrate Biology*. University of Michigan Press, Ann Arbor, Michigan, 261 pp.
- Gans, C. 1976. Aspects of the biology of uropeltid snakes; pp. 191–204 in A. d'A. Bellairs and C. B. Cox (eds.), *Morphology and Biology of Reptiles*. Linnean Society Symposium Series, Number 3. Academic Press, London, U.K.
- Gans, C., and G. C. Lehman. 1973. Studies on amphisbaenians (Amphisbaenia: Reptilia). 5. The species of *Monopeltis* from north of the River Zaire. *Occasional Papers of the Museum of Zoology, University of Michigan* 669:1–34.
- Gans, C., H. C. Dessauer, and D. Baic. 1978. Axial differences in the musculature of uropeltid snakes: the freight-train approach to burrowing. *Science* 199:189–192.
- Gasparini, Z. B. 1971. Los Notosuchia del Cretácico de América del Sur como un nuevo infraorden de los Mesosuchia (Crocodylia). *Ameghiniana* 8:83–103.
- Gasparini, Z., L. M. Chiappe, and M. Fernandez. 1991. A new Senonian peirosaurid (Crocodylomorpha) from Argentina and a synopsis of the South American Cretaceous crocodylians. *Journal of Vertebrate Paleontology* 11:316–333.
- Gasparini, Z., M. Fernandez, and J. Powell. 1993. New Tertiary sebecosuchians (Crocodylomorpha) from South America: phylogenetic implications. *Historical Biology* 7:1–19.
- Gasparini, Z., D. Pol, and L. A. Spalletti. 2006. An unusual marine crocodyliform from the Jurassic-Cretaceous boundary of Patagonia. *Science* 311:70–73.
- Gaymer, R. 1971. New method of locomotion in limbless terrestrial vertebrates. *Nature* 234:150–151.
- Georgi, J. A., and D. W. Krause. 2010. Postcranial axial skeleton of *Simosuchus clarki* (Crocodyliformes: Notosuchia) from the Late Cretaceous of Madagascar; pp. 99–121 in D. W. Krause and N. J. Kley (eds.), *Simosuchus clarki* (Crocodyliformes: Notosuchia) from the Late Cretaceous of Madagascar. *Society of Vertebrate Paleontology Memoir* 10. *Journal of Vertebrate Paleontology* 30 (6, Supplement).
- Girard, L. 1923. Le plan des canaux semi-circulaires horizontaux considéré comme plan horizontal de la tête. *Bulletins et Mémoires de la Société d'Anthropologie de Paris, Série* 7 4:14–33.
- Gnanamuthu, C. P. 1937. Comparative study of the hyoid and tongue of some typical genera of reptiles. *Proceedings of the Zoological Society of London, Series B* 107:1–63.
- Gomani, E. M. 1997. A crocodyliform from the Early Cretaceous dinosaur beds, northern Malawi. *Journal of Vertebrate Paleontology* 17:280–294.
- Graf, W., C. de Waele, and P. P. Vidal. 1995. Functional anatomy of the head-neck movement system of quadrupedal and bipedal mammals. *Journal of Anatomy* 186:55–74.
- Hall, P. M., and K. M. Portier. 1994. Cranial morphometry of New Guinea crocodiles (*Crocodylus novaeguinae*): ontogenetic variation in relative growth of the skull and an assessment of its utility as a predictor of the sex and size of individuals. *Herpetological Monographs* 8:203–225.
- Harris, J. D. 2004. Confusing dinosaurs with mammals: tetrapod phylogenetics and anatomical terminology in the world of homology. *Anatomical Record Part A: Discoveries in Molecular, Cellular, and Evolutionary Biology* 281:1240–1246.
- Hay, O. P. 1930. *Second Bibliography and Catalogue of the Fossil Vertebrata of North America, Volume 2*. Carnegie Institution of Washington, Washington, D.C., 390(2):1–1094.
- Hildebrand, M. 1985. Digging of quadrupeds; pp. 89–109 in M. Hildebrand, D. M. Bramble, K. F. Liem, and D. B. Wake (eds.), *Functional Vertebrate Morphology*. Belknap Press, Cambridge, Massachusetts.
- Hill, R. V. 2010. Osteoderms of *Simosuchus clarki* (Crocodyliformes: Notosuchia) from the Late Cretaceous of Madagascar; pp. 154–176 in D. W. Krause and N. J. Kley (eds.), *Simosuchus clarki* (Crocodyliformes: Notosuchia) from the Late Cretaceous of Madagascar. *Society of Vertebrate Paleontology Memoir* 10. *Journal of Vertebrate Paleontology* 30(6, Supplement).
- Holliday, C. M. 2006. Evolution and function of the jaw musculature and adductor chamber of archosaurs (crocodylians, dinosaurs, and birds). Ph.D. dissertation, Ohio University, Athens, Ohio, 325 pp.
- Holliday, C. M. 2009. New insights into dinosaur jaw muscle anatomy. *Anatomical Record: Advances in Integrative Anatomy and Evolutionary Biology* 292:1246–1265.
- Holliday, C. M., and L. M. Witmer. 2009. The epipterygoid of crocodyliforms and its significance for the evolution of the orbitotemporal region of eusuchians. *Journal of Vertebrate Paleontology* 29:715–733.
- Hopson, J. A. 1979. *Paleoneurology*; pp. 39–146 in C. Gans (ed.), *Biology of the Reptilia, Volume 9: Neurology A*. Academic Press, New York, New York.
- Hotton, N., III. 1955. A survey of adaptive relationships of dentition to diet in the North American Iguanidae. *American Midland Naturalist* 53:88–114.
- Huang, C.-c. 1982. The ecology of the Chinese alligator and changes in its geographical distribution; pp. 54–62 in *Proceedings of the 5th Work-*

- ing Meeting of the Crocodile Specialist Group, 12–16 August 1980, Gainesville, Florida. International Union for Conservation of Nature and Natural Resources, Gland, Switzerland.
- Hullar, T. E. 2006. Semicircular canal geometry, afferent sensitivity, and animal behavior. *Anatomical Record Part A: Discoveries in Molecular, Cellular, and Evolutionary Biology* 288:466–472.
- International Committee on Veterinary Gross Anatomical Nomenclature. 2005. *Nomina Anatomica Veterinaria*, 5th edition. ICVGAN Editorial Committee, Hanover, Germany, Columbia, Missouri, Gent, Belgium, and Sapporo, Japan, 166 pp.
- Iordansky, N. N. 1964. The jaw muscles of the crocodiles and some relating structures of the crocodilian skull. *Anatomischer Anzeiger* 115:256–280.
- Iordansky, N. N. 1973. The skull of the Crocodilia; pp. 201–262 in C. Gans and T. S. Parsons (eds.), *Biology of the Reptilia*, Volume 4: Morphology D. Academic Press, London, U.K.
- Jan, G., and F. Sordelli. 1860–1866. *Iconographie Générale des Ophidiens*, Tome Premier. G. Jan and F. Sordelli, Milan, Italy.
- Jerison, H. J. 1973. *Evolution of the Brain and Intelligence*. Academic Press, New York, New York, 482 pp.
- Joffe, J. 1967. The ‘dwarf’ crocodiles of the Purbeck Formation, Dorset: a reappraisal. *Palaeontology* 10:629–639.
- Jouve, S. 2009. The skull of *Teleosaurus cadomensis* (Crocodylomorpha; Thalattosuchia), and phylogenetic analysis of Thalattosuchia. *Journal of Vertebrate Paleontology* 29:88–102.
- Jouve, S., M. Iarochène, B. Bouya, and M. Amaghazaz. 2006. A new species of *Dyrosaurus* (Crocodylomorpha, Dyrosauridae) from the early Eocene of Morocco: phylogenetic implications. *Zoological Journal of the Linnean Society* 148:603–656.
- Kley, N. J., and M. Kearney. 2007. Adaptations for digging and burrowing; pp. 284–309 in B. K. Hall (ed.), *Fins into Limbs: Evolution, Development, and Transformation*. University of Chicago Press, Chicago, Illinois.
- Krause, D. W., S. E. Evans, and K.-Q. Gao. 2003. First definitive record of Mesozoic lizards from Madagascar. *Journal of Vertebrate Paleontology* 23:842–856.
- Krause, D. W., J. J. W. Sertich, R. R. Rogers, A. H. Rasoamiramanana, S. C. Kast, and G. Buckley. 2010. Overview of the discovery, distribution, and geological context of *Simosuchus clarki* (Crocodyliformes: Notosuchia) from the Late Cretaceous of Madagascar; pp. 4–12 in D. W. Krause and N. J. Kley (eds.), *Simosuchus clarki* (Crocodyliformes: Notosuchia) from the Late Cretaceous of Madagascar. *Simosuchus clarki* (Crocodyliformes: Notosuchia) from the Late Cretaceous of Madagascar. *Journal of Vertebrate Paleontology* 30(6, Supplement).
- LaDuke, T. C., D. W. Krause, J. D. Scanlon, and N. J. Kley. 2010. A Late Cretaceous (Maastrichtian) snake assemblage from the Maevarano Formation, Mahajanga Basin, Madagascar. *Journal of Vertebrate Paleontology* 30:109–138.
- Lakjer, T. 1926. *Studien über die Trigeminus-versorgte Kaumuskulatur der Sauropsiden*. C. A. Reitzel, Copenhagen, Denmark, 154 pp.
- Langston, W. 1973. The crocodilian skull in historical perspective; pp. 263–284 in C. Gans and T. S. Parsons (eds.), *Biology of the Reptilia*, Volume 4: Morphology D. Academic Press, London, U.K.
- Larsson, H. C. E. 2001. Endocranial anatomy of *Carcharodontosaurus saharicus* (Theropoda: Allosauroidea) and its implications for theropod brain evolution; pp. 19–33 in D. H. Tanke and K. Carpenter (eds.), *Mesozoic Vertebrate Life*. Indiana University Press, Indianapolis, Indiana.
- Larsson, H. C. E., and B. Gado. 2000. A new Early Cretaceous crocodyliform from Niger. *Neues Jahrbuch für Geologie und Paläontologie-Abhandlungen* 217:131–141.
- Larsson, H. C. E., and H.-D. Sues. 2007. Cranial osteology and phylogenetic relationships of *Hamadasuchus rebouli* (Crocodyliformes: Mesoeucrocodylia) from the Cretaceous of Morocco. *Zoological Journal of the Linnean Society* 149:533–567.
- Lavocat, R. 1955. Sur une portion de mandibule de Théropode provenant du Crétacé supérieur de Madagascar. *Bulletin du Muséum National d’Histoire Naturelle* 27:256–259.
- Ledebkin, S. 1924. Über die Lage des Canalis semicircularis lateralis bei Säugern. *Anatomischer Anzeiger* 58:447–460.
- Lee, M. S. Y. 2000. The Russian pareiasaurs; pp. 71–85 in M. J. Benton, M. A. Shishkin, D. M. Unwin, and E. N. Kurochkin (eds.), *The Age of Dinosaurs in Russia and Mongolia*. Cambridge University Press, Cambridge, U.K.
- Marinho, T. S., and I. S. Carvalho. 2009. An armadillo-like sphagesaurid crocodyliform from the Late Cretaceous of Brazil. *Journal of South American Earth Sciences* 27:36–41.
- Martinelli, A. G. 2003. New cranial remains of the bizarre notosuchid *Comahuesuchus brachybuccalis* (Archosauria, Crocodyliformes) from the Late Cretaceous of Rio Negro Province (Argentina). *Ameghiniana* 40:559–572.
- Mazza, D., and B. J. Winterson. 1984. Semicircular canal orientation in the adult resting rabbit. *Acta Otolaryngologica* 98:472–480.
- McDowell, S. B. 1974. A catalogue of the snakes of New Guinea and the Solomons, with special reference to those in the Bernice P. Bishop Museum. Part I. *Scolopendria*. *Journal of Herpetology* 8:1–57.
- Montanucci, R. R. 1968. Comparative dentition in four iguanid lizards. *Herpetologica* 24:305–315.
- Mook, C. C. 1921a. Individual and age variations in the skulls of Recent Crocodilia. *Bulletin of the American Museum of Natural History* 44:51–66.
- Mook, C. C. 1921b. Skull characters of Recent Crocodilia, with notes on the affinities of the Recent genera. *Bulletin of the American Museum of Natural History* 44:123–268.
- Mook, C. C. 1964. New species of *Goniopholis* from the Morrison of Oklahoma. *Oklahoma Geology Notes* 24:283–287.
- Navas, C. A., M. M. Antoniazzi, J. E. Carvalho, J. G. Chaui-Berlink, R. S. James, C. Jared, T. Kohlsdorf, M. D. Pai-Silva, and R. S. Wilson. 2004. Morphological and physiological specialization for digging in amphisbaenians, an ancient lineage of fossorial vertebrates. *Journal of Experimental Biology* 207:2433–2441.
- Nobre, P. H., and I. S. Carvalho. 2002. Osteologia do crânio de *Candidodon itapecuruensis* (Crocodylomorpha, Mesoeucrocodylia) do Cretáceo do Brasil; pp. 77–82 in J. C. Castro, D. Dias-Brito, E. A. Musacchio, and R. Rohn (eds.), *Boletim do 6º Simpósio sobre o Cretáceo do Brasil/2º Simposio sobre el Cretácico de América del Sur*. Universidade Estadual Paulista, São Pedro, Brazil.
- Nobre, P. H., and I. S. Carvalho. 2006. *Adamantinasuchus navae*: a new Gondwanan Crocodylomorpha (Mesoeucrocodylia) from the Late Cretaceous of Brazil. *Gondwana Research* 10:370–378.
- Nobre, P. H., I. S. Carvalho, F. M. de Vasconcellos, and P. R. Souto. 2008. Feeding behavior of the Gondwanic Crocodylomorpha *Mariilia suchus amarali* from the Upper Cretaceous Bauru Basin, Brazil. *Gondwana Research* 13:139–145.
- Novas, F. E., D. F. Pais, D. Pol, I. S. Carvalho, A. Scanferla, A. Mones, and M. S. Riglos. 2009. Bizarre notosuchian crocodyliform with associated eggs from the Upper Cretaceous of Bolivia. *Journal of Vertebrate Paleontology* 29:1316–1320.
- O’Connor, P. M., J. J. W. Sertich, N. J. Stevens, E. M. Roberts, M. D. Gottfried, T. L. Hieronymus, Z. A. Jinnah, R. Ridgely, S. E. Ngalala, and J. Temba. 2010. The evolution of mammal-like crocodyliforms in the Cretaceous Period of Gondwana. *Nature* 466:748–751.
- O’Reilly, J. C., D. A. Ritter, and D. R. Carrier. 1997. Hydrostatic locomotion in a limbless tetrapod. *Nature* 386:269–272.
- Ortega, F., Z. Gasparini, A. D. Buscalioni, and J. O. Calvo. 2000. A new species of *Arapipesuchus* (Crocodylomorpha, Mesoeucrocodylia) from the Lower Cretaceous of Patagonia (Argentina). *Journal of Vertebrate Paleontology* 20:57–76.
- Ősi, A. 2008. Cranial osteology of *Iharkutosuchus makadii*, a Late Cretaceous basal eusuchian crocodyliform from Hungary. *Neues Jahrbuch für Geologie und Paläontologie, Abhandlungen* 248:279–299.
- Ősi, A., J. M. Clark, and D. B. Weishampel. 2007. First report on a new basal eusuchian crocodyliform with multicusped teeth from the Upper Cretaceous (Santonian) of Hungary. *Neues Jahrbuch für Geologie und Paläontologie-Abhandlungen* 243:169–177.
- Owen, R. 1850. On the communications between the cavity of the tympanum and the palate in the Crocodilia (gavials, alligators and crocodiles). *Philosophical Transactions of the Royal Society of London* 140:521–527.
- Owen, R. 1854. *The Principal Forms of the Skeleton and of the Teeth*. Blanchard and Lea, Philadelphia, Pennsylvania, 329 pp.
- Owen, R. 1866. *On the Anatomy of Vertebrates*. Volume 1. Fishes and Reptiles. Longmans, Green, and Co., London, U.K., 650 pp.
- Parker, W. K. 1883. On the structure and development of the skull in the Crocodilia. *Transactions of the Zoological Society of London* 11:263–310.

- Peterka, M., J. Y. Sire, M. Hovorakova, J. Prochazka, L. Fougeirol, R. Peterkova, and L. Viriot. 2010. Prenatal development of *Crocodylus niloticus niloticus* Laurenti, 1768. *Journal of Experimental Zoology Part B: Molecular and Developmental Evolution* 314:353–368.
- Peyer, B. 1968. *Comparative Odontology*. University of Chicago Press, Chicago, Illinois, 347 pp.
- Poglayen-Neuwall, I. 1953. Untersuchungen der Kiefermuskulatur und deren Innervation an Krokodilen. *Anatomischer Anzeiger* 99:257–276.
- Pol, D. 1999. El esqueleto postcraneano de *Notosuchus terrestris* (Archosauria: Crocodyliformes) del Cretácico Superior de la Cuenca Neuquina y su información filogenética. Tesis de Licenciatura, Facultad de Ciencias Exactas y Naturales, Universidad de Buenos Aires, 158 pp.
- Pol, D. 2003. New remains of *Sphagesaurus huenei* (Crocodylomorpha: Mesoeucrocodylia) from the Late Cretaceous of Brazil. *Journal of Vertebrate Paleontology* 23:817–831.
- Pol, D., and S. Apesteguía. 2005. New *Araripesuchus* remains from the early Late Cretaceous (Cenomanian–Turonian) of Patagonia. *American Museum Novitates* 3490:1–38.
- Pol, D., and M. A. Norell. 2004a. A new crocodyliform from Zos Canyon, Mongolia. *American Museum Novitates* 3445:1–36.
- Pol, D., and M. A. Norell. 2004b. A new gobiosuchid crocodyliform taxon from the Cretaceous of Mongolia. *American Museum Novitates* 3458:1–31.
- Pol, D., A. H. Turner, and M. A. Norell. 2009. Morphology of the Late Cretaceous crocodylomorph *Shamosuchus djadochtaensis* and a discussion of neosuchian phylogeny as related to the origin of Eusuchia. *Bulletin of the American Museum of Natural History* 324:1–103.
- Pol, D., S.-a. Ji, J. M. Clark, and L. M. Chiappe. 2004. Basal crocodyliforms from the Lower Cretaceous Tugulu Group (Xinjiang, China), and the phylogenetic position of *Edentosuchus*. *Cretaceous Research* 25:603–622.
- Poole, D. F. G. 1961. Notes on tooth replacement in the Nile crocodile *Crocodylus niloticus*. *Proceedings of the Zoological Society of London* 136:131–140.
- Price, L. I. 1945. A new reptil [sic] from the Cretaceous of Brazil. *Notas Preliminares e Estudos, Divisão de Geologia e Mineralogia, Ministério da Agricultura, Rio de Janeiro, Brasil* 25:1–8.
- Price, L. I. 1955. Novos crocodilídeos dos Arenitos da Série Baurú, Cretáceo do Estado de Minas Gerais. *Anais da Academia Brasileira de Ciências* 27:487–498.
- Price, L. I. 1959. Sobre um crocodilídeo notossúquio do Cretácico Brasileiro. *Boletim do Departamento Nacional da Produção Mineral, Divisão de Geologia e Mineralogia, Rio de Janeiro* 188:1–55.
- Purcell, S. W., and D. R. Bellwood. 1993. A functional analysis of food procurement in two surgeonfish species, *Acanthurus nigrofasciatus* and *Ctenochaetus striatus* (Acanthuridae). *Environmental Biology of Fishes* 37:139–159.
- Rajendran, M. V. 1985. *Studies in Uropeltid Snakes*. Publications Division, Madurai Kamaraj University, Madurai, India, 132 pp.
- Ray, C. E. 1965. Variation in the number of marginal tooth positions in three species of iguanid lizards. *Breviora* 236:1–15.
- Reisz, R. R., and H.-D. Sues. 2000. Herbivory in late Paleozoic and Triassic terrestrial vertebrates; pp. 9–41 in H.-D. Sues (ed.), *Evolution of Herbivory in Terrestrial Vertebrates: Perspectives from the Fossil Record*. Cambridge University Press, Cambridge, U.K.
- Rieppel, O. 1993. Studies on skeleton formation in reptiles. V. Patterns of ossification in the skeleton of *Alligator mississippiensis* Daudin (Reptilia, Crocodylia). *Zoological Journal of the Linnean Society* 109:301–325.
- Rogers, R. R. 2005. Fine-grained debris flows and extraordinary vertebrate burials in the Late Cretaceous of Madagascar. *Geology* 33:297–300.
- Rogers, R. R., J. H. Hartman, and D. W. Krause. 2000. Stratigraphic analysis of Upper Cretaceous rocks in the Mahajanga Basin, northwestern Madagascar: implications for ancient and modern faunas. *Journal of Geology* 108:275–301.
- Rogers, R. R., D. W. Krause, K. Curry Rogers, A. H. Rasoamiramanana, and L. Rahantarisoa. 2007. Paleoenvironment and paleoecology of *Majungasaurus crenatissimus* (Theropoda: Abelisauridae) from the Late Cretaceous of Madagascar; pp. 21–31 in S. D. Sampson and D. W. Krause (eds.), *Majungasaurus crenatissimus* (Theropoda: Abelisauridae) from the Late Cretaceous of Madagascar. Society of Vertebrate Paleontology Memoir 8. *Journal of Vertebrate Paleontology* 27(2, Supplement).
- Rogers, S. W. 1999. *Allosaurus*, crocodiles, and birds: evolutionary clues from spiral computed tomography of an endocast. *Anatomical Record* 257:162–173.
- Romer, A. S. 1956. *Osteology of the Reptiles*. University of Chicago Press, Chicago, Illinois, 772 pp.
- Roux-Estève, R. 1974. Révision systématique des Typhlopidae d'Afrique Reptilia-Serpentes. *Mémoires du Muséum National d'Histoire Naturelle. Nouvelle Série. Série A, Zoologie* 87:1–313.
- Rusconi, C. 1933. Sobre reptiles cretáceos del Uruguay (*Uruguaysuchus aznarezi* n. g. n. sp.) y sus relaciones con los notosúquidos de Patagonia. *Boletín del Instituto de Geología y Perforaciones del Uruguay* 19:3–64.
- Rybczynski, N., and R. R. Reisz. 2001. Earliest evidence for efficient oral processing in a terrestrial herbivore. *Nature* 411:684–687.
- Salisbury, S. W., R. E. Molnar, E. Frey, and P. M. A. Willis. 2006. The origin of modern crocodyliforms: new evidence from the Cretaceous of Australia. *Proceedings of the Royal Society of London, Series B* 273:2439–2448.
- Salisbury, S. W., P. M. A. Willis, S. Peitz, and P. M. Sander. 1999. The crocodylian *Goniopholis simus* from the Lower Cretaceous of northwestern Germany. *Special Papers in Palaeontology* 60:121–148.
- Sampson, S. D., and L. M. Witmer. 2007. Craniofacial anatomy of *Majungasaurus crenatissimus* (Theropoda: Abelisauridae) from the Late Cretaceous of Madagascar; pp. 32–102 in S. D. Sampson and D. W. Krause (eds.), *Majungasaurus crenatissimus* (Theropoda: Abelisauridae) from the Late Cretaceous of Madagascar. Society of Vertebrate Paleontology Memoir 8. *Journal of Vertebrate Paleontology* 27(2, Supplement).
- Sampson, S. D., M. T. Carrano, and C. A. Forster. 2001. A bizarre predatory dinosaur from the Late Cretaceous of Madagascar. *Nature* 409:504–506.
- Sampson, S. D., L. M. Witmer, C. A. Forster, D. W. Krause, P. M. O'Connor, P. Dodson, and F. Ravoavy. 1998. Predatory dinosaur remains from Madagascar: implications for the Cretaceous biogeography of Gondwana. *Science* 280:1048–1051.
- Schumacher, G. H. 1973. The head muscles and hyolaryngeal skeleton of turtles and crocodylians; pp. 101–199 in C. Gans and T. S. Parsons (eds.), *Biology of the Reptilia, Volume 4: Morphology D*. Academic Press, London, U.K.
- Sedlmayr, J. C. 2002. *Anatomy, evolution, and functional significance of cephalic vasculature in Archosauria*. Ph.D. dissertation, Ohio University, Athens, Ohio, 398 pp.
- Senter, P. 2008. Homology between and antiquity of stereotyped communicatory behaviors of crocodylians. *Journal of Herpetology* 42:354–360.
- Sereno, P. C. 1991. *Lesothosaurus*, “fabrosaurids,” and the early evolution of Ornithischia. *Journal of Vertebrate Paleontology* 11:168–197.
- Sereno, P. C., and H. C. E. Larsson. 2009. Cretaceous crocodyliforms from the Sahara. *ZooKeys* 28:1–143.
- Sereno, P. C., H. C. E. Larsson, C. A. Sidor, and B. Gado. 2001. The giant crocodyliform *Sarcosuchus* from the Cretaceous of Africa. *Science* 294:1516–1519.
- Sereno, P. C., C. A. Sidor, H. C. E. Larsson, and B. Gado. 2003. A new notosuchian from the Early Cretaceous of Niger. *Journal of Vertebrate Paleontology* 23:477–482.
- Sereno, P. C., J. A. Wilson, L. M. Witmer, J. A. Whitlock, A. Maga, O. Ide, and T. A. [sic] Rowe. 2007. Structural extremes in a Cretaceous dinosaur. *PLoS One* 2:e1230.
- Sertich, J. J. W., and J. R. Groenke. 2010. Appendicular skeleton of *Simosuchus clarki* (Crocodyliformes: Notosuchia) from the Late Cretaceous of Madagascar; pp. 122–153 in D. W. Krause and N. J. Kley (eds.), *Simosuchus clarki* (Crocodyliformes: Notosuchia) from the Late Cretaceous of Madagascar. Society of Vertebrate Paleontology Memoir 10. *Journal of Vertebrate Paleontology* 30(6, Supplement).
- Simons, E. L. R., and G. A. Buckley. 2009. New material of “*Trematochampsia*” *oblita* (Crocodyliformes, Trematochampsidae) from the Late Cretaceous of Madagascar. *Journal of Vertebrate Paleontology* 29:599–604.
- Sondhi, K. C. 1958. The hyoid and associated structures in some Indian reptiles. *Annals of Zoology* 11:155–240.

- Stromer, E. 1914. Ergebnisse der Forschungsreisen Prof. E. Stromers in den Wüsten Ägyptens. II. Wirbeltier-Reste der Baharije-Stufe (unterstes Cenoman). 1. Einleitung und 2. *Libycosuchus*. Abhandlungen der Königlich Bayerischen Akademie der Wissenschaften Mathematisch-physikalische Klasse 27(3):1–16.
- Stromer, E. 1925. Ergebnisse der Forschungsreisen Prof. E. Stromers in den Wüsten Ägyptens. II. Wirbeltier-Reste der Baharije-Stufe (unterstes Cenoman). 7. *Stomatosuchus inermis* Stromer, ein schwach bezahnter Krokodilier und 8. Ein Skelettrest des Pristiden *Onchopristis numidus* Huag sp. Abhandlungen der Königlich Bayerischen Akademie der Wissenschaften Mathematisch-physikalische Klasse 30(6):1–22.
- Sues, H.-D., P. E. Olsen, J. G. Carter, and D. M. Scott. 2003. A new crocodylomorph archosaur from the Upper Triassic of North Carolina. *Journal of Vertebrate Paleontology* 23:329–343.
- Tanner, W. W., and D. F. Avery. 1982. Buccal floor of reptiles, a summary. *Great Basin Naturalist* 42:273–349.
- Taylor, M. P., M. J. Wedel, and D. Naish. 2009. Head and neck posture in sauropod dinosaurs inferred from extant animals. *Acta Palaeontologica Polonica* 54:213–220.
- Thulborn, R. A. 1970. The skull of *Fabrosaurus australis*, a Triassic ornithischian dinosaur. *Palaeontology* 13:414–432.
- Troxell, E. L. 1925. The Bridger crocodiles. *American Journal of Science* 9:29–72.
- Turner, A. H. 2004. Crocodyliform biogeography during the Cretaceous: evidence of Gondwanan vicariance from biogeographical analysis. *Proceedings of the Royal Society of London, Biological Sciences* 271:2003–2009.
- Turner, A. H. 2006. Osteology and phylogeny of a new species of *Araripesuchus* (Crocodyliformes: Mesoeucrocodylia) from the Late Cretaceous of Madagascar. *Historical Biology* 18:255–369.
- Turner, A. H., and G. A. Buckley. 2008. *Mahajangasuchus insignis* (Crocodyliformes: Mesoeucrocodylia) cranial anatomy and new data on the origin of the eusuchian-style palate. *Journal of Vertebrate Paleontology* 28:382–408.
- Turner, A. H., and J. O. Calvo. 2005. A new sebecosuchian crocodyliform from the Late Cretaceous of Patagonia. *Journal of Vertebrate Paleontology* 25:87–98.
- Turner, A. H., and J. J. W. Sertich. 2010. Phylogenetic history of *Simosuchus clarki* (Crocodyliformes: Notosuchia) from the Late Cretaceous of Madagascar; pp. 177–236 in D. W. Krause and N. J. Kley (eds.), *Simosuchus clarki* (Crocodyliformes: Notosuchia) from the Late Cretaceous of Madagascar. *Society of Vertebrate Paleontology Memoir 10*. *Journal of Vertebrate Paleontology* 30 (6, Supplement).
- Tykoski, R. S., T. B. Rowe, R. A. Ketcham, and M. W. Colbert. 2002. *Calosyasuchus valliceps*, a new crocodyliform from the Early Jurassic Kayenta Formation of Arizona. *Journal of Vertebrate Paleontology* 22:593–611.
- Underwood, G. 1970. The eye; pp. 1–97 in C. Gans and T. S. Parsons (eds.), *Biology of the Reptilia*, Volume 2: Morphology B. Academic Press, London, U.K.
- Vasconcellos, F. M., and I. S. Carvalho. 2007. Cranial features of *Baurusuchus salgadoensis* Carvalho, Campos & Nobre 2005, a Baurusuchidae (Mesoeucrocodylia) from the Adamantina Formation, Bauru Basin, Brazil: paleoichnological, taxonomic and systematic implications; pp. 319–332 in I. S. Carvalho, R. C. T. Cassab, C. Schwanke, M. A. Carvalho, A. C. S. Fernandes, M. A. C. Rodrigues, M. S. S. Carvalho, M. Arai, and M. E. Q. Oliveira (eds.), *Paleontologia: Cenários de Vida*. Interciência, Rio de Janeiro, Brazil.
- Vidal, P. P., W. Graf, and A. Berthoz. 1986. The orientation of the cervical vertebral column in unrestrained awake animals. I. Resting position. *Experimental Brain Research* 61:549–559.
- Wake, M. H. 1993. The skull as a locomotor organ; pp. 197–240 in J. Hanken and B. K. Hall (eds.), *The Skull*, Volume 3: Functional and Evolutionary Mechanisms. University of Chicago Press, Chicago, Illinois.
- Walker, A. D. 1970. A revision of the Jurassic reptile *Hallopus victor* (Marsh), with remarks on the classification of crocodiles. *Philosophical Transactions of the Royal Society of London B* 257:323–372.
- Walker, A. D. 1990. A revision of *Sphenosuchus acutus* Houghton, a crocodylomorph reptile from the Elliot Formation (late Triassic or early Jurassic) of South Africa. *Philosophical Transactions of the Royal Society of London Series B, Biological Sciences* 330:1–120.
- Walls, G. L. 1942. The Vertebrate Eye and its Adaptive Radiation. *Cranbrook Institute of Science Bulletin Number 19*. Cranbrook Institute of Science, Bloomfield Hills, Michigan, 785 pp.
- Watanabe, M. E., and C.-c. Huang. 1984. Status of the Chinese alligator in the People's Republic of China; pp. 91–101 in *Proceedings of the 6th Working Meeting of the Crocodile Specialist Group*, 19–30 September 1982, Victoria Falls, Zimbabwe and St. Lucia Estuary, South Africa. International Union for Conservation of Nature and Natural Resources, Gland, Switzerland.
- Wharton, D. S. 2000. An enlarged endocranial venous system in *Steenosaurus pictaviensis* (Crocodylia: Thalattosuchia) from the Upper Jurassic of Les Lourdines, France. *Comptes Rendus de l'Académie des Sciences, Série IIA* 331:221–226.
- Whetstone, K. N., and P. J. Whybrow. 1983. A “cursorial” crocodylian from the Triassic of Lesotho (Basutoland), southern Africa. *Occasional Papers of the Museum of Natural History, University of Kansas* 106:1–37.
- Williston, S. W. 1925. *The Osteology of the Reptiles*. Harvard University Press, Cambridge, Massachusetts, 300 pp.
- Wilson, J. A. 2006. Anatomical nomenclature of fossil vertebrates: standardized terms or ‘lingua franca’? *Journal of Vertebrate Paleontology* 26:511–518.
- Witmer, L. M. 1995. Homology of facial structures in extant archosaurs (birds and crocodylians), with special reference to paranasal pneumaticity and nasal conchae. *Journal of Morphology* 225:269–327.
- Witmer, L. M., and R. C. Ridgely. 2009. New insights into the brain, braincase, and ear region of tyrannosaurs (Dinosauria, Theropoda), with implications for sensory organization and behavior. *Anatomical Record: Advances in Integrative Anatomy and Evolutionary Biology* 292:1266–1296.
- Witmer, L. M., S. Chatterjee, J. Franzosa, and T. Rowe. 2003. Neuroanatomy of flying reptiles and implications for flight, posture and behaviour. *Nature* 425:950–953.
- Witmer, L. M., R. C. Ridgely, D. L. Dufeu, and M. C. Semones. 2008. Using CT to peer into the past: 3D visualization of the brain and ear regions of birds, crocodiles and nonavian dinosaurs; pp. 67–87 in H. Endo and R. Frey (eds.), *Anatomical Imaging: Towards a New Morphology*. Springer-Verlag, Tokyo.
- Wu, X.-c., and S. Chatterjee. 1993. *Dibothrosuchus elaphros*, a crocodylomorph from the Lower Jurassic of China and the phylogeny of the Sphenosuchia. *Journal of Vertebrate Paleontology* 13:58–89.
- Wu, X.-c., and H.-D. Sues. 1996. Anatomy and phylogenetic relationships of *Chimaerasuchus paradoxus*, an unusual crocodyliform reptile from the Lower Cretaceous of Hubei, China. *Journal of Vertebrate Paleontology* 16:688–702.
- Wu, X.-c., A. P. Russell, and S. L. Cumbaa. 2001. *Terminonaris* (Archosauria: Crocodyliformes): new material from Saskatchewan, Canada, and comments on its phylogenetic relationships. *Journal of Vertebrate Paleontology* 21:492–514.
- Wu, X.-c., H.-D. Sues, and Z.-M. Dong. 1997. *Sichuanosuchus shuhanensis*: a new? Early Cretaceous protosuchian (Archosauria: Crocodyliformes) from Sichuan (China), and the monophyly of Protosuchia. *Journal of Vertebrate Paleontology* 17:89–103.
- Wu, X.-c., H.-D. Sues, and A. Sun. 1995. A plant-eating crocodyliform reptile from the Cretaceous of China. *Nature* 376:678–680.
- Zaher, H., D. Pol, A. B. Carvalho, C. Riccomini, D. Campos, and W. Nava. 2006. Redescription of the cranial morphology of *Marilia-suchus amarali*, and its phylogenetic affinities (Crocodyliformes, Notosuchia). *American Museum Novitates* 3512:1–40.

Submitted August 6, 2010; accepted October 12, 2010.

APPENDIX 1. List of anatomical abbreviations.

ac, adductor chamber
acf, anterior carotid foramen
act, area of contact for cartilago transiliens
af ap, articular facet for anterior palpebral
af pp, articular facet for posterior palpebral
amnc, anteromedial narial crest
ang, angular
ang nvf, angular neurovascular foramina
ang ram, angular ramus
ang vlf, angular ventrolateral flange
ang vmp, angular ventromedial process
aof, antorbital fenestra
ap, anterior palpebral
ap af prf, anterior palpebral articular facet for prefrontal
apalf, anterior palatal foramen
apalfos, anterior palatal fossa
apt, anterior palatal trough
art ap, articular anterior process
art bod, articular body
art vmp, articular ventromedial process
asc, anterior semicircular canal (or endocast thereof)
asto, anterior supratemporal ossification
bo, basioccipital
bt, basal tubera
cav ept, cavum epiptericum
cavs, cavernous dural venous sinus (endocast)
cer, cerebrum (endocast)
CN, cranial nerve
CN II, optic nerve (endocast)
CN III, oculomotor nerve (endocast)
CN V, trigeminal nerve (endocast)
CN VI, abducens nerve (endocast)
CN IX + X, glossopharyngeal and vagus nerves (endocast)
CN XII a, anterior rootlets of hypoglossal nerve (endocast)
CN XII p, posterior rootlets of hypoglossal nerve (endocast)
cqc, cranioquadrate canal
ct, 'cranial table'
dals, dorsal alveolar spines
den, dentary
den alg, dentary alveolar groove
den alp, dentary alveolar process
den alp lal, dentary alveolar process labial lamina
den alp lil, dentary alveolar process lingual lamina
den alv, dentary alveolus
den nvf, dentary neurovascular foramina
den pdp, dentary posterodorsal process
den ram, dentary ramus
den sd, dentary subdental process
den smp, dentary submeckelian process
den t, dentary tooth
dls, dorsal longitudinal dural venous sinus (endocast)
dmdals, dorsomedial dorsal alveolar spine
ds, dorsum sellae
ect bod, ectopterygoid body
ect dsp, ectopterygoid descending process
ect pp, ectopterygoid posterior process
emf, external mandibular fenestra
enf, external narial fenestra
eor, external otic recess
ept, epipterygoid
fa, foramen aereum
fl, flocculus (endocast)
fm, foramen magnum
fro, frontal
fro ap, frontal anterior process
fro ap dl, frontal anterior process dorsal lamina
fro dl, frontal dorsal lamina
fro dsp, frontal descending process
fro lc, frontal longitudinal crest
gfos, glenoid fossa
hf, hypophyseal fossa (or endocast thereof)
idr, interdental ridge
ifor, incisive foramen
ifos, incisive fossa
in, internal naris
inf, internal narial fenestra
inpf, internal narial posterior fossa
itf, infratemporal fenestra
jug ap, jugal anterior process
jug ap dc, jugal anterior process dorsal crest
jug ap vlc, jugal anterior process ventrolateral crest
jug ap vmc, jugal anterior process ventromedial crest
jug asp, jugal ascending process
jug pp, jugal posterior process
jug pp vmc, jugal posterior process ventromedial crest
lac can, lacrimal canal
lac can ao, lacrimal canal anterior opening
lac can po, lacrimal canal posterior opening
lac fl, lacrimal facial lamina
lac fl ap, lacrimal facial lamina anterior process
lac fl dsp, lacrimal facial lamina descending process
lac ol, lacrimal orbital lamina
lac plc, lacrimal posterolateral crest
leuf, lateral Eustachian foramen
lpt, lateral palatal trough
ls all, laterosphenoid anterolateral lamina
ls cotc, laterosphenoid cotylar crest
ls cp, laterosphenoid capitate process
ls ped ept, laterosphenoid pedicel for epipterygoid
ls pll, laterosphenoid posterolateral lamina
lsc, lateral semicircular canal (or endocast thereof)
mac, mandibular canal
maf, mandibular adductor fossa
max, maxilla
max alg, maxillary alveolar groove
max alp, maxillary alveolar process
max asp, maxillary ascending process
max nvf, maxillary neurovascular foramina
max pap, maxillary palatal process
max t, maxillary tooth
mc, Meckel's canal
meuf, median Eustachian foramen
meut ab, median Eustachian tube, anterior branch
meut pb, median Eustachian tube, posterior branch
mfis, metotic fissure
mg, Meckel's groove
moc, mid-orbital crest
mr, recess for Meckel's cartilage
nas, nasal
nc, nuchal crest
npc, nasopharyngeal canal
oa, otic aperture
ob, olfactory bulb (endocast)
oc, occipital condyle
ocs, occipital dural venous sinus (endocast)
of, orbital fenestra
oinc, otic incisure
ot, olfactory tract (endocast)
oto, otoccipital (opisthotic-exoccipital)
pal asp, palatine ascending process
pal pap, palatine palatal process
par, parietal
par dl, parietal dorsal lamina

par dsp, parietal descending process
par sin, parietal sinus
parop, paroccipital process
pbs, parabasisphenoid (parasphenoid-basisphenoid)
pbs ros, parabasisphenoid rostrum
pcf, posterior carotid foramen
pgs, postglenoid spine
plnc, posterolateral narial crest
pmx, premaxilla
pmx alg, premaxillary alveolar groove
pmx alp, premaxillary alveolar process
pmx alp al, premaxillary alveolar process anterior lamina
pmx alp pl, premaxillary alveolar process posterior lamina
pmx alv, premaxillary alveolus
pmx dlp, premaxillary dorsolateral process
pmx dmp, premaxillary dorsomedial process
pmx pap, premaxillary palatal process
pmx t, premaxillary tooth
pnfor, perinarial foramen
pnfos, perinarial fossa
po amp, postorbital anteromedial process
po amp dl, postorbital anteromedial process dorsal lamina
po amp ol, postorbital anteromedial process orbital lamina
po dl, postorbital dorsal lamina
po dsp, postorbital descending process
po dsp dpl, postorbital descending process dorsal plate
po dsp ol, postorbital descending process orbital lamina
po dsp pll, postorbital descending process posterolateral lamina
po ol, postorbital orbital lamina
po pp, postorbital posterior process
po pp dl, postorbital posterior process dorsal lamina
pooc, postorbital crest
posf, preotic siphoneal foramen
pp, posterior palpebral
pp af po, posterior palpebral articular facet for postorbital
prf dl, prefrontal dorsal lamina
prf dsp, prefrontal descending process
prf ol, prefrontal orbital lamina
pro, prootic
proc, preorbital crest
psc, posterior semicircular canal (or endocast thereof)
psca, ampulla of posterior semicircular canal (endocast)
psf, parasymphiseal fossa
pss, parasymphiseal spine
psto, posterior supratemporal ossification
pstop, postoccipital process
pt, pterygoid
pt ap, pterygoid anterior process
pt ap dll, pterygoid anterior process dorsolateral lamina
pt ap vnl, pterygoid anterior process ventral lamina
pt ap vrl, pterygoid anterior process vertical lamina
pt dp, pterygoid dorsal process
pt ped ept, pterygoid pedicel for epipterygoid
pt pl, pterygoid plate
pt qp, pterygoid quadrate process
pt tp, pterygoid transverse process
pt tp ac, pterygoid transverse process anterior crest
pt tp dt, pterygoid transverse process dorsal tuberosity
pt tp vc, pterygoid transverse process ventral crest
ptf, posttemporal fenestra
q, quadrate
q adp, quadrate anterodorsal process
q bod, quadrate body
q dp, quadrate dorsal process
q dph, quadrate dorsal primary head
q lhc, quadrate lateral hemicondyle
q mhc, quadrate medial hemicondyle
q ptp, quadrate pterygoid process
qj, quadratojugal
qj ap, quadratojugal anterior process
qj asp, quadratojugal ascending process
qj cpl, quadratojugal central plate
qj tub, quadratojugal tubercle
rap, retroarticular process
rt, replacement tooth
so, supraoccipital
so sin, supraoccipital sinus
soc, supraorbital crest
sof, suborbital fenestra
spl, splenial
spl ml, splenial medial lamina
spl vl, splenial ventral lamina
sps, sphenoparietal dural venous sinus (endocast)
sq, squamosal
sq adsl, squamosal anterior descending lamina
sq ap, squamosal anterior process
sq mp, squamosal medial process
sq pdsl, squamosal posterior descending lamina
sq pp, squamosal posterior process
stfen, supratemporal fenestra
stfos, supratemporal fossa
sur, surangular
sur nvf, surangular neurovascular foramina
sur ram, surangular ramus
sur ram ldf, lateral descending flange of surangular ramus
sur ram mdf, medial descending flange of surangular ramus
sur vmp, surangular ventromedial process
sym, mandibular symphysis
sym tub, symphyseal tubercle
tof, temporo-orbital foramen
ts, transverse dural venous sinus (endocast)
vac, ventral alveolar canal
vaf, ventral alveolar foramen
vag, ventral alveolar groove
vldals, ventrolateral dorsal alveolar spine
vls, ventral longitudinal dural venous sinus (endocast)
vo, vomer
vo asp, vomer ascending process
vo pap, vomer palatal process
III, oculomotor foramen
IV, trochlear foramen
V, trigeminal foramen
V fos, trigeminal fossa
V₂₊₃ gr, maxillomandibular groove
V₃ gr, groove for mandibular nerve
V₃ iab, foramen for internal angular branch of mandibular nerve
V₃ isb, foramen for internal surangular branch of mandibular nerve
VI, abducens canal/foramina
VII, facial foramen
VIII, vestibulocochlear foramen
IX + X, foramen for glossopharyngeal and vagus nerves
XII a, anterior hypoglossal foramen
XII p, posterior hypoglossal foramen